

INFORMATION TO USERS

This manuscript has been reproduced from the microfilm master. UMI films the text directly from the original or copy submitted. Thus, some thesis and dissertation copies are in typewriter face, while others may be from any type of computer printer.

The quality of this reproduction is dependent upon the quality of the copy submitted. Broken or indistinct print, colored or poor quality illustrations and photographs, print bleedthrough, substandard margins, and improper alignment can adversely affect reproduction.

In the unlikely event that the author did not send UMI a complete manuscript and there are missing pages, these will be noted. Also, if unauthorized copyright material had to be removed, a note will indicate the deletion.

Oversize materials (e.g., maps, drawings, charts) are reproduced by sectioning the original, beginning at the upper left-hand corner and continuing from left to right in equal sections with small overlaps.

Photographs included in the original manuscript have been reproduced xerographically in this copy. Higher quality 6" x 9" black and white photographic prints are available for any photographs or illustrations appearing in this copy for an additional charge. Contact UMI directly to order.

Bell & Howell Information and Learning
300 North Zeeb Road, Ann Arbor, MI 48106-1346 USA

UMI[®]
800-521-0600

Copyright
by
Paul Norman Chisholm
1999

**Dry Absorption of Hydrogen Chloride and Sulfur Dioxide by
Calcium-Based Sorbents from Humidified Flue Gas**

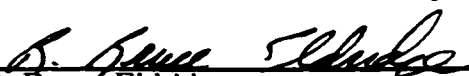
**Approved by
Dissertation Committee:**



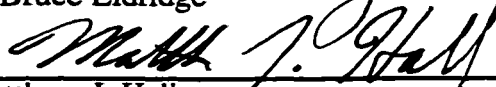
Gary T. Rochelle, Supervisor



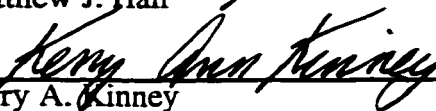
David T. Allen



R. Bruce Eldridge



Matthew J. Hall



Kerry A. Kinney

**Dry Absorption of Hydrogen Chloride and Sulfur Dioxide by
Calcium-Based Sorbents from Humidified Flue Gas**

by

Paul Norman Chisholm, B.S., M.S.

Dissertation

Presented to the Faculty of the Graduate School of

The University of Texas at Austin

in Partial Fulfillment

of the Requirements

for the Degree of

Doctor of Philosophy

The University of Texas at Austin

August, 1999

UMI Number: 9956812

UMI[®]

UMI Microform 9956812

Copyright 2000 by Bell & Howell Information and Learning Company.

**All rights reserved. This microform edition is protected against
unauthorized copying under Title 17, United States Code.**

**Bell & Howell Information and Learning Company
300 North Zeeb Road
P.O. Box 1346
Ann Arbor, MI 48106-1346**

Dedication

This dissertation is dedicated to my high school chemistry teacher, Mr. Kevin Zenewicz, and all the teachers who work hard to develop their students' abilities.

Acknowledgements

I would like to acknowledge first Dr. Gary Rochelle for his ability to create an excellent environment for graduate work. While supervising my research, he provided insightful assistance while still affording me a large measure of independence. Few graduate supervisors can maintain that fine balance with his dexterity. In addition, his creative approach to understanding and solving problems has been a tremendous asset to the completion of this work.

Throughout my tenure at Texas, several of my peers have gone out of their way to assist me. The help given by Chris Nelli and Lia Arthur (now Lia Brodnax) early during my time here expedited considerably my methods development and construction of an experimental apparatus. In addition to Chris and Lia, Sanjay Bishnoi, Mike Dutchuk, and other colleagues have been great sounding boards for technical ideas and discussions. Perhaps more importantly, the camaraderie provided by their company has made an often-frustrating job enjoyable and, at times, downright entertaining. Having read the entire dissertation, Norman Yeh's impressive attention to detail considerably improved this document. Thanks also go out to Joseph Devinentis for his patience and assistance with all my computer-related problems.

Thanks to my parents and brothers for their moral support throughout the years that I have spent in school. Typical of their generation, my parents made many sacrifices to ensure that their children would have a bit more of a headstart in life than they did. I have had the opportunity to complete a Ph.D only because of the lessons they have taught me.

I must thank my fiancée, Carrie O'Brien, for her endless and unconditional support of me. Even a brief discussion with Carrie would undo an entire day's worth of frustration in the laboratory. She is the best friend I could ever wish for.

In conclusion, thanks go to the Separations Research, the Texas Advanced Technology, and the Environmental Solutions Programs for providing the majority of financial support for this work.

Dry Absorption of Hydrogen Chloride and Sulfur Dioxide by Calcium-Based Sorbents from Humidified Flue Gas

Publication No. _____

Paul Norman Chisholm, Ph.D.

The University of Texas at Austin, 1999

Supervisor: Gary T. Rochelle

A fixed-bed experimental apparatus was constructed to simulate acid gas absorption by powdered sorbents on a bag filter. The sorbents studied were hydrated lime and calcium silicate. Key variables included relative humidity, temperature, and the concentrations of HCl, SO₂, NO, NO₂, and O₂. The concentrations of HCl, SO₂, and NO₂ at the outlet of the fixed bed were monitored by an FT-IR with a gas cell.

At a high relative humidity (19%), the HCl absorption rate and sorbent utilization were approximately the same for both hydrated lime and calcium silicate. At low relative humidity (3.5%), calcium silicate was more reactive than hydrated lime. At a concentration from 250 to 1000 ppm HCl, the rate of absorption was first order in HCl concentration with both sorbents.

When HCl and SO₂ were present simultaneously in the absence of O₂ or NO₂, the reactivity of HCl dominated that of SO₂. At the end of an experiment with calcium silicate, no SO₂ remained bound in the solids. With hydrated lime, a small amount of SO₂ would remain with the solids. With both hydrated lime and calcium silicate, the reactivity of SO₂ was increased in the presence of O₂ or NO₂. Even with increased SO₂ reactivity, the absorption of the acid gases by hydrated

lime was still dominated by HCl reactivity. On the other hand, if sufficient NO₂ were in the gas stream (≥ 50 ppm) and the SO₂/HCl ratio was high, the reacted solids contained more sulfur than chloride.

The fixed-bed experiments were modeled using a semiempirical approach based on shrinking core theory. Parameters estimated from the experiments were then used to predict sorbent performance on a bag filter. With calcium silicate at conditions of a municipal waste incinerator, $\geq 90\%$ removal of both HCl and SO₂ is possible at reasonable humidity and NO₂ concentration. At conditions of a coal-fired boiler with calcium silicate, $\geq 90\%$ HCl removal and approximately 60% SO₂ removal is possible at reasonable gas conditions. For both combustors and boilers with hydrated lime, high HCl removal levels are predicted but SO₂ removal is low ($\leq 30\%$).

Table of Contents

List of Tables	xii
List of Figures	xiii
Nomenclature.....	xvii
Chapter 1. Problem Description	1
Chapter 2. Chemistry and Literature Review	6
2.1 Chemistry.....	6
2.1.1 Reactions with Hydrated Lime.....	6
2.1.2 Slurry Reaction Producing Calcium Silicate.....	7
2.1.3 Reactions with Calcium Silicate.....	8
2.2 Literature Review	9
2.2.1 Hydrated Lime.....	9
2.2.2 Calcium Silicate Solids	13
2.2.3 Gas-Solid Reaction Modeling	16
Chapter 3. Experimental Methods	20
3.1 Experimental Apparatus	20
3.2 Experimental Procedure.....	24
3.3 Gas Phase Analysis	25
3.4 Sand and Sorbent Characterization.....	28
3.4.1 Sand	28
3.4.2 Hydrated Lime.....	28
3.4.3 Calcium Silicate	31
3.5 Typical Experimental Data	33
3.6 Experimental Reproducibility.....	35
Chapter 4. Absorption of HCl and SO ₂ by Hydrated Lime.....	38
4.1 HCl and Hydrated Lime.....	39
4.2 SO ₂ and Hydrated Lime.....	42

4.3	HCl-SO ₂ and Hydrated Lime.....	44
4.4	HCl-SO ₂ -O ₂ and Hydrated Lime.....	50
4.5	HCl-SO ₂ -NO _x -O ₂ and Hydrated Lime	52
4.6	Summary	56
Chapter 5. Absorption of HCl and SO ₂ by Calcium Silicate		57
5.1	HCl and Calcium Silicate	58
5.2	SO ₂ and Calcium Silicate	63
5.3	HCl-SO ₂ -NO _x -O ₂ and Calcium Silicate.....	64
5.3.1	Effect of O ₂	64
5.3.2	Effect of NO ₂	66
5.3.3	Effect of NO	71
5.3.4	Effect of Varying Relative Humidity	72
5.3.5	Effect of Varying Inlet SO ₂ /HCl Ratio	74
5.4	SO ₂ -NO _x -O ₂ and Calcium Silicate.....	75
5.5	Summary	78
Chapter 6. Experimental Modeling and Bag Filter Performance Predictions		80
6.1	Modeling Approach	80
6.1.1	Integral Fixed-Bed Reactor Mass Balance	80
6.1.2	Development of Flux Equation	84
6.1.3	Parameter Estimation Package	86
6.1.4	Bag Filter Performance Model	87
6.2	Modeling of HCl-Calcium Silicate	88
6.2.1	Parameter Estimation	88
6.2.2	Bag Filter Performance Projections	93
6.3	Modeling of HCl-Hydrated Lime	99
6.3.1	Parameter Estimation	99
6.3.2	Bag Filter Performance Projections	101
6.4	Modeling of HCl-SO ₂ -Calcium Silicate.....	104
6.4.1	Parameter Estimation	104
6.4.2	Bag Filter Performance Projections	111
6.5	Modeling of HCl-SO ₂ -Hydrated Lime	117

6.5.1	Parameter Estimation	117
6.5.2	Bag Filter Performance Projections	119
6.6	Summary	121
Chapter 7.	Comparison of Hydrated Lime and Calcium Silicate	123
7.1	Flue Gas Containing HCl.....	123
7.2	Flue Gas Containing HCl and SO ₂	125
7.3	Summary	127
Chapter 8.	Conclusions and Recommendations	129
8.1	Bench-Scale Results	129
8.1.1	Hydrated Lime.....	129
8.1.2	Calcium Silicate	130
8.2	Modeling and Bag Filter Performance Projections	131
8.3	Recommendations.....	132
Appendix A.	FT-IR Experimental Procedure	134
A.1	Perkin-Elmer System 2000	134
A.2	Infrared Analysis Gas Cell.....	137
Appendix B.	Sample Calculations	139
Appendix C.	Experimental Conditions and Loading Results	145
Appendix D.	Ion Chromatography Calculations	148
Appendix E.	Modeling Code	151
E.1	HCl Analysis.....	151
E.1.1	Fixed-Bed Code.....	151
E.1.2	HCl Bag Filter Code.....	158
E.2	HCl-SO ₂ Analysis.....	160
E.2.1	Fixed-Bed Code.....	160
E.2.2	HCl-SO ₂ Bag Filter Code.....	168

Appendix F. Data Archive	172
Appendix G. Speculation of Absorption Mechanism	182
Appendix H. Experimental Reproducibility	184
References	188
Vita	193

List of Tables

Table 1.1.1	Comparison of Costs for Acid Gas Control Technologies	3
Table 3.1.1	Range of Experimental Conditions	24
Table 4.0.1	Range of Conditions for Hydrated Lime Experiments	38
Table 5.0.1	Range of Conditions for Calcium Silicate Experiments	57
Table 6.2.1	Results of Parameter Estimation for HCl-Calcium Silicate System.....	90
Table 6.2.2	Results of Parameter Estimation for the Gas Cell Constant	93
Table 6.3.1	Results of Parameter Estimation for HCl-Hydrated Lime System at 9% RH.	100
Table 6.3.2	Results of Parameter Estimation for HCl-Hydrated Lime System at 19% RH.	100
Table 6.4.1	Results of Parameter Estimation for HCl-SO ₂ -Calcium Silicate System.....	107
Table 6.5.1	Results of Parameter Estimation for HCl-SO ₂ -Hydrated Lime System.....	118
Table B.1	Absorbance Values for Acid Gas Calibration	142
Table C.1	Conditions and Final Loading Results for Hydrated Lime Experiments	145
Table C.2	Conditions and Final Loading Results for Calcium Silicate Experiments	146
Table F.1	Experimental Data (in ppm) for Exp. Nos. CS18 and CS25.	172
Table H.1.1	Comparison of Parameters for Three Experiments at the Conditions of CS9.....	184

List of Figures

Figure 1.1.1 Schematic of the duct injection process.....	4
Figure 2.2.1 Utilization of hydrated lime by HCl absorption as a function of relative humidity.	10
Figure 2.2.2 Utilization of hydrated lime by HCl absorption as a function of temperature.	11
Figure 2.2.3 Removal of SO ₂ in the presence of HCl by hydrated lime in a bag filter pilot plant.	13
Figure 2.2.4 Loading of calcium silicate solids by HCl and SO ₂ as a function of approach to saturation.	15
Figure 3.1.1 Schematic with dimensions of the fixed-bed reactors used.....	21
Figure 3.1.2 Schematic of experimental fixed-bed apparatus.....	22
Figure 3.3.1 Example IR spectra of HCl, SO ₂ , and NO ₂	26
Figure 3.4.1 Pore volume distribution of hydrated lime and calcium silicate.	29
Figure 3.4.2 X-Ray diffraction patterns of hydrated lime and calcium silicate hydrate.	30
Figure 3.4.3 SEM of hydrated lime.....	31
Figure 3.4.4 SEM of calcium silicate solids.	32
Figure 3.5.1 Typical experimental data for HCl, SO ₂ , and NO ₂	34
Figure 3.6.1 Comparison of three experiments performed at the same conditions.....	36
Figure 4.1.1 Effect of relative humidity on HCl removal.	39
Figure 4.1.2 Effect of HCl concentration on HCl removal and final loading.	41
Figure 4.2.1 Effect of relative humidity on SO ₂ removal.	43
Figure 4.2.2 Effect of SO ₂ concentration on SO ₂ removal.....	44
Figure 4.3.1 Effect of HCl concentration on SO ₂ removal.	45
Figure 4.3.2 Effect of SO ₂ concentration on HCl removal.	46
Figure 4.3.3 Effect of SO ₂ /HCl feed ratio on fraction of total loading by SO ₂	47
Figure 4.3.4 Sequential absorption of SO ₂ , then HCl, then SO ₂ by hydrated lime.	48

Figure 4.3.5 Sequential absorption of HCl, then 2000 and 500 ppm SO ₂ by hydrated lime.	49
Figure 4.4.1 Effect of O ₂ and HCl concentration on SO ₂ loading.....	51
Figure 4.5.1 Effect of NO and NO ₂ on SO ₂ loading in the presence of HCl.....	53
Figure 4.5.2 Effect of O ₂ and HCl on NO ₂ loading.	55
Figure 5.1.1 Effect of relative humidity on HCl removal.	58
Figure 5.1.2 X-ray powder diffraction results on reaction products from 1.8 and 3.5% RH experiments.	60
Figure 5.1.3 Scanning Electron Microscope picture of a sample of reaction products.....	61
Figure 5.1.4 Effect of HCl concentration on HCl removal.	62
Figure 5.2.1 Effect of relative humidity on SO ₂ removal.	63
Figure 5.2.2 Effect of SO ₂ concentration on SO ₂ removal.....	64
Figure 5.3.1 Effect of O ₂ and HCl on SO ₂ loading.	65
Figure 5.3.2 Effect of NO ₂ on SO ₂ loading in the presence of HCl.	67
Figure 5.3.3 Effect of NO ₂ on HCl loading in the presence of SO ₂	68
Figure 5.3.4 Effect of O ₂ and NO ₂ on NO ₂ removal.	69
Figure 5.3.5 Effect of NO on SO ₂ loading in the presence of HCl.....	72
Figure 5.3.6 Effect of relative humidity on SO ₂ and NO ₂ loading in the presence of HCl.	73
Figure 5.3.7 Effect of HCl/SO ₂ ratio on HCl and SO ₂ Loading.....	75
Figure 5.4.1 Effect of NO ₂ on SO ₂ loading at 150 °C.....	76
Figure 5.4.2 Effect of NO ₂ on SO ₂ Loading at 90 °C.....	77
Figure 6.1.1 Schematic of fixed-bed reactor for the finite element analysis.	82
Figure 6.2.1 Best model fit using the parameters from the simultaneous regression of all HCl-calcium silicate experiments greater than 1.8% RH.	91
Figure 6.2.2 Worst model fit using the parameters from the simultaneous regression of all HCl-calcium silicate experiments greater than 1.8% RH.	92

Figure 6.2.3 Penetration of HCl as a function of relative humidity in a bag filter system using calcium silicate as the sorbent.	94
Figure 6.2.4 Penetration of HCl as a function of sorbent feed ratio in a bag filter system using calcium silicate as the sorbent.	96
Figure 6.2.5 Penetration of HCl as a function of HCl concentration in a bag filter system using calcium silicate as the sorbent.	97
Figure 6.2.6 HCl removal as a function of calcium silicate utilization at varying cycle times.	98
Figure 6.3.1 Penetration of HCl as a function of relative humidity in a bag filter system using hydrated lime as the sorbent.	102
Figure 6.3.2 Penetration of HCl as a function of HCl concentration in a bag filter system using hydrated lime as the sorbent.	103
Figure 6.3.3 HCl removal as a function of hydrated lime utilization at varying cycle times.	104
Figure 6.4.1 Typical model fit for HCl-SO ₂ absorption by calcium silicate.	108
Figure 6.4.2 Effect on penetration of varying $D_{eff,H}$ from the center to the top and bottom of the confidence interval.	109
Figure 6.4.3 Effect on penetration of varying $k_{s,S}$ from the center to the top and bottom of the confidence interval.	110
Figure 6.4.4 Penetration of HCl and SO ₂ as the inlet SO ₂ /HCl concentration ratio changes from 0.25 to 4 in a bag filter system using calcium silicate.	112
Figure 6.4.5 Penetration of HCl and SO ₂ at varying, low HCl concentration in a bag filter system using calcium silicate.	113
Figure 6.4.6 Penetration of HCl and SO ₂ at the same conditions as predicted by two different sets of parameters from Exp. Nos. CS18 and CS25 using calcium silicate.	114
Figure 6.4.7 SO ₂ removal as a function of calcium silicate utilization at varying inlet SO ₂ /HCl concentration ratios in a bag filter system.	115
Figure 6.4.8 HCl removal as a function of calcium silicate utilization at varying inlet SO ₂ /HCl concentration ratios in a bag filter system.	116

Figure 6.5.1 Penetration of HCl and SO ₂ with varying NO ₂ and O ₂ concentrations in a bag filter system using hydrated lime.....	119
Figure 6.5.2 HCl and SO ₂ removal by hydrated lime as a function of cycle time in a bag filter system.....	120
Figure 7.1.1 Comparison of HCl penetration with hydrated lime and calcium silicate.	124
Figure 7.2.1 Comparison of HCl penetration with hydrated lime and calcium silicate at coal-fired combustion flue gas conditions.....	125
Figure 7.2.2 Comparison of SO ₂ penetration with hydrated lime and calcium silicate at coal-fired combustion flue gas conditions.....	126
Figure G.1.1 Schematic of crystallization.	183
Figure H.1.1 Comparison of data from CS9(1) to a individually regressed model and to the model with all CS9 experiments regressed simultaneously.	185
Figure H.1.2 Comparison of data from CS9(2) to a individually regressed model and to the model with all CS9 experiments regressed simultaneously.	186
Figure H.1.3 Comparison of data from CS9(3) to a individually regressed model and to the model with all CS9 experiments regressed simultaneously.	187

Nomenclature

a	Sorbent Surface area Divided by Volume (m^{-1})
A_x	Cross Sectional Area of the Reactor (m^2)
c	Gas Cell Correction Factor
C_A	Concentration of A (mol/m^3)
$C_{A,L} \tau$	Outlet Concentration of A at Distance L in Fixed-Bed at Time τ (mol/m^3)
$C_A^0 \tau$	Gas Cell Concentration of A at Distance L in Fixed-Bed at Time τ (mol/m^3)
CS	Calcium Silicate
C_S	Concentration of the Sorbent (mol/m^3)
D_A	Diffusion Coefficient of Species A (m^2/s)
$D_{A,eff}$	Effective Diffusion Coefficient of Species A (m/s)
$D_{eff}, D_{eff,H}$	Effective Diffusion Coefficient for HCl Modeling (m/s)
$D_{eff,S}$	Effective Diffusion Coefficient for SO ₂ Modeling (m/s)
F_A	Flux of A ($moles/m^2/s$)
G	Objective Function
k_0	Long-Term SO ₂ Absorption Rate Constant ($mol/m^2/s$)
$k_s, k_{s,H}$	Surface First Order Rate Constant for HCl (m/s)
$k_s', k_{s,H}'$	Surface Pseud-Second Order Rate Constant for HCl ($m^4/mol/s$)
$k_{s,S}$	Surface First Order Rate Constant for SO ₂ ($m^4/mol/s$)
HL	Hydrated Lime
n_A	Moles A (mol)
$n_A \tau$	Moles A at Time τ (mol)
Q	Flowrate (m^3/s or L/min)
r	Radius of Nucleus (m)
RH	Relative Humidity
S	Surface Area
S_m	Molar Surface Area (m^2/mol)
t	Time (s)

t^*	Maximum Bag Filter Cycle Time (min)
W	Mechanical Work for Nucleation (J)
x	Conversion
x_T	Termination Conversion
x_i^*	Mole Fraction of i in the Gas Cylinder (ppm)
$x_{i,in}$	Mole Fraction of i in the Reactor Inlet Gas (ppm)
z	Distance in Fixed Bed (m)
α	Stoichiometric Factor (mol/mol)
ΔG	Free Energy (J)
ΔG_c	Free Energy of Reaction (J/mol)
δ	Product Layer Thickness (m)
δ_o	Characteristic Particle/Grain Thickness (m)
ρ_p	Reaction Product Molar Density (mol/m ³)
Ω	Vector of Regressed Constants

Chapter 1. Problem Description

Because of the passage of the Clean Air Act Amendments in 1990, many industrial processes must reduce acid gas emissions, including those of HCl and SO₂. These two gases are emitted together primarily in municipal waste combustors (MWC), hazardous waste incinerators (HWI), and coal-fired power plants. Published regulations (USEPA, 1995) require new MWCs and large MWCs undergoing major modifications to remove 95% of their HCl and 75% of their SO₂ emissions. Medical waste incinerators, a common HWI, must remove 99% of their HCl emissions and reduce the SO₂ concentration to 55 ppm (USEPA, 1997). New coal-fired power plants and those undergoing major modifications must report HCl releases if they exceed ten tons per year. The Acid Rain Program of the Clean Air Act Amendments (Title IV) regulates SO₂ emissions from coal-fired boilers. Title IV is unique in that it puts an overall limit on SO₂ emissions and allows for the buying and selling of emission allowances.

To meet emission limits, several different control strategies are employed. The most common, spray dryer absorption (SDA), neutralizes acid gas by spraying a water-based alkaline slurry into the flue gas. The slurry is atomized and most of the water evaporates, leaving a moist powder. Advantages of SDA over wet systems are that no wastewater is generated, there is considerably less potential for corrosion, and there is less condensation in the stack (Holzman and Atkins, 1988). Another alternative, wet scrubbing, employs both a prescrubber and a scrubber. The prescrubber is an open spray that cools the gas and removes much of the HCl and HF (Donnelly, 1989). The scrubber, then, removes the remaining acid gas. The primary advantage of wet scrubbing is a 30 to 50% reduction in reagent costs over the best dry scrubbing technology. A third control strategy is furnace injection. With this technology, a dry sorbent is injected into the furnace or post-furnace region. The major advantage of furnace injection is its simplicity; no additional reactors or complex reagent preparation is required.

A fourth control strategy is the injection of a dry, alkaline powder into the flue duct leading up to the particulate control device. This approach is

particularly effective if a fabric filter is in place for particulate control. Flue gas containing HCl, SO₂, NO, NO₂, particulates, and other contaminants along with O₂ approach the end of the flue duct with a moderate water vapor content (5-15 vol%) and elevated temperature (150-300 °C) (White and Vancil, 1989). Water is sprayed into the flue gas dropping the temperature (to 60-150 °C), increasing the water content (to 15-35 vol%), and increasing the relative humidity (to 10-60% RH). Once the water has been vaporized, the sorbent is injected into the duct pneumatically. Some of the acid gas will react in the flue duct, but most will react on the surface of the bag filter. The baghouse is a collection of bags similar to those in a vacuum cleaner, hung from a manifold in parallel. Particulates, including fly ash and sorbent particles, collect on the surface of the bags. Once the pressure drop through the filter cake becomes too large, the bag is cleaned by a pulse of air from the reverse side of the bag or is simply shaken.

Compared to spray dryer absorption, dry sorbent injection has a simpler alkaline addition system, does not have problems with the plugging or erosion of nozzles, and is an easier system to retrofit. In general, the advantages of dry sorbent injection over wet scrubbing are the same as those discussed for spray dryer absorption over wet scrubbing. Compared to furnace injection, dry sorbent injection has lower reagent costs due to more efficient utilization of the sorbent. Though dry sorbent injection utilizes the alkaline reagent more efficiently than furnace injection, the chief disadvantage of dry sorbent injection compared to spray dryer absorption and wet scrubbing is its reduced utilization of the sorbent. Costs for the four competing technologies as applied to municipal waste combustion are shown in Table 1.1.1. Details of the calculations for the economic analysis can be found in Holzman and Atkins (1988).

Table 1.1.1 Comparison of Costs for Acid Gas Control Technologies

	Dry Sorbent Injection	Spray Dryer Absorption	Wet Scrubbing	Furnace Injection
\$/Ton Waste Burned [†]	11.60	11.60	20.60	7.00
\$/lb. Acid Gas Removed [†]	0.68	0.68	1.14	0.62

[†]Costs are in 1988 U.S. dollars.

Source: Holzman and Atkins (1988)

The most common sorbent used for dry sorbent injection is hydrated lime, which consists primarily of calcium hydroxide. If a sorbent were developed that provided better utilization than hydrated lime, the economics of dry sorbent injection may be favored over the alternate control technologies for flue gas cleaning. Studies in recent years have produced an effective acid gas sorbent by slurring hydrated lime, a source of silica such as glass or fly ash, and gypsum (Arthur, 1998; Nelli, 1997). After dewatering the slurry, the resulting calcium silicate solid (known as ADVACATE, ADVAnced siliCATE) has a high surface area and has been shown to be more reactive with SO₂ than hydrated lime. A schematic of the dry sorbent injection process that employs the calcium silicate solids is shown in Figure 1.1. The sorbent can be made either on-site or at a central facility and then transported to the site.

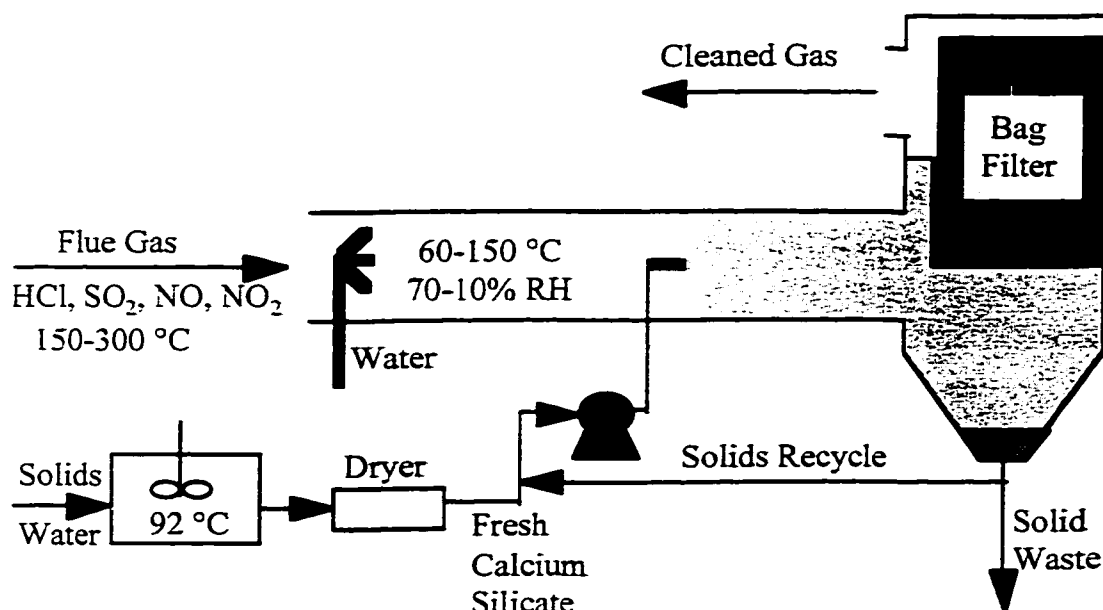


Figure 1.1.1 Schematic of the duct injection process

The objective of this work was to determine whether calcium silicate solids are a suitable replacement for hydrated lime using dry sorbent injection technology with flue gas from municipal waste combustors and coal-fired power plants. A secondary objective was to gain an understanding of and quantify the interactions on alkaline reagents between HCl, SO₂, NO, NO₂, O₂, and water vapor. This understanding then can be applied to systems utilizing not only dry sorbent injection but also spray dryer absorption and perhaps even furnace injection technologies. To reach these objectives, a two phase approach was used. During the first phase, bench-scale absorption data were obtained at various gas conditions with hydrated lime and a representative calcium silicate as the sorbent. Phase two of this study involved modeling of the bench-scale data using a parameter estimation package. The parameters estimated were then used to predict the performance of HCl and SO₂ removal in a bag filter system employing either hydrated lime or calcium silicate solids.

The next chapter gives an overview of the relevant literature that addresses the absorption of HCl and SO₂ by calcium-based sorbents. Chapter 3 details the experimental methods used to obtain acid gas absorption data. Chapters 4 and 5 discuss the results of the bench-scale experiments with hydrated lime and calcium silicate, respectively. Modeling work and bag filter performance projections are presented in Chapter 6. Chapter 7 directly compares performance predictions of calcium silicate to hydrated lime. Conclusions and recommendations are discussed in the final chapter.

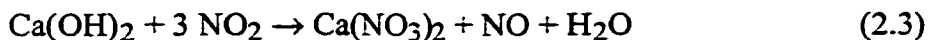
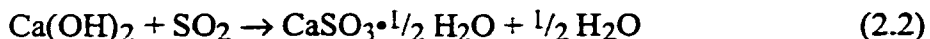
Chapter 2. Chemistry and Literature Review

With both hydrated lime and calcium silicate, simple acid-base reactions describe the absorption of HCl and SO₂ in the absence of O₂ and NO₂. The presence of O₂ and NO₂ promote SO₂ absorption because of the oxidation of sulfur. Other researchers have conducted studies of the absorption of HCl by hydrated lime. Few works have sought to understand the interactions between HCl and SO₂ in the presence of O₂ and NO₂. Even fewer studies have conducted research on the absorption of HCl by calcium silicate. This chapter lays the groundwork for the dissertation by detailing the reaction chemistry and discussing HCl and SO₂ absorption results described in the literature.

2.1 CHEMISTRY

2.1.1 Reactions with Hydrated Lime

The absorption of HCl, SO₂, and NO₂ can be achieved by irreversible acid-base reactions:



Calculations based on thermodynamic data from Sinke et al. (1985) and Garvin et al. (1987) suggested that calcium chloride undergoes a phase transition at 120 °C when the relative humidity (RH) is 2.2%. Above 2.2% RH, the dihydrate is stable; below, the monohydrate is the stable calcium chloride salt. A more detailed discussion of the phase transition calculation is given in Section 5.1. At the temperature and relative humidity range investigated, the most likely solid phase for calcium sulfite was the hemihydrate (Jones et al., 1976).

In this study, it was discovered that when CaSO₃•¹/₂ H₂O is exposed to HCl vapor, SO₂ is evolved and CaCl₂•2 H₂O is formed. Also, when CaCl₂•2

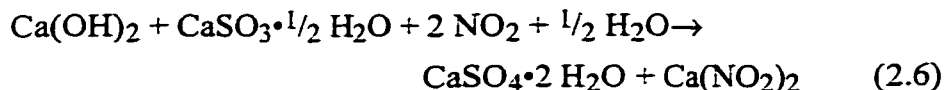
H₂O is exposed to SO₂ in the absence of HCl, HCl is released by the solids and CaSO₃•¹/₂ H₂O is formed. This pseudo-equilibrium reaction is given by Reaction 2.4:



When oxygen is present in the gas phase, S(IV) is oxidized to S(VI). According to Jones et al. (1976), the dihydrate of calcium sulfate (gypsum) converts to a hemihydrate between 120 and 140 °C. Because this study was performed at the lower border of the temperature range, it was assumed that S(VI) exists as gypsum:

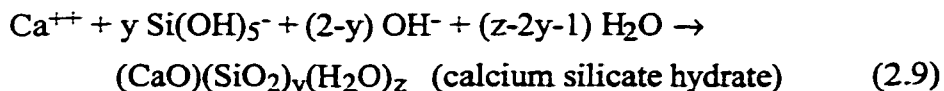
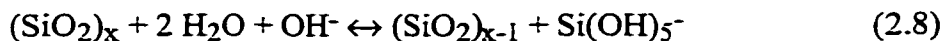


NO₂ is expected to act as a catalyst promoting S(IV) oxidation by Reaction 5 (Shen, 1997). NO₂ may also participate directly in S(IV) oxidation:



2.1.2 Slurry Reaction Producing Calcium Silicate

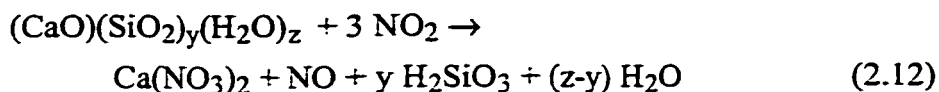
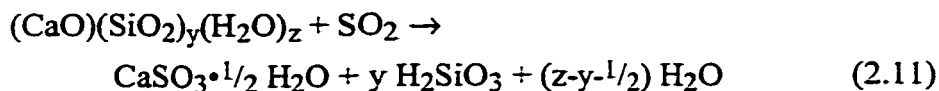
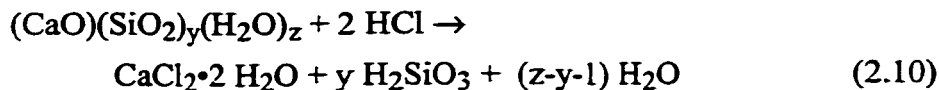
The production of calcium silicate solids from recycled glass is discussed at length by Arthur (1998). Calcium silicate was formed by the slurring of hydrated lime, pulverized silica glass, and gypsum. Reactions 2.7-9 describe the process:



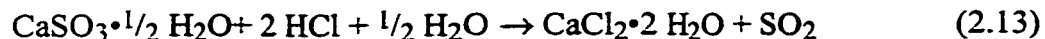
First, the dissolution of lime takes place by Reaction 2.7. The resulting increase in pH causes the accelerated breakdown of the silica matrix in the glass. Once the silica is dissolved, calcium silicate is formed and precipitates on the surface of the glass. The solids have a high-surface area and are amorphous. The value of y for the calcium silicate solids used in this study was 0.67 (Arthur, 1998). More specifics about the calcium silicate used as well as an X-ray diffraction pattern and scanning electron micrograph are given in Section 3.4.3.

2.1.3 Reactions with Calcium Silicate

Calcium silicate absorption closely parallels hydrated lime absorption. Reactions with HCl, SO₂, and NO₂ are shown in Reactions 2.10-12:

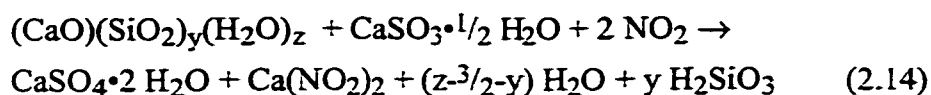


When calcium sulfite is formed through Reaction 2.11 and then exposed to HCl, SO₂ is evolved in favor of calcium chloride. Unlike with hydrated lime, no sulfur remains with the reacted solids; HCl vapor drives off all of the SO₂ that was bound to the solids. Therefore, this reaction is not shown in Reaction 2.13 as an equilibrium reaction:



Reaction 2.13 is valid when SO₂ was absorbed by calcium silicate solids. Reaction 2.4 is appropriate when hydrated lime was used to absorb HCl. It is unclear whether the reversibility with hydrated lime as contrasted to the irreversibility with calcium silicate is due to chemical or mass transfer differences.

As with hydrated lime, S(IV) from the absorption of SO₂ by calcium silicate is oxidized with O₂ by Reaction 2.5. As with hydrated lime, NO₂ may catalyze the oxidation of S(IV) by Reaction 2.5. The oxidation of S(IV) by NO₂ is similar with calcium silicate as with hydrated lime:



2.2 LITERATURE REVIEW

2.2.1 Hydrated Lime

The most comprehensive study of the absorption of HCl by hydrated lime was conducted by Pakrasi (1992). He found that the capacity of hydrated lime for absorption of HCl, like absorption of SO₂, increases with increasing relative humidity. This trend is seen in the data presented in Figure 2.2.1. Other researchers have observed the same influence of relative humidity on HCl absorption (Jozewicz et al., 1990; Fonseca et al., 1998; Weinell et al., 1992). Without water vapor, less than 5% of the hydrated lime was utilized after five minutes reaction time. Nearly complete utilization of the sorbent was found at 44% RH after five minutes reaction time.

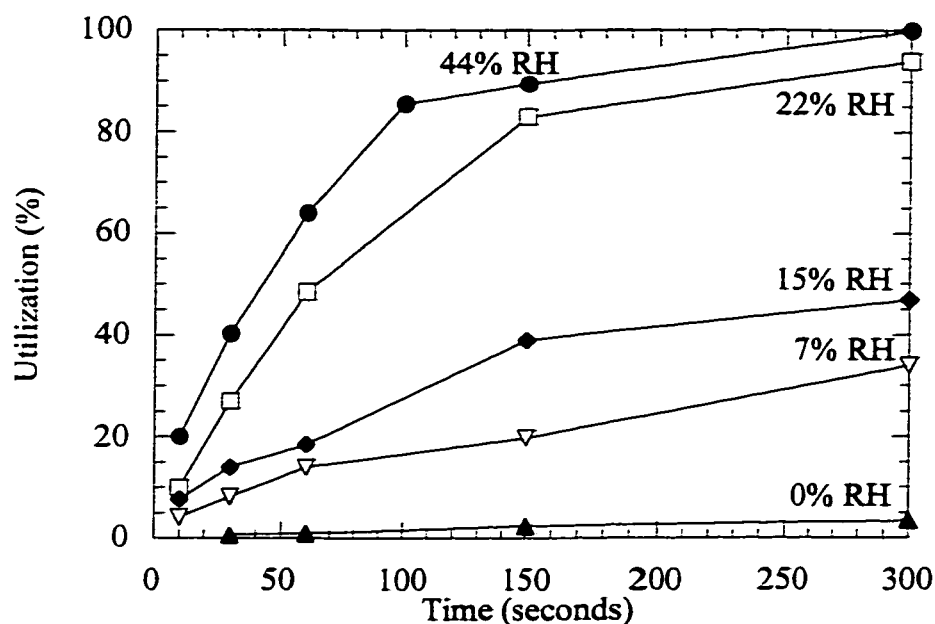


Figure 2.2.1 Utilization of hydrated lime by HCl absorption as a function of relative humidity.

Experiments conducted in a fixed-bed reactor at 79 °C with 1000 ppm HCl and 25 mg hydrated lime; the flowrate was not reported. Data taken from Pakrasi (1992).

Pakrasi (1992) also found that when relative humidity was held constant, an increase in gas temperature from 80 to 107 °C had little impact on the rate of HCl absorption by hydrated lime. The data shown in Figure 2.2.2 supported this conclusion.

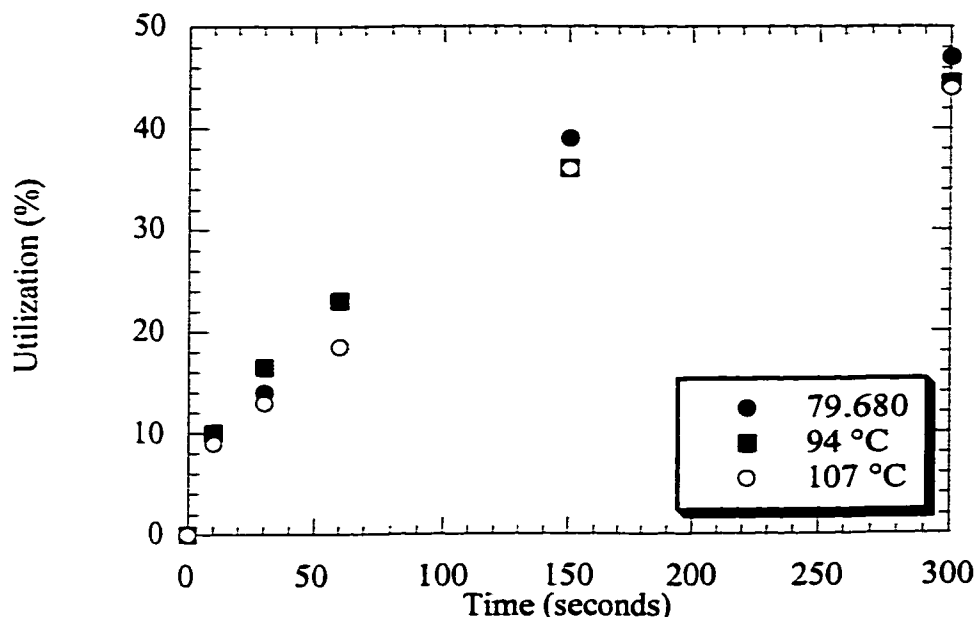


Figure 2.2.2 Utilization of hydrated lime by HCl absorption as a function of temperature.

Experiments conducted in a fixed-bed reactor at 15% RH with 1000 ppm HCl and 25 mg hydrated lime; the flowrate was not reported. Data taken from Pakrasi (1992).

Little work has been performed to understand the effect of changing HCl concentration on absorption in the presence of water vapor. Pakrasi (1992) conducted experiments where the absorption of different concentrations of HCl by hydrated lime were observed for an experimental time of five minutes. The conversion of a fixed mass of sorbent to calcium chloride took place more rapidly with greater HCl concentration. Barring zeroth order behavior, this was expected. With increased gas concentration and fixed sorbent mass, conversion of the solids took place more rapidly at increased concentration. Other studies conducted at various temperatures with calcium-based sorbents (Daoudi and Walters, 1991;

Gullett et al., 1992; Fonseca et al., 1998; Duo et al., 1995) have had success modeling the rate of absorption with hydrated lime as first order in HCl concentration.

Few studies have investigated the interactions between HCl and SO₂ when the acid gases were absorbed by hydrated lime. Chang et al. (1989) found that at low HCl concentration, SO₂ removal was improved with increasing HCl concentration (Figure 2.2.3). They suggested that the deliquescent nature of calcium chloride may have improved SO₂ absorption. At high HCl concentration, SO₂ removal decreased with increasing HCl concentration. This was probably due to the rapid accumulation of a calcium chloride product layer on the surface of the sorbent that blinded the hydrated lime to SO₂ absorption. Some researchers (Matsukata et al., 1996; Jozewicz et al., 1990) have found that increased HCl concentration increased SO₂ absorption rates. Each of those two studies have also shown that the presence of SO₂ has little effect on HCl absorption. Research conducted with a bench-scale spray dryer absorber (Yuan and Fong, 1992) did not confirm that increasing HCl concentration increased SO₂ absorption rates.

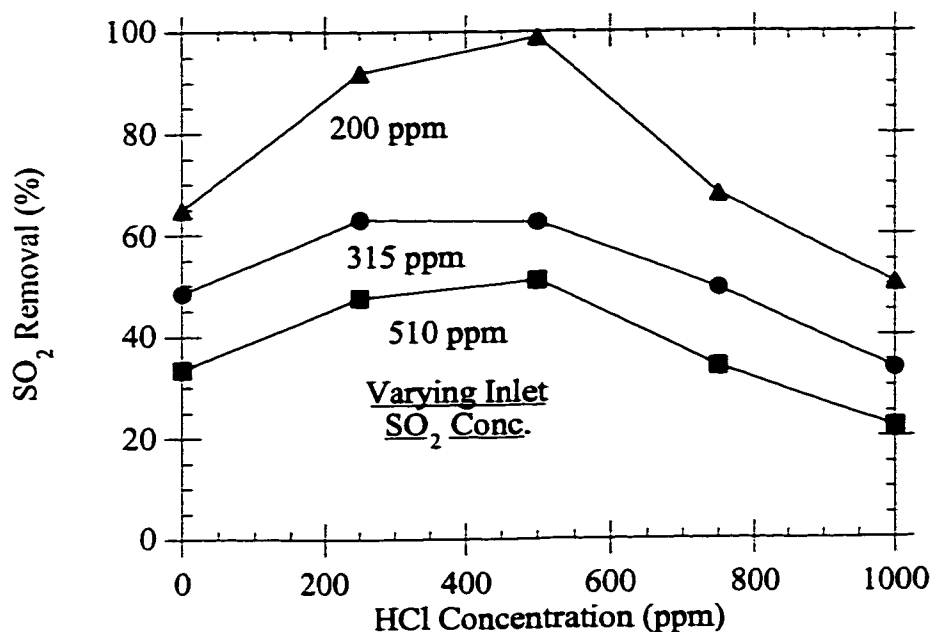


Figure 2.2.3 Removal of SO₂ in the presence of HCl by hydrated lime in a bag filter pilot plant.

Study conducted at 23% RH and 77 °C with an hydrated lime sorbent feed ratio of 3.0. For all data points, $\geq 99\%$ removal of HCl was obtained. Data taken from Chang et al. (1989).

Studies that did not include HCl have investigated the effect of O₂ and NO₂ on SO₂ absorption (Nelli and Rochelle, 1996; Chu and Rochelle, 1989; Littlejohn et al., 1993). These studies have indicated that the absorption rate of SO₂ by hydrated lime increased with the addition of O₂ and/or NO₂ in the gas phase. The reaction chemistry for S(IV) oxidation by O₂ and NO₂ is detailed earlier in this chapter.

2.2.2 Calcium Silicate Solids

The preparation of calcium silicate solids for SO₂ absorption has been studied extensively (Jozewicz and Rochelle, 1986; Fernández et al., 1997; Kind et

al., 1994; Jozewicz et al., 1988). These studies have shown that when the slurrying conditions are properly controlled, the resulting calcium silicate sorbent is more reactive with SO_2 than hydrated lime. Work by Nelli and Rochelle (1996) has shown that the absorption of SO_2 by calcium silicate solids can be increased by the addition of NO_2 to the feed gas mixture.

Considerably less research has been conducted to quantify the reactivity of HCl with calcium silicate. Cain (1993) studied the preparation of calcium silicate solids from various silica sources, including fly ash, amorphous silica, and crystalline silica. The slurry was 6 wt% solids and was maintained at 90°C . To measure the performance of the solids prepared, she reacted the sorbent at 2.1% RH and 149°C with 1000 ppm HCl in a fixed-bed reactor. At these conditions, a calcium silicate sorbent prepared from a 8/1 fly ash to hydrated lime mass ratio and a six hour slurry time exhibited a utilization of 34% after five minutes experimental time. This is an increase from the 18% hydrated lime utilization determined at the same experimental conditions (Pakrasi, 1992). A similar study by Jozewicz et al. (1991) claimed that fly ash-derived calcium silicate solids were "up to three times more reactive with HCl [than] hydrated lime." However, detailed results are not given to support their claim.

Another study (Jozewicz et al., 1990) researched the simultaneous absorption of HCl and SO_2 by calcium silicate solids. Results from that work are shown in Figure 2.2.4. At approaches to saturation of 20 to 40°C with 1000 ppm HCl and 500 ppm SO_2 , they found that after one hour the SO_2 loading of calcium silicate was only slightly greater than the loading of hydrated lime. On the other hand, the loading of HCl was almost double that of hydrated lime. Both HCl and SO_2 exhibited an increase in loading with a decrease in approach to saturation (or an increase in relative humidity).

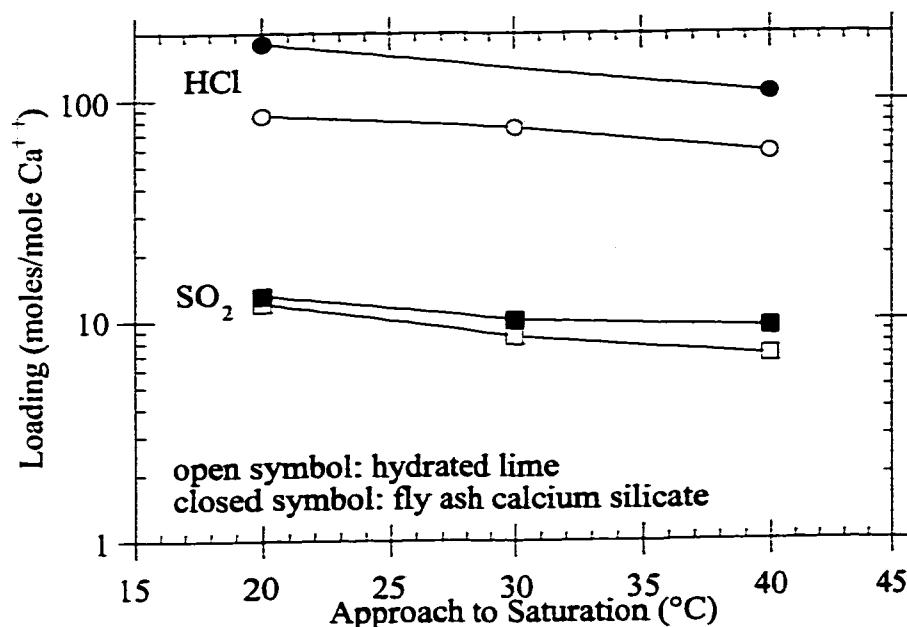


Figure 2.2.4 Loading of calcium silicate solids by HCl and SO₂ as a function of approach to saturation.

Experiments conducted in a fixed bed for one hour with a fixed water vapor feed rate (0.1 g H₂O/g dry gas) and varying temperature. The inlet gas containing 1000 ppm HCl and 500 ppm SO₂ contacted 1 g sorbent. The fly ash calcium silicate was produced at 90 °C with a fly ash to hydrated lime mass ratio of 10:1. Data taken from Jozewicz et al. (1990).

The discussion from this section has included an overview of the information found in the literature for the absorption of HCl by hydrated lime. This reaction has been studied thoroughly, especially by Pakrasi (1992). However, the absorption of HCl in the presence of SO₂ much less O₂ and NO₂ has seen only limited attention. The same can be said for the absorption of HCl by calcium silicate solids. This study attempted to fill in the gaps in

understanding for the multi-component hydrated lime system and the calcium silicate system. Results are discussed in Chapters 4 through 7.

2.2.3 Gas-Solid Reaction Modeling

The most common tool for modeling noncatalytic gas-solid reactions is the shrinking core model (Levenspiel, 1962; Szekeley et al., 1976). Many studies have used this approach to more thoroughly understand laboratory data (Gullett et al., 1992; Wang et al., 1996; Pakrasi, 1992). The theory assumes that the absorption rate of an acid gas A, is limited by a series of mass transfer steps:

1. As gas A approaches a single sorbent particle, it must diffuse from the bulk of the gas through a boundary layer to the external surface of the particle.
2. Assuming the particle is nonporous, the next resistance to reaction is the diffusion through any non-reactive product layer that has formed which covered the surface of the reactive core of the particle. The diffusing species through the product layer can be the gas, the solid, or a combination of both species.
3. After the reacting species have diffused to meet each other, the rate of absorption is limited by the reaction rate as dictated by kinetics.

In general, the rate of absorption is not limited by gas-film resistance. Calculations by Nelli (1997) for similar sorbents and experimental conditions supported this hypothesis. With fresh sorbent, the rate of absorption is limited only by the reaction rate. However, as the reaction of a given particle proceeds, the product layer thickness increases as the reactive core of the particle shrinks. The absorption rate of gas A falls to zero when there is no more reactive core remaining. Assuming that first order kinetics and diffusion through the product layer are the rate-limiting steps, the flux of A to a sorbent particle is described by Equation 2.1:

$$F_A = \frac{C_A}{\frac{1}{k_s} + \frac{\delta}{D_A}} \quad (2.1)$$

where k_s is the first order surface rate constant, δ is the product layer thickness, and D_A is the diffusion coefficient of the diffusing species through the product layer. Equation 2.1 also assumes planar geometry for the sake of simplicity.

A modification to the shrinking core model, called the grain model, has allowed for the application of shrinking core theory to porous particles (Szekely et al., 1976; Fonseca et al., 1998; Dam-Johansen et al., 1991). Grain theory states that a porous sorbent particle is comprised of smaller, nonporous grains of uniform size. As gas A reacts with the sorbent, each grain undergoes a chemical conversion described by shrinking core theory. Beside the three resistances described by the shrinking core theory, an extra resistance is introduced. After approaching the external surface of the particle, gas A must diffuse through the pores of the particle before reaching the product layer.

The grain model has been modified to take into account the fact that reaction products may have a greater molar volume than the sorbent (Szekely et al., 1976; Wang et al., 1996; Gullett et al., 1992). The reaction products of HCl and SO₂ absorption in this study -- CaCl₂•2 H₂O, CaSO₃•¹/₂ H₂O and CaSO₄•2 H₂O -- have larger pore volumes than hydrated lime (mostly Ca(OH)₂). Consequently, when these acid gases react with a grain of hydrated lime, the grain grows in size. The thickness of the product layer grows more rapidly when the reaction product has a large pore volume. Also, as the grains grow pores may become plugged.

As alkaline grains and particles react with acid gases, most researchers have found that the rate of absorption is limited primarily by product layer diffusion. Consequently, several researchers have studied this diffusion step in detail (Borgwardt et al., 1987; Bhatia and Perlmutter, 1981; Hsia et al., 1993). They found that diffusion coefficients predicted by the shrinking core or grain theories were on the order of solid state diffusion, 10⁻¹² to 10⁻¹⁴ m²/s. When SO₂ was absorbed by calcium-based sorbents, these researchers concluded that the diffusing species was the calcium ion. Hsia et al. (1993) employed platinum as a tracer to reach this conclusion. Borgwardt et al. (1987) concluded Ca⁺² was the

diffusing species by varying the impurities in the sorbent. With increasing impurities in the crystalline structure of the sorbent, an increase in regressed diffusion coefficients was observed.

The major shortcoming with the shrinking core and grain theories as stated is that both predict that the sorbent is eventually completely converted to the product. Many of the studies already discussed have demonstrated that even if the solids are exposed to HCl or SO₂ for extended periods of time, a fraction of the sorbent does not react. Simons and Garman (1986) have suggested that pore plugging prevented H₂S and SO₂ from contacting all of the sorbent, CaO. Using BET surface area data for reacted solids, they argued that deactivation of the sorbent was due to the plugging of small pores.

While Simons and Garman (1986) have proposed an explanation of why sorbent particles are not completely utilized, the role of relative humidity has not been incorporated into their theory. It has been seen throughout the literature that an increase in relative humidity increases acid gas reaction rates and calcium-based sorbent utilization. Neither shrinking core nor grain theories suggests that gas absorption is related to relative humidity. Garea et al. (1997) and Irabien et al. (1992) have studied the absorption of SO₂ by fly ash calcium silicate and hydrated lime, respectively. They concluded that the rate limiting step is the adsorption of SO₂ on the surface of the sorbent. The presence of water vapor on the surface of the solid changed the activation energy and heat of adsorption.

Another proposed model for acid gas absorption by calcium-based sorbents is given in Duo et al. (1994) and Duo et al. (1995). They point out that when HCl is absorbed by hydrated lime, the calcium chloride product has a greater molar volume than hydrated lime. The product layer grows nonuniformly by nucleation and crystallization of calcium chloride on the surface of the sorbent. As a nucleus is formed, it encounters mechanical resistance from the surrounding sorbent solids. To nucleate successfully, it must fracture the surrounding solids to allow for additional crystal growth and HCl absorption. When the mechanical energy required for fracture is too large, the sorbent does not nucleate. In the absence of nucleation, calcium chloride blankets the surface of the sorbent as it

precipitates and deactivates the sorbent. As long as the free energy for nucleation is greater than zero, HCl absorption will take place. The free energy equation summing surface energy, reaction energy, and mechanical energy for a spherical nucleus is shown in Equation 2.2:

$$\Delta G = 4\pi r^2 \sigma + \frac{4}{3}\pi r^3 \rho_p \Delta G_c + W \quad (2.2)$$

where ΔG is free energy, r is the radius of the nucleus, σ is the specific surface energy of the product, ρ_p is the molar density of the product, ΔG_c is the free energy due to chemical reaction, and W is the mechanical work from nucleation. Duo et al. (1994) suggest that there is an optimal range of ΔG_c , perhaps between -50 and -70 kJ/mol, that allows for rapid absorption of an acid gas by hydrated lime. When water vapor is involved in acid gas absorption reaction chemistry, its concentration will influence the value of ΔG_c . It is this influence on ΔG_c that may describe the role of relative humidity in acid gas absorption systems.

All of the discussion in this section has concerned the absorption of a single acid gas. No studies have been found in the literature that model rigorously the simultaneous absorption of HCl and SO₂.

Chapter 3. Experimental Methods

The foundation of the experimental work in this study is a bench-scale, fixed-bed reactor. This reactor and the analytical method employed are discussed in this chapter. A description of the sorbents used, the experimental procedure, typical data, and a discussion of the reproducibility of the data are also addressed.

3.1 EXPERIMENTAL APPARATUS

The nucleus of the apparatus was a Pyrex® glass fixed-bed reactor with a extra coarse frit near the reactor outlet. Two reactors were used, one for hydrated lime and the other for calcium silicate experiments. Because a greater mass of sorbent was used for calcium silicate, the reactor for those experiments was larger. A schematic with the dimensions of the reactor is shown in Figure 3.1.1.

A schematic of the rest of the experimental system used is shown in Figure 3.1.2. The sorbent was dispersed in quartz sand to prevent channeling of the gas and agglomeration of the solids. For hydrated lime, the mass ratio of sand to sorbent was 100. Because dispersing calcium silicate uniformly was more difficult, the mass ratio used was 200. In general, the pressure drop through the reactor (solids + frit) was less than 1 psi. The reactor was suspended in a fluidized sand (alumina) bath (Tecam, Model SBL-2D) that was usually maintained at 120 °C.

HCl, SO₂, NO₂, and NO were stored as low concentration (≤ 1 vol%) blends in nitrogen. All gases but NO₂ are known to be stable in nitrogen. A blend of NO₂ and N₂ will cause a low level of NO formation. Tests on the NO₂ cylinder by Dutchuk (1999) indicated that less than 0.1% of the NO_x was NO. When air was used as part of the simulated flue gas mixture, house air was filtered through two stainless steel, 0.5 μ m, in-line filters configured in series. All of the gases but HCl were fed through Brooks mass flow controllers (Models 5850 and 5850E). Ranges of the flow controllers varied from 0.01 to 2 SLPM (standard conditions: 21.1°C and 1 atm).

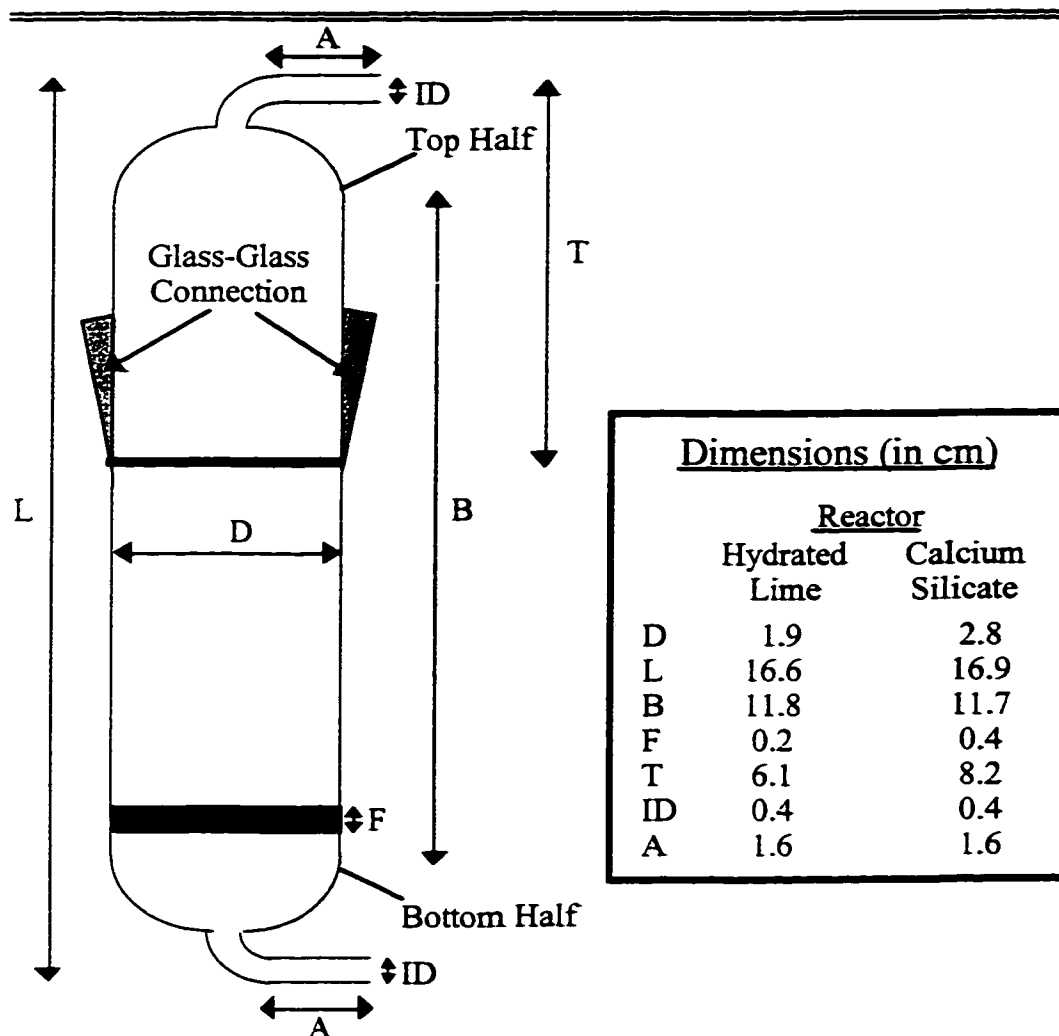


Figure 3.1.1 Schematic with dimensions of the fixed-bed reactors used.

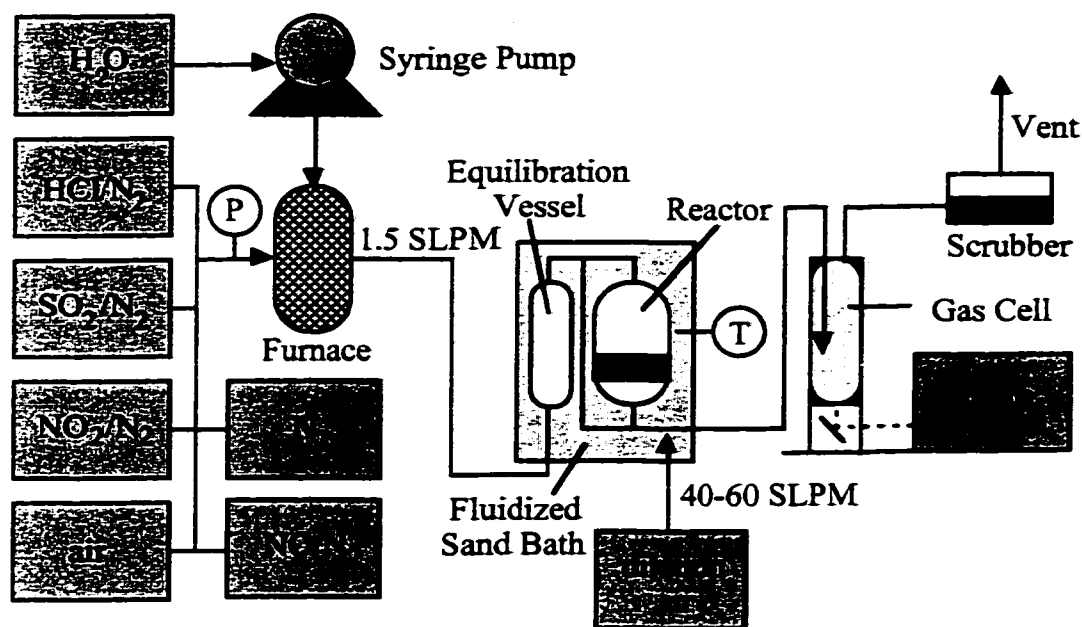


Figure 3.1.2 Schematic of experimental fixed-bed apparatus.

There were considerable difficulties with the introduction of HCl to the system. Early attempts to use Brooks controllers to add HCl to the gas mixture resulted in corroded controllers. Corrosion took place even when care was taken to purge the HCl-wetted lines with nitrogen after an experiment. Consequently, a rotameter with Teflon® fittings at the inlet and outlet was used (Matheson, Model E1G-A101-E302). The rotameter tube was made of borosilicate glass and contained a sapphire float. The maximum flowrate with the float used was 0.54 SLPM. Corrosion problems elsewhere in the apparatus were avoided by ensuring that surfaces that were wetted with high concentration HCl (≥ 50 ppm) were constructed of either TFE or PFA (a perfluoroalkoxy polymer).

The second major experimental problem was determining the HCl concentration in the gas cylinders. Cylinders were ordered for 5000 ppm HCl and delivered, as measured by the manufacturer, within 5% of the ordered concentration. Initially, the HCl concentration supplied by the manufacturer was

used in mass balance calculations. Later, it was determined that a more accurate concentration was needed for the mass balances. A method was developed where HCl from the gas cylinder at a known flowrate was sparged into a 4 L flask. The gas outlet from the flask was monitored by IR to ensure HCl absorption was complete. The change in conductivity with respect to time was measured with a conductance meter (Yellow Springs Instrument Co., Model 32). Aqueous HCl concentration was confirmed independently by titration with NaOH and an ion selective electrode (Fisher Scientific, Catalog Number 13-620-518). The method for determining gas cylinder HCl concentration was accurate but not precise. The gas cylinder concentration for all the experiments presented in this work was 5404 (± 222.5) ppm HCl.

As the gases from the cylinders were being blended, deionized water was fed through a syringe pump (Harvard Apparatus, Model 908) to a furnace that was held at approximately 300 °C. The water was vaporized in a helical glass tube suspended in the furnace and was mixed with the gas from the cylinders. The simulated flue gas exited the furnace and was sent to a 0.8 L glass equilibration vessel that was submerged in the sand bath. The purpose of the vessel was to ensure the gas was at the bath temperature and to dampen out fluctuations caused by the evaporation of water in the furnace. After leaving the glass vessel, the gas was sent to the reactor. The reactor outlet was diluted heavily -- by a factor of 25 to 50 -- with house air. The purpose of the dilution was twofold. By diluting, the water vapor concentration was dropped below its dew point at room temperature. Dilution also reduced corrosion by HCl in the gas cell. Oil particulates in the house air line were partially removed with a stainless steel, 0.5 μm , in-line filter. The flowrate of the dilution air was calibrated approximately with the pressure of the flue gas at the furnace inlet using a high air flow rotameter (Gilmont, F1760). As the dilution flowrate increased, the pressure of the flue gas at the furnace inlet also increased.

Once the reactor outlet was diluted, it left the sand bath and was sent to the gas cell (Infrared Analysis, Model G-5-22-V-AU). The gas cell was mounted vertically on a FT-IR (Perkin-Elmer, System 2000). The cell was 13 cm in

diameter, 56 cm long, had a volume of 7.4 L and an equivalent pathlength of 24 meters. A gold-plated, square mirror sat at the bottom and two gold-plated, semi-circular mirrors were suspended at the top of the gas cell. The mirrors at the top were adjusted for alignment and pathlength. A laser (Uniphase, Model 1108) and power source (Uniphase, Model 1205-1) were used as a guide for adjusting for proper IR alignment and pathlength. In general, the signal to noise ratio for the IR was maximized with increased pathlength. Once the gas was analyzed by the IR in the gas cell, it was sent to a liquid scrubber maintained at a pH of approximately 12.5 and then vented. The range of conditions studied is shown in Table 3.1.1.

Table 3.1.1 Range of Experimental Conditions

Variable	Range
Relative Humidity	0-19% RH
HCl Concentration	0-3500 ppm
SO ₂ Concentration	0-2000 ppm
NO ₂ Concentration	0-150 ppm
O ₂ Concentration	0-5.5%
NO Concentration	0-150 ppm
Temperature	90-150 °C
Sorbent Loading	18-72 mg
Flowrate	0.65-1.5 SLPM

3.2 EXPERIMENTAL PROCEDURE

The first step for each experiment was to weigh out the proper amount of sorbent and sand. The sorbent and sand were mixed in a small beaker and poured into the reactor. The reactor was then submerged in the sand bath. Extreme care was required while placing the reactor in the sand bath so the reactor outlet did not snap. The sand bath was then brought up to the experimental temperature. A gas stream of water vapor and nitrogen at 1.5 SLPM was sent through the system, bypassing the reactor for about 30 minutes. After this time, a background scan was made and the response of the IR was monitored for 10 minutes. Assuming the apparatus was behaving well, the moist nitrogen gas was directed to the

reactor so that the solids could adsorb water in accordance with the isotherm at the appropriate relative humidity.

Once this had taken place, flow was directed to bypass the reactor again. The gases -- HCl, SO₂, NO₂, O₂, and NO -- were introduced into the gas stream. The system was allowed to reach steady-state over an extended period of time. This time ranged from 20 minutes when no HCl was present in the system to 120 minutes when HCl was present at low concentrations and high humidity. When long experiments were anticipated, the water syringe was refilled during this period of time. Once steady-state was reached, the simulated flue gas was redirected from the bypass loop to the reactor. After allowing the solids to react until absorption rates dropped to zero, flow was directed again to the bypass loop. This last step allowed for an estimation of drift over the course of the experiment. After about 10 minutes, the check for drift was completed and acid gas flowrates were halted. The apparatus was then purged with nitrogen to prevent corrosion.

3.3 GAS PHASE ANALYSIS

Detailed instructions for using the FT-IR are provided in Appendix A. At a resolution of 8 cm⁻¹, the IR generated a full spectrum from 6500 to 500 cm⁻¹ every three seconds. Five spectra were averaged over fifteen seconds to produce one value for absorbance. The data point was reported at the time when the last of the five averaged scans was taken. Averaging five spectra was the product of a tradeoff between precise, time-resolved data (less averaging) and reduced noise (more averaging). Example spectra for HCl, SO₂, and NO₂ are shown in Figure 3.3.1.

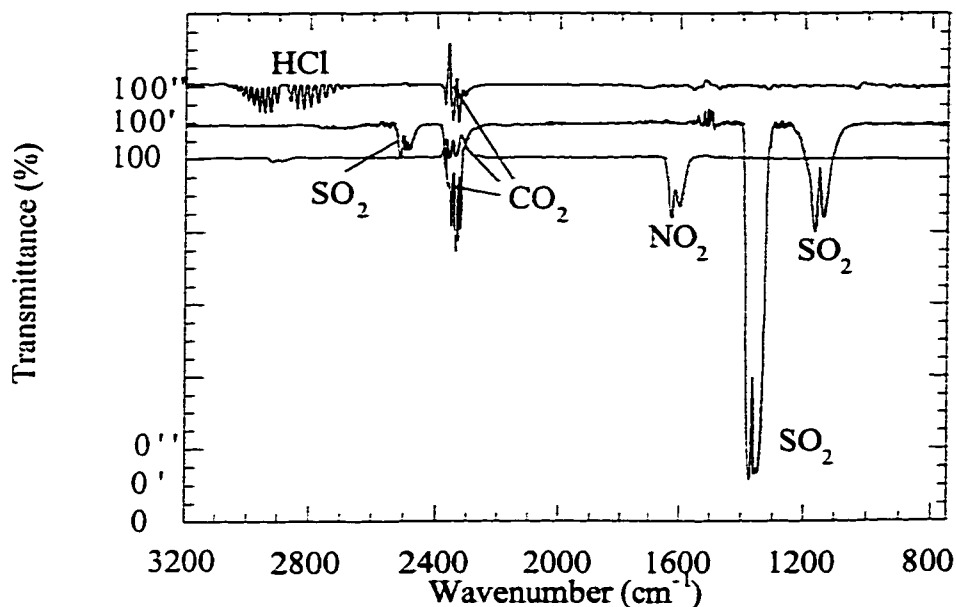


Figure 3.3.1 Example IR spectra of HCl, SO₂, and NO₂.

The spectra were taken with a 24 m pathlength at 25 °C and 1 atm. The approximate gas concentrations were as follows: HCl, 25 ppm; SO₂, 40 ppm; and NO₂, 5 ppm.

The peaks for NO, ranging from 1950 to 1800 cm⁻¹, were overlapped beyond the point of being quantitatively useful. For each of the three gases analyzed, a specific peak was chosen for quantitative analysis to determine concentration. The peak used for HCl was located from 2828 to 2814 cm⁻¹; for SO₂, from 1360 to 1340 cm⁻¹; for NO₂, 1655 to 1615 cm⁻¹. These peaks were chosen because they were relatively large and offered a high signal to noise ratio. However, they were not so large such that there was a nonlinear response of absorbance to concentration. Over the course of an experiment, the baseline taken at the beginning of the experiment tended to drift. Consequently, the area of a small range of wavenumbers next to each peak was determined. This baseline

correction area was subtracted from the area of the peak analyzed to determine a corrected absorbance. The ranges used for the baseline correction for HCl was 2830.5-2830 cm^{-1} ; for SO_2 , 1241-1240 cm^{-1} ; and for NO_2 , 1660-1659 cm^{-1} .

The analysis for SO_2 proved to have the greatest signal to noise ratio. SO_2 is a strong absorber in the IR band and its peaks do not overlap with water. On the other hand, HCl is a fairly weak absorber. In addition, its peaks were located adjacent to water peaks. Consequently, any drift in the water signal led to relatively noisy HCl data. The HCl data were most noisy at low HCl concentration and high relative humidity. NO_2 is a fairly strong absorber in the IR range but the concentration in the gas cell after dilution was fairly low (≤ 5 ppm). Also, the peak analyzed -- the least noisy for NO_2 -- was in the same wavenumber range as several water peaks. The combination of low NO_2 concentration and the overlapping of the water peaks led to somewhat noisy NO_2 data.

After an experiment, the area under the peak for each gas being analyzed was calculated for every fifteen seconds during the experiment. The concentrations were calculated based on a two point calibration. Absorbance at one of the two points, 0 ppm, was taken early in the experiment before any acid gases were introduced into the apparatus. The second of the two points was taken after the acid gases had been introduced to the system as they were bypassing the reactor. Once the gases reached steady-state and before flow was redirected to the reactor, the acid gas was at a nominal concentration (e.g., 1000 ppm) before being diluted. This nominal concentration, then, corresponds to an absorbance value which is the second of the two point calibration. The actual concentration in the gas cell was not known precisely. But because the dilution air flowrate was constant over the course of the experiment, the concentration of a given acid gas at the reactor outlet can be determined by the two point calibration.

Knowing the reactor inlet gas concentration and concentration as a function of time during the experiment, the number of moles absorbed between fifteen second time intervals was calculated. The moles of acid gas absorbed was compared to the known moles of sorbent placed in the reactor before the

experiment. Sorbent loading and conversion (or utilization) was then determined. See Appendix B for sample calculations.

3.4 SAND AND SORBENT CHARACTERIZATION

3.4.1 Sand

As discussed above, quartz sand from Aldrich was used to disperse the sorbent in the reactor. The same sand was used as a sorbent dispersant by previous researchers (Arthur, 1998; Nelli, 1997). The specific surface area of the quartz sand, as measured by nitrogen porosimetry (Micromeritics, Model ASAP 2000), was $0.183 \pm 0.002 \text{ m}^2/\text{g}$. The particle size determined by Aldrich is between 70 and 50 mesh.

Several experiments were performed to determine the extent of HCl absorption by water on the surface of sand particles. Experiments conducted at 1000 ppm HCl, 58% RH, and 70 °C showed that after 80 minutes, 2.0×10^{-5} moles HCl/g sand were adsorbed. Electrostatic interactions between the sand and HCl molecules increased HCl concentration in the water adsorbed on the surface of the sand to exceed saturation by almost a factor of 100. At 58% RH and 70 °C, a greater amount of HCl adsorbed than would have at the relative humidity (usually 3.5-19%) and temperature (usually 120 °C) of the sorbent experiments. With this overestimation, an HCl loading of 2.0×10^{-5} moles/g sand equates to less than 1% of the reactivity of both hydrated lime and calcium silicate. Therefore, the adsorption of HCl on quartz sand was ignored when experiments were analyzed. Adsorption of HCl on quartz sand was found to be less than with Ottawa sand standard and sea sand (both from Fisher).

3.4.2 Hydrated Lime

Hydrated lime was donated by the Mississippi Lime Company (MLC). Arthur (1998) and Nelli (1997) used the same sample. The specific surface area, as measured by the BET method, was $21.1 \pm 0.4 \text{ m}^2/\text{g}$. Pore size distributions for hydrated lime and calcium silicate are shown in Figure 3.4.1. Assuming the pores were cylindrical, the volume of void space for pores between 24 and 1830 Å in

diameter was $0.110 \text{ cm}^3/\text{g}$. The largest normalized pore volume was in the range of 20 to 30 Å. According to MLC, the hydrated lime was composed of 97% calcium hydroxide with the balance mostly calcium carbonate.

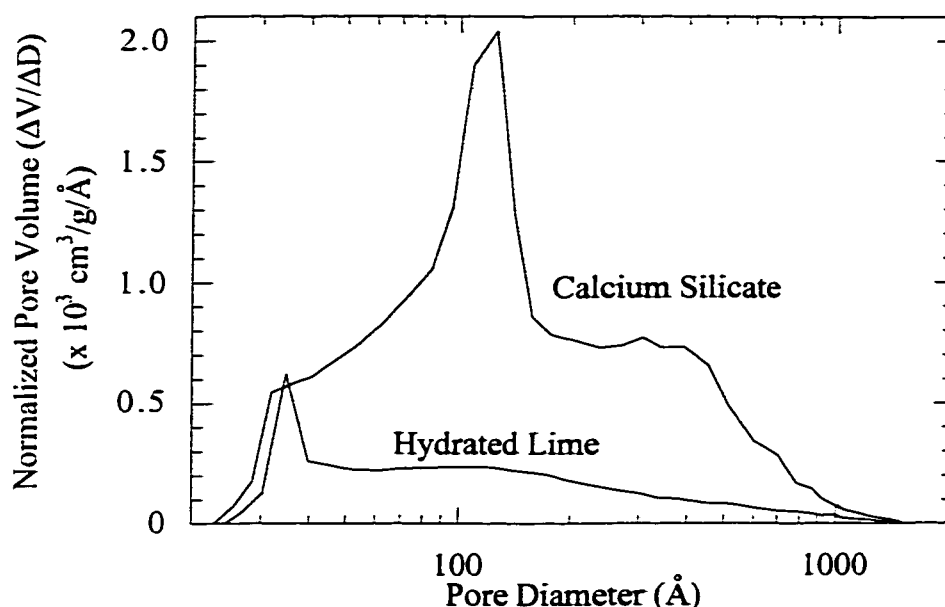


Figure 3.4.1 Pore volume distribution of hydrated lime and calcium silicate.

The data were acquired by nitrogen porosimetry. The calcium silicate distribution courtesy of Arthur (unpublished).

An X-Ray diffraction analysis (Philips, Model PW 1720 X-ray generator and APD 3520 data collection system) of hydrated lime showed no peaks except calcium hydroxide. X-ray diffraction patterns for hydrated lime and calcium silicate are shown in Figure 3.4.2. As determined by sieving, all the particles were smaller than 149 microns; 92% (by mass) were smaller than 45 microns. A scanning electron micrograph (JEOL, Model JSM35C) of hydrated lime shown in Figure 3.4.3 shows that particles tend to agglomerate into larger flakes.

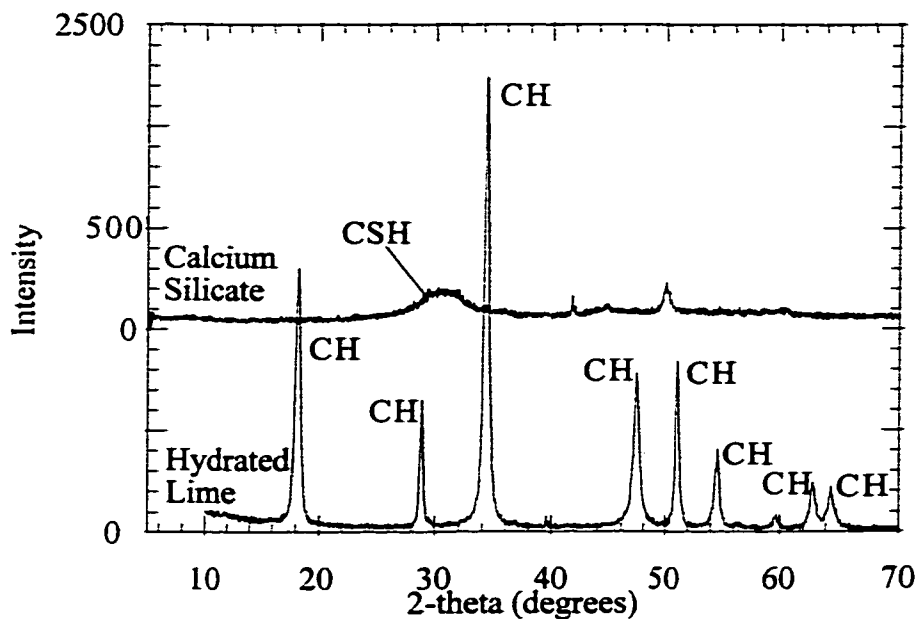


Figure 3.4.2 X-Ray diffraction patterns of hydrated lime and calcium silicate hydrate.

Peaks labeled CH are characteristic of calcium hydroxide. The rounded peak labeled CSH indicated a low level of crystallinity in the calcium silicate hydrate. Calcium silicate hydrate pattern courtesy of Arthur (1998).



Figure 3.4.3 SEM of hydrated lime.

Hydrated lime donated by the Mississippi Lime Company. The darker shadows appear because of the mounting tape. A dark 10 μm bar is located toward the bottom right of the figure. This micrograph was taken with a magnification of 1000.

3.4.3 Calcium Silicate

The solids that were used for all calcium silicate experiments were taken from the same sorbent preparation batch. A detailed description of the preparation of the sorbent can be found in Arthur (1998). The calcium silicate solids were generated by slurring a 1/1/0.5 mass ratio of hydrated lime, recycled glass, and gypsum for 50 hours at 92 °C with 20 wt% solids. The resulting solids were a calcium silicate hydrate with a calcium to silicate mole ratio of 1.5 (Arthur, 1998). The BET surface area of the solids was $87.5 \pm 0.7 \text{ m}^2/\text{g}$. The pore volume

between 22 and 1700 Å was 0.538 cm³/g. The greatest normalized pore volume was at approximately 130 Å (see Figure 3.4.1). A scanning electron micrograph of the calcium silicate sorbent shown in Figure 3.4.4 suggested that the calcium silicate solids may have agglomerated less than the hydrated lime.

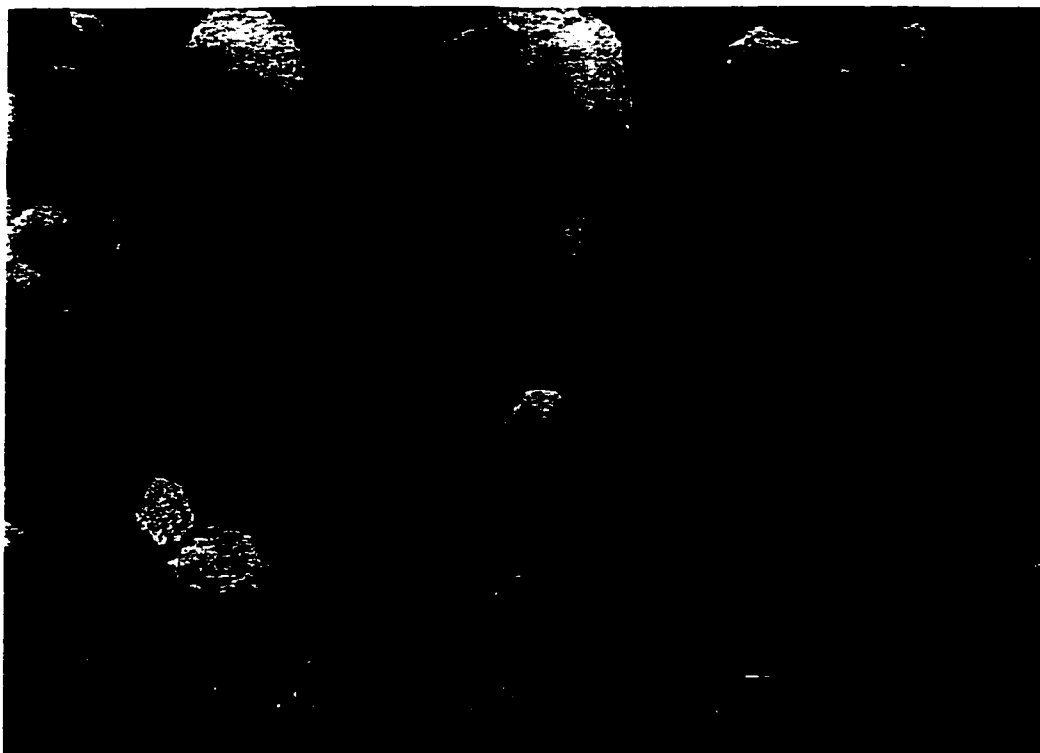


Figure 3.4.4 SEM of calcium silicate solids.

Calcium silicate solids formed by slurring a 1/1/0.5 mass ratio of hydrated lime, recycled glass, and gypsum for 50 hours at 92 °C with 20 wt% solids. This micrograph was taken with a magnification of 1000 and is courtesy of Arthur (1998).

X-ray diffraction analysis of the calcium silicate showed that the solids were almost completely amorphous (see Figure 3.4.2). To determine the capacity of the sorbent to absorb acid gases (defined herein as alkalinity), the solids were dissolved in an HCl solution at a pH of approximately 3. After titrating to a

phenolphthalein endpoint with NaOH, the divalent alkalinity of the calcium silicate was found to be 6.49 mmoles $\text{Ca(OH)}_2/\text{g}$ sorbent. Using atomic absorption (AA) spectroscopy, the moles of calcium and sodium were found to be 6.20 and 0.894 mmoles/g sorbent, respectively. It should be noted that the alkalinity of hydrated lime, 13.5 mmoles $\text{Ca(OH)}_2/\text{g}$ sorbent, is more than double the alkalinity of calcium silicate.

3.5 TYPICAL EXPERIMENTAL DATA

Figure 3.5.1 gives concentration as a function of time for HCl, SO_2 , and NO_2 for Exp. No. CS20. (Note that Appendix C gives a detailed listing of experimental conditions and results. The abbreviation HL indicates a hydrated lime experiment; CS is a calcium silicate experiment.) The experiment shown in Figure 3.5.1 was performed at 19% RH. At high humidity and a low inlet concentration, the noise of the HCl concentration with this experiment represents the most noise seen with HCl. Because NO_2 is at a high concentration, the signal to noise ratio from this experiment is slightly higher than with experiments conducted at lower NO_2 inlet concentration. At all experimental conditions, the signal to noise ratio for SO_2 was very high. With the data shown in Figure 3.5.1, gas absorption rates were calculated. By knowing the reaction stoichiometry, a mass balance was performed to calculate the sorbent conversion (or utilization). A detailed sample calculation is shown in Appendix B.

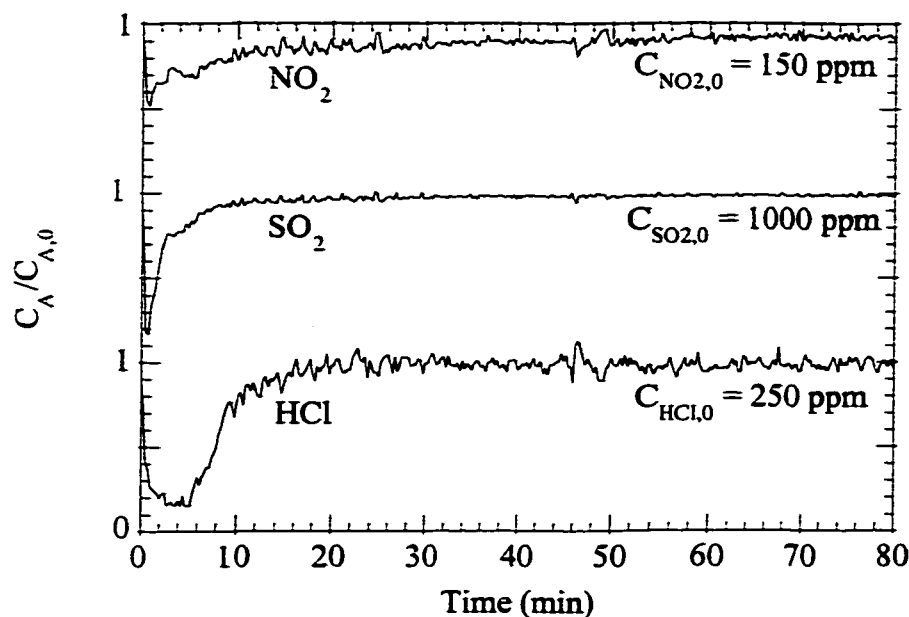


Figure 3.5.1 Typical experimental data for HCl, SO₂, and NO₂.

These data are taken from Exp. No. CS20. The conditions are as follows: 250 ppm HCl, 1000 ppm SO₂, 150 ppm NO₂, 2.5% O₂, 36 mg calcium silicate at 19% RH, 120 °C, and 1.5 SLPM. Note that each gas concentration is normalized to its inlet concentration. The curves all vary from 0 to 1 but are shifted to prevent overlap.

At time zero, the simulated flue gas was redirected from the reactor bypass to the reactor. For SO₂ and NO₂, the normalized gas concentration dropped to a minimum very quickly, generally within the first 30 seconds of the experiment. On the other hand, it took about five minutes for HCl to reach the minimum HCl concentration. This lag time for HCl was due to the absorption of HCl into the layer of water adsorbed on the surfaces of the gas cell. When experiments were run at 19% RH and 120 °C in the reactor, the relative humidity in the gas cell even after dilution was approximately 40% at 25 °C. This high level of humidity combined with the high solubility of HCl in water led to the damping of HCl

absorbance. At time zero, the gas cell was in equilibrium with, for example, 6 ppm HCl (250 ppm diluted by 40 LPM of house air). When flow was directed to the reactor, nearly all of the 250 ppm HCl was removed by the sorbent. Therefore, the surfaces of the gas cell were in contact with approximately 0 ppm HCl. The imbalance led to a 6 ppm driving force and desorption of HCl from the gas cell surfaces. For Exp. No. CS20 shown in Figure 3.5.1, this desorption took place for about five minutes. After five minutes, HCl broke through the sorbent bed and began to absorb into the water layer in the gas cell. This caused the HCl breakthrough curve to appear less steep than it would have without adsorption.

This HCl sorption phenomenon led to some added complexity when modeling HCl absorption by the sorbent. The behavior of the fresh sorbents when exposed to HCl was confounded with the gas cell effect. To overcome this problem, an additional equation was introduced into the model to account for the HCl sorption. The approach used is discussed in detail in Chapter 6.

3.6 EXPERIMENTAL REPRODUCIBILITY

At times throughout this study, experiments at the same conditions were performed to measure reproducibility or to lend confidence to an unexpected result. On the whole, the reproducibility of the apparatus was acceptable. Two experiments would produce nearly the same breakthrough curves; utilization from one experiment generally ended up within a few percent of the other.

Figure 3.6.1 shows three experiments performed at the same conditions of CS9. Clearly there was a spread in the breakthrough curves. Though the lack of reproducibility shown in Figure 3.6.1 was worse with these three experiments than usual, these data sets demonstrate a shortcoming of the experimental system. Though each of these experiments ended up at approximately the same final conversion, the path to that final conversion differed. It was suspected that uneven dispersion of the sorbent in the reactor often led to differences in breakthrough curves. For example, if the sorbent was unevenly distributed such that one side of the reactor contained more sorbent than the other, breakthrough occurred more quickly. However, eventually the side that contained more sorbent reacted and reached the same final conversion as an experiment with perfect

sorbent dispersion. On a concentration versus time curve, the experiment with uneven sorbent distribution exhibited a “tail” as the reactor outlet concentration approached the inlet concentration. If two experiments were performed at the same conditions and had different breakthrough profiles, the experiment that had less of a tail was assumed to be more accurate because of a more uniform sorbent distribution.

Understanding the reproducibility of the apparatus is paramount when, in Chapter 6, the experimental data are compared to a modeled fit. See Appendix H

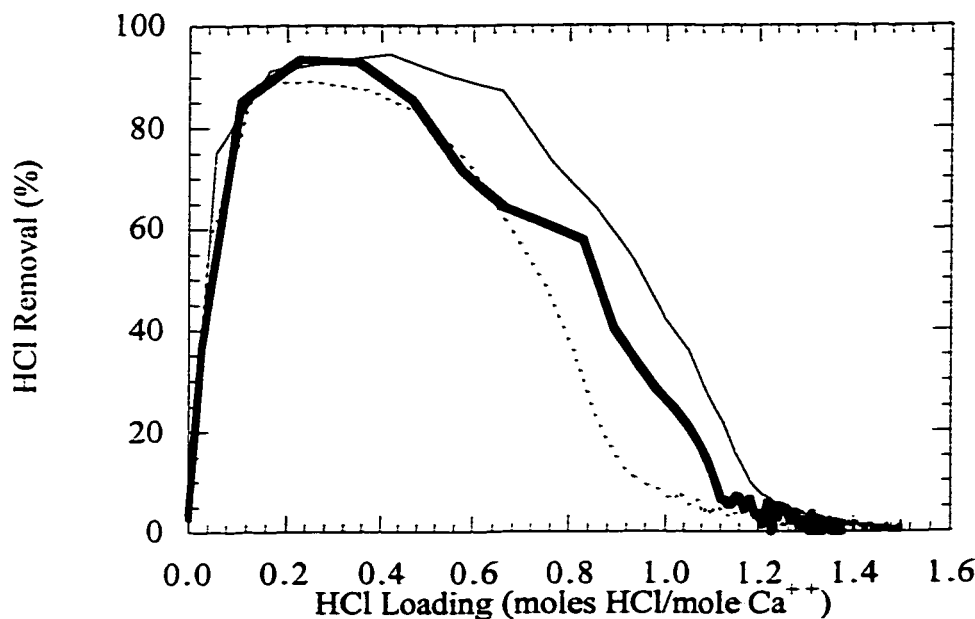


Figure 3.6.1 Comparison of three experiments performed at the same conditions.

The conditions for each experiment were those of Exp. No. CS9. The experiments were performed at 3.5% RH, 120 °C, and 1.5 SLPM with 2000 ppm HCl, 36 mg calcium silicate.

for a discussion of how the differences in experimental reproducibility shown in Figure 3.6.1 manifest in fixed-bed modeling.

Chapter 4. Absorption of HCl and SO₂ by Hydrated Lime

Experimentally, absorption by hydrated lime (HL) was studied first followed by absorption by calcium silicate. With both sorbents, experiments reacting a single gas with HCl, then SO₂, were performed first. Multi-gas experiments were conducted later. The analysis of the more complicated systems was made easier by the understanding gained from the results of the single gas experiments. The gas systems investigated can be divided into five groups:

- (1) HCl
- (2) SO₂
- (3) HCl and SO₂
- (4) HCl, SO₂, and O₂
- (5) HCl, SO₂, and O₂ with NO or NO₂

The range of conditions studied is shown in Table 4.0.1:

Table 4.0.1 Range of Conditions for Hydrated Lime Experiments

Variable	Low Value	High Value
Rel. Humidity (%)	0	19
HCl Conc. (ppm)	0	3500
SO ₂ Conc. (ppm)	0	2000
O ₂ Conc. (%)	0	5.5
NO ₂ Conc. (ppm)	All expts. including NO ₂ had 150 ppm	
Temperature (°C)	All expts. performed at 120°C	
Flowrate (SLPM)	All expts. but one performed at 1.5 SLPM	

Experimental results are discussed in this chapter in the order listed above. Modeling efforts aimed at describing the data in this chapter will be addressed in Chapter 6. Throughout this chapter, Experiment Numbers (Exp. Nos.) will be cited. A table matching Experiment Numbers to experimental conditions and final sorbent loadings can be found in Appendix C.

4.1 HCL AND HYDRATED LIME

As expected, the absorption of HCl by hydrated lime (HL) was found to be sensitive to relative humidity. Figure 4.1.1 shows that HCl removal and HL loading increased dramatically with an increase in relative humidity. Loading of

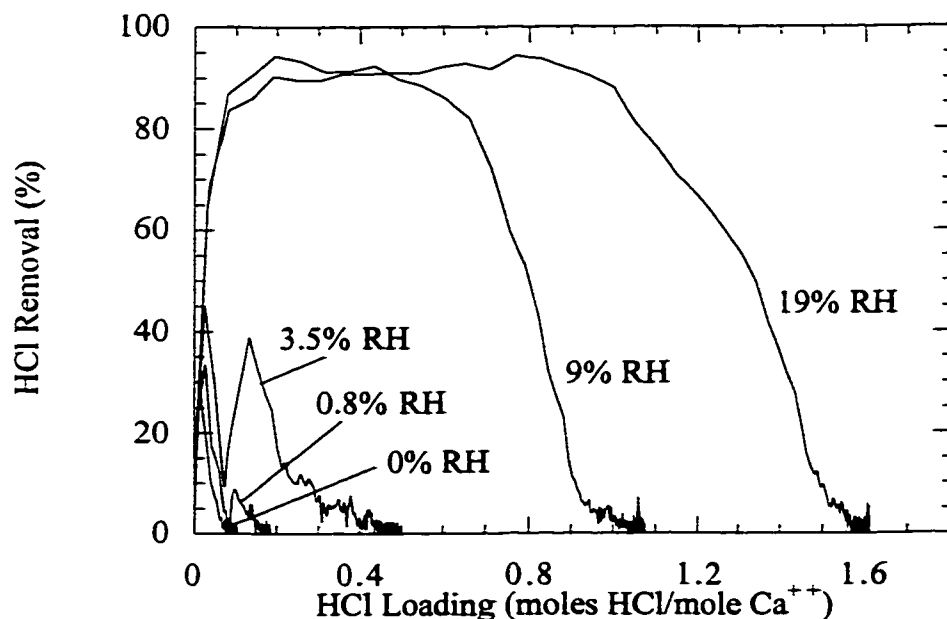


Figure 4.1.1 Effect of relative humidity on HCl removal.

Experiments performed at 1000 ppm HCl, 120 °C, 18 mg hydrated lime, and 1.5 SLPM. Exp. Nos. HL1-5.

an individual gas is defined as the total moles absorbed of that gas divided by the moles of calcium in the sorbent.

These data agree well with Pakrasi (1992). For example, he found that the HCl loading after 5 minutes was 0.52 moles HCl/mole Ca^{++} at 107 °C and 5.4% RH. A calculation based on the densities of hydrated lime and calcium chloride dihydrate and on the pore volume of the sorbent indicated that the pores could be completely plugged at an HCl loading of 0.21 moles/mole Ca^{++} . Based on the comparison of this loading value to the experimental data, it is unclear how the dihydrate salt deposits on the solids.

Close inspection of Figure 4.1.1 reveals that at 3.5% RH, HCl removal reached a maximum of 45% at the beginning of the experiment, decreased to about 10% removal at 0.10 moles HCl/mole Ca^{++} loading, and then increased to about 40% removal before finally tapering off to 0% removal at 0.48 moles HCl/mole Ca^{++} loading. The same trend, though less pronounced, was evident in the experiment at 0.8% RH. The experiment at 3.5% RH was reproduced four times; the experiment at 0.8% RH was duplicated. Each of the seven experiments showed the same drop in reactivity at about 0.10 moles HCl/mole Ca^{++} loading and then a resumption of reactivity. While it is not evident in Figure 4.1.1, there was a greater time lapse before the reaction restarted with the experiment at 0.8% RH than with the experiment 3.5% RH.

The deliquescent nature of calcium chloride may explain this unexpected phenomenon. The solids reacted to about 0.10 moles HCl/mole Ca^{++} loading producing a layer of $\text{CaCl}_2 \cdot 2 \text{H}_2\text{O}$ on the HL particles per Reaction 2.1. The calcium chloride then absorbed water from the vapor phase. The reaction started up again once there was a sufficient degree of surface water on the particles. The same phenomenon may have occurred with the higher relative humidity experiments but because the water vapor rates were much greater, the rehydration of the particles took place too quickly to observe. While this behavior is interesting scientifically, further studies were not conducted to conclusively explain its cause.

Over the typical HCl concentration range in flue gas for municipal waste combustors and coal-fired boilers, HCl removal rate was first order in HCl concentration. Also, final HL loading was not a function of HCl concentration at typical HCl concentrations. However, at an HCl concentration of 2000 and 3500 ppm, increased HCl concentration decreased final loading. This trend is evident in Figure 4.1.2. From 250 to 1000 ppm HCl, HCl removal was equal within experimental error up to the final loading of 1.64 moles HCl/mole Ca^{++} . With greater HCl concentration, HCl removal remained high until about 0.60 moles HCl/mole Ca^{++} loading. However, the absorption shut off more quickly to a final loading of 1.44 moles HCl/mole Ca^{++} at 2000 ppm HCl and 1.28 moles HCl/mole Ca^{++} at 3500 ppm HCl. The experiments at 2000 and 3500 ppm were each

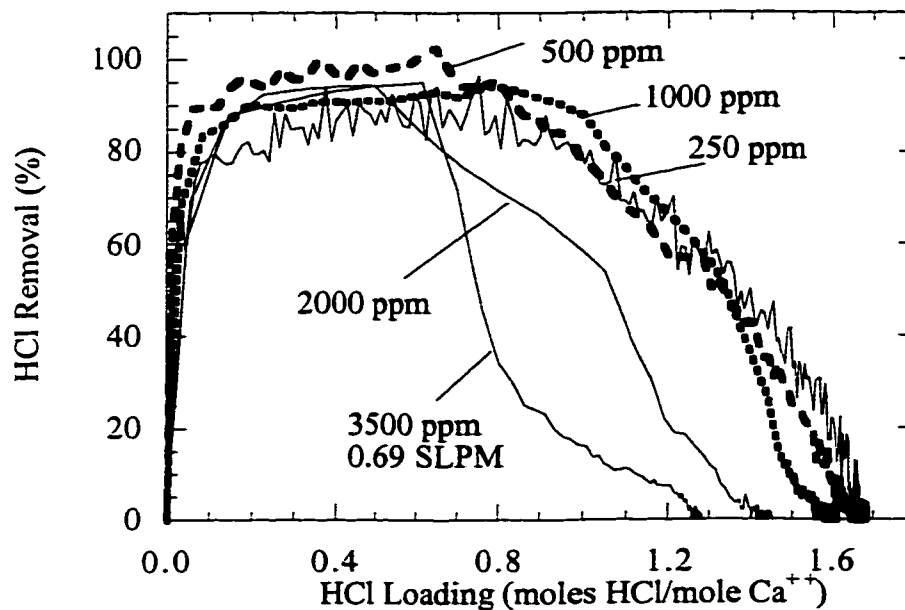


Figure 4.1.2 Effect of HCl concentration on HCl removal and final loading.

Experiment performed at 19% RH, 120 °C, 18 mg hydrated lime, and 1.5 SLPM (unless indicated otherwise). Exp. Nos. HL5-9.

reproduced two times. Experimental constraints prohibited experiments with a concentration greater than 3500 ppm.

Previously, only Pakrasi (1992) had investigated the effect of increased HCl concentration on final sorbent loading. The results of his experiments, which were conducted at conditions similar to those in Figure 4.1.2, did not reveal a decrease in HL utilization with HCl concentration varying from 1000 to 5000 ppm. However, his analysis to determine HL loading was done with a maximum sorbent exposure time of only five minutes. While the sorbent would have been deactivated by five minutes with 5000 ppm HCl, absorption would continue past five minutes with low HCl concentration. Therefore, the loading at five minutes does not represent an accurate *final* loading and conclusions about the effect of HCl concentration are difficult to draw from Pakrasi's work.

Reduced final sorbent loading at higher HCl concentration may have been due to an increase in the plugging of the pores of the sorbent. Simons' (1992) analysis of the reaction of calcined limestone with SO₂ showed that under certain conditions, loading of SO₂ does not reach 1 mole SO₂/mole Ca⁺⁺ because pores get plugged near the external particle surface. This blockage leaves the interior of the sorbent unavailable for reaction. When the HCl concentration in the gas was high, the rate of reaction at the surface of the particle was greater. Therefore, reaction products accumulated at the opening of the pore, eventually leading to plugging. When the HCl concentration was low, the lower reaction rate at the surface of the solid allowed for increased diffusion of the gas into the interior of the particle. The results shown in Figure 4.1.2 suggested that at a concentration of 1000 ppm and below, the reaction rate at the surface of the particle was low enough to allow the HCl to diffuse into the pores and utilize more alkalinity.

4.2 SO₂ AND HYDRATED LIME

As with HCl, the reactivity of SO₂ with HL in the absence of HCl increased with increasing relative humidity. This trend is illustrated in Figure 4.2.1. At the low relative humidity range studied, the utilization of the solid is low. Even at the highest relative humidity studied, the loading of the solids barely exceeded 0.10 moles SO₂/mole Ca⁺⁺ after 40 minutes.

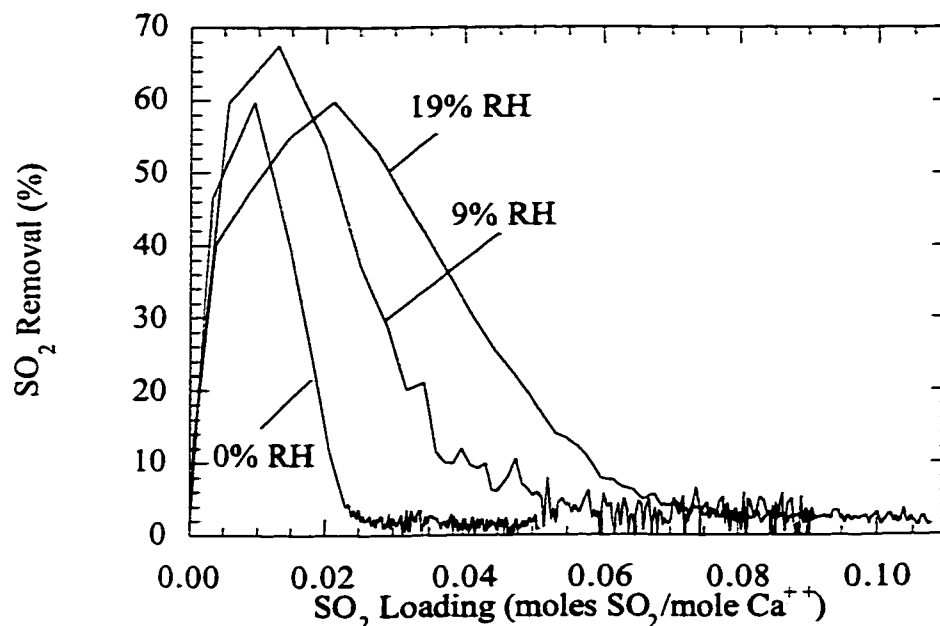


Figure 4.2.1 Effect of relative humidity on SO₂ removal.

Experiment performed at 1000 ppm SO₂, 120 °C, 100 mg hydrated lime, and 1.5 SLPM for 40 min. Exp. Nos. HL10-12.

Unlike with HCl, decreasing SO₂ concentration increased the maximum SO₂ removal. This trend is evident by the two experiments compared in Figure 4.2.2. The maximum removal at 500 ppm SO₂ was 90% while the maximum removal at 1000 ppm SO₂ was less than 60%. These effects of relative humidity and SO₂ concentration on SO₂ removal followed the same trends as those found by other researchers (Jorgensen et al., 1986; Klingspor et al., 1984; Ruiz-Alsop and Rochelle, 1985).

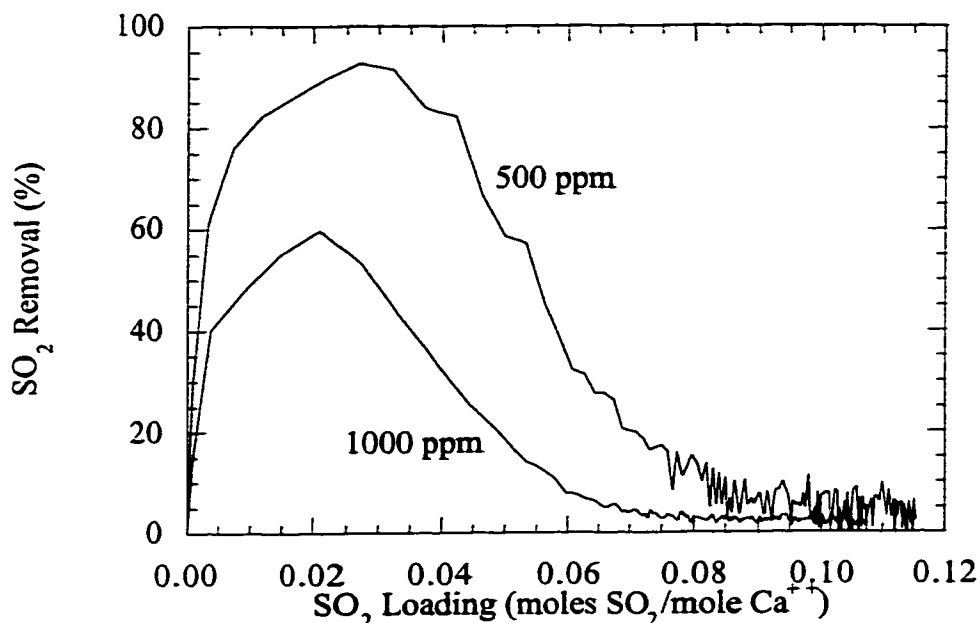


Figure 4.2.2 Effect of SO₂ concentration on SO₂ removal.

Experiments performed at 19% RH, 120 °C, 100 mg hydrated lime, 1.5 SLPM for 40 min. Exp. Nos. HL12-13.

4.3 HCL-SO₂ AND HYDRATED LIME

Before discussing the experimental results of the HCl-SO₂ and hydrated lime system, the definition of loading must be made clear. Loading of an individual gas is defined as the moles absorbed of that gas divided by the moles of calcium in the sorbent. However when total loading is discussed, the stoichiometry of a reaction is usually taken into account. For example, two moles of HCl absorbed by hydrated lime per Reaction 2.1 will contribute one mole of total loading because of the reaction stoichiometry. However, one mole of SO₂ absorption by Reaction 2.2 will contribute one mole of total loading because of the reaction stoichiometry. If one mole of HCl and one mole of SO₂ are absorbed

simultaneously by one mole of hydrated lime, the individual loading of both HCl and SO₂ is 1 mole/mole Ca⁺⁺. However, if the absorption took place by Reactions 2.1 and 2.2, the total loading is 1.5 (0.5*moles HCl+moles SO₂)/moles Ca⁺⁺.

Most of the experiments performed with the HCl-SO₂-HL system were at high relative humidity (19%). This was done because at lower relative humidity, the reactivity of SO₂ is too low to observe trends within acceptable precision. At early experimental times, the absorption of SO₂ was limited by having to compete with HCl for alkalinity. The increase in SO₂ absorbance with lower HCl concentration is evident in Figure 4.3.1. Later in the experiment, as the alkalinity

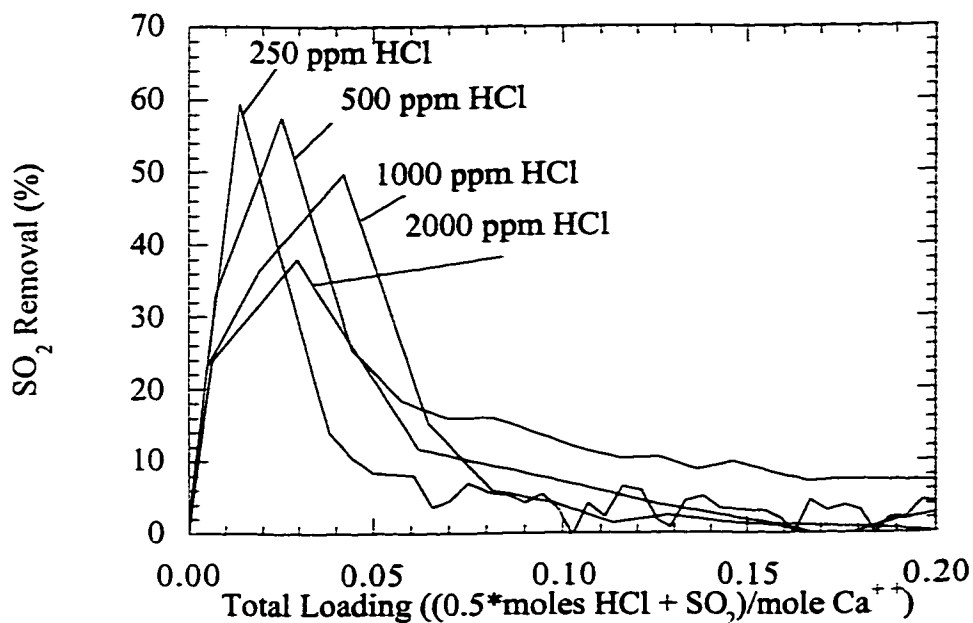


Figure 4.3.1 Effect of HCl concentration on SO₂ removal.

Experiments performed at 19% RH, 1000 ppm SO₂, 35 mg hydrated lime, 120 °C, and 1.5 SLPM. Exp. Nos. HL14-17.

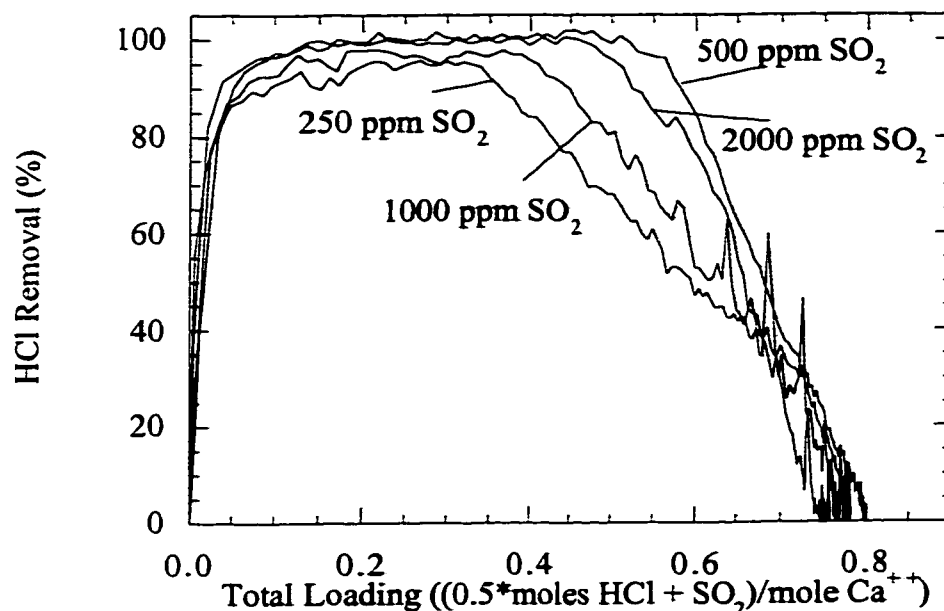


Figure 4.3.2 Effect of SO₂ concentration on HCl removal.

Experiments performed at 19% RH, 1000 ppm HCl, 35 mg hydrated lime, 120 °C, and 1.5 SLPM. Exp. Nos. HL14-17.

of the sorbent became consumed, HCl reacted with $\text{CaSO}_3 \cdot \frac{1}{2} \text{H}_2\text{O}$ releasing SO₂ as indicated by Reaction 2.4.

It was found that the concentration of SO₂ in the gas phase had little effect on the reactivity of HCl. This is evident in Figure 4.3.2. As discussed in Section 3.6, the differences in the breakthrough curves can be attributed to differences in the quality of the distribution of HL in the reactor. The fact that all the experiments ended up at approximately the same final conversion implies that there is, at most, only a minor effect of SO₂ conversion on HCl removal.

In all of the HCl-SO₂ experiments in the absence of O₂ or NO₂, the sorbent utilization achieved was the same as the utilization achieved with only HCl in the gas stream. At 19% RH and an HCl concentration of 1000 ppm and

less, this final loading, adjusted for the reaction stoichiometry in Reactions 2.1 and 2.2, was 0.82 (0.5*moles HCl+moles SO₂)/moles Ca⁺⁺. This fact implies that with HCl and SO₂, there seemed to be a maximum available alkalinity primarily defined by relative humidity regardless of the feed gas composition. When the ratio of SO₂/HCl in the feed gas increased, slightly less CaCl₂•2 H₂O was formed in favor of a greater amount of CaSO₃•1/2 H₂O. Though with some scatter, this trend is evident in Figure 4.3.3.

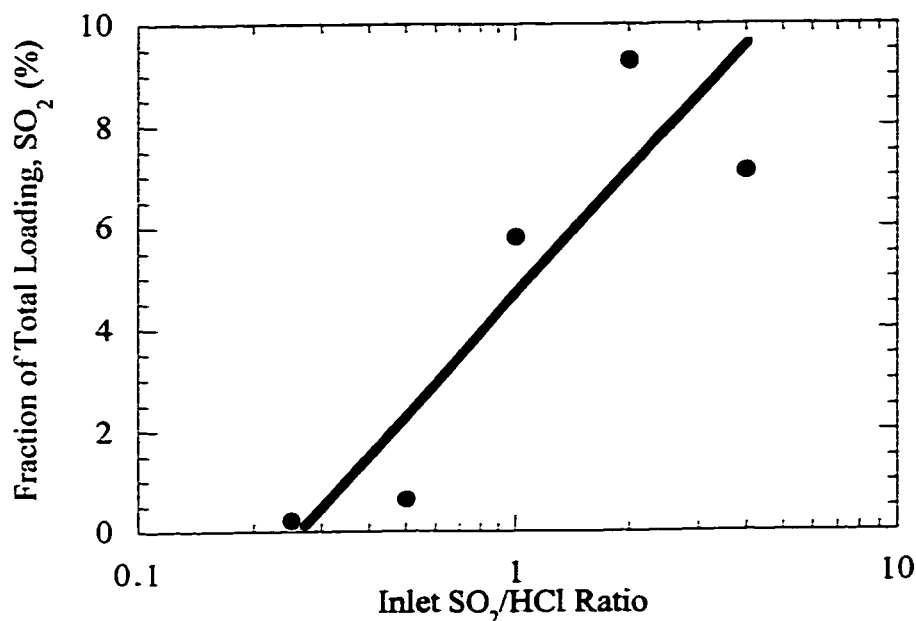


Figure 4.3.3 Effect of SO₂/HCl feed ratio on fraction of total loading by SO₂.

Experiments performed at 19% RH, 35 mg hydrated lime, 120 °C, and 1.5 SLPM. Two data points had the same fraction of total loading by SO₂ of 9.3% at an inlet SO₂/HCl ratio of 2. Exp. Nos. HL14-19.

The fact that the final solids product composition was a function of the feed gas composition suggested that a pseudo-equilibrium existed, probably in

accordance with Reaction 2.4. One explanation of the pseudo-equilibrium may be reaction kinetics. Another explanation may be that the chemistry dictates that HCl would react completely with $\text{CaCl}_2 \cdot 2 \text{H}_2\text{O}$. However, $\text{CaSO}_3 \cdot \frac{1}{2} \text{H}_2\text{O}$ became trapped in pores and was inaccessible to HCl.

Experiments where solids were exposed to just HCl or SO_2 in sequence showed that not only could HCl react to drive off SO_2 but that the reverse was also true. Figure 4.3.4 shows an experiment where, during Phase I, hydrated lime

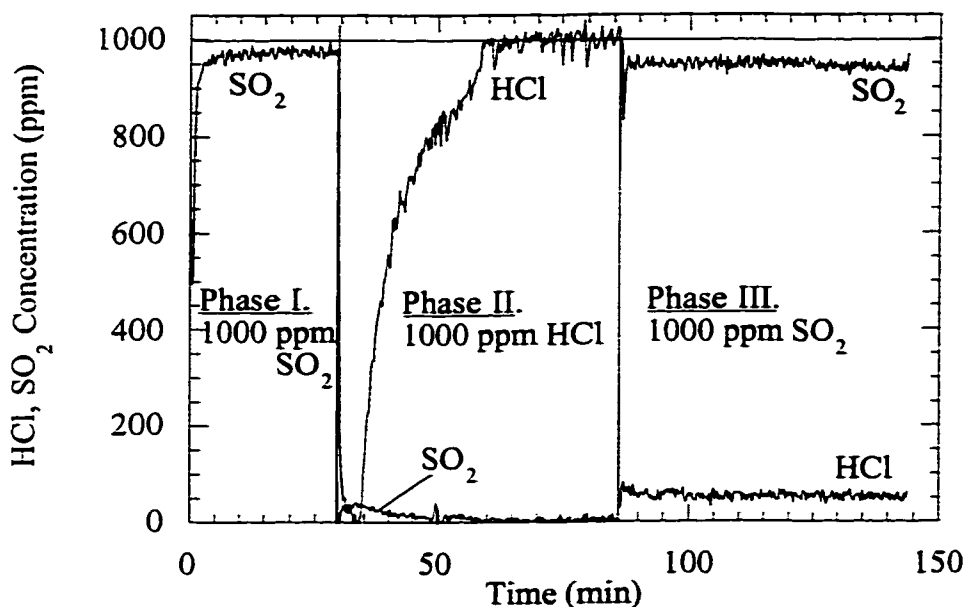


Figure 4.3.4 Sequential absorption of SO_2 , then HCl, then SO_2 by hydrated lime.

Experiments performed at 19% RH, 120 °C, 35 mg hydrated lime, and 1.5 SLPM.

was exposed to 1000 ppm SO_2 . Then 1000 ppm HCl contacted the solids, mostly hydrated lime with some $\text{CaSO}_3 \cdot \frac{1}{2} \text{H}_2\text{O}$, during Phase II. In the final phase, 1000 ppm SO_2 was passed through the reactor which, at that point, contained

mostly $\text{CaCl}_2 \cdot 2 \text{H}_2\text{O}$ with some hydrated lime. A mass balance showed that during Phase II, the HCl drove off all of the SO_2 that had reacted during Phase I. Most of the SO_2 desorbed early during Phase II as HCl was breaking through the fixed bed. During Phase III, the SO_2 exposed to the chloride salt drove off HCl at an average rate of about 54 ppm from 85 to 145 minutes.

Another similar experiment, shown in Figure 4.3.5, tested whether an

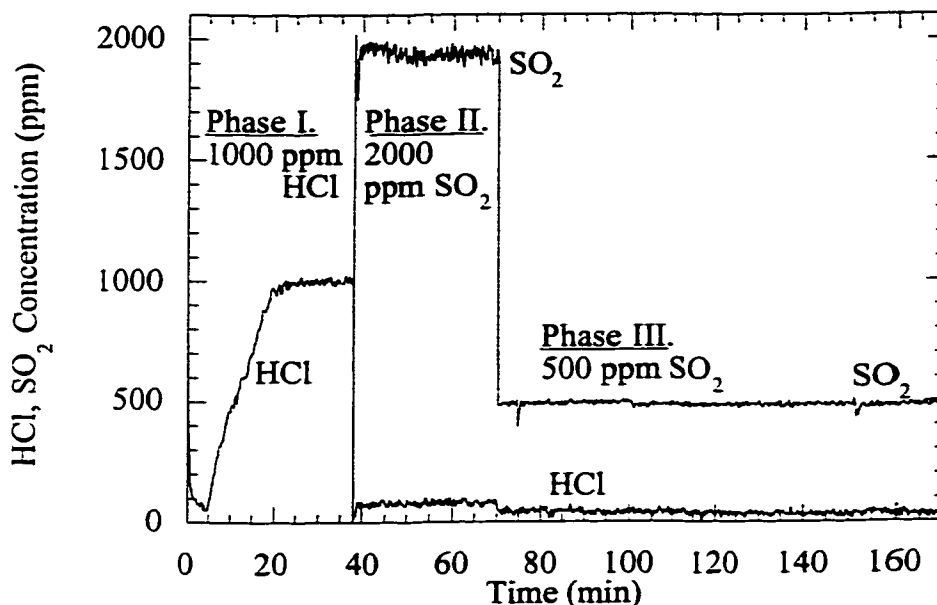


Figure 4.3.5 Sequential absorption of HCl, then 2000 and 500 ppm SO_2 by hydrated lime.

Experiments performed at 19% RH, 120 °C, 35 mg hydrated lime, and 1.5 SLPM.

increase in SO_2 concentration over $\text{CaCl}_2 \cdot 2 \text{H}_2\text{O}$ would increase HCl desorption. During Phase I, the hydrated lime was loaded with HCl. Then during Phases II and III, the solids, mostly $\text{CaCl}_2 \cdot 2 \text{H}_2\text{O}$, were exposed sequentially to 2000 and 500 ppm SO_2 . During Phase II, the average concentration of HCl emissions was

80 ppm. The average concentration of HCl emissions during Phase III was 39 ppm. Clearly, increasing the concentration of SO₂ contacting the chloride salt increased the amount of HCl desorbed from the solids. Another test (data not shown) demonstrated that reagent grade calcium chloride also absorbed SO₂ while simultaneously emitting HCl. While the ability of calcium chloride to absorb SO₂ is interesting scientifically, the low removal obtained (a maximum of 5% with 2000 ppm SO₂ at 19% RH) indicates that calcium chloride would not be a suitable sorbent for SO₂.

4.4 HCL-SO₂-O₂ AND HYDRATED LIME

Adding air to a dilute HCl gas stream did not affect HCl reactivity (data not shown). With a similar sorbent, Chu and Rochelle (1989) have found that the presence of oxygen in the feed gas led to greater SO₂ removal and final sorbent loading. With air present in the HCl-SO₂ gas mixture, the oxidation of S(IV) to S(VI) by Reaction 2.5 can take place. Figure 4.4.1 shows the effect of air when added to the HCl-SO₂ mixture.

Several conclusions can be drawn from the experiments shown in Figure 4.4.1. First, the presence of O₂ increased the reactivity of SO₂ with HL. This is clear particularly in the experiments without HCl. Comparing the experiments containing 5.5% O₂ with and without 250 ppm HCl, it is apparent that there was a slight increase in SO₂ reactivity early in the experiment due to the presence of HCl. However, once the HCl moving front pushed to the end of the reactor and alkalinity started to become scarce (at about 35 minutes or 0.55 (0.5*moles HCl+moles SO₂)/moles Ca⁺⁺ total loading), HCl reacted with CaSO₃•¹/₂ H₂O producing SO₂ emissions. As the concentration of oxygen increased, the amount of sulfur that remained bound with the solids also increased. This suggested that with a greater oxygen concentration, there was a greater amount of S(VI) formed through the irreversible Reaction 2.5. When there was only 250 ppm HCl in the gas stream, the SO₂ did not have to aggressively compete with HCl; the SO₂ absorption probably took place at the back of the reactor where HCl had not broken through. But when the concentration of HCl was increased to 1000 ppm, the competition for alkalinity led to reduced SO₂ reactivity. This effect is seen

clearly in the comparison of the experiments with 250 and 1000 ppm HCl with a constant O₂ concentration of 5.5%.

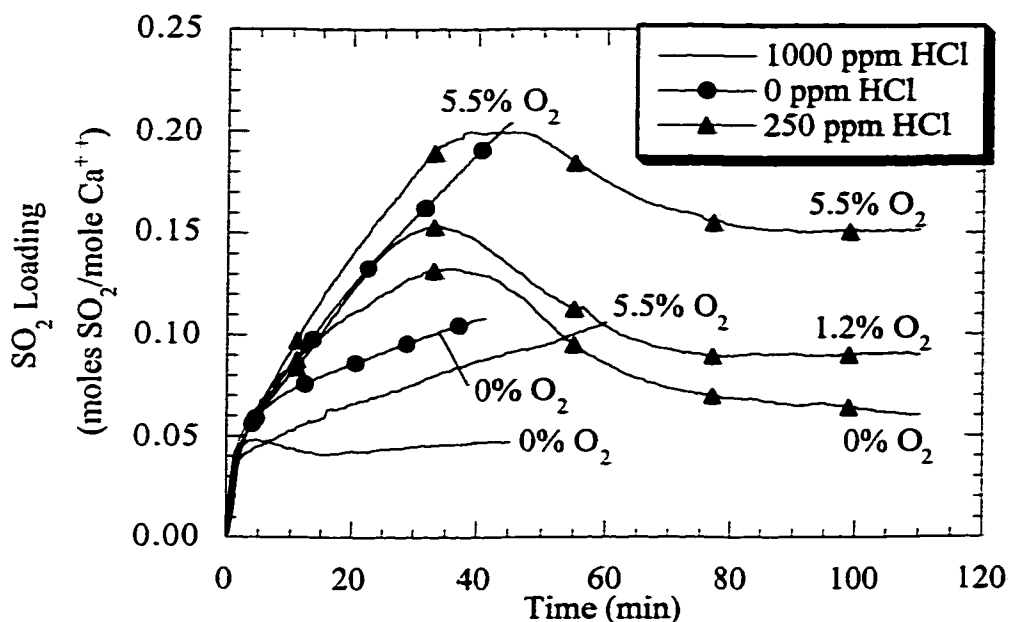


Figure 4.4.1 Effect of O₂ and HCl concentration on SO₂ loading.

Experiments performed at 19% RH, 1000 ppm SO₂, 35 mg hydrated lime, 120 °C, and 1.5 SLPM. Exp. Nos. HL12, HL14, 16HL, HL21-24.

In summary, if SO₂ did not have to compete with HCl for alkalinity, it reacted almost as if the HCl were not in the feed gas. Once SO₂ reacted, the presence of oxygen in the gas stream allowed the irreversible oxidation of S(IV). But the oxidation did not take place quickly enough to force all the bound sulfur to S(VI). Consequently, SO₂ was emitted as HCl began to break through to the back of the bed. At a high HCl concentration, SO₂ had to compete with HCl for alkalinity. This competition caused a reduction in SO₂ reactivity, even in the presence of oxygen.

While the dynamics of SO₂ absorption in the presence of HCl and O₂ were somewhat complex, HCl reactivity was relatively uninteresting. For each of the experiments shown in Figure 4.4.1, the final loading of HCl was 1.5 moles HCl/moles Ca⁺⁺ within experimental error. Therefore, in the experiments where there was a greater loading of SO₂, the total loading also increased. Without oxygen present, the final loading of the HCl-SO₂ system is about 0.82 (0.5*moles HCl+moles SO₂)/moles Ca⁺⁺ at 19% RH. The experiment with 250 ppm HCl, 1000 ppm SO₂, and 5.5% O₂ at 19% RH yielded a final conversion of 0.91 (0.5*moles HCl+moles SO₂)/moles Ca⁺⁺ -- 76% by HCl and 15% by SO₂.

4.5 HCL-SO₂-NO_x-O₂ AND HYDRATED LIME

In general, NO accounts for approximately 90% of the NO_x emitted in flue gas; the remaining 10% is NO₂. Yuan and Fong (1992) studied the reactivity of the HCl-SO₂-NO system with calcium hydroxide slurry in a simulated spray drying apparatus. Their results showed that fractional removal of NO by the slurry is an order of magnitude less than for HCl and SO₂. They concluded that increasing NO concentration had a slight positive effect on SO₂ absorption. In a study done without HCl, Nelli (1997) found that increasing NO₂ concentration improved SO₂ reactivity. Greater SO₂ concentration also enhanced NO₂ absorption.

The experiments investigating the effect of NO_x in the feed gas were performed at 250 ppm HCl. This was done so that the absorption of SO₂ and NO_x could be observed without those gases having to compete aggressively with HCl for alkalinity. A high concentration of SO₂ and a low concentration of HCl most closely represents coal-fired boiler flue gas. However, it is expected that the conclusions drawn below are qualitatively applicable to flue gases with other SO₂/HCl ratios. Experiments performed in this study generally confirm the trends found by previous researchers. Figure 9 shows the effects of NO and NO₂ on SO₂ removal.

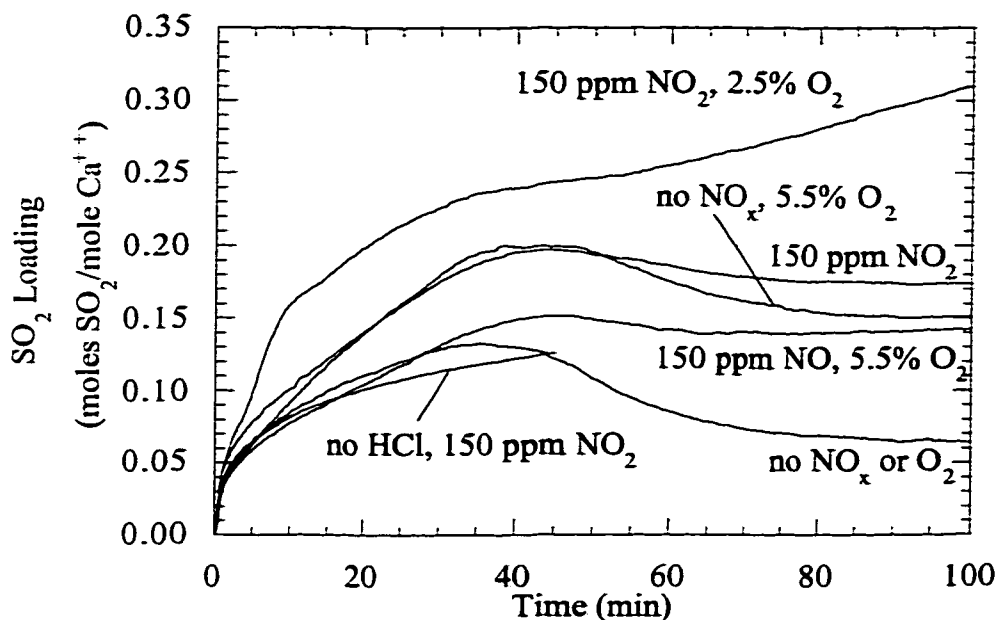


Figure 4.5.1 Effect of NO and NO₂ on SO₂ loading in the presence of HCl.

Experiments performed at 19% RH, 250 ppm HCl, 1000 ppm SO₂, 35 mg hydrated lime, 120 °C, and 1.5 SLPM. Exp. Nos. HL22-23, HL25-28.

Through fifty minutes, the presence of 150 ppm NO decreased SO₂ loading by 0.05 moles SO₂/mole Ca⁺⁺ when all other variables were held constant. This effect was probably due to the competition between SO₂ and NO for available alkalinity at the back of the sorbent bed. In the experiment without NO, by 100 minutes the HCl reactivity had forced the emission of SO₂ by Reaction 2.4. Therefore, loading by SO₂ in the experiments with and without NO ended up within 0.01 moles SO₂/mole Ca⁺⁺ of each other.

Loading of the solids by NO could not be accurately calculated because the NO peaks in the IR spectrum were washed out by water peaks. Though water was taken as part of the background, fluctuations in the syringe pump and dilution

air water content made the NO signal too noisy for a mass balance. Utilizing the data from the noisy NO peaks qualitatively, it was apparent that NO reacted at early experimental times but ceased absorbing (or desorbing) after about three minutes.

One strategy for NO capture is to oxidize the relatively unreactive NO to NO₂ by injecting a hydrocarbon such as methanol into the flue gas (Lyon et al., 1990). With this strategy in mind, experiments with NO₂ added to the feed gas were conducted. The presence of NO₂ clearly increased the reactivity of SO₂ with HL. When 150 ppm NO₂ was added to the gas stream in the absence of oxygen, the final loading by SO₂ was 0.11 moles SO₂/moles Ca⁺⁺ greater than in the absence of NO₂. With 150 ppm NO₂ and 2.5% O₂ in the feed gas, final loading by SO₂ reached 0.31 moles SO₂/moles Ca⁺⁺. Even as the solids loading approached 1 (0.5*moles HCl+moles SO₂)/moles Ca⁺⁺, the reactivity of the solids with SO₂ continued. This is probably due to enhanced sorbent utilization from the formation of sulfur-nitrogen compounds (Nelli, 1997).

Sorbent loading due to NO₂ was calculated by means of the gas phase mass balance. Figure 4.5.2 plots loading of NO₂ for the same experiments shown in Figure 4.5.1. The addition of 250 ppm HCl to the system increased the loading of HL by NO₂. However, adding 2.5% O₂ caused a reduction in loading by NO₂ by 2.5 moles NO₂/moles Ca⁺⁺. This reduction in reactivity arose because with the oxygen in the feed stream, S(IV) could be oxidized to S(VI). If S(IV) was oxidized by oxygen, it was not available to react with NO₂ by Reaction 2.6.

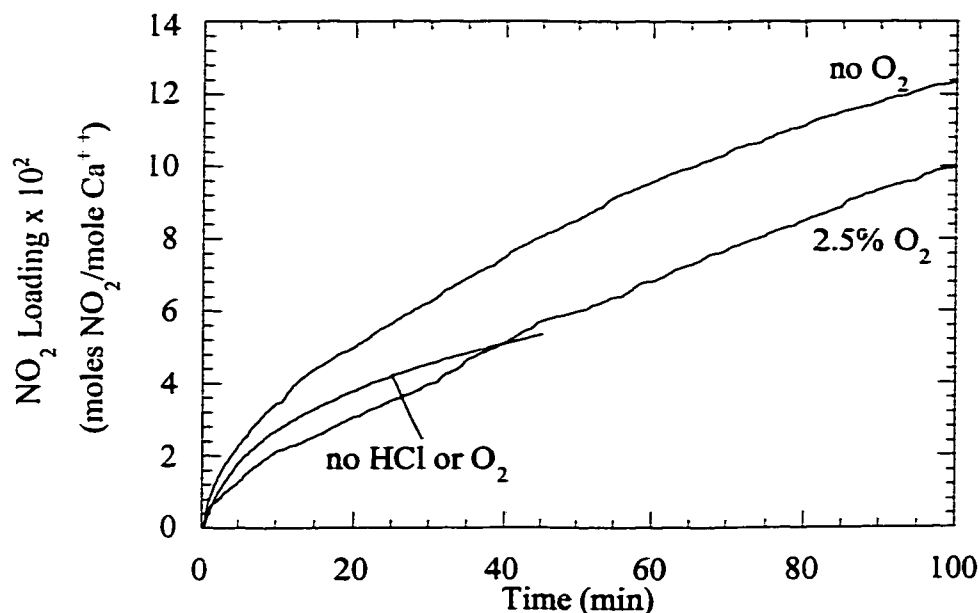


Figure 4.5.2 Effect of O₂ and HCl on NO₂ loading.

Experiments performed at 19% RH, 250 ppm HCl, 1000 ppm SO₂, 150 ppm NO₂, 35 mg hydrated lime, 120 °C, and 1.5 SLPM. Exp. Nos. HL25, HL26, HL28.

As with the HCl-SO₂-O₂ system, the reactivity of HCl when NO_x is added did not change considerably. Without NO_x or oxygen in the gas, an experiment with 250 ppm HCl and 1000 ppm SO₂ yielded an HCl loading of 1.58 moles/moles Ca⁺⁺. Loading of SO₂ for the same experiment was 0.06 moles/moles Ca⁺⁺. Under conditions with the most SO₂ and NO_x reactivity (150 ppm NO₂ and 2.5% O₂), the loading by HCl dropped to 1.34 moles/moles Ca⁺⁺ while loading by SO₂ and NO₂ was 0.31 moles SO₂/moles Ca⁺⁺ and 0.10 moles NO₂/moles Ca⁺⁺, respectively. So even when HCl must compete the most for alkalinity, its reactivity still suffers only minimally.

4.6 SUMMARY

In the HCl gas system, the reactivity of HCl with hydrated lime (HL) increased considerably with increasing relative humidity. At 1000 ppm HCl and below, the rate of absorption was first order with respect to HCl concentration and final loading was constant. At 2000 and 3500 ppm HCl, increasing concentration decreased final HL loading. The decrease in final loading may have been due to pore plugging near the external particle surface.

When SO₂ was the only gas in the reactor inlet, increased relative humidity increased SO₂ loading. Unlike with HCl, lower inlet SO₂ concentration increased the maximum SO₂ removal.

When HCl and SO₂ were simultaneously exposed to HL, the final total loading of the solids did not depend on SO₂/HCl feed ratio. However, as the SO₂/HCl ratio increased, the fraction of the loaded solids that consisted of CaSO₃•¹/₂ H₂O increased while the fraction of CaCl₂•2 H₂O decreased slightly. This phenomenon implies that there was an pseudo-equilibrium between the reaction products and the acid gases. The addition of oxygen to the HCl-SO₂ system enhanced SO₂ absorption but did not affect HCl reactivity.

The presence of NO in the HCl-SO₂-O₂ system did not affect final loading by HCl or SO₂. On the other hand, the presence of NO₂ enhanced SO₂ absorption. While the presence of O₂ improved SO₂ reactivity, the presence of O₂ caused a decrease in HL loading of NO₂. Increasing SO₂ and NO₂ reactivity had a minor negative effect on the absorption of HCl. The conditions that maximize sorbent utilization are high relative humidity, SO₂ concentration, NO₂ concentration, and oxygen concentration and low HCl concentration.

Chapter 5. Absorption of HCl and SO₂ by Calcium Silicate

The experimental work performed with calcium silicate solids closely paralleled studies with hydrated lime. An essential element in determining whether calcium silicate solids would be more suitable for HCl and SO₂ absorption applications than hydrated lime is to be able to directly compare the results from experiments with similar conditions. The discussion of experimental results is grouped into four gas systems:

- a. HCl
- b. SO₂
- c. HCl, SO₂, NO_x, and O₂
- d. SO₂, NO_x, and O₂

The first three sets were the original scope of this study. However, experimental data from the third set led to additional experiments that focused on gaining an understanding of the interactions of SO₂ and NO₂ as a function of

Table 5.0.1 Range of Conditions for Calcium Silicate Experiments

Variable	Low Value	High Value
Rel. Humidity (%)	0	19
HCl Conc. (ppm)	0	3250
SO ₂ Conc. (ppm)	0	2000
O ₂ Conc. (%)	0	5.5
NO ₂ Conc. (ppm)	0	150
Temperature (°C)	90	150
Flowrate (SLPM)	All expts. but one performed at 1.5 SLPM	

temperature and relative humidity. Table 5.0.1 shows the range of conditions for experiments with calcium silicate as the sorbent.

A tabulation matching Experiment Numbers (Exp. Nos.) to experimental conditions and final sorbent loadings can be found in Appendix C. This chapter does not discuss modeling of the experimental data or attempt to give a detailed comparison between the performance of hydrated lime and calcium silicate. Those subjects are addressed in Chapters 6 and 7.

5.1 HCL AND CALCIUM SILICATE

As seen in Figure 5.1.1, the final HCl loading increased from 0.32 to 0.86 moles HCl/mole Ca^{++} when the relative humidity was increased from 0 to 1.8%.

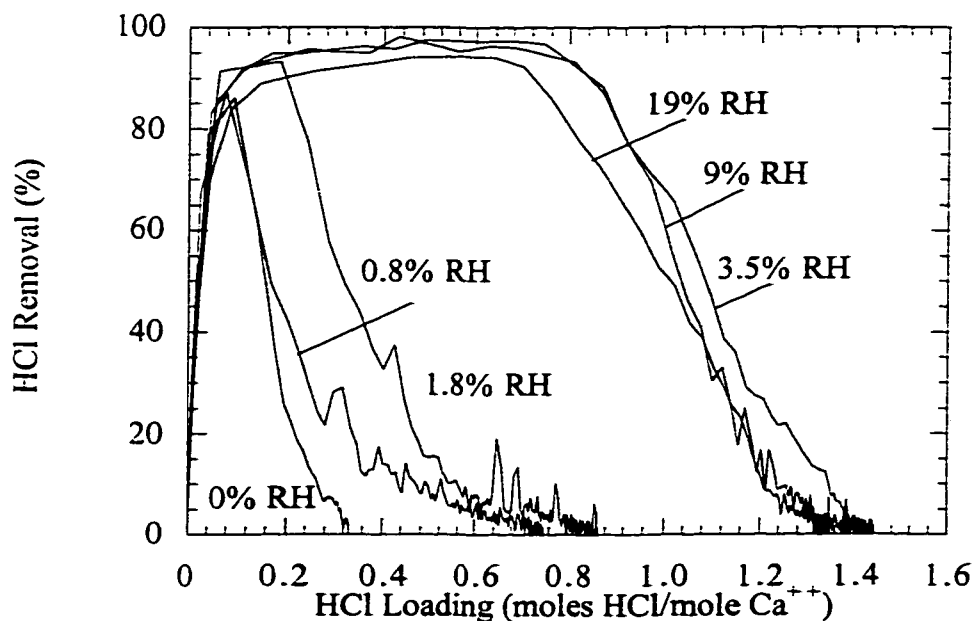


Figure 5.1.1 Effect of relative humidity on HCl removal.

Experiments performed at 1000 ppm HCl, 120 °C, 36 mg calcium silicate, and 1.5 SLPM. Experiment Nos. CS1-6.

RH. However, from 3.5 to 19% RH, HCl loading throughout the experiments was not a function of relative humidity. In each experiment, the HCl removal approached 100% until about 0.8 moles HCl/mole Ca^{++} and then fell off to zero HCl removal at approximately 1.4 moles HCl/mole Ca^{++} . As discussed in Chapter 2, previous work with both hydrated lime and calcium silicate solids indicated that as relative humidity was increased, reactivity of acid gases almost invariably also increased. Because these results were unexpected, each of the 3.5, 9, and 19% RH experiments were reproduced two times.

In light of the reactivity at 3.5% RH, it was expected that at some higher relative humidity, complete utilization of the solids (an HCl loading of 2 moles HCl/moles Ca^{++}) could be achieved. But because increasing relative humidity did not increase HCl loading, it appears that the maximum calcium silicate loading is 1.4 moles HCl/mole Ca^{++} or 70% utilization. A calculation using the densities of calcium silicate (Kind, 1994), calcium chloride dihydrate, and silicic acid (Perry, 1984) and the void volume of calcium silicate (Section 3.4.3) indicated that the pores would become plugged at an HCl loading of 1.58 moles/mole Ca^{++} . It is possible that an increase in relative humidity above 3.5% RH did not increase final HCl loading because the pores became plugged.

Sinke et al. (1985) reported that the triple point for $\text{CaCl}_2 \cdot \text{H}_2\text{O}$, $\text{CaCl}_2 \cdot 2\text{H}_2\text{O}$, and saturated calcium chloride existed at 176 °C. Using this information and heats of formation from Garvin et al. (1987), it was calculated that at 120 °C and a relative humidity less than 2.2%, the monohydrate was the stable solid phase. At a relative humidity greater than 2.2%, the dihydrate salt was the stable solid phase. It is possible that increasing relative humidity above 2.2% did not increase HCl loading because the larger dihydrate salt blocked the pores. Because the pores were blocked, HCl could not diffuse into the center of the particle and react with the 30% of the calcium that remained unutilized.

In an attempt to confirm the existence of two different levels of hydration, two experiments, one at 1.8 and the other at 3.5% RH, were performed where calcium silicate was dispersed in glass wool instead of quartz sand. The conditions were the same as Exp. Nos. CS3 and CS4. X-ray powder diffraction

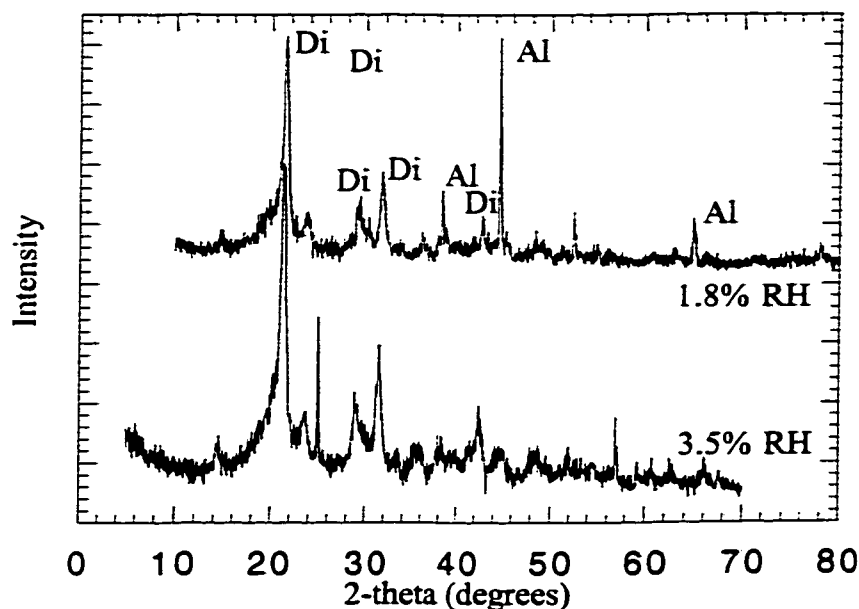


Figure 5.1.2 X-ray powder diffraction results on reaction products from 1.8 and 3.5% RH experiments.

The reactions products were taken from experiments performed at 1000 ppm HCl, 120 °C, 36 mg calcium silicate, and 1.5 SLPM. The conditions were similar to those of Exp. Nos. CS3-4. Peaks labeled Al are the result of the aluminum stage upon which the 1.8% RH sample was taken. Peaks labeled Di indicate characteristic $\text{CaCl}_2 \cdot 2 \text{H}_2\text{O}$ peaks as given by the standard from Hanawalt et al. (1938).

analyses were performed on samples of both reacted sorbents in an attempt to understand the discontinuity in the effect of relative humidity. The X-ray analyses, depicted in Figure 5.1.2, show that both samples contained the dihydrate of calcium chloride based on a standard from Hanawalt et al. (1938). Clearly these results did not confirm the calculation regarding the hydrate phase transition discussed above. It is possible that during the time interval (~ 30 minutes) between extracting the solids from the reactor and loading them in the X-ray

diffractometer, the monohydrate may have converted to the dihydrate salt. The results of the study by Sinke et al. (1985) may support this conclusion as they found the monohydrate to be unstable.

Scanning Electron Microscopy (SEM) pictures were taken on the same reaction products analyzed with X-Ray Powder Diffraction. The objective of the SEM studies was to determine if there was any visible difference in the reaction products of the experiments conducted at 1.8 and 3.5% RH. Both samples looked nearly identical under the electron microscope and very similar to the fresh sorbent shown in Figure 3.4.3. Consequently the SEM analyses, like the X-ray powder diffraction analyses, did not confirm different levels of hydration of the

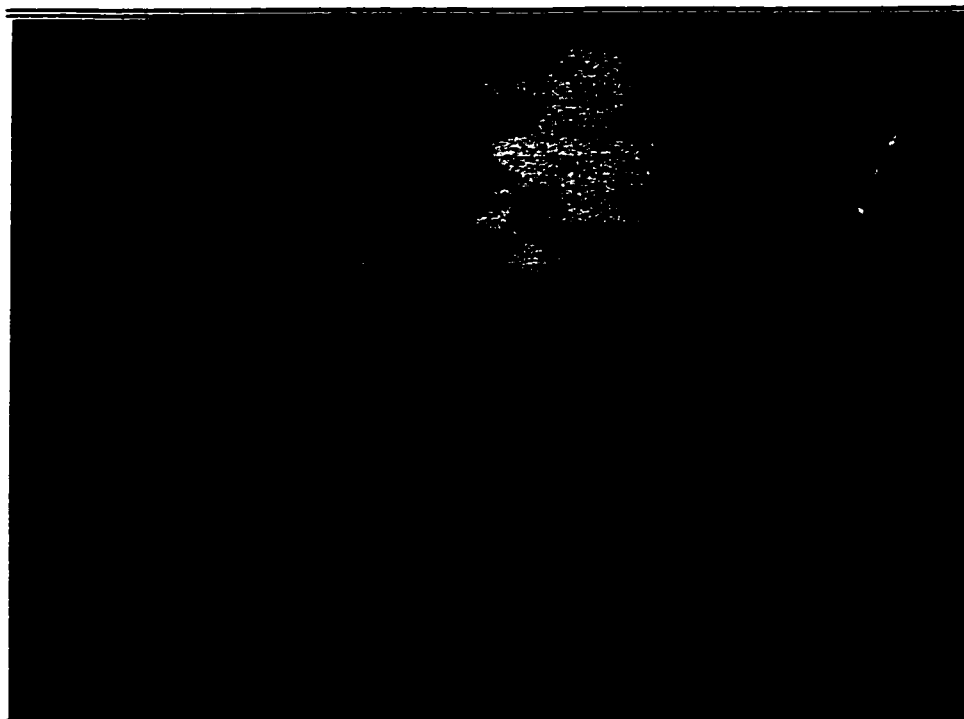


Figure 5.1.3 Scanning Electron Microscope picture of a sample of reaction products.

The reactions products were taken from an experiment performed at 1.8% RH, 1000 ppm HCl, 120 °C, 36 mg calcium silicate, and 1.5 SLPM. The conditions similar to those of Exp. No. CS3.

reaction products. The SEM picture taken of the sample from the experiment performed at 1.8% RH is shown in Figure 5.1.3.

Analysis of the reactivity of HCl as a function of concentration is more straightforward than the reactivity as a function of relative humidity. It is shown in Figure 5.1.4 that at concentrations ranging from 250 to 3250 ppm, HCl removal as a function of HCl loading was zeroth order with respect to concentration within experimental error. This indicates that the absorption rate was first order with respect to HCl concentration at a fixed HCl loading.

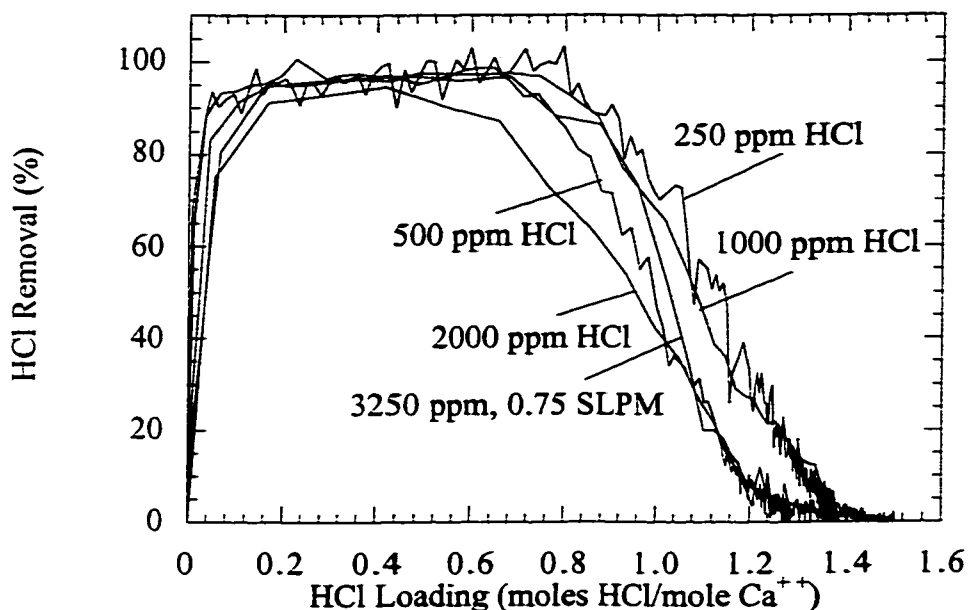


Figure 5.1.4 Effect of HCl concentration on HCl removal.

Experiments performed at 3.5% RH, 120 °C, 36 mg calcium silicate, and 1.5 SLPM. Exp. Nos. CS4, CS7-10.

5.2 SO₂ AND CALCIUM SILICATE

As other researchers had found (Nelli, 1997; Arthur, 1998), increasing relative humidity increased the reactivity of SO₂ with calcium silicate. This trend is evident in Figure 5.2.1. Unlike HCl, SO₂ continued to react, albeit at a very low rate, even after thirty minutes. With HCl, a final loading was reached where the absorption rate of HCl dropped to zero. It is unclear whether the difference between HCl and SO₂ is due to differences with the mass transfer mechanisms or with the thermodynamics of the reactions.

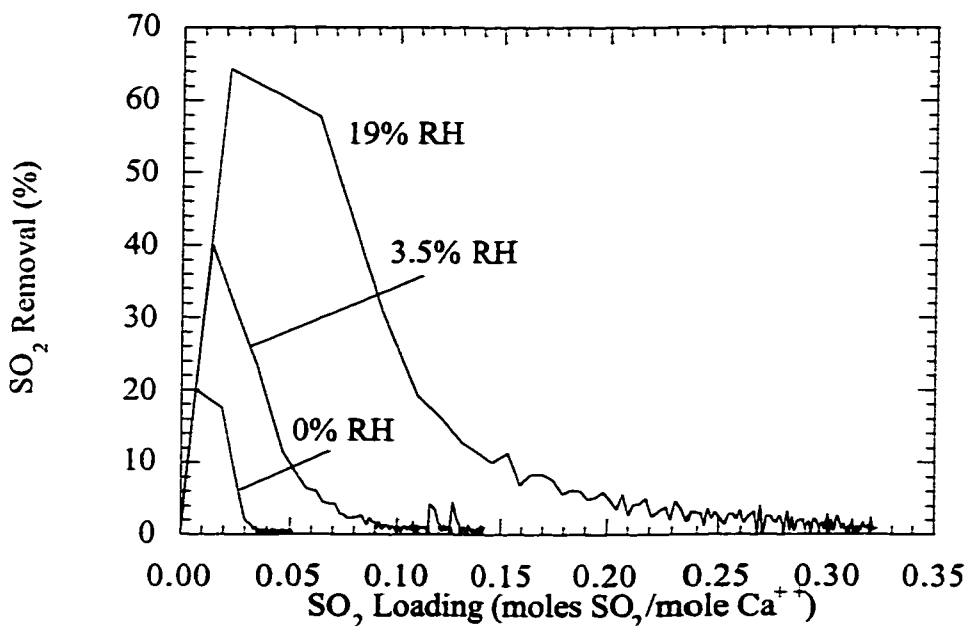


Figure 5.2.1 Effect of relative humidity on SO₂ removal.

Experiments performed for 30 minutes at 1000 ppm SO₂, 120 °C, 36 mg calcium silicate, and 1.5 SLPM. Exp.Nos. CS11-13.

As with hydrated lime, increasing the SO₂ concentration decreased the SO₂ removal early in experimental time. Data from two experiments, one at 500 and the other at 1000 ppm SO₂, are presented in Figure 5.2.2. These results

suggest that SO_2 absorption on fresh sorbent may have been controlled by a process that was less than first order.

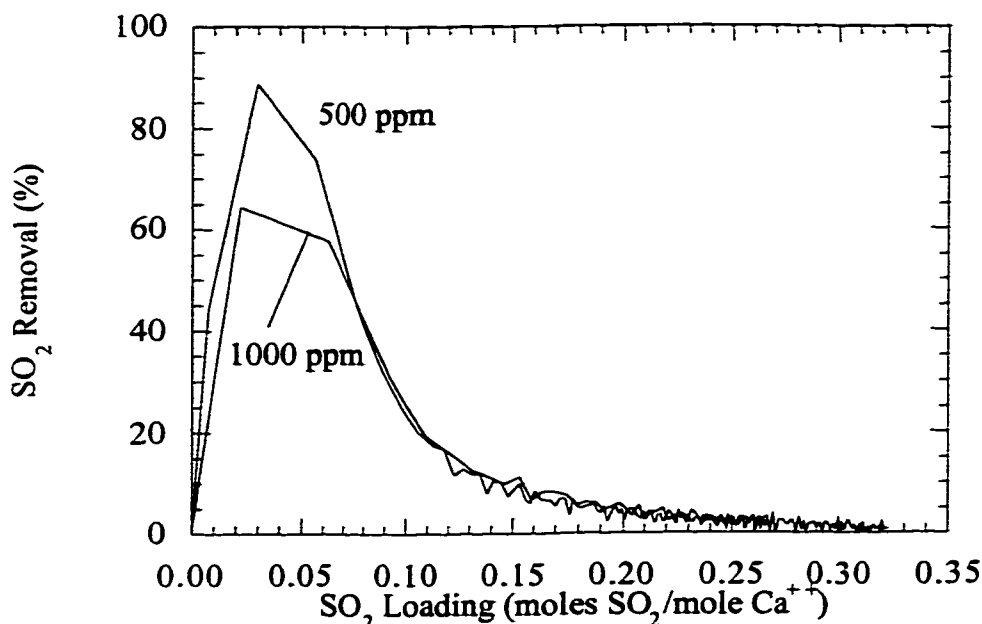


Figure 5.2.2 Effect of SO_2 concentration on SO_2 removal.

Experiments performed for 30 minutes at 19% RH, 120 °C, 36 mg calcium silicate, and 1.5 SLPM. Exp. Nos. CS13-14.

5.3 HCL-SO₂-NO_x-O₂ AND CALCIUM SILICATE

5.3.1 Effect of O₂

Most of the experiments absorbing SO_2 and HCl simultaneously were performed at 19% RH and 120 °C. This high humidity was chosen because HCl, SO_2 , and NO_2 reactivity generally increased with increasing relative humidity. Conducting experiments at 19% allowed for better quantification of acid gas interactions. It was found that when both HCl and SO_2 were present in the

absence of an S(IV) oxidizing agent (O_2 or NO_2), the absorption of HCl led to the emission of SO_2 from the reacted solids. This phenomenon is shown by the lower curve in Figure 5.3.1:

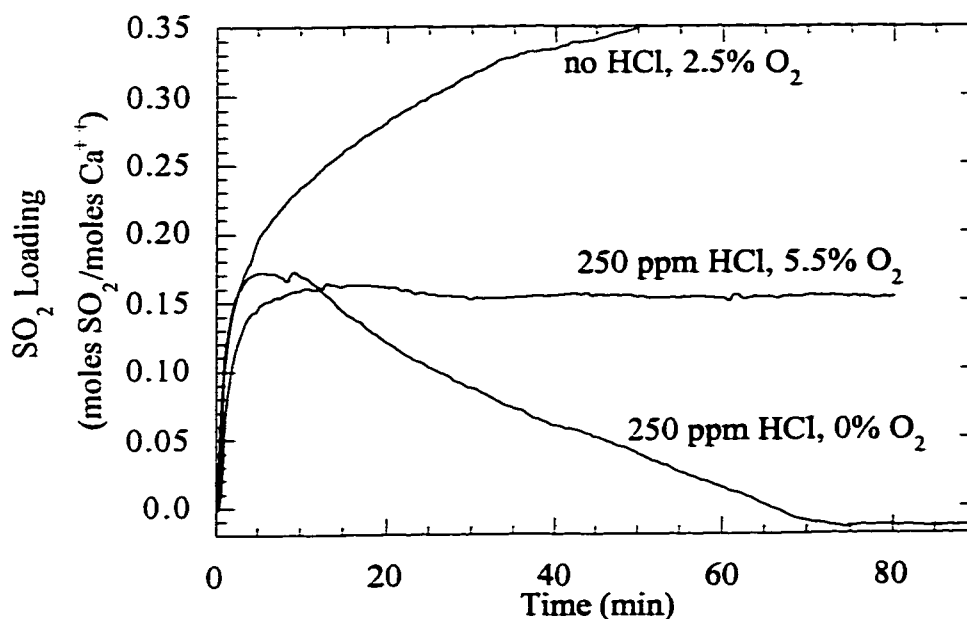


Figure 5.3.1 Effect of O_2 and HCl on SO_2 loading.

Experiments performed at 19% RH, 1000 ppm SO_2 , 120 °C, 36 mg calcium silicate, and 1.5 SLPM. Exp. Nos. CS15-17.

When both HCl and SO_2 were present in the gas phase, each gas had a moving reactivity zone in the bed. In these zones, HCl reacted to form $CaCl_2 \cdot 2 H_2O$ while SO_2 formed $CaSO_3 \cdot \frac{1}{2} H_2O$. When the calcium silicate solids that were available for reaction were consumed, HCl would react with any available calcium sulfite per reaction 2.13. Consequently, SO_2 was emitted from the solids in favor of increased HCl reactivity. As shown in Figure 5.3.1, the fixed-bed continued to remove SO_2 through about ten minutes. After ten minutes, the reaction of calcium sulfite with HCl caused SO_2 to be released, decreasing the

SO₂ loading. The curve showing HCl loading as a function of time was essentially the same with 1000 ppm SO₂ as without any SO₂. This fact suggests that the absorption rates of HCl with both calcium silicate and CaSO₃•¹/₂ H₂O are approximately the same.

When 5.5% O₂ was added to the gas stream, SO₂ reacted with the solids and maintained the SO₂ loading. The presence of O₂ allowed for the oxidation of S(IV) to S(VI) per reaction 2.5. Unlike calcium sulfite hemihydrate, when gypsum was exposed to HCl it was stable and did not emit SO₂. The HCl loading at the end of the experiment was 0.10 moles HCl/mole Ca⁺⁺ less when SO₂ and O₂ were present than when they were absent from the gas mixture. The total loading with SO₂ and O₂ present was 0.82 (0.5*moles HCl+moles SO₂)/mole Ca⁺⁺; the total loading in the HCl only system was 0.70 (0.5*moles HCl)/mole Ca⁺⁺.

5.3.2 Effect of NO₂

The addition of NO₂ to the simulated flue gas greatly enhanced SO₂ absorption. This effect is shown in Figure 5.3.2. Assuming there was no effect of differing oxygen concentrations from 2.5 to 5.5%, the addition of 50 ppm NO₂ increased SO₂ loading to 0.73 from 0.15 moles SO₂/mole Ca⁺⁺. Tripling the NO₂ concentration from 50 to 150 ppm NO₂ led to a 42% increase in SO₂ loading.

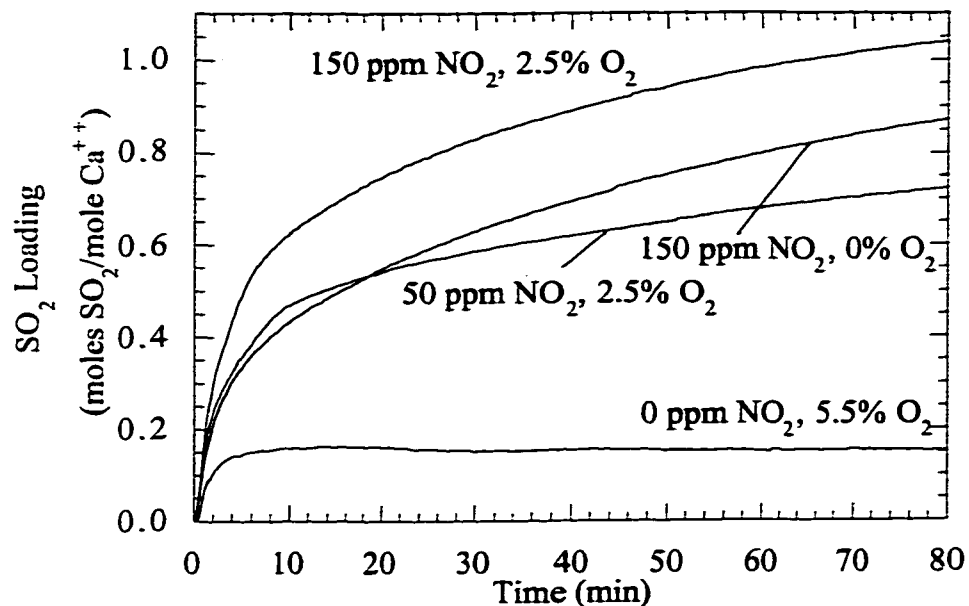


Figure 5.3.2 Effect of NO₂ on SO₂ loading in the presence of HCl.

The experiment was performed at 19% RH, 250 ppm HCl, 1000 ppm SO₂, 120 °C, 36 mg calcium silicate, and 1.5 SLPM. Exp. Nos. CS16, CS18-20.

The increase in SO₂ reactivity with calcium silicate by the addition of NO₂ and O₂ was partially at the expense of reduced reactivity of HCl. This reduction is apparent in Figure 5.3.3. In the presence of varying levels of NO₂, the nature of the competition changed from a system dominated by HCl reactivity to one dominated by SO₂. With the addition of 150 ppm NO₂, final SO₂ loading increased by a factor of 6.8. Conversely, adding 150 ppm NO₂ decreased final HCl loading by a factor of 2.6.

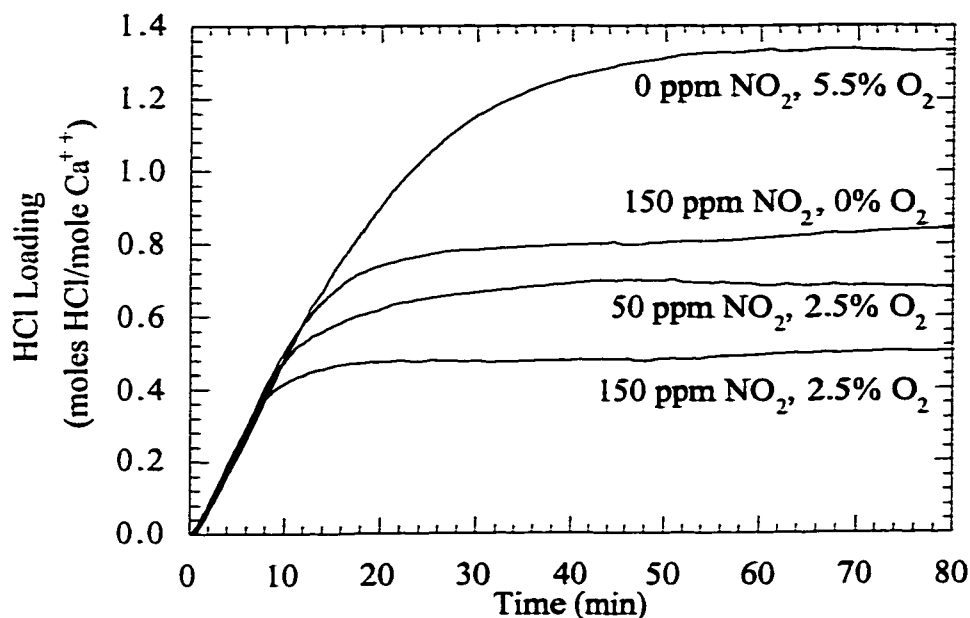


Figure 5.3.3 Effect of NO₂ on HCl loading in the presence of SO₂.

The experiment was performed at 19% RH, 250 ppm HCl, 1000 ppm SO₂, 120 °C, 36 mg calcium silicate, and 1.5 SLPM.
Experiment Nos. CS16, CS18-20.

As seen in Figure 5.3.2, increasing the NO₂ and O₂ concentration causes an increase in SO₂ absorption. However, adding O₂ to a gas stream that contains NO₂ reduces the reactivity of NO₂ with the sorbent (see Figure 5.3.4). The loading of NO₂ continues almost linearly with respect to time even after 100% utilization is surpassed. In addition, the rate of NO₂ loading is not first order in NO₂ concentration. In the presence of calcium sulfite, the primary mechanism for NO₂ removal is through the oxidation of S(IV) to S(VI) (reaction 2.14). When O₂ is present, some of the S(IV) is oxidized by O₂ and is therefore not available for reaction with NO₂.

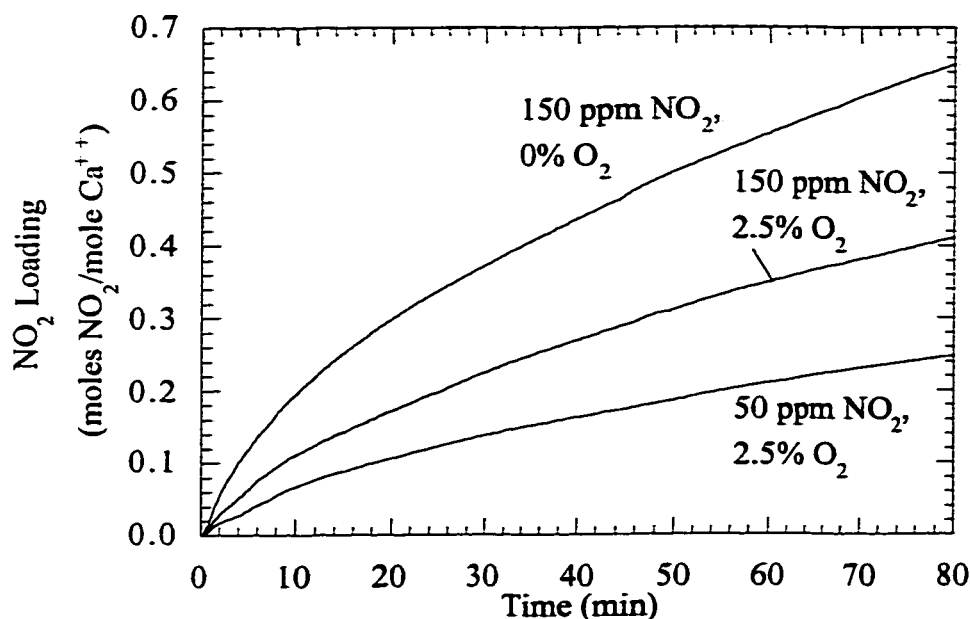


Figure 5.3.4 Effect of O₂ and NO₂ on NO₂ removal.

The experiment was performed at 19% RH, 250 ppm HCl, 1000 ppm SO₂, 120 °C, 36 mg calcium silicate, and 1.5 SLPM, Exp. Nos. CS18-20.

Assuming that the only reaction products of HCl, SO₂, and NO₂ with calcium silicate were the chloride, sulfite (or sulfate), and nitrate (or nitrite) salts of calcium, there was a limit to the absorption capacity of the sorbent. Based on the stoichiometry of these salts, utilization can be defined in terms of the moles of HCl, SO₂, and NO₂ loaded onto the solids:

$$\text{utilization} = \frac{\frac{1}{2}n_{\text{HCl}} + n_{\text{SO}_2} + \frac{1}{2}n_{\text{NO}_2}}{n_{\text{Ca}}} \times 100$$

If only calcium salts were the reaction products, the maximum utilization would have been 100%. However, in the experiments with NO₂ and O₂,

utilization was calculated to be as high as 167% with SO₂ absorption accounting for 104% utilization. This fact suggested that there may be other reaction products. Others (Nelli, 1997; Jarvis et al., 1985) have found sulfur-nitrogen species such as hydroxyaminedisulfonate (HADS) and aminedisulfonate (ADS) when reaction systems have included SO₂ and NO₂. With respect to stoichiometry, neither HADS nor ADS consume any of the available calcium or sodium. Therefore, any sulfur-nitrogen compound formation would be like “free” reactivity because the SO₂ or NO₂ absorption would not be at the expense of alkalinity.

An ion chromatography method was developed similar to Nelli's (1997) to analyze for HADS and ADS (see Appendix D). Reaction products were recovered from the reactor at the end of experiments with conditions of Exp. Nos. CS20 and CS30 and analyzed to determine the reaction products. The conditions of the experiment were set to maximize SO₂ absorption: high humidity (19% RH), low HCl concentration (0 and 250 ppm), high SO₂ concentration (1000 ppm), and high NO₂ concentration (150 ppm) with O₂ added (2.5%). Surprisingly, only chloride, sulfate, nitrate and low levels of nitrite and sulfite were present in the reaction products solution. No HADS, ADS, or any other unidentified peaks were seen. A mass balance for the sulfur closed to within 7 and 8% of the gas phase mass balance for Exp. Nos. CS30 and CS20, respectively. With Exp. No. CS30, the nitrogen balance of the reaction products closed to within 11% of the gas phase balance. Though calculations for chlorine and nitrogen balances were less precise with Exp. No. CS20 due to overlapping chromatograph peaks, mass balances for chlorine and nitrogen closed within 20% and 5%, respectively. See Appendix D for the detailed calculations.

The inconclusive results of the IC analysis made it difficult to confidently ascertain the reaction products. It is possible that the true reaction products changed when the solids were dissolved in water at room temperature.

It was also suspected that the production of H₂SO₄ in the layer of surface water on the solids may have accounted for the SO₂ absorption in excess of 100% utilization. When the reacted solids were removed and dissolved in 100 ml water,

the pH of the resulting solution was measured to be 4.3. If it were assumed that all the acid gas loading over 100% utilization was due to H₂SO₄ formation, the pH of the solution with the reacted solids would have to have been approximately 2.9. A potentiometric titration of fresh calcium silicate solids was performed to check for the existence of any buffers such as bicarbonate that may have led to utilization in excess of 100%. No buffers were found. In summary, the results of the IC analysis, the pH calculation of the reacted solid solution, and the potentiometric titration did not lend any clear insight to the mechanism of the "super-absorption" of SO₂.

5.3.3 Effect of NO

It was not expected that the addition of NO would increase SO₂ reactivity. Within experimental error, this hypothesis was proven correct (see Figure 5.3.5). However, the simultaneous addition of NO and O₂ to the simulated flue gas increased SO₂ absorption. When both NO and O₂ were present, low levels of NO₂ were seen in the IR spectrum. It is likely that the reaction



took place in the experimental equipment, perhaps in the water vaporization furnace. This low level of NO₂ in the reactor inlet then led to slightly increased levels of SO₂ absorption. The elevated final SO₂ loading of 0.33 moles SO₂/mole Ca⁺⁺ was considerably less than the final loading of 0.73 SO₂/mole Ca⁺⁺ when the gas inlet included 50 ppm NO₂.

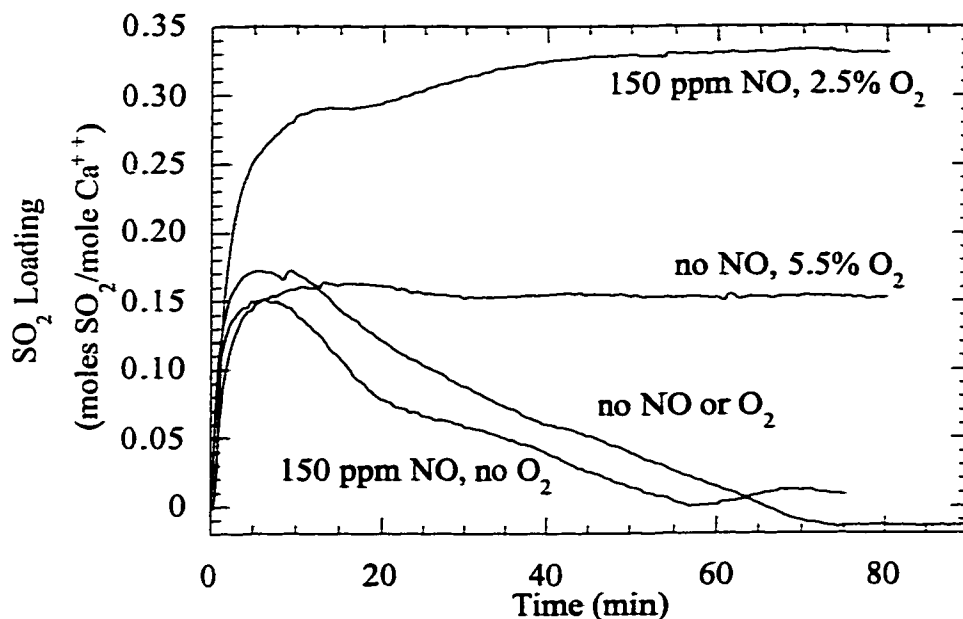


Figure 5.3.5 Effect of NO on SO₂ loading in the presence of HCl.

The experiments were performed at 19% RH, 250 ppm HCl, 1000 ppm SO₂, 120 °C, 36 mg calcium silicate, and 1.5 SLPM. Exp. Nos. CS. 15-16, CS21-22

5.3.4 Effect of Varying Relative Humidity

All of the experiments discussed above were performed at 19% RH. It was shown earlier that increasing relative humidity above 3.5% had no positive effect on HCl reactivity. However, it was expected that high humidity levels would provide for increased reactivity of SO₂ and NO₂. 19% RH at 120 °C corresponds to 35 vol% water vapor, a concentration greater than what is generally found in most municipal waste combustor and coal-fired boiler flue gases. Therefore, two additional experiments, both at 120 °C, were conducted at

9% RH (16 vol% water) and 0.8% RH (1.5 vol% water). The comparison of these experiments with the one conducted at 19% RH is shown in Figure 5.3.6:

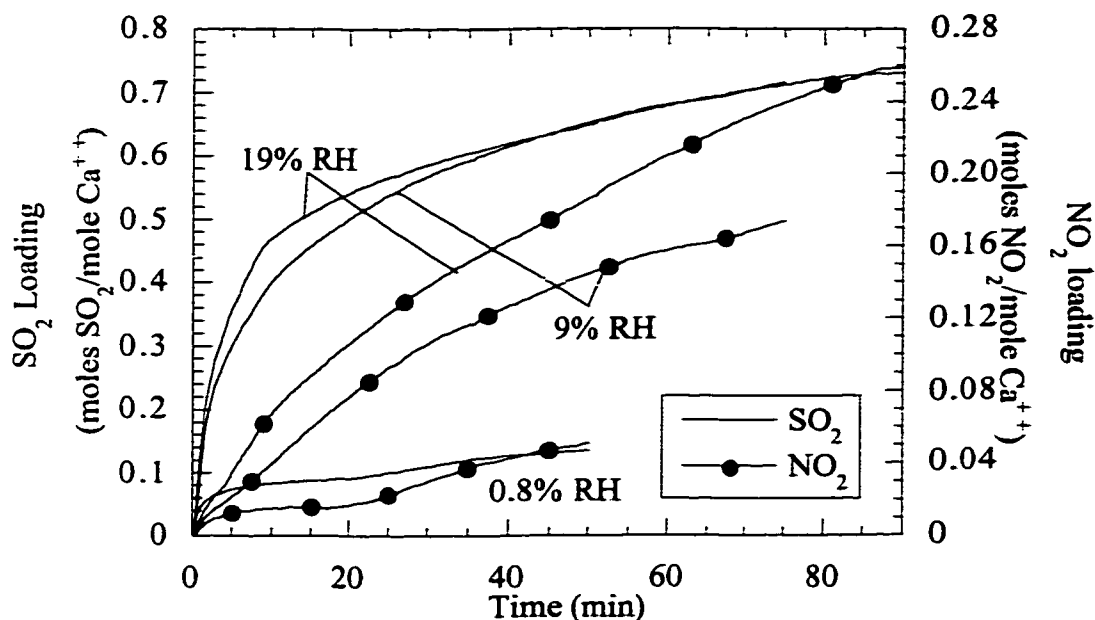


Figure 5.3.6 Effect of relative humidity on SO₂ and NO₂ loading in the presence of HCl.

Experiments were performed at 250 ppm HCl, 1000 ppm SO₂, 50 ppm NO₂, 120 °C, 36 mg calcium silicate, and 1.5 SLPM. Exp. Nos. CS18, CS23-24.

The final HCl loading for the 9 and 19% RH experiments shown in Figure 5.3.6 was essentially the same at 0.74 and 0.68 moles HCl/mole Ca⁺⁺, respectively. These data show that, within experimental error, HCl and SO₂ reacted the same under these conditions at 9 and 19% RH. As shown in Figure 5.1.1, it was not expected that HCl absorption would change between the 9 and 19% RH. However other experiments involving just SO₂ showed increased SO₂ loading when gas phase humidity was increased from 3.5 to 19%. Because the

HCl loading profile for the two high humidity experiments were the same, the SO₂ that passed through the sorbent bed was exposed to the same mass of the chloride salt in both experiments. It appears that the deliquescent nature of calcium chloride caused a fixed level of surface moisture to be associated with the solids in both high humidity experiments. Therefore, the important parameter that dictated SO₂ absorption was surface moisture, not vapor phase water concentration. Provided there was enough NO₂ and O₂ available to prevent the emission of SO₂, the calcium chloride bound to the solids acted to eliminate relative humidity as the important variable. Experiments were performed without HCl at 9 (CS33) and 19% (CS34) RH and 120 °C with 1000 ppm SO₂, 150 ppm NO₂, and 2.5% O₂. The experiment at 9% RH showed a final SO₂ loading of 0.76 moles SO₂/mole Ca⁺⁺ while the experiment at 19% RH had a final SO₂ loading of 0.91 moles SO₂/mole Ca⁺⁺. These results along with those presented in Figure 5.3.6 supported the idea that the presence of calcium chloride on the surface of the sorbent compensated for differences in gas phase humidity.

When the relative humidity was dropped to 0.8% RH, the HCl loading at the end of the experiment dropped to 0.34 moles HCl/mole Ca⁺⁺. Without sufficient calcium chloride associated with the solids or enough gas phase humidity, the reactivity of SO₂ dropped considerably. Though there was sufficient NO₂ and O₂ to prevent emission of SO₂, there was insufficient moisture to induce appreciable absorption of SO₂.

5.3.5 Effect of Varying Inlet SO₂/HCl Ratio

Most of the experiments discussed thus far were conducted with 250 ppm HCl and 1000 ppm SO₂. When these concentrations were reversed, reactivity of HCl was increased considerably at the expense of SO₂ reactivity. The data showing this behavior are shown in Figure 5.3.7. Both experiments indicated that in the presence of 50 ppm NO₂ and 2.5% O₂, both HCl and SO₂ loading increased dramatically with increasing gas concentration.

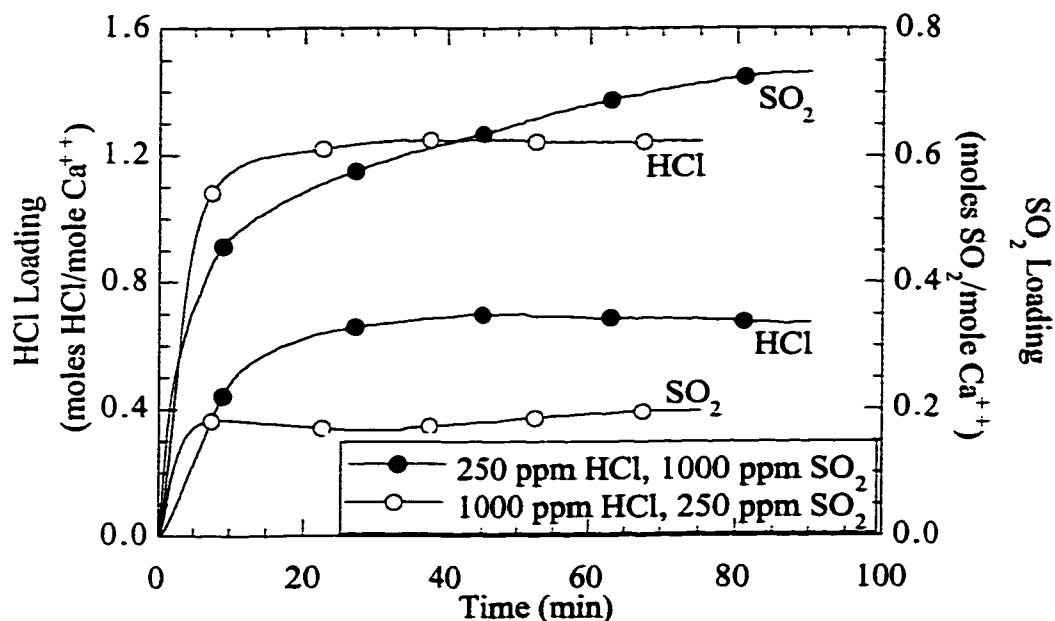


Figure 5.3.7. Effect of HCl/SO₂ ratio on HCl and SO₂ Loading.

Experiments performed at 19% RH, 120 °C, 50 ppm NO₂, 2.5% O₂, 36 mg calcium silicate, and 1.5 SLPM. Exp. Nos. CS18, CS25.

5.4 SO₂-NO_x-O₂ AND CALCIUM SILICATE

As shown in Figure 5.3.2, the final SO₂ loading in the presence of HCl increased from 0.15 to 1.04 moles SO₂/mole Ca⁺⁺ when 150 ppm NO₂ was added to the gas phase. Nelli (1997) observed an increase in final SO₂ loading from 0.71 to 0.91 moles SO₂/mole Ca⁺⁺ with the addition of 223 ppm NO₂ at 70 °C and 60% RH with no HCl in the inlet gas. To better understand the role of temperature in the SO₂-NO₂ interaction, several experiments were conducted at varying temperatures in the absence of HCl. Three experiments, performed at 150 °C, are shown in Figure 5.4.1.

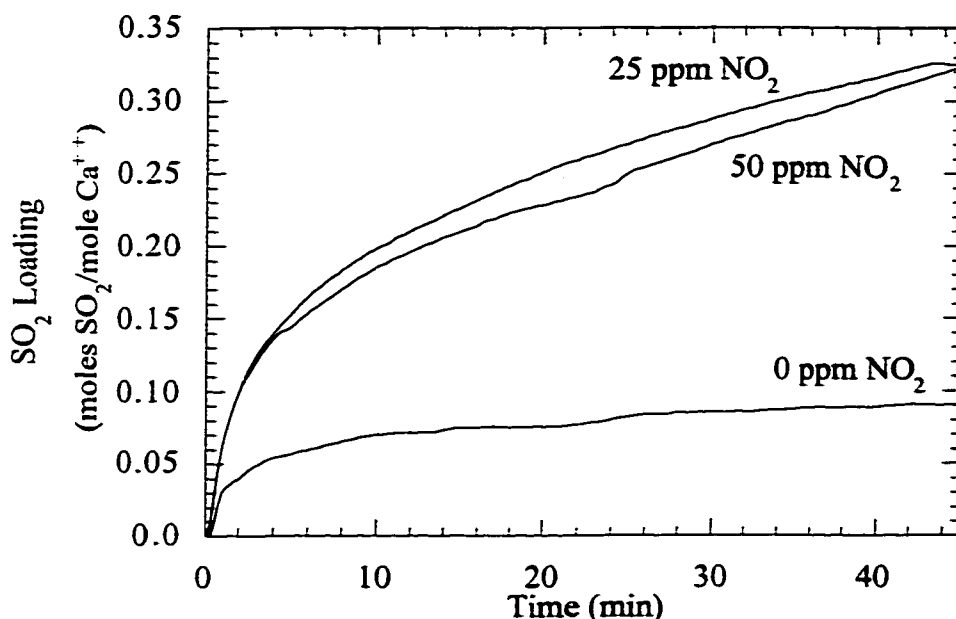


Figure 5.4.1 Effect of NO₂ on SO₂ loading at 150 °C.

The experiments were conducted at 1.5% RH, 150 °C, 0 ppm HCl, 1000 ppm SO₂, 2.5% O₂, 36 mg calcium silicate, and 1.5 SLPM. Exp. Nos. CS26-28.

This set of experiments suggested that there existed a ceiling concentration of NO₂ above which additional NO₂ did not assist SO₂ absorption. The maximum benefit of NO₂ addition at 150 °C was seen at some concentration less than or equal to 25 ppm NO₂. Assuming that the presence of HCl did not strongly impact the SO₂-NO₂ interaction, Figure 5.3.2 shows that changing NO₂ concentration from 50 to 150 ppm had a definite positive influence on SO₂ absorption. It may be concluded then that at 120 °C, the ceiling level of NO₂-assisted SO₂ absorption was above 150 ppm NO₂.

As seen in Figure 5.4.1, the addition of 25 ppm NO₂ to 1000 ppm SO₂ at 1.5% RH and 150 °C increased final SO₂ loading from 0.090 to 0.32 moles

SO₂/mole Ca⁺⁺ or by 356%. Experiments were also conducted at 10% RH and 90 °C. The results are shown in Figure 5.4.2. Increasing the NO₂ concentration from 0 to 150 ppm increased final SO₂ loading from 0.31 to 0.54 moles SO₂/mole Ca⁺⁺ or by 74%. It is clear that low levels of NO₂ can have a much greater positive impact on SO₂ absorption at higher temperature.

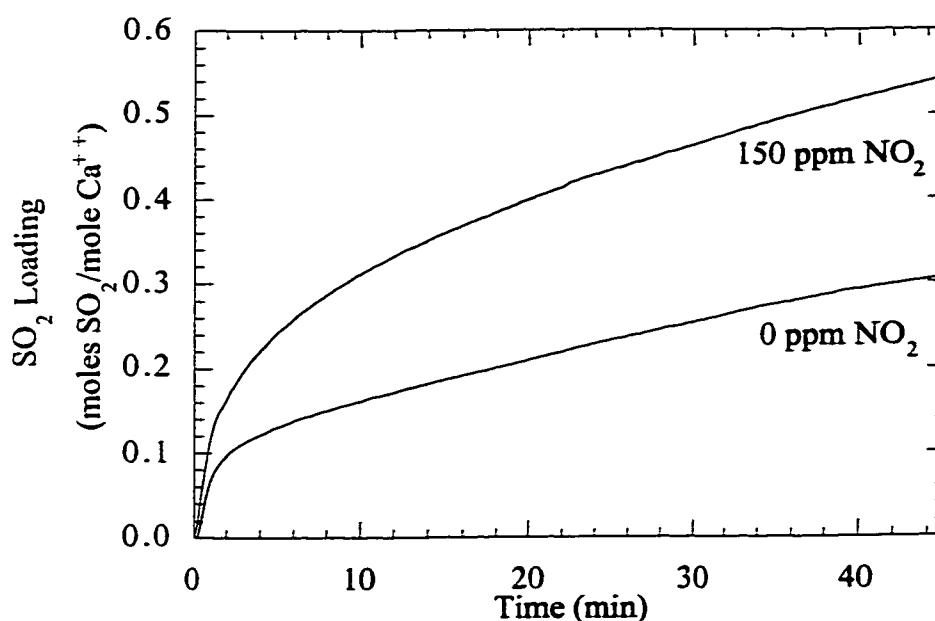


Figure 5.4.2 Effect of NO₂ on SO₂ Loading at 90 °C.

Experiments conducted at 10% RH, 90 °C, 1000 ppm SO₂, 2.5% O₂, 36 mg calcium silicate, 1.5 SLPM. Exp. Nos. CS29-30.

The experiments conducted at 1.5% RH and 150 °C had the same water vapor concentration as those at 10% RH and 90 °C. In a real system, these two conditions represented the same gas except that the gas at 90 °C had been cooled more than the gas at 150 °C. It is clear that SO₂ absorption is greater at the lower temperature and greater relative humidity. Even if a high level of NO₂ (≥ 25 ppm NO₂) is present in the high temperature flue gas, SO₂ loading and sorbent

utilization will not increase beyond the low temperature utilization even with no NO_2 present.

5.5 SUMMARY

With HCl as the only acid gas, utilization and removal increased with increasing relative humidity from 0 to 3.5% RH. No increase in HCl reactivity was seen with increased relative humidity from 3.5 to 19% RH. HCl absorption was determined to be first order in HCl concentration from 250 to 3250 ppm.

The trends with SO_2 absorption as a function of relative humidity and concentration by calcium silicate solids closely resemble those with the SO_2 -hydrated lime system. Increased relative humidity increased final sorbent loading and SO_2 removal. Decreased SO_2 concentration led to greater maximum SO_2 removal. However, experiments at 500 and 1000 ppm SO_2 converged to the same loading after 40 minutes.

In the absence of any oxidizing species (O_2 or NO_2), feeding HCl and SO_2 simultaneously led to HCl reacting completely with any deposited S(IV). Therefore, the solids at the end of the experiment had a loading of HCl but no SO_2 . With the addition of O_2 , loaded S(IV) was oxidized to S(VI). This oxidation led to a nonzero loading of SO_2 at the end of experiments. At low HCl and high SO_2 concentration, adding 150 ppm NO_2 helped the calcium silicate solids to absorb almost seven times the SO_2 absorbed in the absence of NO_2 . It is suspected, but was not proven, that this increase in calcium silicate reactivity may be due to the formation of sulfur-nitrogen compounds that do not consume calcium ions. The simultaneous addition of NO and O_2 improved SO_2 reactivity probably due to the formation of NO_2 upstream of the reactor. In gas systems with a high HCl concentration and low SO_2 concentrations, loading of HCl increases at the expense of SO_2 loading. The reverse was also true with gas systems where SO_2 concentration was high and HCl concentration is low.

In studies with SO_2 , NO_2 , and O_2 in the absence of HCl, low concentrations of NO_2 were found to facilitate greater SO_2 absorption at higher temperature. Experimental evidence suggested that at a given temperature there

existed an NO₂ concentration above which no added SO₂ loading took place. This NO₂ concentration ceiling decreased with increasing temperature.

Chapter 6. Experimental Modeling and Bag Filter Performance Predictions

Chapters 4 and 5 describe the results from experiments where HCl absorption was quantified and conclusions were drawn regarding the interactions among HCl, SO₂, NO₂, and O₂. The objective of this study was to predict HCl and SO₂ absorption by hydrated lime and calcium silicate solids in a bag filter absorption system. Clearly, the operation of the fixed-bed reactor apparatus used to extract gas-solid reaction data is different than that of a bag filter. However, the data from the fixed-bed reactor can be used to extract absorption rates. The rate expression derived from the experimental data can then be used to predict the performance of a bag filter with conditions similar to those of the experiments.

The primary objective of modeling the experimental results was to match the data with a set of equations that accurately described HCl and SO₂ concentration over the course of an experiment. The primary objective was *not* to prove conclusively any of the gas-solid reaction models discussed in Chapter 2.

This chapter discusses the mass balance employed to account for HCl and SO₂ absorption in the fixed-bed reactor. Projections are given for the performance of HCl and SO₂ absorption by hydrated lime and calcium silicate solids on the surface of a bag filter at diverse operating conditions.

6.1 MODELING APPROACH

6.1.1 Integral Fixed-Bed Reactor Mass Balance

The first step to modeling the gas system was to set up the appropriate mass balance equations for the absorption of a gas by a solid in a fixed-bed reactor. With the downflow reactor shown in Figure 6.1.1, it was assumed that the gas flowed with a flat velocity profile through the sorbent. This assumption is justified by the existence of at least a 1 psi pressure drop through the sorbent bed and frit. Non-steady state experiments were performed under integral conditions where there existed a concentration gradient through the bed in the same direction

as gas flow. The gas concentration as a function of time and distance is described by Equation 6.1:

$$F_A = \frac{\partial C_A}{\partial t} - \frac{Q}{aA_x} \frac{\partial C_A}{\partial z} \quad (6.1)$$

where F_A is the flux of A to the sorbent in the fixed-bed, C_A is the concentration of species A, t is experimental time, z is distance in the bed, Q is the gas flowrate, a is the sorbent surface area per unit volume, and A_x is the cross-sectional area of the reactor. In most cases, the time derivative is much less than the spatial derivative (von Rosenberg et al., 1977). Therefore, Equation 6.1 can be reduced to

$$F_A = - \frac{Q}{aA_x} \frac{dC_A}{dz} \quad (6.2)$$

The solid phase reactivity is described by Equation 6.3:

$$F_A = - \frac{\alpha}{a} \frac{dC_S}{dt} = \frac{\alpha}{S_m} \frac{dx}{dt} \quad (6.3)$$

where C_S is the concentration of the sorbent, α is a stoichiometric factor ($\alpha = 2$ for HCl; $\alpha = 1$ for SO_2), S_m is the molar surface area of the sorbent, and x is conversion.

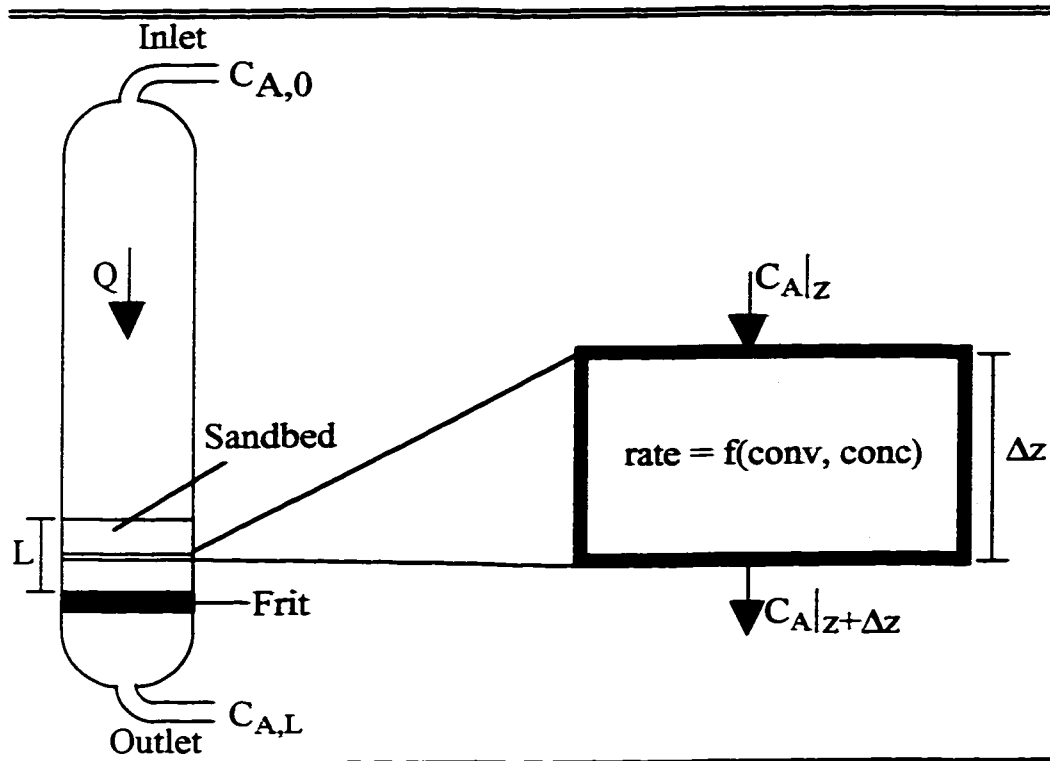


Figure 6.1.1 Schematic of fixed-bed reactor for the finite element analysis.

Experimental time and reactor distance from Equations 6.2 and 6.3 can be discretized, thereby transforming a differential equation into an algebraic equation:

$$F_A = \frac{Q}{aA_x} \frac{C_{A|t,z} - C_{A|t,z+\Delta z}}{\Delta z} = \frac{\alpha}{S_m} \frac{x_{|z,t+\Delta t} - C_{A|z,t}}{\Delta t} \quad (6.4)$$

Using Euler's method, expressions for $C_{A|z+\Delta z}$ at a given t and $x_{|t+\Delta t}$ at a given z are given by

$$C_{A|z+\Delta z} = C_{A|z} - \frac{aA_x \Delta z}{Q} F_{A|z} \quad (6.5a)$$

$$x_{|t+\Delta t} = x_{|t} + \frac{S_m \Delta t}{\alpha} F_{A|z} \quad (6.5b)$$

Because Euler's method was employed, care was taken to ensure that sufficiently small time and distance steps were taken during parameter estimation calculations. During an estimation, time and distance intervals were reduced until a decrease in an interval led to zero decrease in the sum of squares to three significant figures. Discretizing the sorbent bed into 100 slices and performing calculations once for every three second interval generally minimized the sum of squares to three significant figures.

To estimate parameters in a flux equation (discussed in Section 6.1.2), calculations began at the top of the reactor at time zero. See Appendix E for the FORTRAN code that performed the reactor integration. The spatial boundary condition was the inlet concentration of acid gas to the bed, a constant, for each time step. The initial condition was a sorbent conversion of zero for each spatial step throughout the bed. With these two conditions, the flux was calculated through the bed from the inlet to the outlet at time τ . A spatial mass balance in a finite element generated the inlet to the next finite element downstream. Another mass balance in the finite element determined the conversion for the next time step in the same element. Calculations were performed through the bed to generate an outlet concentration, $C_{A,L}|\tau$ from the reactor at time τ .

For SO_2 , $C_{\text{SO}_2,L}|\tau$ was compared directly to the datum taken at time τ , $C_{\text{SO}_2}|\tau$. However, with the more soluble HCl, water absorption on the surfaces of the gas cell caused confounding effects. Therefore, the gas cell surfaces were modeled as a well-mixed absorber/stripper where $C_{\text{HCl},L}|\tau$ was the inlet to the gas cell. The equation used to generate a modeled concentration, $C_{\text{HCl}}^o|\tau$, to a concentration datum obtained at the same t , $C_{\text{HCl}}|\tau$, is given below:

$$C_{\text{HCl}}^o|\tau = C_{\text{HCl},L}|\tau - \frac{c}{\Delta\tau} (C_{\text{HCl},L}|\tau - C_{\text{HCl}}^o|\tau - \Delta\tau) \quad (6.6)$$

where c is an empirical parameter estimated uniquely for each experiment. The driving force in Equation 6.6 accounted for molecules of HCl stripping out of or absorbing into the water layer on the surfaces of the gas cell.

Once outlet concentrations were generated from the model at time τ , they were compared to the data taken for the same time. The same calculations through the bed were performed for each of the time intervals and compared to the experimental data. Once this was completed for an entire experiment, parameters were adjusted to improve the fit and the calculations started again from the top of the bed at time zero.

6.1.2 Development of Flux Equation

Difficulty with modeling arose not with the mass balances discussed above but with the identification of an accurate equation describing the flux of the acid gases, F_A . As it was discussed in Chapter 2, many researchers have employed shrinking core models, either with particles or grains within particles. These models described the rate of absorption of an acid gas as being dictated by mass transfer resistances in series. In most systems with small particles, the gas film and pore diffusion resistances do not limit the rate of gas absorption. At early times in an experiment before a product layer has deposited on the surface of a reactant particle, the rate of gas absorption was limited only by the kinetics of the surface reaction. As the acid gas continued to react with the sorbent particle, a product layer formed. This product layer then acted as a barrier between the gas and the reactive solid core of the particle, thereby limiting the rate at which the gas was absorbed. Assuming first order kinetics and diffusion through the product layer were the limiting rates in gas absorption, the following equation describes the flux of gas A:

$$R_{A/S} = F_A = \frac{C_A}{\frac{1}{k_s} + \frac{\delta}{D_A}} \quad (6.7)$$

where k_s is the first order surface rate constant, δ is the product layer thickness, and D_A is the diffusion coefficient of the diffusing species through the product layer.

In developing Equation 6.7, planar rather than spherical geometry was used. This was done primarily to simplify the flux expression. Because the internal surface area of the sorbents studied is much greater than the external surface area, this assumption seems reasonable. In addition, when the sorbents absorbed the acid gases studied, the volume of the particles expanded. This expansion of the particle was discussed in Section 2.2.3. This effect was ignored again in the interest of simplicity. As shown in Equation 6.7, the flux was a function of the product layer thickness. This thickness was not measured at any time. Because conversion, x , was proportional to product layer thickness, δ was replaced by $\delta_0 x$.

Throughout the literature and in this study, it was apparent that most sorbents generally were not totally converted from the alkaline particle to the salt product. At some point during an experiment, the absorption rate declined to zero despite the fact that there was still unreacted sorbent in the reactor. However, the shrinking core model predicts that the rate will not drop to zero until all the sorbent has been consumed. Reasons for incomplete utilization, including pore plugging and crystal fracture, were discussed in Section 2.2.3. Because of the discrepancy between the shrinking core model and the experimental results, a driving force based on conversion was added to Equation 6.7:

$$F_A = \frac{C_A(x_T - x)}{\frac{1}{k_s} + \frac{\delta_0 x}{D_A}} \quad (6.8)$$

x_T is defined as the conversion when reactivity of the sorbent terminated. The three regressed parameters in Equation 6.8 are x_T , k_s , and D_A/δ_0 . Throughout this chapter, the value D_A/δ_0 will be referred to as $D_{A,eff}$. Principles leading to Equation 6.8 are used with both the single gas system (HCl) and with the multi-gas system (HCl and SO₂). However, another modification to the flux equation for SO₂ was found to be necessary. This modification will be discussed later in this chapter.

This modification to the shrinking core equation and the other assumptions discussed above led to a semiempirical model for the flux. However, the primary objective of the modeling of experiments was to describe the data. The goal of modeling was not to conclusively determine an absorption mechanism or exact physical constants.

6.1.3 Parameter Estimation Package

The parameter estimation package utilized, Generalized REGression (GREG), is a nonlinear estimation package that is suitable for single and multi-response data (Caracotsios, 1986) written in FORTRAN. GREG, Level 10 was employed in this work to estimate parameters with multi-variable inputs but only one response vector. Code was written to link GREG with the fixed-bed integration routine. Solutions are determined through the minimization of an objective function given by Equation 6.9:

$$G(\Omega) = \sum_{\tau=0}^n \left(\frac{C_{A^0}|\tau}{C_{A,0}} - \frac{C_{A}|\tau}{C_{A,0}} \right)^2 \quad (6.9)$$

where G is the objective function, Ω is the vector of parameters being estimated, τ is time, n is the number of data points available, $C_{A^0}|\tau$ is the modeled A concentration in the gas cell at time τ , $C_{A}|\tau$ is the experimental concentration of A in the gas cell at time τ , and $C_{A,0}$ is the reactor inlet HCl concentration. A comprehensive treatment of the numerical methods used to converge to Ω can be found in Caracotsios' dissertation (1986) or in Stewart et al. (1992).

After converging to a solution vector Ω , estimates from GREG of the parameters were given as well as 2σ confidence intervals, and the normalized covariances of the parameter estimates. The integration routine output estimates of $C_{A^0}|\tau$, the concentration at the end of the reactor, $C_{A,L}|\tau$, and average conversion of the solids in the bed.

6.1.4 Bag Filter Performance Model

The objective of the modeling effort was to project how well hydrated lime and calcium silicate would perform absorbing HCl and SO₂ on the surface of a bag filter. The bag filter system is different physically from the experimental system used in this study. In the fixed-bed reactor, high concentration acid gas contacts highly converted sorbent in the front of the reactor. Conversely, in a bag filter the high concentration gas will pass through fresh sorbent first and will contact the most highly converted solids just before it escapes the filter. In addition, the bag filter system has sorbent continually added to the filter cake whereas the experimental system has a batch loading of sorbent.

Because of these differences, predicting how well a sorbent would perform under given circumstances was not straightforward using only the experimental data. The bag filter performance model (FORTRAN code archived in Appendix E) assumed that the flux expressions that govern the absorption of HCl and SO₂ in the experimental system also described the flux expressions for the baghouse. Also, it was assumed that the sorbent contacts the surface of the bag to form a uniformly thick layer. No reaction took place in the duct between the introduction of the sorbent and when it reached the baghouse. In addition, it was assumed that the presence of any other contaminants, gas or solid, would not influence the acid gas absorption. Changes in pressure drop with increased filter cake thickness were not calculated or considered in any fashion.

One of the key operational conditions that impacted the performance projections was the sorbent feed ratio. This ratio was the number of moles of sorbent fed to the system divided by the number of moles needed to remove all the acid gas assuming 100% conversion of the solids by simple acid-base reactions. For example, if one mole each of SO₂ and HCl entered a flue duct, a sorbent feed ratio of 2 meant 3 moles ($2 \times (1 \text{ mole} + 0.5 \text{ moles})$) of sorbent was fed into the duct.

The second important operational variable in a bag filter system was the cycle time -- the period between cleanings of the bag. Bag filters are generally cleaned by a reversed air stream, a pulse jet, or are simply shaken. After a bag

was cleaned, it was assumed that there was no cake on the surface of the filter. Consequently, removal from that bag was lowest immediately after being cleaned and increased with increasing cycle time.

The calculations for bag filter performance used the surface of the filter as the origin. As the cycle time continued, the filter became thicker. As the cake grew away from the filter, the spatial boundary condition moved with the outermost layer. Over time, t^* , the average penetration of gas A was defined as the time average of the instantaneous penetration of A from 0 to t^* :

$$\begin{aligned} \text{Average Penetration of A} = \\ 1 - \text{Removal of A} = \frac{1}{t^*} \int_0^{t^*} \frac{C_A(t) dt}{C_{A,in}} \end{aligned} \quad (9)$$

where $C_A(t)$ is the instantaneous concentration of A leaving the baghouse and $C_{A,in}$ is the inlet concentration of A to the baghouse.

The quality of the bag filter performance projections were only as good the model fit of the data. The experiments attempt to quantify phenomena as accurately and precisely as possible. Imperfections with the data and the modeling, then, will multiply and may manifest in the performance projections. Consequently, caution should be used such that the precision of the performance projections are not over-estimated.

6.2 MODELING OF HCL-CALCIUM SILICATE

6.2.1 Parameter Estimation

The results of the parameter estimations for the system with calcium silicate absorbing HCl are given in Table 6.2.1. For each of the experiments listed in the table, a separate regression was performed. For the experiments at 3.5, 9, and 19% RH, no effect on HCl absorption was seen when relative humidity, HCl concentration, or sorbent was loading was changed. For this reason, the last seven experiments shown in Table 6.2.1 were regressed simultaneously to produce global absorption parameters.

Regressed values of D_{eff} and x_T were found to be constant at each concentration, loading, and relative humidity from 3.5 to 19%. This was expected as the experiments showed no effect of these variables over the ranges mentioned. The value of k_s , though with considerable scatter, was found to be constant for all the experiments.

There were two minor problems with the parameter estimation results shown in Table 6.2.1. For the experiments at 0.8 and 1.8% RH, the value of x_T was set at the value determined experimentally. Without setting x_T for these two regressions, the routine had difficulty converging on a reasonable solution. In general, the values of k_s were found to have wide confidence intervals. In two of the regressions, the value of k_s was set to the value determined by the global estimation. Problems with x_T at low humidity and k_s arose due to a moderately high (≈ 0.8) normalized covariance between D_{eff} and k_s . The large covariance was probably due to the fact that after a differential element had undergone a few time steps of contact with HCl, x changes at a very slow rate. Consequently, the two terms in the denominator of Equation 6.8 are of similar form -- a constant. Therefore, the value of k_s is determined over only a few time steps before considerable reaction takes place in a finite element. The difficulties in obtaining accurate D_{eff} and k_s values with small confidence intervals persisted throughout the modeling effort.

Table 6.2.1 Results of Parameter Estimation for HCl-Calcium Silicate System

CS Exp No.	Rel. Hum. (%)	HCl Conc. (ppm)	Sorb. Load. (mg)	$D_{eff} \times 10^5$ (m/s)	$k_s \times 10^4$ (m/s)	x_T	Mean Model Error (%) †	Simult. Mean Model Error (%) §
2	0.8	1000	36	0.178	13.6	0.37*	4.05	
2 σ :				0.014	2.2	-		
3	1.8	1000	36	0.275	21.3	0.43*	2.61	
2 σ :				0.032	0.12	-		
This set of parameters are from the simult. modeling of exps. at 3.5-19% RH.								
Exp. Nos. 4-9, 31				2.23	6.22	0.644	-	4.56
2 σ :				0.18	3.25	0.006		
4	3.5	1000	36	1.53	6.22°	0.641	3.86	4.65
2 σ :				0.13	-	0.017		
7	3.5	250	36	2.80	4.88	0.670	4.12	5.72
2 σ :				0.35	2.83	0.009		
8	3.5	500	36	2.35	9.43	0.603	3.77	4.48
2 σ :				0.37	13.30	0.011		
9	3.5	2000	36	1.93	12.0	0.642	3.46	3.49
2 σ :				0.48	10.7	0.024		
31	3.5	1000	72	2.58	15.6	0.617	2.43	6.45
2 σ :				0.14	6.8	0.013		
5	9	1000	36	1.17	6.22°	0.680	4.05	2.73
2 σ :				.069	-	0.011		
6	19	1000	36	2.76	2.67	0.626	2.61	2.67
2 σ :				0.58	1.37	0.012		

All experiments took place at 1.5 SLPM.

† The error reported is the square root of the average model error squared multiplied by 100 when the experiment was modeled individually.

§ The error reported is the square root of the average model error squared multiplied by 100 when the experiments were modeled simultaneously.

* The x_T value was fixed at the value determined by the gas phase mass balance to allow for independent estimation of D_{eff} and k_1 .

° Value was fixed at the value determined by the simultaneous regression value to allow for independent estimation of D_{eff} and x_T .

The mean model error for the set of parameters was an indicator of how well the model fit the data. For the set of data modeled simultaneously, the error for an experiment with the global set of parameters was greater than the error for the individually regressed set of parameters. This was due to the fact that with an

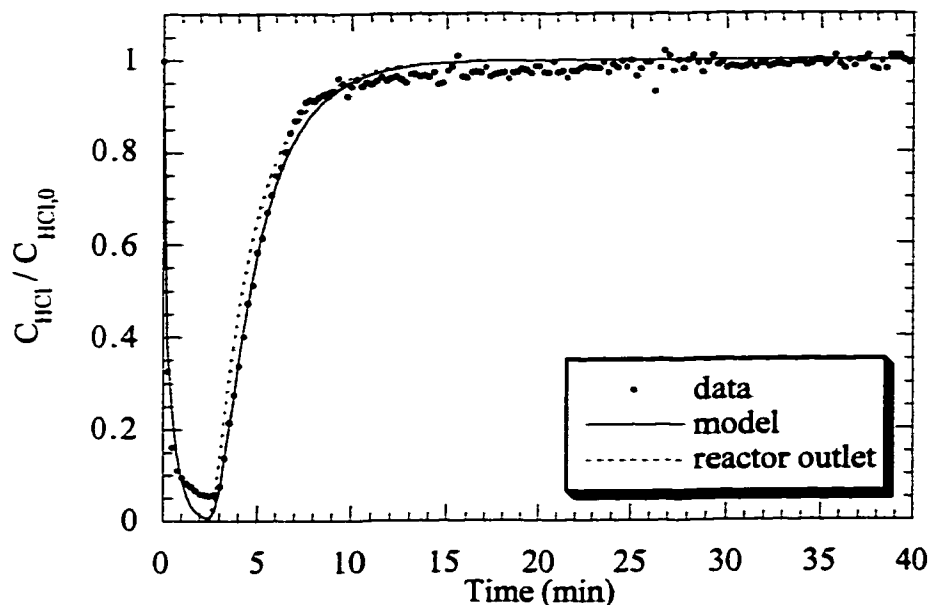


Figure 6.2.1 Best model fit using the parameters from the simultaneous regression of all HCl-calcium silicate experiments greater than 1.8% RH.

Experiment performed at 19% RH, 1000 ppm HCl, 36 mg calcium silicate, 120 °C, and 1.5 SLPM. The mean model error was 2.67%.
Exp. No. CS6.

experiment being regressed individually, the parameters can adjust to any specific trend or error of that experiment. Constrained by a global averaging of sorts from the six other experiments, experimental errors are “averaged out” and the estimation routine can more accurately determine parameters. Plots of the best fit (Exp. No. CS6) and the worst fit (Exp. No. CS31) based on the results from the

simultaneous regression are shown in Figures 6.2.1 and 6.2.2. It is likely that the fit for Exp. No. CS5 was not as good as the other experiments because of either non-uniform dispersion of calcium silicate in the reactor or because of signal drift with the FT-IR.

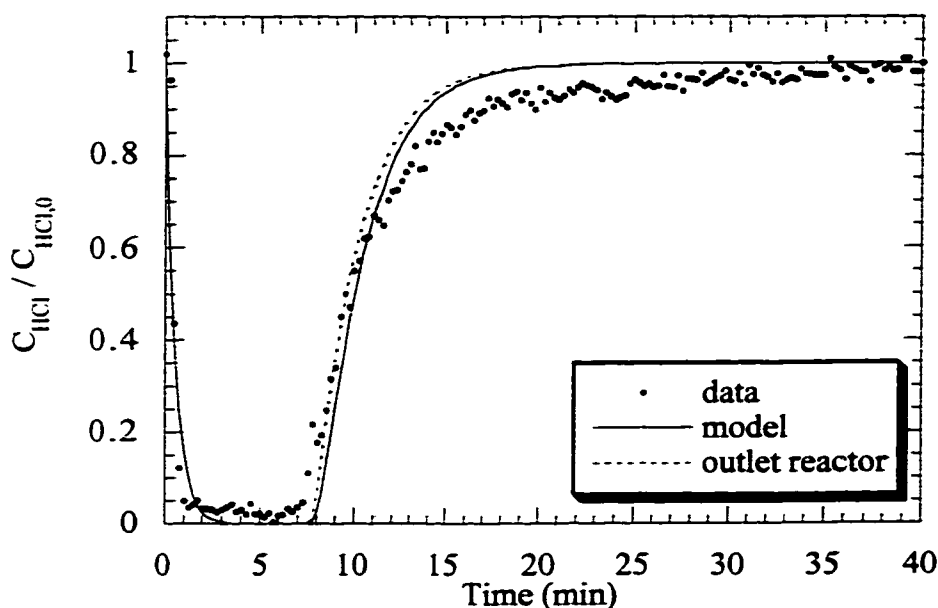


Figure 6.2.2 Worst model fit using the parameters from the simultaneous regression of all HCl-calcium silicate experiments greater than 1.8% RH.

Experiment performed at 19% RH, 1000 ppm HCl, 72 mg calcium silicate, 120 °C, and 1.5 SLPM. The mean model error was 6.45%. Exp. No. CS31.

A parameter that played an important role in fitting the data was the gas cell correction term, c , defined by Equation 6.6. This term took into account adsorption and desorption of HCl on the surfaces in the gas cell. Except for Exp. No. CS5, all the gas cell constants that were determined by the simultaneous regression (c') closely approximated the value of the gas cell constant estimated

with the individual regression (c). The gas cell constant tended to have a low covariance (<0.3) with the other estimated parameters. Table 6.2.2 shows the values of the gas cell constants estimated for both the individual regressions and the simultaneous regression.

Table 6.2.2 Results of Parameter Estimation for the Gas Cell Constant

CS Exp. No.	Relative Humidity (%)	c (s) Individual Regressions [†]	c' (s) Simultaneous Regressions [§]
2	0.8	2.74	
3	1.8	6.27	
4	3.5	9.63	9.21
7	3.5	9.74	10.7
8	3.5	8.97	8.84
9	3.5	8.54	8.94
31	3.5	9.65	9.45
5	9	9.60	6.81
6	19	9.41	9.30

[†] Gas cell correction when the experiment was modeled individually.

[§] Gas cell correction when the seven experiments were modeled simultaneously.

The values for c from one experiment to the next were not the same. This was because, in part, each of the experiments had different dilution air flowrates. Differing dilution rates would induce different adsorption and desorption rates. Also, during experiments with greater relative humidity, the effect of the gas cell was more pronounced because there was more water adsorbed in the gas cell. It was expected that in the experiments with greater humidity, the value of c would also be greater. This trend was apparent when the values for c from the high humidity experiments are compared with those from the low humidity experiments.

6.2.2 Bag Filter Performance Projections

The parameters estimated from the fixed-bed reactor were used to estimate the absorption dynamics of HCl by calcium silicate in a bag filter system. The same flux equation was used for the performance projections as was used in the

fixed-bed modeling. For experiments greater than 1.8% RH at any HCl concentration, the parameters used for the flux equation were the global parameters. A comparison of absorption performance at 3.5% RH versus 0.8% RH is shown in Figure 6.2.3.

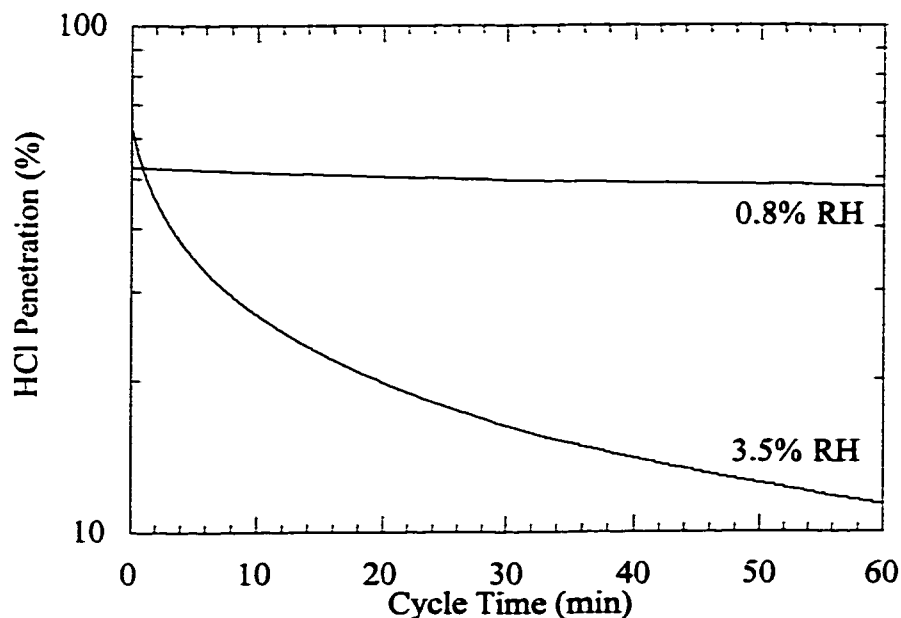


Figure 6.2.3 Penetration of HCl as a function of relative humidity in a bag filter system using calcium silicate as the sorbent. .

Performance projection with 1000 ppm HCl at 120 °C with a sorbent feed ratio of 1.5. The curve at 3.5% RH uses the global parameters given in Table 6.2.1; the 0.8% RH curve uses parameters from the individual regression shown in Table 6.2.1.

Looking first at the 3.5% RH curve in Figure 6.2.3, as cycle time increased the HCl penetration decreased. This was due to the fact that the solids that were added to the filter early in the cycle time are given a long time (up to 60 minutes) to react the maximum conversion possible, x_T . While most of the HCl removal took place at any given time by the fresh sorbent most recently added to the

system, the increasingly thick filter cake allowed solids closer to the surface of the filter to steadily increase HCl removal with cycle time.

Clearly, the penetration of HCl is less at 3.5% RH compared to 0.8% RH. This was expected as the experimental data indicated that an increase in relative humidity increased both reaction rate and sorbent capacity. The slope of the penetration curve for the projection at 0.8% RH was less than the projection at 3.5% RH. The relatively flat curve at 0.8% RH is explained by the values of the parameters determined with the estimation. The value of k_s , 13.6×10^{-4} m/s, was greater than the value of k_s found for the global, high humidity experiments. Conversely, the value of D_{eff} for 0.8% RH was an order of magnitude less than the D_{eff} determined as part of the global, high humidity parameters. The combination of a large k_s and a small D_{eff} led to rapid conversion of the fresh sorbent followed by very slow absorption once any appreciable conversion had been reached. Thus, the model suggested that high HCl removal is possible at early cycle times but an increase in cycle time improved HCl removal only slightly.

As the sorbent feed ratio was increased, HCl absorption at a given cycle time also increased. This trend is evident in Figure 6.2.4. As the sorbent feed ratio increased, the HCl penetration decreased. In addition, the increase in sorbent feed ratio from 1 to 2 decreased penetration more than an increase in sorbent feed rate from 2 to 3.

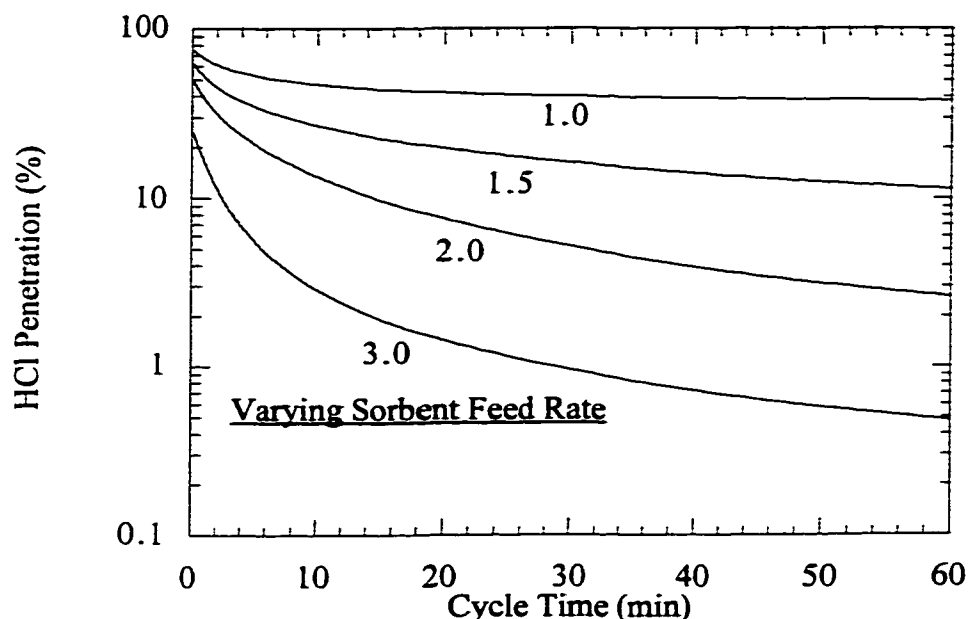


Figure 6.2.4 Penetration of HCl as a function of sorbent feed ratio in a bag filter system using calcium silicate as the sorbent.

Performance projection at 3.5% RH, 1000 ppm HCl at 120 °C.
The curves use the global parameters given in Table 6.2.1.

Figure 6.2.5 shows the effect of varying HCl concentration while holding the sorbent feed ratio constant. As the HCl concentration increases, the mass of sorbent fed to the system also increased. Therefore, there is more sorbent available to react with greater concentrations of HCl. The fraction of HCl absorbed immediately once it contacts fresh sorbent was the same for all concentrations. But because the bed is thicker with more inlet HCl, a greater fraction of HCl is removed by solids at high (but less than x_T) conversion.

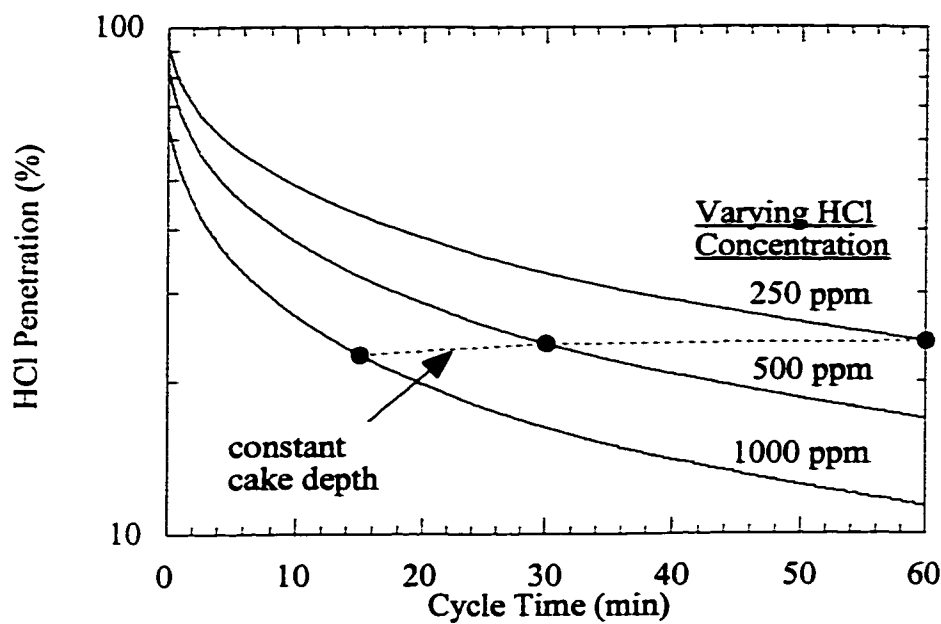


Figure 6.2.5 Penetration of HCl as a function of HCl concentration in a bag filter system using calcium silicate as the sorbent.

Performance projection with a sorbent feed ratio of 1.5, 3.5% RH, and 120 °C. The curves use the global parameters given in Table 6.2.1.

The curve labeled “constant cake depth” in Figure 6.2.5 plots the penetration of HCl at 250, 500, and 1000 if the bag filter was cleaned when sorbent accumulation on the filter reached a given depth. This curve assumed that the only contribution to the filter cake was sorbent addition. Because the sorbent feed rate (*not* ratio) is four times greater with 1000 ppm HCl versus 250 ppm, the time required to accumulate the same cake thickness for the 1000 ppm case was a quarter of the time for the 250 ppm case. When this thickness was reached, the penetration at 250 ppm was essentially the same as at 1000 ppm. The constant cake depth curve was added to point out that when taking pressure drop into

account, increased HCl concentration did not significantly decrease HCl penetration.

Perhaps the most useful depiction of the results of the performance projection is the curve shown in Figure 6.2.6. The utilization, defined as the average through the filter cake of the moles of HCl absorbed corrected for reaction stoichiometry, is an indication of how much of the sorbent is actually used. Ideally, high HCl removal would have been possible at high sorbent utilization. The shape of the curves shown in Figure 6.2.6 illustrates the tradeoff between increasing sorbent utilization while at the same time decreasing HCl removal. This figure indicates that to remove greater than 90% of the inlet gas at

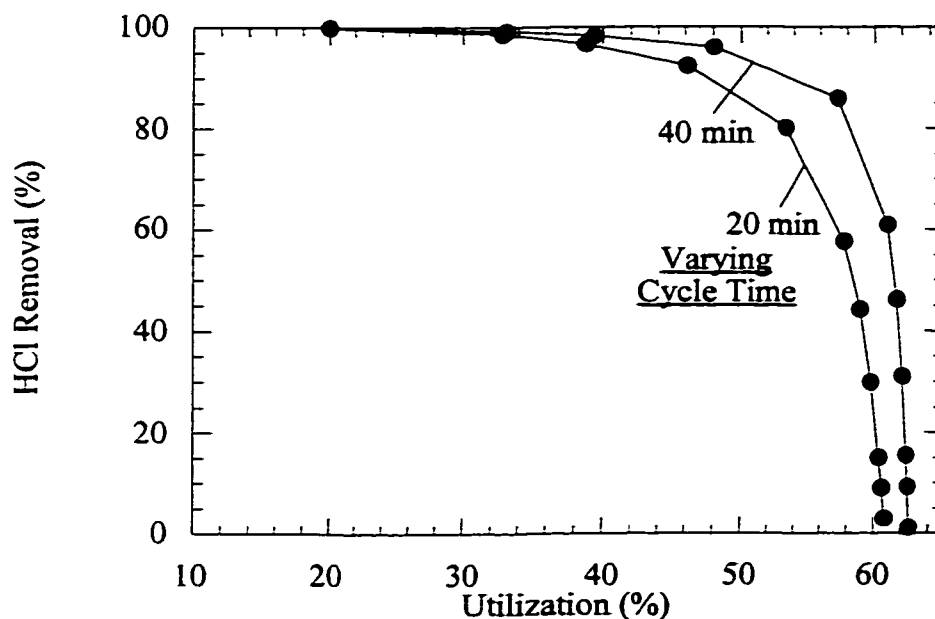


Figure 6.2.6 HCl removal as a function of calcium silicate utilization at varying cycle times.

Performance projection with 3.5% RH, 1000 ppm HCl at 120 °C.
The curves use the global parameters given in Table 6.2.1.

1000 ppm HCl and 3.5% RH, less than half of the sorbent will actually be involved in HCl absorption. A utilization of less than half under these gas conditions with a 40 minute cycle time translates to a sorbent feed ratio of greater than 2.

6.3 MODELING OF HCL-HYDRATED LIME

6.3.1 Parameter Estimation

The focus of parameter estimation for the HCl-hydrated lime system was the experiments conducted at 9 and 19% humidity. As discussed in Chapter 4, the experiments at 0.8 and 3.5% RH exhibited unexpected, transient behavior. Because of the potential difficulty in modeling the data at these low relative humidities, the emphasis of modeling was placed on the high humidity experiments. In addition, the high concentration data (2000 and 3500 ppm HCl) were not modeled because those experiments exhibited different final conversion than the data taken at low and intermediate HCl concentration.

The data for the absorption of HCl by hydrated lime was first modeled with the flux described by Equation 6.8. Using Equation 6.8, the estimation routine systematically overpredicted the rate of HCl absorption in the first five minutes of each experiment. For each of the data sets, 100% removal of HCl was predicted for nearly all the experiments. For this reason, Equation 6.8 was modified to a pseudo-second order dependence on HCl concentration at early experimental times to better describe absorption. At the longer experimental times, HCl absorption was still described as first order in HCl. Equation 6.11 was used as the flux equation for absorption of HCl by hydrated lime:

$$F_A = \frac{C_{HCl}(x_T - x)}{\frac{l}{k_s C_{HCl}} + \frac{x}{D_{eff}}} \quad (6.11)$$

The results of parameter estimation for experiments run at 9 and 19% at concentrations less than 2000 ppm are given in Tables 6.3.1 and 6.3.2,

respectively. Note the different units of k_s' required for the pseudo-second order dependence of the flux on HCl concentration.

Table 6.3.1 Results of Parameter Estimation for HCl-Hydrated Lime System at 9% RH.

HL Exp No.	HCl Conc. (ppm)	Sorb. Load. (mg)	$D_{eff} \times 10^4$ (m/s)	k_s' (m ⁴ /mol/s)	x_T	Mean Model Error †	Simult. Mean Model Error †
Simult. Model			3.20	0.613	0.497	-	4.22
2 σ :			0.36	0.185	0.006		
4	1000	18	3.03	0.352	0.465	3.09	4.13
2 σ :			0.55	0.230	0.011		
29	1000	36	3.90	0.172	0.508	3.48	4.20
2 σ :			0.97	0.063	0.008		
30	500	18	4.33	0.872	0.465	4.29	4.76
2 σ :			0.93	0.568	0.010		

† The error reported is the square root of the average model error squared multiplied by 100.

Table 6.3.2 Results of Parameter Estimation for HCl-Hydrated Lime System at 19% RH.

HL Exp No.	HCl Conc. (ppm)	Sorb. Load. (mg)	$D_{eff} \times 10^4$ (m/s)	k_s' (m ⁴ /mol/s)	x_T	Mean Model Error †	Simult. Mean Model Error †
Simult. Model			2.67	0.160	0.795	-	4.09
2 σ :			0.20	0.015	0.008		
5	1000	18	3.38	0.112	0.748	2.63	3.08
2 σ :			0.46	0.029	0.012		
6	250	18	4.23	0.129	0.802	4.76	5.20
2 σ :			0.98	0.015	0.012		
7	500	18	1.87	0.243	0.794	2.59	3.14
2 σ :			0.11	0.045	0.010		

† The error reported is the square root of the average model error squared multiplied by 100.

There was less difficulty obtaining independent estimates of the D_{eff} , k_s' , and x_T than with the HCl-calcium silicate system. This is probably due to the fact

that the flux equation for hydrated lime had the second order HCl concentration term with k_s' . This left the two terms in the denominator, $1/k_s' C_{HCl}$ and x/D_{eff} with two changing values -- C_{HCl} and x . Because there were two values changing in a finite element, the two terms varied more independently than with the calcium silicate system. As shown by the mean model error, the quality of the fit with the hydrated lime system was comparable to the quality of the calcium silicate system.

6.3.2 Bag Filter Performance Projections

The trends for the bag filter performance predictions were similar to those predicted for HCl-calcium silicate. Figure 6.3.1 shows that increasing relative humidity from 9 to 19% decreases HCl penetration for most reasonable cycle times. The curve for 9% RH is flat because the estimated k_s' was large, 0.613 $m^4/mol/s$. The sorbent reacted to its termination conversion, x_T , the instant that it contacted any HCl. Therefore, the rest of the filter cake between the outer sorbent surface and the actual filter did not react at all with HCl. The absence of any HCl absorption throughout the rest of the filter cake flattens the penetration profile with respect to cycle time. The parameter k_s' had a fairly wide confidence interval which indicated that the fixed-bed data were not particularly sensitive to it. On the other hand, the bag filter performance projection is fairly sensitive to k_s' .

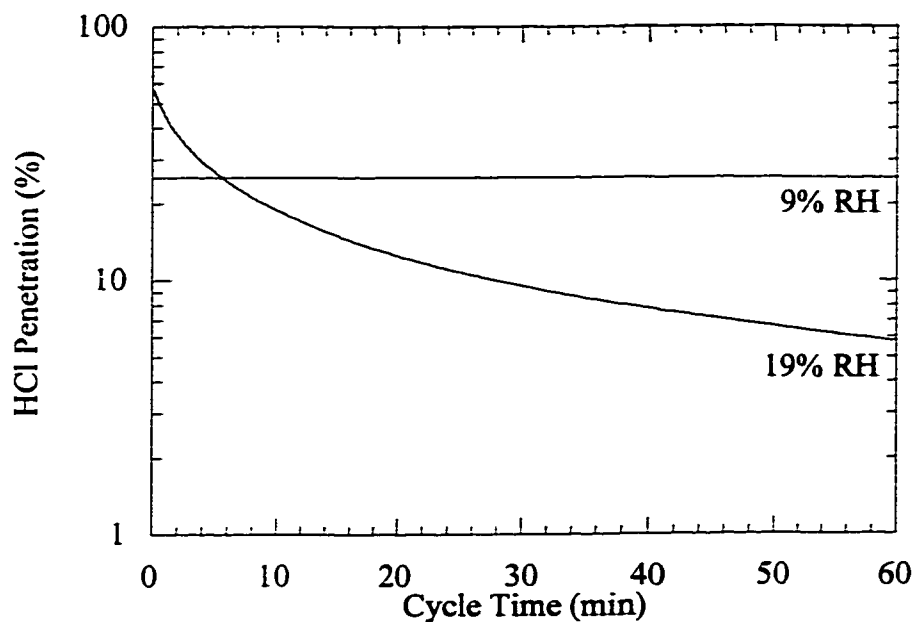


Figure 6.3.1 Penetration of HCl as a function of relative humidity in a bag filter system using hydrated lime as the sorbent.

Performance projection with a sorbent feed ratio of 1.5, 1000 ppm HCl, and 120 °C. The curves use the global parameters given in Table 6.3.2.

Similar to HCl absorption by calcium silicate, the penetration of HCl is greater with hydrated lime as the concentration of HCl decreased. This effect is shown in Figure 6.3.2:

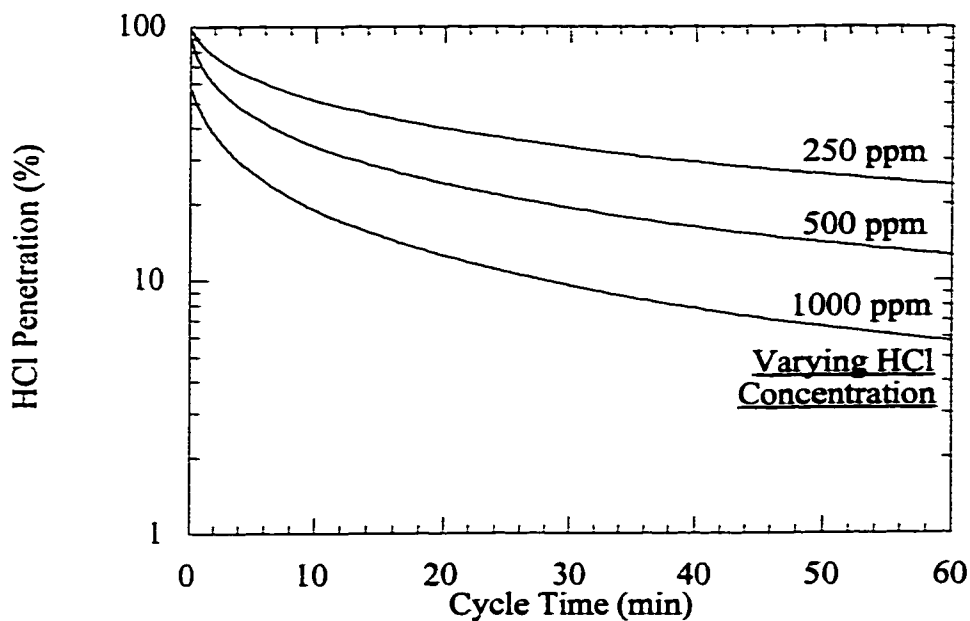


Figure 6.3.2 Penetration of HCl as a function of HCl concentration in a bag filter system using hydrated lime as the sorbent.

Performance projection with a sorbent feed ratio of 1.5, 19% RH HCl, and 120 °C. The curves use the global parameters given in Table 6.3.2.

The plot showing the tradeoff between sorbent utilization and HCl removal is shown in Figure 6.3.3. This figure shows that to achieve 90% removal, only slightly more than half the sorbent will be utilized. A detailed comparison between the performance of hydrated lime and calcium silicate will be discussed in Chapter 7.

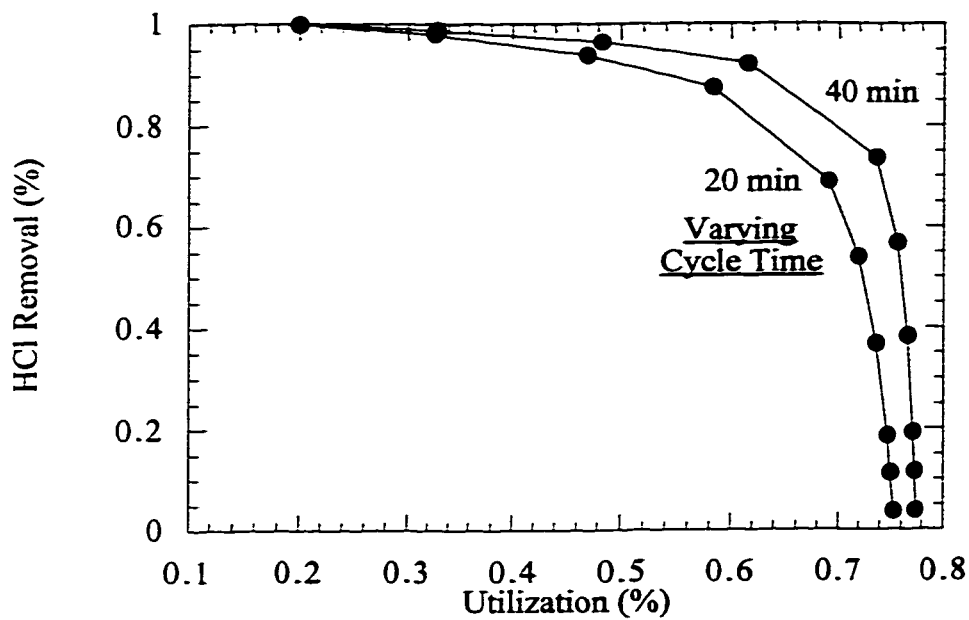


Figure 6.3.3 HCl removal as a function of hydrated lime utilization at varying cycle times.

Performance projection with 19% RH, 1000 ppm HCl at 120 °C.
The curves use the global parameters given in Table 6.2.1.

6.4 MODELING OF HCL-SO₂-CALCIUM SILICATE

6.4.1 Parameter Estimation

The addition of SO₂ to the inlet gas stream led to an increase in the complexity of the modeling approach, especially with the concurrent addition of NO₂ and O₂ with SO₂. Though analysis of the gas system became more complex, the flux equation for HCl was the same as the one used for the HCl-only system given by Equation 6.8. With respect to SO₂ absorption, it was shown in Chapter 5 that the presence of O₂ and NO₂ as oxidizing agents of S(IV) had a positive influence on SO₂ absorption. The positive impact of oxidizing agents on SO₂

absorption was particularly clear over long experimental times when SO₂ absorption was reduced to a slow but steady rate. At a high inlet SO₂/HCl ratio, the presence of NO₂ or O₂ led to SO₂ absorption rates never quite dropping to zero. The HCl absorption rate, on the contrary, did drop to zero when the conversion of the solids reached x_T . While the flux equation for SO₂ absorption was similar in form to the flux equation for HCl, the flux equation for SO₂ took into account long-term, nonzero absorption rates. The equations describing SO₂ absorption took the following form:

$$\text{I. For } x \leq 0.95x_T, \quad F_{\text{SO}_2} = \frac{C_{\text{SO}_2}(x_T - x)}{\frac{1}{k_{s,S}C_{\text{HCl}}} + \frac{x}{D_{\text{eff},S}}} \quad (6.12a)$$

$$\text{II. For } 0.95x_T \leq x \leq x_T, \quad F_{\text{SO}_2} = \frac{C_{\text{SO}_2}(x_T - x)}{\frac{1}{k_{s,S}C_{\text{HCl}}} + \frac{x}{D_{\text{eff},S}}} + \frac{k_0}{x} \quad (6.12b)$$

$$\text{III. For } x \geq x_T, \quad F_{\text{SO}_2} = \frac{k_0}{x} \quad (6.12c)$$

where x at time τ is the sum of the moles of HCl, n_{HCl} , and SO₂, n_{SO_2} , that have been absorbed since time zero, adjusted for reaction stoichiometry and divided by initial moles of alkalinity:

$$x_\tau = \frac{1/2n_{\text{HCl}}|_\tau + n_{\text{SO}_2}|_\tau}{n_{\text{Ca}+2}}$$

The SO₂ flux was described by two mechanisms: reaction with the sorbent and long-term absorption, perhaps due to sulfur-nitrogen compound formation. It was necessary to break down the flux equation into three regimes because once conversion became greater than the termination conversion, x_T , the term $(x_T - x)$ became negative. With this term negative, the model predicted the desorption of both HCl and SO₂. The transition regime between these two mechanisms is described by Equation 6.12b. The lower border, $0.95x_T$, was set somewhat

arbitrarily. Neither estimated parameters nor the sum of squares was sensitive to the transition regime lower border from $0.75x_T$ to $0.97x_T$. It was necessary to include a transition regime to allow for a smooth bridge from the regime governed by sorbent absorption to the regime with long-term, slow SO_2 absorption. The expression for the long-term SO_2 absorption included a $1/x$ term because it was noted that the absorption rate, though fairly steady, did slow slightly as utilization values increased in excess of 100%.

At early experimental time ($x \rightarrow 0$) equations 6.12a and 6.12b described the SO_2 flux as being first order in both SO_2 and HCl concentration. It is believed that the deliquescent nature of CaCl_2 salts improved SO_2 absorption. This same effect was seen by other researchers (Matsukata et al., 1996; Jozewicz et al., 1990). As seen in Figure 5.2.1, an increase in relative humidity over calcium silicate increased SO_2 absorption. If the solids had surface solution that was saturated to CaCl_2 , the partial pressure of water over the solids would have increased. This increase in water vapor partial pressure, then, would have increased SO_2 absorption. Several other forms of Equation 6.12a were regressed, including equations where the order on SO_2 concentration was varied widely. However, only Equation 6.12a estimated the same approximate value of k_s with experiments ranging from 250 ppm HCl /1000 ppm SO_2 to 1000 ppm HCl /250 ppm SO_2 .

While the flux equation employed for SO_2 absorption clearly did not evolve from first principles, it is important to recall that the primary object was to describe the experimental data. With HCl and SO_2 in the inlet gas stream, Equations 6.8 (HCl) and 6.12 (SO_2) indeed described the data effectively. The results of the parameter estimations for seven experiments from the HCl - SO_2 -calcium silicate system are given in Table 6.4.1.

Table 6.4.1 Results of Parameter Estimation for HCl-SO₂-Calcium Silicate System

All experiments performed at 19% RH, 120 °C, 36 mg calcium silicate, and 1.5 SLPM, unless otherwise noted.

CS Exp. No.	HCl conc. (ppm)	SO ₂ conc. (ppm)	NO ₂ conc. (ppm)	O ₂ conc. (%)	Deff,H x 10 ⁵ (m/s)	k _{s,H} x 10 ⁵ (m/s)	x _T	Deff,S x 10 ⁶ (m/s)	k _{s,S} x 10 ² (m ⁴ /m/s)	k ₀ x 10 ⁹ (mol/ m ² /s)	c _i (s)	error † (%)
20	250	1000	150	2.5	11.3	5.73	0.935	4.37	2.35	8.0	11.3	4.08
				2σ	8.0	2.12	0.037	0.43	1.54	§	0.3	
19	250	1000	150	0	5.43	7.68	0.942	1.30	4.45	8.0	12.3	4.10
				2σ	1.20	1.13	0.040	0.11	1.09	§	0.2	
18	250	1000	50	2.5	6.38	6.62	0.943	2.08	2.78	3.8	12.3	4.75
				2σ	1.93	1.95	0.048	0.20	1.88	§	0.2	
24*	250	1000	50	2.5	∞	4.88	0.843	2.87	0.503	5.2	12.4	6.82
				2σ	∞	1.95	0.074	1.39	0.370	§	0.4	
16	250	1000	0	5.5	56.2	2.93	0.843	0.083	15.4	0	12.2	3.81
				2σ	207	0.025	0.013	§	∞	§	0.2	
25	1000	250	50	2.5	2.33	15.0	0.827	7.82	2.17	0	10.2	3.32
				2σ	0.45	6.2	0.019	0.85	1.15	§	0.3	
32	1000	250	NO:140 NO ₂ :10	2.5	2.22	3.22	0.766	5.33	5.15	0	11.5	4.10
				2σ	0.48	2.18	0.023	0.79	4.63	§	0.3	

† The error reported is the square root of the average model error squared multiplied by 100 when the experiment was modeled individually.

* Experiment performed at 9% RH.

§ Parameter was determined manually to two significant figures and does not have a 2σ estimate.

∞ Parameter was determined to be very large or had a very large confidence interval.

The value of k_0 was determined by manually adjusting it to match the average slope of the increase in conversion with respect to time after x_T was surpassed. The values given in Table 6.4.1 are the best values within two significant figures. The parameter estimation routine could not determine accurate values of k_0 because it was using concentrations, given by Equation 6.9, as the objective function. Generally, GREG would estimate the parameter to be zero with an infinite 2σ value because concentration was not sufficiently sensitive to k_0 . However, with k_0 set to zero, the outlet concentration from the reactor was systematically over-predicted. This problem led to an under-prediction of sorbent

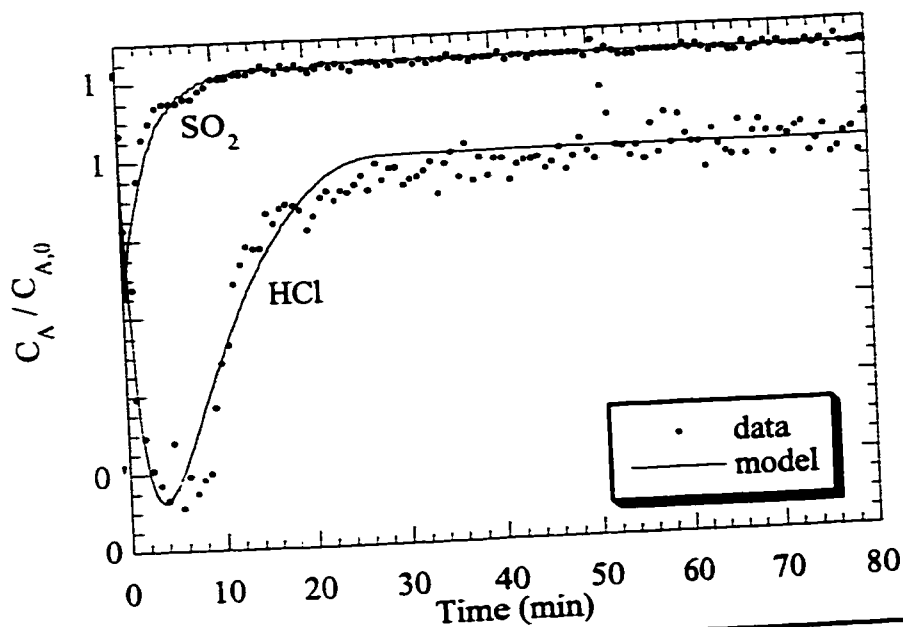


Figure 6.4.1 Typical model fit for HCl-SO₂ absorption by calcium silicate.

Experiment performed at 19% RH, 250 ppm HCl, 1000 ppm SO₂, 50 ppm NO₂, 2.5% O₂ with 36 mg calcium silicate at 120 °C and 1.5 SLPM. Exp. No. CS18.

conversion at values greater than x_T . To capture the “super-absorption” of SO_2 by calcium silicate well in excess of 100% utilization (or conversion), k_0 was estimated manually. The comparison between the data and the modeled concentration is shown in Figure 6.4.1 for both HCl and SO_2 .

Similar to the regression results for HCl absorption by calcium silicate, problems arose due to large normalized covariance (≥ 0.8) between $D_{\text{eff,H}}$, $k_{s,H}$, and $k_{s,S}$. With large covariance, some of the parameters had rather wide confidence intervals. Wide confidence intervals for a parameter indicated that the experimental data were not particularly sensitive to that parameter. However,

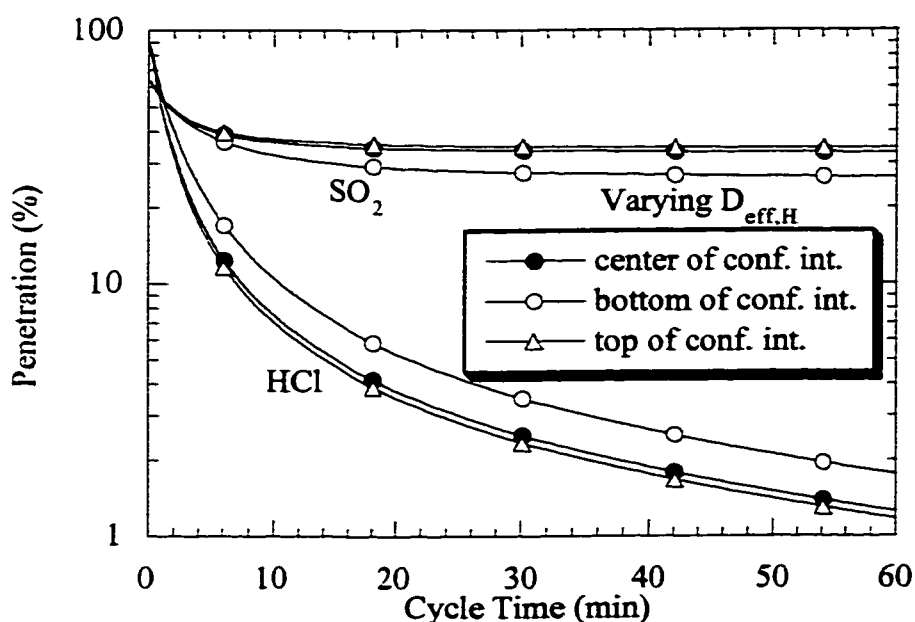


Figure 6.4.2 Effect on penetration of varying $D_{\text{eff,H}}$ from the center to the top and bottom of the confidence interval.

Performance projection with a calcium silicate feed ratio of 1.5 at 19% RH, 250 ppm, 1000 ppm SO_2 , 150 ppm NO_2 , 2.5% O_2 , and 120 °C. Exp. No. CS20.

when the parameters were used to predict bag filter performance, the bag filter model may be more sensitive to some terms than the fixed-bed model. Figures 6.4.2 and 6.4.3 show the effect of changing a parameter from its regressed value to the top and bottom of the 2σ confidence interval. In general, $D_{\text{eff,H}}$ and $k_{s,S}$ tended to give the widest confidence intervals so they are used as examples for the figures. The curves shown in Figures 6.4.2 and 6.4.3 provide a qualitative measurement of the limits on precision of the bag filter performance projections due to large confidence intervals.

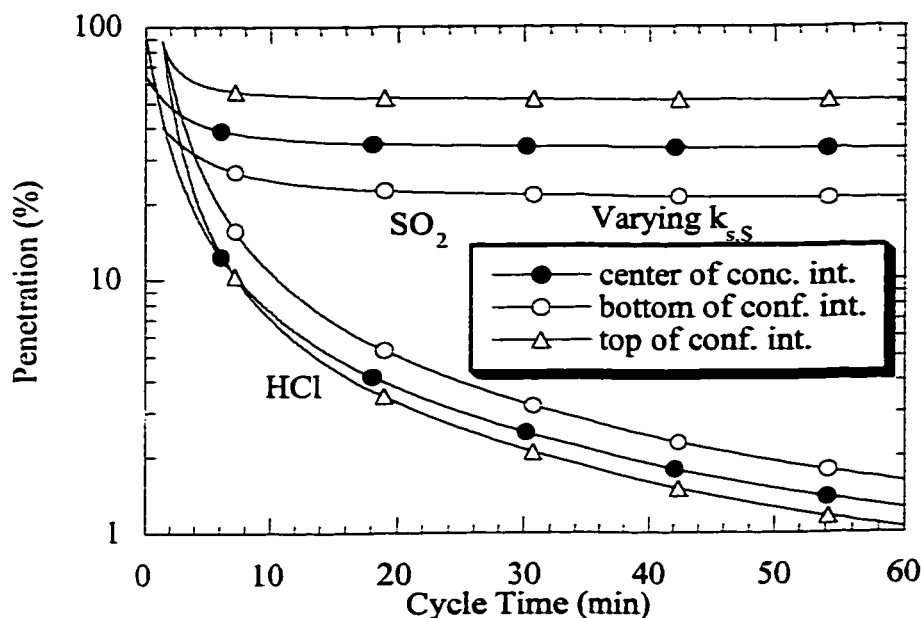


Figure 6.4.3 Effect on penetration of varying $k_{s,S}$ from the center to the top and bottom of the confidence interval.

Performance projection with a calcium silicate feed ratio of 1.5 at 19% RH, 250 ppm, 1000 ppm SO₂, 150 ppm NO₂, 2.5% O₂, and 120 °C. Exp. No. CS20.

Based on the two examples shown in Figures 6.4.2 and 6.4.3, the effect of varying a parameter through its 2σ confidence interval seems to have less of an effect on HCl penetration than SO₂ penetration. When $D_{\text{eff,H}}$ is decreased, SO₂ penetration decreases because SO₂ has slightly less competition for alkalinity due to the increase in HCl penetration. There is a considerable effect on SO₂ penetration when $k_{\text{s,S}}$ is decreased to the bottom of the confidence interval. SO₂ penetration increases from 33 to 51% when $k_{\text{s,S}}$ is decreased from 2.35 to 0.81 m⁴/m/s. Exp. No. CS20 was chosen as the example for discussion because the results of the parameter estimation produced relatively large confidence intervals. With this in mind, the results from Exp. No. CS20 represented a worst case scenario of sorts.

6.4.2 Bag Filter Performance Projections

A comparison of HCl and SO₂ penetration for conditions at a low inlet SO₂/HCl ratio (250 ppm SO₂/1000 ppm HCl) and a high inlet SO₂/HCl ratio (1000 ppm SO₂/250 ppm HCl) is shown in Figure 6.4.4. At a low SO₂/HCl ratio, the penetration for both acid gases is approximately 5% after a cycle time of 60 minutes. But when the ratio of SO₂/HCl increases to 4.0, SO₂ penetration increases to almost 40% while HCl penetration decreases to 1%. The increase in SO₂ absorption with large HCl concentrations may be due to the deliquescent effect of CaCl₂.

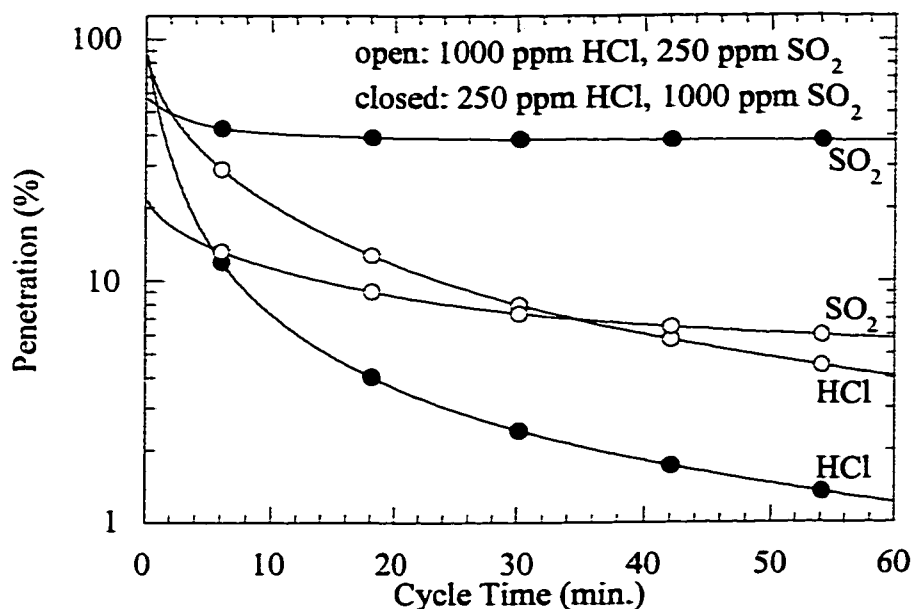


Figure 6.4.4 Penetration of HCl and SO₂ as the inlet SO₂/HCl concentration ratio changes from 0.25 to 4 in a bag filter system using calcium silicate.

Performance projection with a sorbent feed ratio of 1.5, 19% RH, 50 ppm NO₂, 2.5% O₂, and 120 °C. The curves use the parameters given in Table 6.4.1 for Exp. Nos CS18, CS25.

Experimentally, the lowest HCl concentration that could have been studied in the presence of high levels of water vapor (19% RH) was 250 ppm. However, most coal-fired boilers do not have HCl levels as high as 250 ppm HCl. The parameters estimated for Exp. No. CS18, obtained at 250 ppm HCl with 1000 ppm SO₂, 50 ppm NO₂, and 2.5% O₂, were used to extrapolate to 50 and 150 ppm HCl. The results of that extrapolation are shown in Figure 6.4.5. Decreasing HCl concentration from 250 to 50 ppm HCl increased SO₂ penetration from 38 to 66%. This drop in SO₂ removal occurred because the flux for SO₂ was dependent on HCl concentration (see Equation 6.12). The penetration of HCl decreased

slightly with decreasing HCl concentration because there was more unreacted sorbent available for reaction due to less competition with SO₂.

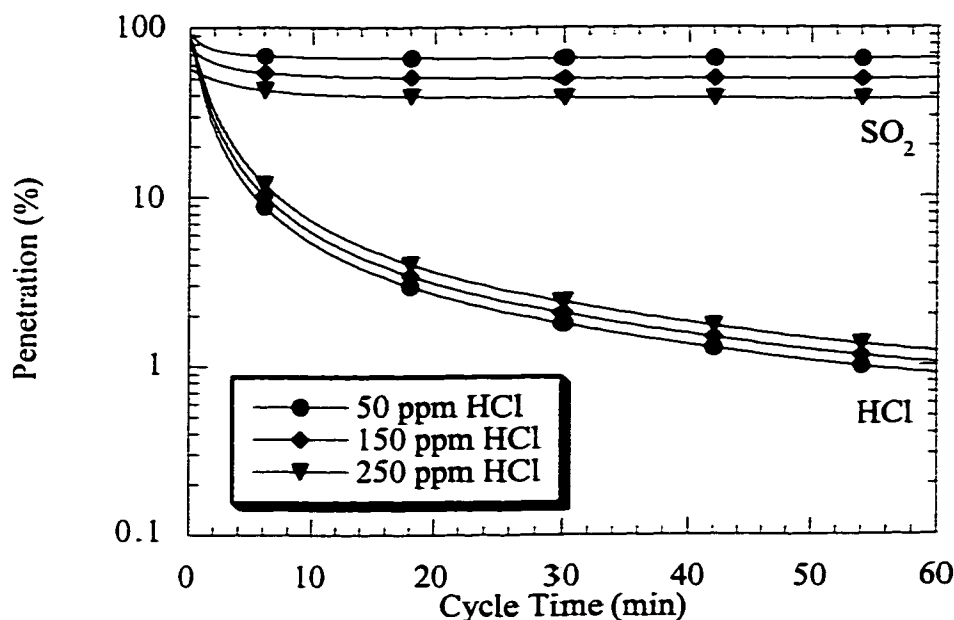


Figure 6.4.5 Penetration of HCl and SO₂ at varying, low HCl concentration in a bag filter system using calcium silicate.

Performance projection with a sorbent feed ratio of 1.5, 19% RH, 1000 ppm SO₂, 50 ppm NO₂, 2.5% O₂, and 120 °C. The curves at 50 and 150 ppm HCl are extrapolations from the parameters, given in Table 6.4.1, for Exp. No. CS18.

As with the single gas systems discussed earlier in this chapter, plots of removal versus sorbent utilization were developed. The predictions were for high (4.0) and low (0.25) ratios of inlet SO₂/HCl concentration under the conditions of Exps. No. CS18 and CS25. An unexpected profile was predicted for SO₂ removal. No modeled experiments had equal concentrations of HCl and SO₂ in the reactor inlet. With the objective in mind of using the modeled parameters to extrapolate to a SO₂/HCl ratio of 1, the parameters for CS18 were used to predict

penetration of HCl and SO₂ at conditions of CS25 and vice versa. The comparison for conditions at 250 ppm HCl, 1000 ppm SO₂, 50 ppm NO₂, 2.5% O₂ at 19% RH and 120 °C are shown in Figure 6.4.6. Both sets of parameters predicted almost exactly the same HCl penetration through 60 minutes cycle time. The predictions for SO₂ penetration did not match as well but were still within 10% penetration throughout 60 minutes cycle time.

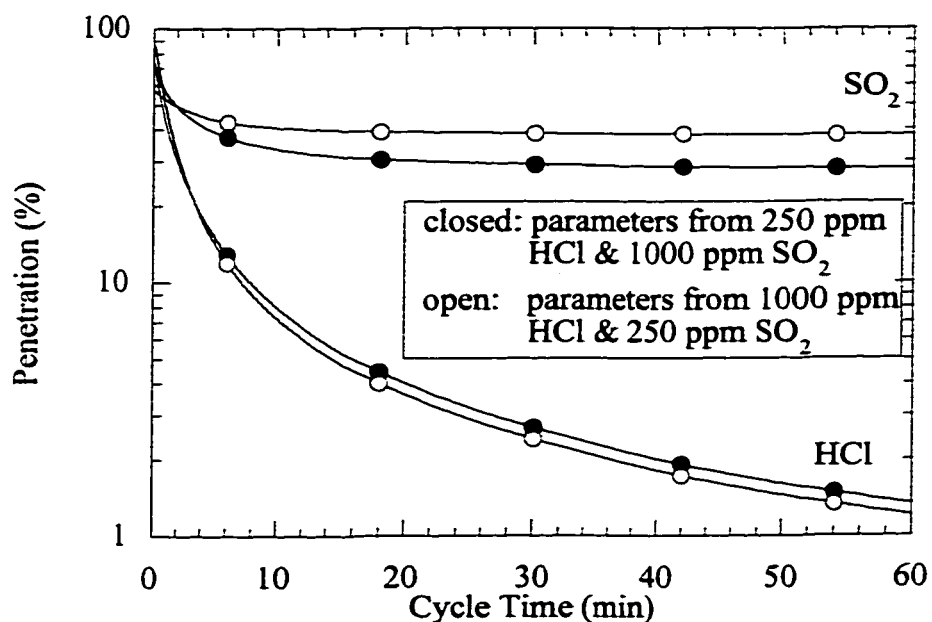


Figure 6.4.6 Penetration of HCl and SO₂ at the same conditions as predicted by two different sets of parameters from Exp. Nos. CS18 and CS25 using calcium silicate.

Performance projection with 250 ppm HCl, 1000 ppm SO₂, 50 ppm NO₂, 2.5% O₂ at 19% RH and 120 °C. Parameters for both sets of projections listed in Table 6.4.1 from Exp. Nos. CS18 and CS25.

With some confidence in the ability for the parameters from CS25 to predict absorption at conditions other than those under which the original data

were taken, bag filter performance was estimated at 500 ppm HCl and SO₂. Under these conditions, the effect of inlet SO₂/HCl concentration ratio could be compared not only at 0.25 and 4.0 from the modeled data but also at 1.0 from the extrapolated data. SO₂ removal is shown in Figure 6.4.7 and HCl removal is shown in Figure 6.4.8.

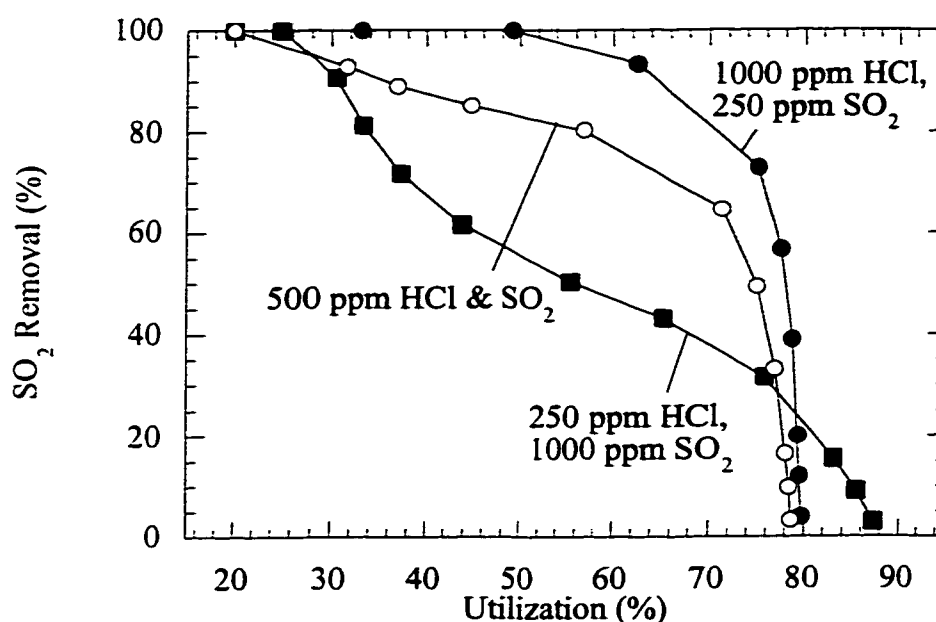


Figure 6.4.7 SO₂ removal as a function of calcium silicate utilization at varying inlet SO₂/HCl concentration ratios in a bag filter system.

Performance projection at 40 min. cycle time with 19% RH, 50 ppm NO₂, 2.5% O₂ at 120 °C. The curve for 250 ppm HCl/1000 ppm SO₂ was generated by the parameters listed in Table 6.4.1 for Exp. No. CS18. The curves for 1000 ppm HCl/250 ppm SO₂ and 500 ppm HCl & SO₂ were generated from parameters listed in the same table for Exp. No. CS25.

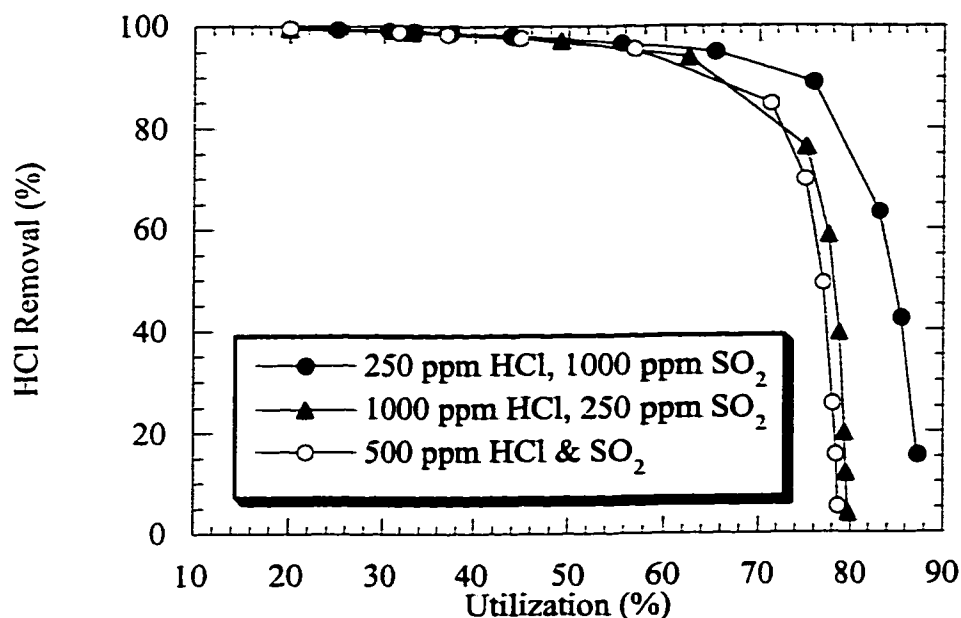


Figure 6.4.8 HCl removal as a function of calcium silicate utilization at varying inlet SO₂/HCl concentration ratios in a bag filter system.

Performance projection at 40 min. cycle time with 19% RH, 50 ppm NO₂, 2.5% O₂ at 120 °C. The curve for 250 ppm HCl/1000 ppm SO₂ was generated by the parameters listed in Table 6.4.1 for Exp. No. CS18. The curves for 1000 ppm HCl/250 ppm SO₂ and 500 ppm HCl&SO₂ were generated from parameters listed in the same table for Exp. No. CS25.

At a greater inlet SO₂/HCl concentration ratio, as utilization drops (and sorbent feed ratio increases) from approximately 70 to 45%, the slope of the SO₂ removal curve became less negative. This suggested that at a high SO₂/HCl ratio, the additional sorbent preferentially reacts with HCl. Once HCl is entirely removed, the slope on the SO₂ removal curve again became more negative, indicating that the additional sorbent was reacting with SO₂. While the flattening

of the SO₂ removal curve is most pronounced at an inlet SO₂/HCl ratio of 4, it was also evident with the extrapolated curve with its inlet SO₂/HCl ratio of 1.

6.5 MODELING OF HCl-SO₂-HYDRATED LIME

6.5.1 Parameter Estimation

Because long-term reactivity of SO₂ with hydrated lime was not observed as it was with calcium silicate, the flux equation for the HCl-SO₂-hydrated lime system was simpler. The flux of HCl, given by Equation 6.11, was modeled with the same equation used when HCl was the only reacting gas. The flux equation for SO₂ is the same as that from the first absorption regime when calcium silicate is used as the sorbent:

$$F_{SO_2} = \frac{C_{SO_2}(x_T - x)}{\frac{1}{k_{s,S}CHCl} + \frac{x}{D_{eff,S}}} \quad (6.12a)$$

The results of the parameter estimation for six experiments from the HCl-SO₂-hydrated lime series of experiments are given in Table 6.5.1.

In general, there were fewer difficulties encountered in obtaining parameter estimates with relatively small confidence intervals than with calcium silicate. As with the modeling of HCl only, the second order dependence of the flux on HCl concentration helped reduce covariance. With some hydrated lime experiments, there were large confidence intervals for some SO₂ flux parameters due to the fact that the small amount of SO₂ absorption took place over a rather narrow range of experimental time. Consequently, there were not enough data in some cases to accurately estimate parameters.

Table 6.5.1 Results of Parameter Estimation for HCl-SO₂-Hydrated Lime System

All experiments performed at 19% RH, 120 °C, 35 mg hydrated lime, and 1.5 SLPM, unless otherwise noted.

Exp. No.	HCl conc. (ppm)	SO ₂ conc. (ppm)	NO ₂ conc. (ppm)	O ₂ conc. (%)	D _{eff,H} x 10 ⁴ (m ⁴ /mol/s)	k _s ' x 10 ² (m/s)	x _T	D _{eff,S} x 10 ⁷ (m/s)	k ₂ x10 ² (m ⁴ /m/s)	c _i (s)	error † (%)
28	250	1000	150	2.5	2.33	18.5	0.951	9.80	5.87	12.7	4.08
				2σ:	0.23	2.9	0.028	2.10	2.90	0.2	
27	250	1000	150	0	3.87	6.60	0.939	5.35	4.47	13.6	4.91
				2σ:	1.05	0.75	0.031	1.63	7.22	0.1	
23	250	1000	0	5.5	2.08	7.28	0.974	2.92	15.4	12.9	5.03
				2σ:	0.18	0.84	0.029	0.86	∞	0.2	
24	1000	1000	0	5.5	0.443	7.35	0.802	1.52	1.43	9.21	3.38
				2σ:	0.025	0.62	0.018	∞	0.42	0.45	
20	1000*	2000	0	0	1.36	14.6	0.794	0.405	2.40	7.68	2.53
				2σ:	0.06	2.3	0.011	0.235	0.11	0.35	
16	1000	1000	0	0	0.987	10.8	0.861	2.97	1.93	10.9	2.93
				2σ:	0.054	1.6	0.015	1.14	0.29	0.2	

† The error reported is the square root of the average model error squared multiplied by 100 when the experiment was modeled individually.

* Experiment performed with 50 mg hydrated lime.

∞ Parameter was determined to be very large or had a very large confidence interval.

6.5.2 Bag Filter Performance Projections

Predictions of HCl and SO₂ penetration under two sets of conditions that allowed for improved SO₂ absorption are illustrated in Figure 6.5.1. High levels of HCl removal were achieved regardless of NO₂ and O₂ concentration. On the other hand, almost 70% of the inlet SO₂ penetrated through the bag filter even in the presence of 150 ppm NO₂ and 2.5% O₂.

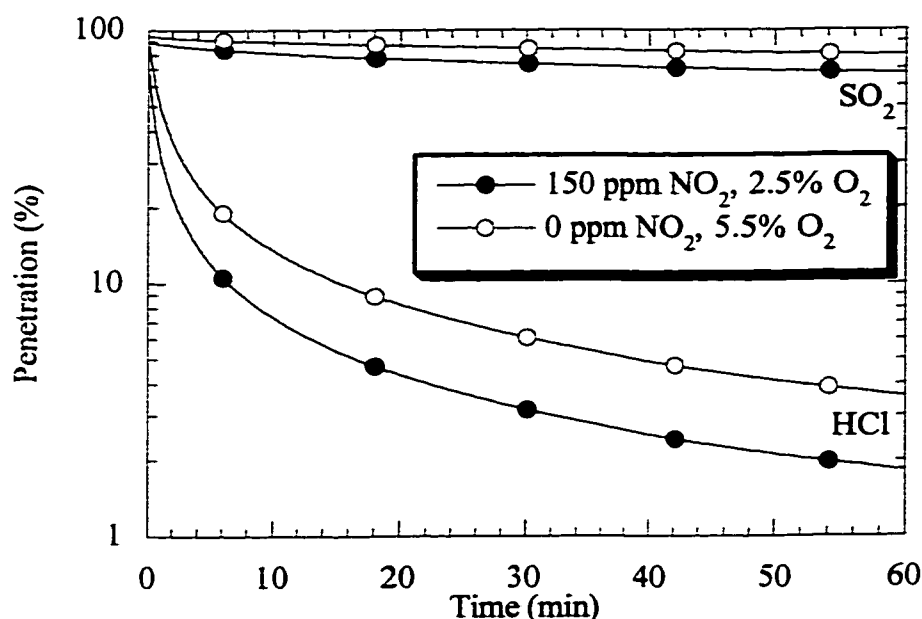


Figure 6.5.1 Penetration of HCl and SO₂ with varying NO₂ and O₂ concentrations in a bag filter system using hydrated lime.

Performance prediction with a sorbent feed ratio of 1.5 at 19% RH and 120 °C with 250 ppm HCl, and 1000 ppm SO₂. Parameters used are taken from Table 6.5.1 for Exp. Nos. HL23, HL28.

A curve of HCl and SO₂ removal as a function of sorbent utilization is given in Figure 6.5.2. To achieve 90% HCl removal, hydrated lime utilization

dropped below 30%. At this utilization, only 10% of the SO_2 fed to the bag filter was removed. It is worthwhile to point out that the conditions for the prediction depicted in Figure 6.5.2 delivered the greatest SO_2 loading in the fixed-bed experiments. So the projection given in the figure below represents a best case scenario for SO_2 absorption with hydrated lime. Further analysis of hydrated lime as a potential sorbent and a comparison of it to calcium silicate is the subject of the next chapter.

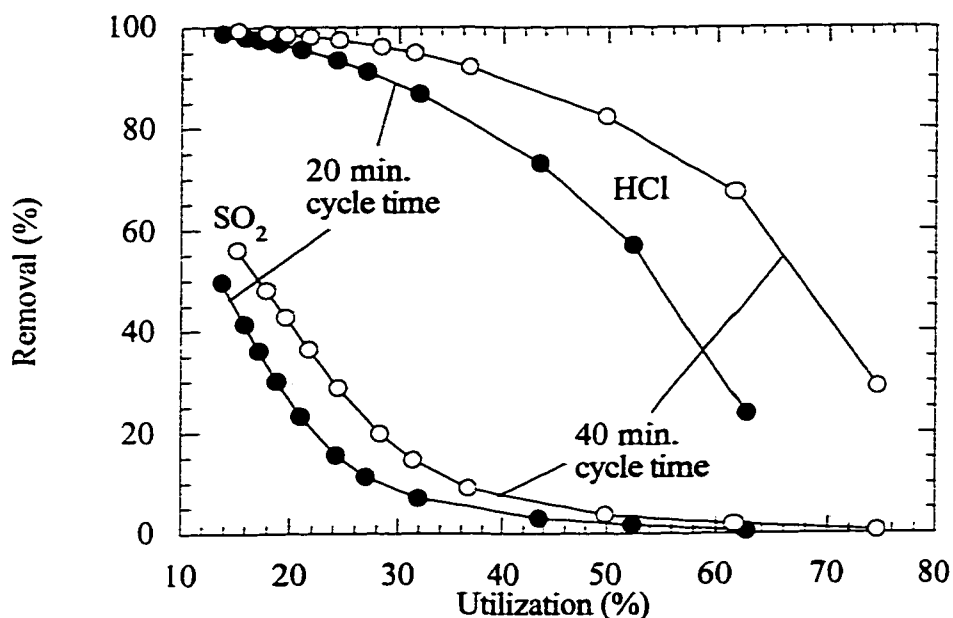


Figure 6.5.2 HCl and SO_2 removal by hydrated lime as a function of cycle time in a bag filter system.

Performance prediction at 19% RH and 120° C and 250 ppm HCl, 1000 ppm SO_2 , 150 ppm NO_2 , 2.5% O_2 . Parameters used are taken from Table 6.5.1 for Exp. No. HL28.

6.6 SUMMARY

A model was developed to describe the experimental data presented in Chapters 4 and 5. FORTRAN code was written that divided experimental time and distance through the fixed-bed into finite elements. Semi-empirical flux equations for HCl and SO₂ were developed that fit the data well. Caracotsios' (1986) Generalized Regression (GREG) routine was employed to estimate parameters in the flux equations. The objective function GREG minimized was the sum of the squares of the differences between modeled and experimental reactor outlet concentration data normalized by the gas inlet concentration. An expression to correct for transient effects due to absorption of HCl in the gas cell was included. Regressed parameters were used to predict the removal of HCl and SO₂ in a bag filter system.

Based on bag filter predictions, calcium silicate is an effective sorbent for HCl control at moderate to high relative humidity. At a relative humidity of 3.5% or greater and reasonable operating conditions, bag filter performance projections for HCl absorption by calcium silicate showed that penetration can be dropped to almost 10%. At 1.8% RH with the same operating conditions, HCl penetration is about 50%. As was expected, increasing the sorbent feed ratio increased HCl removal. Decreasing HCl concentration from 1000 to 250 ppm HCl increased HCl penetration from 11 to 24%. At reasonable operating conditions, less than 20% penetration of HCl was possible with a sorbent utilization of 50%.

Injection of hydrated lime was projected to be an effective sorbent for HCl absorption only at high relative humidity. Predictions of HCl absorption by hydrated lime at showed that HCl penetration could be reduced to 6% at 19% RH at reasonable operating conditions. Almost 10% HCl penetration was predicted for a sorbent utilization of 50% at 19% RH.

In the presence of NO₂, calcium silicate solids were predicted to be effective for simultaneous HCl and SO₂ control, especially at a low SO₂/HCl ratio. Penetration of HCl was predicted to be low at nearly all conditions studied. SO₂ removal decreased with an increasing SO₂/HCl ratio. When HCl and SO₂ are simultaneously absorbed by calcium silicate, an inlet SO₂/HCl ratio of 0.25

led to about 5% penetration of both HCl and SO₂ in the presence of 50 ppm NO₂. As the SO₂/HCl ratio increased, reactivity of HCl increased and SO₂ reactivity decreased. At reasonable bag filter conditions, 5% HCl and about 60% SO₂ penetration was predicted with a sorbent utilization of 50%.

High levels of HCl removal while only limited SO₂ removal were predicted for HCl and SO₂ absorption by hydrated lime. At conditions maximizing SO₂ absorption, about 70% of the SO₂ penetrated the bag filter. At the same conditions, penetration of HCl was predicted to be less than 2%. At conditions that optimize SO₂ reactivity but do not necessarily reflect real flue gas (19% RH and 150 ppm NO₂), predictions for penetration at 50% sorbent utilization were 20 and 95% for HCl and SO₂, respectively.

Chapter 7. Comparison of Hydrated Lime and Calcium Silicate

One of the primary objectives of this study was to determine whether calcium silicate was a more suitable sorbent for HCl and SO₂ absorption than hydrated lime. The experimental work in Chapters 4 and 5 laid the groundwork for the modeling and predictions discussed in Chapter 6. The purpose of this chapter is to compare the expected performance of hydrated lime and calcium silicate.

7.1 FLUE GAS CONTAINING HCL

Figure 7.1.1 shows HCl penetration as a function of sorbent utilization in a bag filter system. The hydrated lime curve is shown at conditions of high relative humidity. At 19% RH and 120 °C, the mole fraction of water in the inlet gas was 35 vol%, a value that is greater than most flue gases. On the other hand, the calcium silicate curve is shown at conditions greater than or equal to 3.5% RH. Recall that between 3.5 and 19% RH, there was no effect of relative humidity on absorption by calcium silicate. Hydrated lime clearly approaches a greater sorbent utilization, almost 80% at high HCl penetration. If a reasonable sorbent utilization was assumed to be between 40 and 60% (1 to 2.5 sorbent feed ratio), the difference between the reactivity of the gas with hydrated lime and calcium silicate over most of the reasonable range of utilization is not large. At low utilization and penetration conditions, calcium silicate demonstrated better HCl removal probably due to the fact that, at low sorbent utilization, absorption on fresh sorbent by hydrated lime was second order while absorption by calcium silicate was first order in HCl concentration.

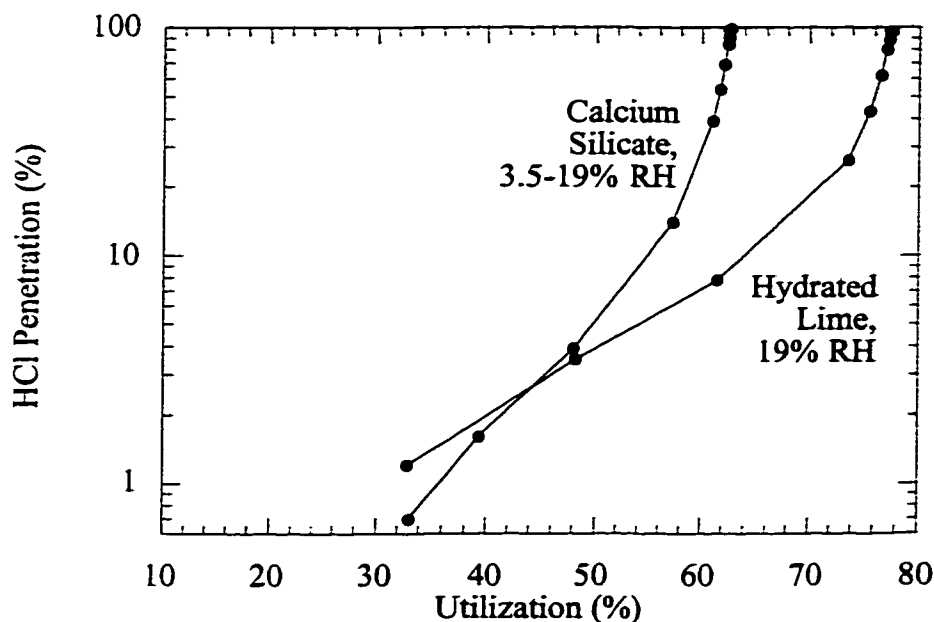


Figure 7.1.1 Comparison of HCl penetration with hydrated lime and calcium silicate.

Performance projection at 40 min. cycle time with absorption by hydrated lime and calcium silicate with 1000 ppm HCl and 120 °C. Global parameters for calcium silicate and hydrated lime projections were taken from Tables 6.2.1 and 6.4.2, respectively.

In the bench-scale experiments, the maximum utilization of calcium silicate was only 71%, less than the 82% by HL. However, low levels of relative humidity ($\geq 3.5\%$ RH) also reached a calcium silicate utilization of 71%. These results suggest that if there is a very high water contact (≥ 35 vol%) intrinsic to a flue gas, the use of hydrated lime is recommended in lieu of calcium silicate. However, typical water vapor levels in flue gas will be enough to induce high absorption rates and sorbent utilization of HCl with calcium silicate. If the increased costs of using calcium silicate offset the capital costs and maintenance

problems of spraying water into a flue duct for removal by hydrated lime, calcium silicate may be more suitable than hydrated lime.

7.2 FLUE GAS CONTAINING HCl AND SO₂

At conditions typical of flue gas derived from coal combustion, calcium silicate was found to be more reactive with HCl than hydrated lime. The comparison of HCl penetration with respect to sorbent utilization for both

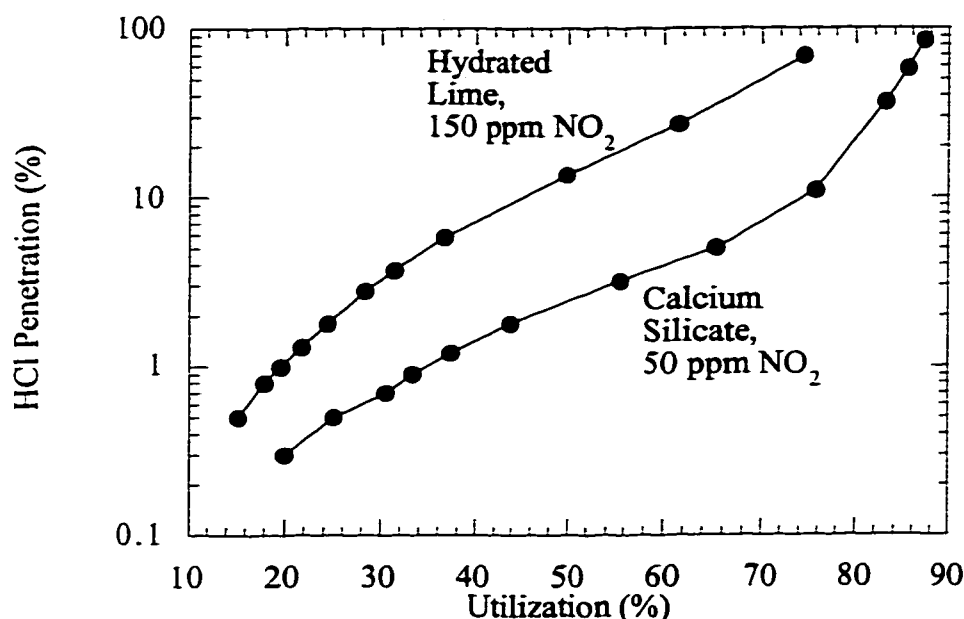


Figure 7.2.1 Comparison of HCl penetration with hydrated lime and calcium silicate at coal-fired combustion flue gas conditions.

Performance projection at 40 min. cycle time with absorption by hydrated lime and calcium silicate with 250 ppm HCl, 1000 ppm SO₂, 2.5% O₂ and 120 °C. Global parameters for calcium silicate and hydrated lime projections were taken from Tables 6.3.1 and 6.5.2, respectively. The experiments that generated the parameters were HL28 and CS18.

sorbents is given in Figure 7.2.1. Through the entire range of utilization shown, penetration of HCl with hydrated lime was about half an order of magnitude greater than absorption by calcium silicate. This conclusion is not obvious given the fixed-bed data discussed in Chapters 4 and 5.

The decrease in SO₂ penetration with calcium silicate relative to hydrated lime was more pronounced than HCl penetration. The comparison between sorbents is shown in Figure 7.2.2. In light of all the data obtained for hydrated

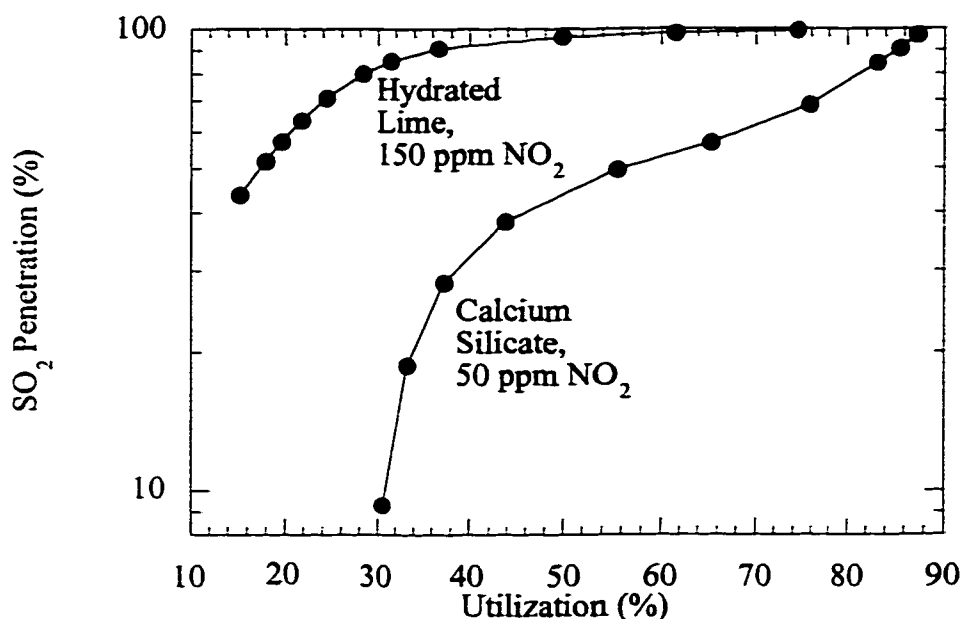


Figure 7.2.2 Comparison of SO₂ penetration with hydrated lime and calcium silicate at coal-fired combustion flue gas conditions.

Performance projection at 40 min. cycle time with 250 ppm HCl, 1000 ppm SO₂, 2.5% O₂ and 120 °C. Global parameters for calcium silicate and hydrated lime projections were taken from Tables 6.3.1 and 6.5.2, respectively. The experiments that generated the parameters were HL28 and CS18.

lime and calcium silicate, the most obvious advantage of using calcium silicate over hydrated lime is the ability of calcium silicate to react not only with HCl but to simultaneously react with SO₂ as well. Based on the data from this study, a coal-fired power plant that required considerable SO₂ emissions reduction could not employ hydrated lime as an effective means to control SO₂. However, using calcium silicate at a utilization of 50% would remove approximately 60% of the SO₂ in the flue gas.

As discussed in Chapter 6, removal of HCl and SO₂ from simulated incinerator flue gas (high HCl, low SO₂ concentrations) was shown to reach almost 90% for both gases with calcium silicate employed as the sorbent. No experiments were performed or modeled with hydrated lime as the sorbent under simulated incinerator flue gas conditions. These experiments were not performed because SO₂ loading of hydrated lime was almost zero with experiments where the inlet SO₂/HCl ratio was less than one. The small measure of reactivity that would occur would have been lost in the time lag introduced by the gas cell. With this qualitative knowledge, it is reasonable to conclude that hydrated lime would not absorb sufficient SO₂ at incinerator flue gas conditions to merit its usage.

7.3 SUMMARY

At a very high water vapor concentration (≥ 35 vol%), hydrated lime removes more HCl than calcium silicate at a constant sorbent utilization. At a relative humidity typical of coal-fired boiler or incinerator flue gas, calcium silicate is more reactive than hydrated lime. However, the increase in absorption rate and capacity with calcium silicate is not large. Therefore, hydrated lime is most likely more suitable than calcium silicate for HCl absorption at all conditions, especially at very high flue gas water content.

When both HCl and SO₂ must be removed from a flue gas, calcium silicate is more reactive than hydrated lime at all conditions studied. The salient element of this conclusion is that SO₂ reactivity with hydrated lime in the presence of HCl is very low. With a simulated coal-fired flue gas, SO₂ penetration after 40 minutes cycle time in a bag filter is about 40% for calcium silicate and 90% for hydrated lime at 50% utilization. Though not studied

specifically, SO₂ absorption by hydrated lime at incinerator conditions were not expected to be any better than at coal-fired boiler conditions. For both coal-fired boiler and incinerator flue gases, HCl penetration was predicted to be approximately 10% or less when calcium silicate was used. Unlike SO₂ absorption, HCl absorption by hydrated lime at coal-fired boiler conditions was projected to be only slightly less reactive than calcium silicate at the same conditions.

Chapter 8. Conclusions and Recommendations

This study utilized a fixed-bed reactor system to measure absorption rates of HCl and SO₂ by hydrated lime and calcium silicate at varying NO₂, O₂, and water vapor concentrations. The data from the experiments were analyzed by estimating parameters of a semi-empirical model. The parameters were then used to predict HCl and SO₂ removal by the two sorbents in a bag filter system. This chapter will summarize the results described in greater detail in Chapters 4 through 7. Recommendations for future work will also be discussed.

8.1 BENCH-SCALE RESULTS

8.1.1 Hydrated Lime

The absorption of HCl by hydrated lime improved with increasing relative humidity from 0 to 19% RH. The utilization of the sorbent was 82% at 19% RH. At 0.8 and 3.5% RH, transient, unexpected behavior was seen at early experimental times. This behavior may have been due to the ability of calcium chloride to absorb moisture from the simulated flue gas. At 250 to 1000 ppm, the rate of HCl absorption over the course of the experiment was first order in HCl concentration. At 2000 and 3500 ppm HCl, removal was high until about 30% utilization. However, the rate of absorption shut down more abruptly to a lower final utilization at 2000 and 3500 ppm than at 250 to 1000 ppm.

SO₂ absorption was considerably less than HCl at all studied reaction conditions. In the absence of any oxidizing species (O₂ or NO₂), there was a pseudo-equilibrium between calcium chloride and calcium sulfite dictated by the inlet SO₂/HCl concentration ratio. As the SO₂/HCl ratio increased, more sulfite and slightly less chloride was bound to the sorbent at the end of the experiment. When O₂ was added to the simulated flue gas, SO₂ absorption was increased due to the oxidation of S(IV) to S(VI). The addition of NO₂ to the gas system increased SO₂ absorption by S(IV) oxidation. At the optimal conditions for SO₂ absorption studied (250 ppm HCl, 1000 ppm SO₂, 150 ppm NO₂, and 2.5% O₂ at

19% RH and 120 °C), the final conversion of hydrated lime by SO₂ accounted for 31% utilization while HCl accounted for 67% utilization. HCl reactivity remained nearly constant regardless of the concentrations of SO₂, NO₂, or O₂.

8.1.2 Calcium Silicate

The absorption of HCl by calcium silicate increased with increasing relative humidity from 0 to 3.5% RH. From 3.5 to 19% RH, increased relative humidity had no effect on the rate of HCl absorption. It was suspected but not proven that at the greater humidity range, the dihydrate chloride was the reaction product while the monohydrate formed at the lower humidity range. The fraction of HCl removal was not dependent on HCl concentration from 250 to 3250 ppm. The maximum utilization was found to be 71% at 3.5 to 19% RH.

Without NO₂ and O₂ and in the presence of HCl, absorbed SO₂ was not stable when bound with calcium silicate. Experiments showed that while SO₂ would react in the back of the fixed-bed where there was no HCl, as soon as HCl broke through to the back of the bed all absorbed SO₂ was emitted. However, when NO₂ or O₂ was added to the inlet gas, the oxidation of S(IV) to S(VI) allowed for the SO₂ that had absorbed in the back of the bed to stay bound later in the experiment when HCl broke through. It was demonstrated that at a high SO₂/HCl ratio as NO₂ concentration increased, reaction of the solids became dominated increasingly by SO₂. Utilization of calcium silicate reached as high as 167%, suggesting the existence of alternate absorption routes of SO₂ such as the formation of sulfur-nitrogen compounds. Even at a low SO₂/HCl ratio, reactivity of SO₂ in the presence of moderate levels of NO₂ (50 ppm) was appreciable (20% utilization). In general, increases in SO₂ reactivity came partly at the expense of a reduction in HCl reactivity.

A limited number of experiments investigating the effects of relative humidity and temperature on the interaction between SO₂ and NO₂ were conducted. These experiments suggested that at a certain temperature, there existed a ceiling NO₂ concentration above which additional NO₂ did not increase SO₂ absorption. At 150° C, the ceiling NO₂ concentration was less than or equal to 25 ppm. The ceiling NO₂ concentration decreased with increasing temperature.

8.2 MODELING AND BAG FILTER PERFORMANCE PROJECTIONS

The experimental data were modeled by dividing experimental time and distance through the fixed-bed into finite elements. Flux equations based on shrinking core theory were modified to describe localized HCl and SO₂ absorption in a finite element. Parameters for the flux equations were estimated by a nonlinear, single response estimation package. The semi-empirical model was found to fit the data well.

The parameters estimated from the bench-scale data were used to predict the absorption of HCl and SO₂ on the surface of a bag filter. When HCl is absorbed alone, the performance of hydrated lime and calcium silicate were comparable at high relative humidity. This observation suggests that at high relative humidity, the additional cost of manufacturing calcium silicate probably does not justify its usage. Because calcium silicate is more reactive at low humidity, systems requiring removal of HCl may reach removal targets cheaper by utilizing calcium silicate rather than by increasing the humidity of the gas and adding hydrated lime.

Modeling of data acquired at conditions similar to coal-fired boiler flue gas (high SO₂/HCl concentration ratio) showed that at a 50% calcium silicate utilization, about 90% removal of HCl and 60% removal of SO₂ could be achieved with 50 ppm NO₂ at 19% RH. With 150 ppm NO₂ and the same water content, removal of HCl and SO₂ at 50% hydrated lime utilization was approximately 80 and 10%, respectively. In general, SO₂ was considerably more reactive with calcium silicate than with hydrated lime.

Over the range of HCl and SO₂ concentration studied, increasing HCl concentration tends to increase SO₂ removal. This effect may be due to the deliquescent nature of calcium chloride. Therefore, at conditions typical of municipal waste combustors (low SO₂/HCl concentration ratio), removal of SO₂ was greater than with conditions typical of coal-fired boilers. At a calcium silicate utilization of 50%, HCl and SO₂ removal both were approximately 90%. Experiments with hydrated lime were not available at combustor conditions.

However, it was expected that hydrated lime would compare no better at combustor conditions than at coal-fired boiler conditions.

The primary objective of this work was to determine if calcium silicate solids are a suitable replacement for hydrated lime in dry sorbent injection applications for municipal waste combustion and coal-fired boiler applications. To meet this objective conclusively, pilot testing and a detailed economic analysis is required. However, based on data and modeling from this study, the increased reactivity of SO_2 with calcium silicate, especially in the presence of NO_2 , suggests that the additional operating costs associated with calcium silicate production may be recovered through increased SO_2 removal.

8.3 RECOMMENDATIONS

This body of research was designed to quantify the effect of interactions between HCl , SO_2 , NO_2 , O_2 , and water vapor. In some instances, the desire to gain an understanding from first principles of a specific interaction was made subordinate to the pressing interest in studying a representative, simulated flue gas. Therefore, several of the recommendations listed below relate to gaining an understanding of some of the interactions and variables whose effects were observed.

1. Though theories have been put forth in the literature, no researchers have proven with confidence the role of relative humidity. A theory has been suggested (see Appendix G) that may explain the effect of relative humidity on acid gas absorption. The fundamentals of this subject need to be studied so that any modeling efforts or process optimization can be based on an understanding of the role of humidity, rather than accepting the effect of increasing humidity empirically.
2. At low (but not zero) relative humidity the absorption of HCl by hydrated lime started with fresh sorbent, ceased abruptly, started up again, and then tailed off to a moderate utilization. Deliquescence of the reaction products may explain this phenomenon but further studies could confirm the cause.
3. Absorption by hydrated lime decreased with increasing HCl concentration above 2000 ppm. It was expected that pore blockage was responsible, but

confirmation of the cause may shed light on pore blockage in the general case.

4. The absorption capacity of calcium silicate for SO_2 in the presence of NO_2 was very large. Utilizations well over 100% were observed. Further studies could speciate the sulfur and nitrogen absorbed more precisely than ion chromatography.
5. Calcium silicate was clearly more reactive than hydrated lime, especially with SO_2 . A future study could confirm whether this is due to increased surface area or different reaction thermodynamics.
6. The introduction of a solids recycle to the bag filter performance model would allow for better process optimization. Pressure drop calculations as a function of filter cake thickness would improve operating conditions recommendations.

Appendix A. FT-IR Experimental Procedure

This appendix gives detailed instructions on how to operate the Perkin-Elmer System 2000 (Perkin-Elmer, 1995a) with the attached Infrared Analysis gas cell (Hanst and Hanst, 1995). The operating instructions assume that Spectrum for Windows™ (Perkin-Elmer, 1995b) and TR-IR (Perkin-Elmer, 1992) software packages are controlling the IR. The instructions are detailed and include some recommendations for troubleshooting common problems.

A.1 PERKIN-ELMER SYSTEM 2000

1. Turn on the IR by flipping the switch to the rear, right side of the machine. Note that the green lights “Power On”, “Laser On”, and “Ready” are lit on the IR display.
2. Turn on the computer and monitor. Type “win” when a DOS prompt appears. Once Windows™ has been launched, double click on the “Spectrum for Windows”. Click on the “Instrument” icon. The software is attempting to communicate with the IR. A window will pop up asking if you want to initialize the machine. Click “OK”. The IR goes through a series of adjustments to the IR and laser beams to optimize energy throughput.
3. After initializing, the Instrument Setup window will appear. The important fields in this window are “Resolution” and “Gain”. Set the resolution at 8 cm^{-1} and the gain at 8. For a resolution of 8 cm^{-1} , one scan takes three seconds. At lower values of resolution, a full scan takes more time. A gain of 8 means that the signal received by the detector is multiplied by 8. With the loss in energy due to the gas cell mirrors, a gain of 8 provides for the maximum signal to noise ratio. Allow the other fields to remain at their default setting: Apodization--Strong; OPD Velocity--0.2 cm/s; Interferogram--Bi-Directional and One-Sided; Phase Correction--Self and 256. Click on “Update”.

4. Click on "Monitor" and "OK". The amount of energy reaching the detector is output. If the IR beam and the gas cell mirrors are aligned properly, the value of energy should be between 700 and 1200. Particles on the gas cell mirrors will reduce the energy value. If laboratory air is in the gas cell, the value will be reduced because of the water vapor. (Note: If the gain is set too high, the IR source will overwhelm the detector. If the Monitor window appears with "ADC Overload", reduce the gain. This may happen when the beam has been changed to the other detector but the gain has been set to 8. In this case, change the beam configuration through the "Instrument Setup" and "Beam" windows.)
5. If an acceptable energy level is found by monitoring, enter "Alt" and "Tab" simultaneously on the keyboard. Launch "TR-IR". Under "File", "Open Method", click on "PCHCL.GMT" and "OK". Under "Method", "Scan Conditions...", the resolution is set at 8 cm^{-1} and the other fields are set to their default: Instrument Setup--Current; Scan Composition--Default. Under "Method", "Data Collection Parameters...", the following settings are used: Scan Time--900 min.; Scans/Slice--5; # Background Scans--8; Interval Between Slices, Delay, and Baseline Interval--0 min.; Peak Threshold--10 min.; Gram-Schmidt [gram Points--25 to 75. A high setting for Scan Time ensures that TR-IR will not cease scanning during an experiment. A Scans/Slice value of 5 means that every five scans will be averaged to one scan. At a resolution of 8 cm^{-1} with 5 scans/slice, a data point is produced every 15 seconds.
6. Under "Method", "Monitor...", click on "Energy" on the "Select Type" field and enter "OK". Ensure that the energy level output by TR-IR is approximately the same as that output by Spectrum for Windows™.
7. The IR is now prepared to record data. In TR-IR, under "Method", click on "Background..." and then on "Continue" in the window that appears. Once the background is registered, click on "Scan..." under

- “Method”**. Click on **“Trigger”** in the window that appears. The IR is now scanning. When you want to halt scanning to end an experiment, type F5 and then **“y”** on the keyboard.
8. To change the output range during scanning, enter **“a”** for the Spectrum window or **“b”** for the Gram-Schmidt Chromatogram window. Use the arrows on the keyboard to indicate which range is to be modified. Enter the number you want the relevant axis to adjust to. Adjustments to the view of the two plots will not affect data acquisition.
 9. After an experiment, to generate absorbance versus time data, click on **“Contour Plot”** under **“View Results”**. Enter the wavenumber range on the window that appears. The resulting plot shows absorbance in arbitrary units as a function of time. The chromatogram plot can be saved under the **“Process Data”** menu. The plot can be opened in Spectrum for Windows and then saved in ASCII format. The plot in ASCII format can be opened in Excel.

Notes:

1. The IR takes approximately 3 hours to warm-up completely. It can be used immediately for data acquisition but there will be increased baseline drift.
2. The IR must be initialized through Spectrum for Windows™ before TR-IR can be launched. If the proper order is not followed, a message **“Cannot Access Transputer”** will appear and the instrument will not scan.
3. Do not change programs through the **“Alt/Tab”** keys while TR-IR is controlling scanning. This will crash the program.
4. If TR-IR randomly shuts down during an experiment, this may indicate that the laser from the IR needs replacement. It is moderately easy for the user to replace the laser and power source. The parts can be ordered directly from Uniphase. Do not request a service call from Perkin-Elmer.
5. If the IR is to sit idle for more than two days, shut it down. This will prolong the life of the laser.

6. The only maintenance required is a periodic (e.g., monthly) nitrogen purge. Using the attached nitrogen line, allow flow *at a very low flowrate* to enter the IR housing. Be sure the detectors are also being purged. At the same time, take the desiccant bed from its chamber and dewater it in a low temperature oven. The location of the desiccant bed can be identified using the User's Manual.

A.2 INFRARED ANALYSIS GAS CELL

The gas cell presently attached to the IR is owned by Dr. Matt Hall from the Department of Mechanical Engineering at the University of Texas at Austin. Once the gas cell has been set up, it requires no daily startup or maintenance. Periodically, the mirrors of the cell develop an accumulation of particles. When the energy being transmitted to the detector drops below 500, the mirrors need to be cleaned. Below, a rough outline of the cleaning process is detailed.

1. Turn off the IR to avoid looking into the laser.
2. Remove all the hex-screws from the top and bottom of the gas cell.
Keep the base of the gas cell securely fastened to the IR.
3. Remove inlet and outlet lines from top of the gas cell.
4. Remove the top metal plate from the gas cell.
5. Remove the glass cylinder and mirror support structure from the IR.
6. Using the house air line, blow any large particles off the mirrors. Very carefully, clean the mirrors using Kimwipes. Use extreme caution to avoid scratching the mirrors.
7. Once the mirrors are clean, reassemble the gas cell by reversing the order of steps 1 through 5.
8. Use the external laser and laser power source to track the laser beam. Pass the laser beam through the transparent window at the top of the gas cell such that it strikes the small, square piece of the bottom mirror that juts out from the rest of the mirror. Adjust the two screw knobs on the top metal plate to align the mirrors so that a reasonable energy level is produced. In general, the signal to noise ratio increases with greater

pathlength. Detailed instructions for mirror alignment can be found in Hanst and Hanst (1995).

9. If no energy is reaching the detector, the mirrors below and external to the gas cell may need adjustment. Use a white card to identify where the laser from the IR is striking and adjust the external mirrors as necessary.

Appendix B. Sample Calculations

The purpose of this appendix is to show how absorption rates, sorbent loading, and total sorbent utilization were calculated. The experiment that is used as an example (CS23) included HCl, SO₂, NO₂, and O₂. The calculations began with the determination of the inlet flowrate, gas concentrations, relative humidity, and moles of sorbent that the experiment is using. SO₂, NO₂, O₂, and N₂ were added by mass flow controllers (MFC) that had been calibrated.

$$\begin{aligned}\text{SO}_2: \quad Q_{\text{SO}_2} &= 9.73 \times 10^{-4} + 4.90 \times 10^{-3} \times \text{Setting} \\ &= 9.73 \times 10^{-4} + 4.90 \times 10^{-3} \times 61.5 \\ &= 0.300 \text{ SLPM}\end{aligned}$$

$$\begin{aligned}\text{NO}_2: \quad Q_{\text{NO}_2} &= -4.13 \times 10^{-2} + 1.24 \times 10^{-2} \times \text{Setting} \\ &= -4.13 \times 10^{-2} + 1.24 \times 10^{-2} \times 15.0 \\ &= 0.144 \text{ SLPM}\end{aligned}$$

$$\begin{aligned}\text{N}_2: \quad Q_{\text{N}_2} &= 3.02 \times 10^{-2} + 2.40 \times 10^{-2} \times \text{Setting} \\ &= 3.02 \times 10^{-2} + 2.40 \times 10^{-2} \times 10.7 \\ &= 0.287 \text{ SLPM}\end{aligned}$$

For this experiment, air was fed to the system through an MFC using a two point calibration:

$$\text{Setting: } 75.9, Q = 0.191 \text{ SLPM}$$

$$\text{Setting: } 65.1, Q = 0.161 \text{ SLPM}$$

$$\text{Setting: } 71.2 \Rightarrow Q_{\text{air}} = 0.180 \text{ SLPM}$$

HCl was fed to the system through a rotameter that was calibrated at the correct flowrate as a function of downstream pressure drop. For a flowrate of 0.069 SLPM with a downstream pressure of 1.50 psig, the setting on the rotameter was 27. Water vapor was fed to the system through a calibrated syringe pump. At the

setting of 7, the flowrate of water was 0.39 ml/min = 0.39 g/min. The volumetric rate of water vapor is

$$\begin{aligned}
 Q_{H_2O} &= \frac{m_{H_2O}RT}{M_{H_2O}P} \\
 &= \frac{0.39 \text{ g/min} \times 0.08206 \text{ L}\cdot\text{atm/gmol/K} \times (273.15+21.1 \text{ K})}{18 \text{ g/gmol} \times 1 \text{ atm}} \\
 &= 0.523 \text{ SLPM}
 \end{aligned} \tag{B.1}$$

The total flowrate was the sum of each flow: 0.300+0.144+0.287+0.180+0.533 = 1.50 SLPM.

Cylinders containing HCl, SO₂, and NO₂ blended in nitrogen were the sources of acid gas. The concentration (x_i^*) of HCl, SO₂, and NO₂ in the cylinders was 5404, 5001, and 517 ppm, respectively. To determine molar flowrates of each of the gases, the following calculations were performed:

$$n_{i,in} = \frac{P x_i^* Q_i}{RT} \tag{B.2}$$

$$\begin{aligned}
 \text{HCl:} \quad n_{\text{HCl},in} &= \frac{1 \text{ atm} \times 5404 \times 10^{-6} \times 0.069 \text{ L/min}}{0.08206 \text{ L}\cdot\text{atm/gmol/K} \times (273.15+21.1 \text{ K})} \\
 &= 1.54 \times 10^{-5} \text{ mol/min} \\
 \text{SO}_2: \quad n_{\text{SO}_2,in} &= \frac{1 \text{ atm} \times 5001 \times 10^{-6} \times 0.300 \text{ L/min}}{0.08206 \text{ L}\cdot\text{atm/gmol/K} \times (273.15+21.1 \text{ K})} \\
 &= 6.22 \times 10^{-5} \text{ mol/min} \\
 \text{NO}_2: \quad n_{\text{NO}_2,in} &= \frac{1 \text{ atm} \times 517 \times 10^{-6} \times 0.144 \text{ L/min}}{0.08206 \text{ L}\cdot\text{atm/gmol/K} \times (273.15+21.1 \text{ K})} \\
 &= 3.09 \times 10^{-6} \text{ mol/min} \\
 \text{air:} \quad n_{\text{air},in} &= \frac{1 \text{ atm} \times 1 \times 0.180 \text{ L/min}}{0.08206 \text{ L}\cdot\text{atm/gmol/K} \times (273.15+21.1 \text{ K})} \\
 &= 7.37 \times 10^{-3} \text{ mol/min} \\
 \text{H}_2\text{O:} \quad n_{\text{H}_2\text{O},in} &= \frac{1 \text{ atm} \times 1 \times 0.523 \text{ L/min}}{0.08206 \text{ L}\cdot\text{atm/gmol/K} \times (273.15+21.1 \text{ K})} \\
 &= 0.0217 \text{ mol/min}
 \end{aligned}$$

The calculation of O₂ was straightforward:

$$\text{O}_2: \quad n_{\text{O}_2,\text{in}} = 0.21 \times n_{\text{air}} = 1.55 \times 10^{-3} \text{ mol/min}$$

The calculation leading to the molar flow of N_2 is long and tedious. Molar flow of N_2 is the summation of all the gas flow except what had already been accounted for by HCl , SO_2 , NO_2 , O_2 , and water. The calculation is similar to the calculation for HCl , SO_2 , and NO_2 .

$$\text{N}_2: \quad n_{\text{N}_2,\text{in}} = 0.0390 \text{ mol/min}$$

To determine the concentration of the acid gases and O_2 , the molar flows were divided by the total molar flow, n_T :

$$n_T = \frac{1 \text{ atm} \times 1.5 \text{ L/min}}{0.08206 \text{ L}\cdot\text{atm/gmol/K} \times (273.15 + 21.1 \text{ K})} \\ = 0.0621 \text{ mol/min}$$

$$\text{HCl:} \quad x_{\text{HCl},\text{in}} = \frac{1.54 \times 10^{-5} \text{ mol/min}}{0.0621 \text{ mol/min}} \times 1 \times 10^6 \\ = 248 \text{ ppm}$$

$$\text{SO}_2: \quad x_{\text{SO}_2,\text{in}} = \frac{6.22 \times 10^{-5} \text{ mol/min}}{0.0621 \text{ mol/min}} \times 1 \times 10^6 \\ = 1000 \text{ ppm}$$

$$\text{NO}_2: \quad x_{\text{NO}_2,\text{in}} = \frac{3.09 \times 10^{-6} \text{ mol/min}}{0.0621 \text{ mol/min}} \times 1 \times 10^6 \\ = 49.6 \text{ ppm}$$

$$\text{O}_2: \quad x_{\text{O}_2,\text{in}} = \frac{1.55 \times 10^{-3} \text{ mol/min}}{0.0621 \text{ mol/min}} \times 100 \\ = 2.49\%$$

$$\text{H}_2\text{O:} \quad x_{\text{H}_2\text{O},\text{in}} = \frac{0.0217 \text{ mol/min}}{0.0621 \text{ mol/min}} \times 100 \\ = 34.9\%$$

To determine the relative humidity, the partial pressure of water in the reactor (total pressure recorded as 1.5 psig) was divided by the saturation pressure of water at the experimental temperature, 120 °C.

$$RH = \frac{(14.7+1.5 \text{ psia}) \times 0.349}{29.76 \text{ psia}} \times 100$$

$$= 19.0\%$$

A titration indicated that the capacity of calcium silicate was 6.49×10^{-3} mol/g. The mass of sorbent weighed out was 36.1 g so the moles of sorbent was 2.34×10^{-4} moles.

Once all the preliminary calculations were performed, the experiment was conducted. The output was three sets of time versus absorbance data, one each for HCl, SO₂, and NO₂. Before any of these acid gases were introduced into the experimental apparatus, an absorbance value at 0 ppm for each gas was calculated. These averages were calculated from 20 data points taken over five minutes. Another average of 20 points was taken after the acid gases had been introduced to the apparatus but had not been sent to the reactor. These averages are the values of absorbance for the inlet concentrations for HCl, SO₂, and NO₂. With absorbances at 0 ppm and at the inlet concentration of each gas, the concentration of each gas throughout the experiment was calculated based on the two-point calibration. The values for the two point calibration are given in Table B.1:

Table B.1 Absorbance Values for Acid Gas Calibration

	Concentration (ppm)	Absorbance
HCl	0	2.67
	248	544
SO ₂	0	-87.4
	1000	39900

NO ₂	0	-182
	49.6	3920

At time zero, the absorbences of HCl, SO₂, and NO₂ were 494, 39600, and 3310. Using the values shown in Table B.1 for interpolation, the concentrations of HCl, SO₂, and NO₂ were 221, 993, and 46.9 ppm, respectively. After 15 seconds reaction time, the absorbences reported corresponded to 207, 823, 33.3 ppm for HCl, SO₂, and NO₂, respectively. At 30 seconds, the concentrations of HCl, SO₂, and NO₂ were 138, 223, and -1.35 (experimental noise) ppm, respectively.

To calculate the moles of each gas that was absorbed at each time interval, a mass balance was performed. Looking at HCl, from 0 to 15 seconds, the average concentration at the outlet was ($1/2(221+207 \text{ ppm})$) 214 ppm. To determine the moles absorbed, Equation B.3 was used:

$$\begin{aligned}
 n_{\text{HCl}} &= (n_{\text{HCl},\text{in}} - n_{\text{HCl},\text{out}}) \times \Delta t & (\text{B.3}) \\
 &= (n_{\text{HCl},\text{in}} - x_{\text{HCl}} \times n_{\text{T}}) \times \Delta t \\
 &= (1.54 \times 10^{-5} \text{ mol/min} - 221/10^6 \times 0.0621 \text{ mol/min}) \\
 &\quad \times 0.25 \text{ min} \\
 &= 5.30 \times 10^{-7} \text{ moles HCl}
 \end{aligned}$$

Similarly, between 15 and 30 seconds, 1.18×10^{-6} moles of HCl were absorbed. With Equation B.3, the moles of HCl, SO₂, and NO₂ can be calculated for each time step through the entire experiment.

To determine the cumulative moles of acid gas that has been absorbed up to a certain time, the moles of HCl absorbed for each time interval was summed. For example, the cumulative moles of HCl that was absorbed through 30 seconds was ($5.30 \times 10^{-7} + 1.18 \times 10^{-6}$ moles) 1.71×10^{-6} moles. The loading of HCl normalized by the original moles of sorbent after 30 seconds is (1.71×10^{-6} moles HCl / 2.34×10^{-4} moles Ca⁺⁺) 7.31×10^{-3} moles HCl/mole Ca⁺⁺.

To determine the utilization of the sorbent, the loading of all the acid gases, corrected for reaction stoichiometry, are summed. Two moles of HCl utilize one mole of Ca^{++} (Reaction 2.1); one mole of SO_2 utilizes one mole of Ca^{++} (Reaction 2.2); two moles of NO_2 utilizes one mole Ca^{++} (Reaction 2.6). Through thirty seconds, the loading of HCl, SO_2 , and NO_2 are 7.31×10^{-3} , 0.0378, and 2.88×10^{-3} moles, respectively. Therefore, the utilization is

$$\begin{aligned}\text{utilization} &= (1/2(7.31 \times 10^{-3} + 2.88 \times 10^{-3} \text{ moles/moles } \text{Ca}^{++}) \\ &\quad + 0.0378 \text{ moles } \text{SO}_2/\text{moles } \text{Ca}^{++}) \times 100 \\ &= 4.29\%\end{aligned}$$

This calculation was performed at every time step to determine utilization as a function of time.

Finally, to determine the removal of an acid gas at any given time, Equation B.4 was used:

$$\text{Removal} = (1 - \frac{x_i}{x_{i,\text{in}}}) \times 100$$

For example, after 15 seconds the concentration at the outlet of the reactor was 221 ppm. Therefore, HCl removal was

$$\begin{aligned}\text{HCl Removal} &= (1 - \frac{221 \text{ ppm}}{248 \text{ ppm}}) \times 100 \\ &= 10.9\%.\end{aligned}$$

This calculation was performed for the entire experiment for HCl, SO_2 , and NO_2 .

Appendix C. Experimental Conditions and Loading Results

Table C.1 Conditions and Final Loading Results for Hydrated Lime Experiments

All tabulated data taken at 120 °C and 1.5 SLPM, unless otherwise indicated.

HL Exp No.	Rel. Hum. (%)	mass sorbent (mg)	time (min)	HCl conc. (ppm)	SO ₂ conc. (ppm)	O ₂ conc. (%)	NO _x conc. (ppm)	HCl load. †	SO ₂ load. †	NO ₂ load. †	Total Util. (%) §
1	0	18	24	1000	0	0	0	0.101	0	0	5.05
2	1	18	45	1000	0	0	0	0.173	0	0	8.65
3	3.5	18	45	1000	0	0	0	0.488	0	0	24.4
4	9	18	45	1000	0	0	0	1.07	0	0	53.5
5	19	18	45	1000	0	0	0	1.61	0	0	80.5
6	19	18	55	250	0	0	0	1.66	0	0	83.0
7	19	18	45	500	0	0	0	1.66	0	0	83.0
8	19	18	45	2000	0	0	0	1.43	0	0	71.5
9*	19	18	45	3500	0	0	0	1.27	0	0	63.5
10	0	100	40	0	1000	0	0	0	0.0574	0	5.74
11	9	100	40	0	1000	0	0	0	0.0968	0	9.68
12	19	100	40	0	1000	0	0	0	0.108	0	10.8
13	19	100	40	0	500	0	0	0	0.119	0	11.9
14	19	35	110	250	1000	0	0	1.58	0.0606	0	85.6
15	19	35	65	500	1000	0	0	1.47	0.0748	0	81.0
16	19	35	45	1000	1000	0	0	1.52	0.0469	0	80.7
17	19	35	45	2000	1000	0	0	1.48	0	0	74.0
18	19	50	45	965	250	0	0	1.60	1.79e-3	0	80.2
19	19	50	45	1000	500	0	0	1.54	5.02e-3	0	77.5
20	19	50	45	1000	2000	0	0	1.37	0.0704	0	75.5
21	19	35	45	0	945	5.5	0	0	0.204	0	20.4
22	19	35	110	250	1000	1.2	0	1.48	0.0903	0	83.0
23	19	35	110	250	1000	5.5	0	1.52	0.152	0	91.2
24	19	35	60	1000	1000	5.5	0	1.50	0.106	0	85.6

HL Exp No.	Rel. Hum. (%)	mass sorbent (mg)	time (min)	HCl conc. (ppm)	SO ₂ conc. (ppm)	O ₂ conc. (%)	NO _x conc. (ppm)	HCl load. †	SO ₂ load. †	NO ₂ load. †	Total Util. (%) §
25	19	35	100	250	1000	0	NO:150	1.52	0.143	0	90.3
26	19	35	45	0	1000	0	NO ₂ :150	0	0.126	0.0534	15.3
27	19	35	100	250	1000	0	NO ₂ :150	1.44	0.174	0.123	95.6
28	19	35	100	250	1000	2.5	NO ₂ :150	1.33	0.310	0.100	102
29	9	36	45	1000	0	0	0	1.122	0	0	56.1
30	9	18	45	500	0	0	0	1.020	0	0	51.0

† Loading of acid gas A is given by moles A/moles Ca⁺⁺.

§ Total Utilization takes into account stoichiometry:

$$\text{Total Utilization} = \frac{1/2n_{\text{HCl}} + n_{\text{SO}_2} + 1/2n_{\text{NO}_2}}{n_{\text{Ca}}} \times 100$$

* Total Flowrate: 0.69 SLPM

Table C.2 Conditions and Final Loading Results for Calcium Silicate Experiments

The flowrate and sorbent loading for all the experiments were 1.5 SLPM and 36 mg, unless otherwise noted.

CS Exp No.	Rel. Hum. (%)	Temp (°C)	Time (min.)	HCl conc. (ppm)	SO ₂ conc. (ppm)	O ₂ conc. (%)	NO _x conc. (ppm)	HCl load. †	SO ₂ load. †	NO ₂ load. †	Total Util. (%) §
1	0	120	8.5	1000	0	0	0	0.33	0	0	16.5
2	0.8	120	45	1000	0	0	0	0.746	0	0	37.3
3	1.8	120	45	1000	0	0	0	0.862	0	0	43.1
4	3.5	120	39	1000	0	0	0	1.421	0	0	71.1
5	9	120	45	1000	0	0	0	1.342	0	0	67.1
6	19	120	45	1000	0	0	0	1.412	0	0	70.6
7	3.5	120	60	250	0	0	0	1.374	0	0	68.7
8	3.5	120	45	500	0	0	0	1.283	0	0	64.2
9	3.5	120	45	2000	0	0	0	1.499	0	0	75.0
10*	3.5	120	45	3250	0	0	0	1.397	0	0	69.9
11	0	120	30	0	1000	0	0	0	0.0489	0	4.89
12	3.5	120	30	0	1000	0	0	0	0.142	0	14.2
13	19	120	30	0	1000	0	0	0	0.322	0	32.2
14	19	120	30	0	500	0	0	0	0.266	0	26.6
15	19	120	100	250	1000	0	0	1.440	0	0	72.0

CS Exp No.	Rel. Hum. (%)	Temp (°C)	Time (min.)	HCl conc. (ppm)	SO ₂ conc. (ppm)	O ₂ conc. (%)	NO _x conc. (ppm)	HCl load. †	SO ₂ load. †	NO ₂ load. †	Total Util. (%) §
16	19	120	80	250	1000	5.5	0	1.332	0.153	0	81.9
17	19	120	50	0	1000	2.5	0	0	0.350	0	35.0
18	19	120	90	250	1000	2.5	NO ₂ :50	0.672	0.732	0.259	120
19	19	120	90	250	1000	0	NO ₂ :150	0.853	0.901	0.690	167
20	19	120	80	250	1000	2.5	NO ₂ :150	0.503	1.040	0.411	150
21	19	120	75	250	1000	0	NO:150	1.427	0.009	0	72.3
22	19	120	80	250	1000	2.5	NO:150	1.116	0.331	0	88.9
23	0.8	120	50	250	1000	2.5	NO ₂ :50	0.344	0.135	0.051	30.7
24	9	120	75	250	1000	2.5	NO ₂ :50	0.745	0.716	0.174	118
25	19	120	75	1000	250	2.5	NO ₂ :50	1.244	0.197	0.067	85.3
26	1.5	150	45	0	1000	2.5	0	0	0.091	0	9.10
27	1.5	150	45	0	1000	2.5	NO ₂ :25	0	0.324	0.022	33.5
28	1.5	150	45	0	1000	2.5	NO ₂ :50	0	0.322	0.060	35.2
29	10	90	45	0	1000	2.5	0	0	0.306	0	30.6
30	10	90	45	0	1000	2.5	NO ₂ :150	0	0.542	0.183	63.4
31†	3.5	120	50	1000	0	0	0	1.468	0	0	73.4
32	19	120	60	1000	250	2.5	NO: 140 NO ₂ : 10	1.324	0.145	0	80.7
33	9	120	45	0	1000	2.5	NO ₂ :150	0	0.761	0.208	86.5
34	19	120	45	0	1000	2.5	NO ₂ :150	0	0.915	0.115	97.2

† Loading of acid gas A is given by moles A/moles Ca⁺⁺.

§ Total Utilization takes into account stoichiometry:

$$\text{Total Utilization} = \frac{1/2n_{\text{HCl}} + n_{\text{SO}_2} + 1/2n_{\text{NO}_2}}{n_{\text{Ca}}} \times 100$$

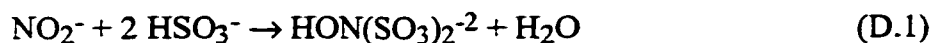
* Total Flowrate: 0.75 SLPM

‡ Calcium silicate loading: 72 mg

Appendix D. Ion Chromatography Calculations

The objective of performing analyses on reacted solids was to determine the speciation of sulfur and nitrogen after the absorption of SO₂ and NO₂. Based on Nelli's work (1997), it was expected that the formation of sulfur-nitrogen compounds led to calcium silicate utilization in excess of 100%. A method was developed to check for the presence of hydroxyaminedisulfonate (HADS) and aminedisulfonate (ADS) (Oblath et al., 1981; Oblath et al., 1982; Nelli, 1997). This method was then employed to check the reacted solids for these sulfur-nitrogen compounds.

When nitrite combines with bisulfite, HADS can be formed according to Reaction D.1. HADS can react further to produce ADS.

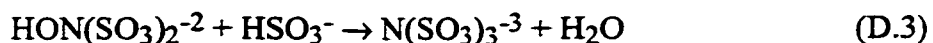


HADS



ADS

Depending on reaction conditions, HADS can also react to form aminetrisulfonate (ATS) or hydroxylaminesulfonate (HAMS) according to reactions D.3 and D.4, respectively:



ATS



HAMS

Note that both HADS and ADS have a sulfur/nitrogen ratio of 2. ATS and HAMS have S/N ratios of 3 and 1, respectively.

To generate a sample of HADS, a solution containing 0.0397 M NO₂⁻ and 0.244 M HSO₃⁻ was prepared. The bisulfite was added using sodium metabisulfite solids (Fisher Scientific). After these ions were mixed, ideally the

concentrations of NO_2^- and HSO_3^- could have been monitored directly. However, once HSO_3^- was diluted to a manageable range for IC analysis, some of it oxidized to SO_4^{2-} . Therefore, the complete oxidation was forced with a small amount of H_2O_2 and SO_4^{2-} was measured. Throughout this appendix, when measuring HSO_3^- is discussed the actual ion being analyzed is SO_4^{2-} .

After nitrite and bisulfite were mixed, their concentrations were measured. Within (Sample #1) two minutes, over 50% of the nitrite was consumed. A sample taken after (#2) 85 minutes indicated that almost 70% of the nitrite had disappeared. Comparing the moles of nitrite that reacted with the reduction in the moles of bisulfite in solution, a S/N ratio of 1.93 was determined at 85 minutes. Samples taken at (#3) 5 hr., 45 min., (#4) 15 hr., 15 min., (#5) 20 hr., (#6) 24 hr., 45 min., and (#7) 46 hr. all exhibited a reaction stoichiometry where the S/N ratio was 2.0 ± 0.16 . A S/N ratio of 2 suggested that HADS and/or ADS was being formed, not HAMS or ATS.

When analyzed individually, solutions containing NO_2^- or HSO_3^- exhibited only one peak. However, the sample taken two minutes after the two ions were mixed showed a peak at 26 minutes retention time. It was suspected that the peak at 26 minutes was HADS. The peak was considerably smaller in magnitude than the bisulfite peak but was easily recognized at a lower detector sensitivity (10 μS). The peak maintained its size through sample (#3). When sample (#4) was analyzed, the area of the peak was less than half the area of the same peak from sample (#3). The area of the HADS peak continued to drop through sample (#7). An eighth and final sample was taken after (#8) three days. The HADS peak had disappeared completely and another, even smaller peak was present at 31 minutes retention time. It was suspected that the peak at 31 minutes was the ADS peak. The reacted S/N ratio for sample (#8) was also approximately 2.

Through this analysis, it was clear that the existence of HADS and perhaps ADS could be identified by a peak at the proper retention time -- 26 minutes for HADS and 31 minutes for ADS. IC could be used as a qualitative tool for HADS

and ADS but it was not expected that precise concentrations of these sulfur-nitrogen compounds could have been determined.

With this method sufficiently developed, two experiments were run where the conditions were designed to produce relatively high levels of sulfur-nitrogen compounds. The experiments that were conducted were at the same conditions as CS20 and CS30. (For the experiment that was similar to CS20, 72 mg calcium silicate was used instead of 36 mg.) Before taking the solids out of the reactor at the end of the CS30 experiment, calibrations were established for NO_2^- , NO_3^- and SO_4^{2-} . The solids were placed in 100 ml water with 1 ml 30% H_2O_2 and the solution was analyzed. The total concentration of $\text{NO}_2^- + \text{NO}_3^-$ was 0.124 mM; the concentration of SO_4^{2-} was 0.864 mM. These concentrations correspond to 89% nitrogen and 93% sulfur recovery compared to the gas phase balance. No other peaks beside NO_2^- , NO_3^- and SO_4^{2-} appeared, including HADS and ADS.

The solids from the experiment that was conducted at the same conditions as CS20 also showed no sign of HADS or ADS. When these solutions were analyzed, the chloride and nitrate peaks overlapped. Therefore, the concentrations of Cl^- and NO_3^- could not be determined precisely. An approximate analysis using peak heights indicated that about 95% of the nitrogen and 80% of the chloride was recovered compared to the gas phase balance. An analysis for SO_4^{2-} showed that 92% of the sulfur was recovered.

The bottom line of the IC analysis is that it did not prove that sulfur-nitrogen compound formation took place and was responsible for calcium silicate utilization in excess of 100%.

Appendix E. Modeling Code

This appendix is an archive of the FORTRAN code that was used to model experimental data and predict bag filter performance. Other researchers (Nelli, 1997; Arthur, 1998) have written similar code.

E.1 HCL ANALYSIS

Shown below are the three subroutines that comprised the code used to analyze HCl absorption by calcium silicate solids. It can also be used to model HCl-hydrated lime absorption. Below, the seven experiments (see Table 6.2.1) modeled simultaneously are used for this example. Section E.1.2 includes the code for a bag filter performance prediction.

E.1.1 Fixed-Bed Code

```
C      Program written by Paul Chisholm
C      28 August 1998
C
C      The purpose of this routine is to (1) read data from
C      a file, (2) calculate concentrations of gas throughout
C      the bed at a certain experimental time, (3) call
C      on GREG and the associated subroutines, (4) and
C      ultimately to return an estimation for the unknown,
C      regressed parameters.
C
      PROGRAM ONEGAS
      IMPLICIT DOUBLE PRECISION (A-H, O-Z)
      DOUBLE PRECISION LOAD
      INTEGER START,END
      EXTERNAL MODEL
      DIMENSION OBS(1200),PAR(10),BNDLW(10),BNDUP(10)
      DIMENSION DSC(15000),ISC(36),CHMAX(10),DEL(10),RAW(1200)
C
C      The following DO loop reads the data from an input file.
C
      OPEN (UNIT=12, FILE='RUN3.inp', STATUS='UNKNOWN')
      OPEN(UNIT=13, FILE='RUN3-250.inp', STATUS='UNKNOWN')
      OPEN(UNIT=14, FILE='RUN3-500.inp', STATUS='UNKNOWN')
      OPEN(UNIT=15, FILE='RUN3-2000.inp', STATUS='UNKNOWN')
      OPEN(UNIT=16, FILE='RUN3-72.inp', STATUS='UNKNOWN')
```

```

OPEN(UNIT=17, FILE='RUN9.inp', STATUS='UNKNOWN')
OPEN(UNIT=18, FILE='RUN19.inp', STATUS='UNKNOWN')
C
C
C   The following declarations initialize the arguments for GREG.
C
C   MDSC=14117
C   MISC=36
C
C   Input the number of parameters and the number of experiments
C   that are being modeled simultaneously. NOB is the total
C   number of data points for all the experiments.
C
C   NPAR=10
C   NEXP=7
C   NOB=NEXP*161
C
C   Read the raw data from files. The temperature and the
C   pressure are also recorded so that the conc. (ppm) vs. time data
C   can be converted to conc. (mol/m**3) vs. time data.
C
C   START and END are used so the program knows when to switch to the
C   next file. NOBS is the number of data points for each
C   individual experiment. Other variables: PPM=Inlet
C   Concentration (ppm); LOAD=Sorbent Mass (mg); TEMP=
C   Temperature (C); SFLRT=Flowrate at Standard Conditions (SLPM);
C   SA=Normalized Surface Area (m**2/g); DT=Data Interval (min.);
C   RH=Relative Humidity (%); CONCIN=Inlet Concentration
C   (mol/m**3).
C
C   START=1
C   DO 876 I=1,NEXP
C   READ(11+I,*) PPM,LOAD,TEMP,SFLRT,PRESS,SA,DT,RH,NOBS
C   CONCIN=((14.696D0+PRESS)*6.89476D3*PPM*1D-6/
C   &      (273.15D0+TEMP)/8.314D0
C   END=START+NOBS-1
C   DO 987 ID=START,END
C   READ(11+I,*) RAW(ID)
C   OBS(ID)=((14.696D0+PRESS)*6.89476D3*RAW(ID)*1D-6/
C   &      (273.15D0+TEMP)/8.314D0)/CONCIN
C   987 CONTINUE
C   CLOSE(11+I)
C   START=END+1
C   876 CONTINUE
C
C   Enter the initial guesses.
C

```

```

PAR(1)=1D-3
PAR(2)=1D-3
PAR(3)=0.8D0
PAR(4)=0.5D0
PAR(5)=0.7D0
PAR(6)=0.7D0
PAR(7)=0.6D0
PAR(8)=0.6D0
PAR(9)=0.6D0
PAR(10)=0.7D0

C
C Initialize the the integer vector ISC. ISC(1)=1 is a user
C number; ISC(2)=10 means the 10 subroutine using least squares
C regression will determine the parameters; ISC(3)=0 means
C several variables will use their default values; ISC(4)-ISC(6)
C are not defined explicitly so their default values will be used.
C
C Set the upper and lower boundaries and the maximum change for
C a parameter.
C
ISC(1)=1
ISC(2)=10
ISC(3)=1
ISC(4)=25
ISC(5)=2
ISC(6)=1

C
C Set major default parameters.
C
DO 765 J=1,NPAR
    BNDLW(J)=1D-30
    BNDUP(J)=1D30
    CHMAX(J)=1D30
    DEL(J)=-0.01D0
765 CONTINUE
RPTOL=1D-5
RSTOL=1D-1
APIV=1D-2

C
C This routine now calls GREG.
C
CALL GREG(NOB,OBS,NPAR,PAR,BNDLW,BNDUP,CHMAX
&      DEL,MDSC,DSC,MISC,ISC,IOBS,IDET,EMOD,VPIV,
&      APIV,RPTOL,RSTOL,MODEL)
C
STOP

```

END

```
C      Paul Chisholm
C      28 August 1998
C
C      The purpose of this program is to send data to the BED
C      subroutine to crunch the numbers. This routine does
C      little more than manage the datafiles.
C
C      SUBROUTINE MODEL (PAR, F, NOB, NPAR, IDER, DERIV,
&      MINFO)
C      IMPLICIT DOUBLE PRECISION (A-H, O-Z)
C      DOUBLE PRECISION LOAD
C      INTEGER START,END,COUNTR
C      DIMENSION PAR(10),F(1200),RAW(1200),OBS(1200),RXR(1200)
C
C      OPEN(UNIT=12, FILE='RUN3.inp', STATUS='UNKNOWN')
C      OPEN(UNIT=13, FILE='RUN3-250.inp', STATUS='UNKNOWN')
C      OPEN(UNIT=14, FILE='RUN3-500.inp', STATUS='UNKNOWN')
C      OPEN(UNIT=15, FILE='RUN3-2000.inp', STATUS='UNKNOWN')
C      OPEN(UNIT=16, FILE='RUN3-72.inp', STATUS='UNKNOWN')
C      OPEN(UNIT=17, FILE='RUN9.inp', STATUS='UNKNOWN')
C      OPEN(UNIT=18, FILE='RUN19.inp', STATUS='UNKNOWN')
C
C      Enter the number of experiments being modeled simultaneously.
C
C      NEXP=7
C
C      The same variable names are used in this subroutine that
C      were used in ONEGAS.
C
C      START=1
C      DO 876 I=1,NEXP
C      READ(11+I,*)PPM,LOAD,TEMP,SFLRT,PRESS,SA,DT,RH,NOBS
C      CONCIN=((14.696D0+PRESS)*6.89476D3*PPM*1D-6/
&      (273.15D0+TEMP)/8.314D0
C      END=START+NOBS-1
C      DO 987 ID=START,END
C      READ(11+I,*) RAW(ID)
C      OBS(ID)=((14.696D0+PRESS)*6.89476D3*RAW(ID)*1D-6/
&      (273.15D0+TEMP)/8.314D0)/CONCIN
C      987 CONTINUE
C      CLOSE(11+I)
C      COUNTR=I
```

```

      CALL BED(LOAD,PPM,SA,PRESS,TEMP,SFLRT,DT,PAR,
&          NOBS,F,START,END,NPAR,COUNTR,NEXP,RXR)
      START=END+1
876  CONTINUE
C
C      After BED regresses parameters, the data and values of
C      important vectors are output to 'conc'.
C
      OPEN(UNIT=23, FILE='conc', STATUS='UNKNOWN')
      DO 765 J=1,END
          WRITE(23,1)DBLE(J)/4D0-0.25D0,OBS(J),F(J),
&          RXR(J),OBS(J)-F(J)
765  CONTINUE
      CLOSE(23)
1    FORMAT (E15.7,5X,E15.7,5X,E15.7,5X,E15.7,5X,E15.7)
C
      RETURN
      END

```

```

C      Program written by Paul Chisholm
C      28 August 1998
C
C      The purpose of this program is to generate a vector of
C      modeled concentrations in the gas cell. The concentration
C      of HCl and conversion are calculated through the bed based
C      on a flux equation. The concentration at the outlet of
C      the reactor is modified with the gas cell correction.
C
C      SUBROUTINE BED(LOAD,PPM,SA,PRESS,TEMP,SFLRT,DT,PAR,
&          NOBS,F,START,END,NPAR,COUNTR,NEXP,RXR)
C
C      IMPLICIT DOUBLE PRECISION (A-H, O-Z)
C      DOUBLE PRECISION MOLE, LOAD
C      INTEGER START,END,COUNTR,FREQM,FREQD
C      DIMENSION PAR(10),F(1200),CONC(5001,501),CONV(5001,501)
C      DIMENSION TIME(5001),FLUX(5001,501),RXR(1200)
C
C      Define the time vector. FREQM is the frequency of time points
C      in a minute that is calculated with the model. FREQD is
C      the number of data points in a minute. NFACT is the factor
C      of model points compared to data points.
C      NTIME is the total number of time points that will be calculated.
C
      FREQM=32

```



```

FREQD=4
NFACT=FREQM/FREQD
NTIME=NOBS*NFACT
TIME(1)=0.0D0
DO 543 J=2,NTIME+1
    TIME(J)=TIME(J-1)+1D0/DBLE(FREQM)
543 CONTINUE
C
C     The next few lines convert the experimental conditions into
C     important variables. MOLE is the number of moles in the rxr.
C     AREA is the normalized total surface area of the sorbent
C     (m**2/g), AFLRT is the actual flowrate (m**3/min.) of the
C     gas through the reactor.
C
MOLE=LOAD*1D-3/154.08D0
AREA=LOAD*1D-3*SA
AFLRT=SFLRT*1D-3*(TEMP+273.15D0)/294.25D0*14.696D0/
& (14.696D0+PRESS)
CONCIN=(14.696D0+PRESS)*6.89476D3*PPM*1D-6/
& (273.15D0+TEMP)/8.314D0
C
C     Begin the DO loops to determine the concentration at the outlet
C     of the bed. N is the number of differential distances in the bed. The
C     outer loop provides the calculations through time. The inner loop
C     calculates calculation of concentration as a function of distance through
C     the bed. The initial value of conversion in the bed is set to 1x10-5. This
C     was not necessary but generally allowed for more rapid convergence to a
C     solution.
C
N=100
DO 987 I=1,NTIME
    CONC(I,1)=CONCIN
    DO 876 J=1,N
        CONV(I,J)=1D-5
        IF (CONV(I,J) .GE. 1.0D0) THEN
            FLUX(I,J)=0.0D0
        ELSE IF (CONC(I,J) .EQ. 0.0D0) THEN
            FLUX(I,J)=0.0D0
        ELSE
            FLUX(I,J)=CONC(I,J)/(CONV(I,J)
& /PAR(1)+1D0/PAR(2))
& *(PAR(3)-CONV(I,J))
        ENDIF
    END DO
C
C     The next part of the code calculates the mass balances.
C

```

```

CONC(I,J+1)=CONC(I,J)-FLUX(I,J)*AREA/DBLE(N)/AFLRT
IF (CONC(I,J+1) .LE. 0.0D0) CONC(I,J+1)=0.0D0
CONV(I+1,J)=CONV(I,J)+AFLRT*(CONC(I,J)-CONC(I,J+1))/
& DBLE(FREQM)/2D0/MOLE*DBLE(N)
IF (CONV(I+1,J) .GT. 1.0D0 .AND. CONV(I,J)
& .LT. 1.0D0) THEN
CONV(I+1,J)=1.0D0
CONC(I,J+1)=CONC(I,J)-(1D0-CONV(I,J))
& *MOLE/DBLE(N)*2D0*DBLE(FREQM)/AFLRT
ENDIF
876 CONTINUE
IF (NFACT .EQ. 1) ITER=0
ITER=ITER+1
987 CONTINUE
C
C The following part of the code calculates the concentration in
C the gas cell based on the outlet of the reactor. Modeled points are
C generated to match the data points taken. The variable ITER
C tracks which of the reactor outlet modeled points is used to compare
C to the experimental points in GREG.
C
ITER=1
DO 765 I=1,NTIME
IF (I .EQ. 1) THEN
F(START)=1D0
RXR(START)=CONC(I,N)/CONCIN
GOTO 765
ENDIF
IF (ITER .EQ. NFACT) THEN
& F(START+I/NFACT)=(CONC(I,N)/CONCIN-
& PAR(NPAR-NEXP+COUNTR)*
& (CONC(I,N)/CONCIN-F(START+I/NFACT-1)))
RXR(START+I/NFACT)=CONC(I,N)/CONCIN
ITER=0
ENDIF
IF (NFACT .EQ. 1) ITER=0
ITER=ITER+1
765 CONTINUE
C
RETURN
END

```

E.1.2 HCl Bag Filter Code

```
C      Program written by Paul Chisholm
C      8 November 1998
C
C      The purpose of this program is to take information from
C      sand bed experiments to predict sorbent performance
C      on a bag filter.
C
C      PROGRAM FILTER
C      PARAMETER (M=1801)
C      IMPLICIT DOUBLE PRECISION (A-H, O-Z)
C      DOUBLE PRECISION MOLEQ
C      DIMENSION PAR(10),CONC(M,M),CONV(M,M),AVEREM(M)
C      DIMENSION TIME(M),FLUX(M,M),REM(M),TOTREM(M)
C      DIMENSION AVERMH(M),TOTCON(M),UTIL(M)
C
C      OPEN(UNIT=12, FILE='filter',STATUS='UNKNOWN')
C
C      Set important filter conditions. HCLIN is the inlet
C      concentration of HCl in ppm. RATIO is the mole ratio
C      of hydrated lime to HCl. WEIGHT is the molecular
C      weight of the sorbent. AREA is the normalized surface
C      area of the sorbent.
C
C      PPM=1000D0
C      RATIO=1D0
C      WEIGHT=154.08D0
C      AREA=87.5D0
C
C      NTIME is the number of time steps. DT is the interval
C      between time steps (min.). A few basic calculations are
C      performed. AFLRT is the actual gas flowrate (m**3/min.);
C      HCLQ is the flowrate of HCl (mol/m**3); HCLIN is the
C      concentration of HCl in the inlet (mol/m**3); SORBENT is the
C      mole rate of sorbent (mol/min.); and AREART is the rate of
C      addition of sorbent area (m**2/min.)
C
C      NTIME=1201
C      DT=1D0/20D0
C      TEMP=120D0
C      Q=1.5D0
C      AFLRT=Q/1.0D3*(273.15+TEMP)/(273.15+21.1)
C      HCLQ=Q/1.0D3*1.013D5*PPM/1.0D6/(273.15D0+21.1D0)/8.314D0
C      HCLIN=1.013D5*PPM/1E6/(273.15D0+TEMP)/8.314D0
C      SORBENT=HCLQ*0.5D0*RATIO
```

```

AREART=AREA*SORBENT*WEIGHT
C
C
C
Set the flux equation parameters:
PAR(1)=2.23D-5
PAR(2)=6.22D-4
PAR(3)=0.644D0
C
C
C
C
C
C
C
C
C
The calculations are similar to those from the fixed-bed
in many ways. There is no gas cell correction. The
origin is at the bag filter surface. The outside of
the filter cake is a moving boundary with a moving
boundary condition. PAR(1) and PAR(2) are divided by
60 to convert minutes to seconds. TOTCON is the
total conversion added up through the entire bed.
C
C
N=2
DO 987 I=1,NTIME
  CONC(I,N)=HCLIN
  CONV(I,N)=0.0D0
  TOTCON(I)=0D0
DO 876 J=N,1,-1
  IF (CONV(I,J) .GE. PAR(3)) THEN
    FLUX(I,J)=0.0D0
  ELSE IF (CONC(I,J) .EQ. 0.0D0) THEN
    FLUX(I,J)=0.0D0
  ELSE
    FLUX(I,J)=CONC(I,J)/(CONV(I,J)
&      /PAR(1)/60D0+1D0/PAR(2)/60D0)
&      *(PAR(3)-CONV(I,J))
  ENDIF
  IF (J .EQ. 1) GOTO 876
  CONC(I,J-1)=CONC(I,J)-FLUX(I,J)*AREART*DT/AFLRT
  IF (CONC(I,J-1) .LE. 0.0D0) CONC(I,J-1)=0.0D0
  CONV(I+1,J)=CONV(I,J)+AFLRT*(CONC(I,J)-CONC(I,J-1))
&      /2.0D0/SORBENT
  IF (CONV(I+1,J) .GE. PAR(3) .AND. CONV(I,J)
&      .LT. PAR(3)) THEN
    CONV(I+1,J)=PAR(3)
    CONC(I,J-1)=CONC(I,J)-(PAR(3)-CONV(I,J))
&      *SORBENT*2D0/AFLRT
  ENDIF
  TOTCON(I)=TOTCON(I)+CONV(I+1,J)
876 CONTINUE
REM(I)=(HCLIN-CONC(I,1))/HCLIN
IF (I .EQ. 1) THEN

```

```

          TOTREM(I)=REM(I)
          GOTO 987
      ENDIF
C
C      TOTREM is the removal through a single bag. AVEREM
C      is the average removal over an entire baghouse.
C      UTIL is the sorbent utilization.
C
      TOTREM(I)=TOTREM(I-1)+REM(I)
      AVEREM(I)=TOTREM(I)/DBLE(N)
      UTIL(I)=TOTCON(I)/DBLE(N)
      WRITE(12,1)DBLE(I)*DT,AVEREM(I),UTIL(I)
C
C      This calculation increases the bed thickness.
C
      N=N+1
987      CONTINUE
C
      CLOSE(12)
1      FORMAT(E15.4,E15.4,E15.4,E15.4)
      RETURN
      END

```

E.2 HCL-SO₂ ANALYSIS

Shown below are the three subroutines that were used to model the simultaneous absorption of HCl and SO₂ by calcium silicate. The same code can also be used for absorption by hydrated lime. The code shown is for the modeling of Exp. No. CS18. FORTRAN code for bag filter performance predictions is shown in Section E.2.2.

E.2.1 Fixed-Bed Code

```

C      Program written by Paul Chisholm
C      11 November 1998
C
C      The purpose of this routine is to (1) read data from
C      a file, (2) calculate concentrations of gas throughout
C      the bed at a certain experimental time, (3) call
C      on GREG and the associated subroutines, (4) and
C      ultimately to return an estimation for the unknown,
C      regressed parameters.
C

```

```

PROGRAM TWOGAS
IMPLICIT DOUBLE PRECISION (A-H, O-Z)
DOUBLE PRECISION LOAD
INTEGER START,END
EXTERNAL MODEL
DIMENSION OBS(2000),PAR(10),BNDLW(10),BNDUP(10)
DIMENSION DSC(13000),ISC(36),CHMAX(10),DEL(10)
DIMENSION RAW(2000)

```

The following DO loop reads the data from an input file.

```

OPEN(UNIT=12, FILE='RUN250-1000-500-O2.inp',
&      STATUS='UNKNOWN')

```

The following declarations initialize the arguments for GREG.

```

MDSC=25000
MISC=60

```

Input the number of parameters and the number of experiments that are being modeled simultaneously. For HCl+SO₂ regressions, only one experiment was modeled at a time. NOB is the total number of data points for all the experiments.

```

NPAR=7
NEXP=1
NOB=NEXP*2*321

```

Read the raw data from a file. Data for HCl is read first followed by data for SO₂. The temperature and the pressure are also recorded so that the conc. (ppm) vs. time data can be converted to conc. (mol/m³) vs. time data.

START and END are used so the program knows when to switch to the next file. NOBS is the number of data points for each individual experiment. Other variables: PPMH and PPMS=Inlet Concentration (ppm); LOAD=Sorbent Mass (mg); TEMP=Temperature (C); SFLRT=Flowrate at Standard Conditions (SLPM); SA=Normalized Surface Area (m²/g); DT=Data Interval (min.); RH=Relative Humidity (%); HClIN and SO₂IN=Inlet Concentration (mol/m³).

```

START=1
DO 876 I=1,NEXP
READ(11+I,*) PPMH,PPMS,LOAD,TEMP,SFLRT,PRESS,

```

```

&          SA,DT,RH,NOBS
&          HCLIN=(14.696D0+PRESS)*6.89476D3*PPMH*1D-6/
&              (273.15D0+TEMP)/8.314D0
&          SO2IN=(14.696D0+PRESS)*6.89476D3*PPMS*1D-6/
&              (273.15D0+TEMP)/8.314D0
&          END=START+2*NOBS-1
&          DO 987 ID=START,END
&              READ(11+I,*) RAW(ID)
&              IF (ID .LT. START+NOBS) THEN
&                  OBS(ID)=((14.696D0+PRESS)*6.89476D3*
&                      RAW(ID)*1D-6/(273.15D0+TEMP)/8.314D0)
&                      /HCLIN
&              ELSE
&                  OBS(ID)=((14.696D0+PRESS)*6.89476D3*
&                      RAW(ID)*1D-6/(273.15D0+TEMP)/8.314D0)
&                      /HCLIN
&              ENDIF
987 CONTINUE
    CLOSE(11+I)
    START=END+1
876 CONTINUE
C
C      Enter the initial guesses.
C
    PAR(1)=1D-3
    PAR(2)=1D-2
    PAR(3)=0.95D0
    PAR(4)=5D-5
    PAR(5)=1D0
    PAR(6)=3D-7
    PAR(7)=0.8D0

C
C      Initialize the the integer vector ISC. ISC(1)=1 is a user
C      number; ISC(2)=10 means the 10 subroutine using least squares
C      regression will determine the parameters; ISC(3)=0 means
C      several variables will use their default values; ISC(4)-ISC(6)
C      are not defined explicitly so their default values will be used.
C
C      Set the upper and lower boundaries and the maximum change for
C      a parameter.
C
    ISC(1)=1
    ISC(2)=10
    ISC(3)=1
    ISC(4)=25
    ISC(5)=2

```

```

ISC(6)=1
C
C      Set major default parameters.
C
      DO 765 J=1,NPAR
          BNDLW(J)=1D-30
          BNDUP(J)=1D30
          CHMAX(J)=1D30
          DEL(J)=-0.01D0
765    CONTINUE
          RPTOL=1D-5
          RSTOL=1D-1
          APIV=1D-2
C
C      This routine now calls GREG.
C
      CALL GREG(NOBS,OBS,NPAR,PAR,BNDLW,BNDUP,
&          CHMAX,DEL,MDSC,DSC,MISC,ISC,IOBS,IDET,
&          EMOD,VPIV,APIV,RPTOL,RSTOL,MODEL)
C
      STOP
      END

```

```

C      Paul Chisholm
C      11 November 1998
C
C      The purpose of this program is to send data to the BED
C      subroutine to crunch the numbers. This routine does
C      little more than manage the datafiles.
C
      SUBROUTINE MODEL (PAR, F, NOB, NPAR, IDER, DERIV,
&          MINFO)
      IMPLICIT DOUBLE PRECISION (A-H, O-Z)
      DOUBLE PRECISION LOAD
      INTEGER START,END,COUNTR
      DIMENSION PAR(10),F(2000),RAW(2000),OBS(2000),
      DIMENSION RXR(2000),AVCONH(2000),AVCONS(2000)
      DIMENSION AVGCON(2000)
C
      OPEN(UNIT=12,FILE='RUN250-1000-500-O2.inp',
C      &          STATUS='UNKNOWN')
C
      Enter the number of experiments being modeled simultaneously.
C

```



```

C      NEXP=1
C
C      The same variable names are used in this subroutine that were used in
C      TWOGAS. HCl and then SO2 data are read from the file.
C
      START=1
      DO 876 I=1,NEXP
        READ(11+I,*) PPMH,PPMS,LOAD,TEMP,SFLRT,
&          PRESS,SA,DT,RH,NOBS
        HCLIN=(14.696D0+PRESS)*6.89476D3*PPMH*1D-6/
&          (273.15D0+TEMP)/8.314D0
        SO2IN=(14.696D0+PRESS)*6.89476D3*PPMS*1D-6/
&          (273.15D0+TEMP)/8.314D0
        END=START+2*NOBS-1
      DO 987 ID=START,END
        READ(11+I,*) RAW(ID)
        IF (ID .LT. START+NOBS) THEN
          OBS(ID)=((14.696D0+PRESS)*6.89476D3*
&          RAW(ID)*1D-6/(273.15D0+TEMP)/8.314D0)
&          /HCLIN
        ELSE
          OBS(ID)=((14.696D0+PRESS)*6.89476D3*
&          RAW(ID)*1D-6/(273.15D0+TEMP)/8.314D0)
&          /HCLIN
        ENDIF
987    CONTINUE
      CLOSE(11+I)
      COUNTR=I
      CALL BED(LOAD,PPMH,PPMS,SA,PRESS,TEMP,SFLRT,DT,PAR,
&          NOBS,F,START,END,NPAR,COUNTR,NEXP,RXR,
&          AVGCON,AVCONH,AVCONS)
      START=END+1
876    CONTINUE
C
C      After BED regresses parameters, the data and values of
C      important vectors are output to 'conc'.
C
      OPEN(UNIT=23, FILE='conc', STATUS='UNKNOWN')
      DO 765 J=1,END
        WRITE(23,1)DBLE(J)/4D0-0.25D0,OBS(J),F(J),RXR(J),
&          OBS(J)-F(J),AVGCON(J),AVCONH(J),AVCONS(J)
765    CONTINUE
      CLOSE(23)
1      FORMAT (E15.7,2X,E15.7,2X,E15.7,2X,E15.7,2X,E15.7,2X,E15.7,
&          2X,E15.7,2X,E15.7)
C

```

RETURN
END

```
C      Program written by Paul Chisholm
C      11 November 1998
C
C      The purpose of this program is to generate a vector of
C      modeled concentrations in the gas cell. The concentration
C      of HCl and SO2 and conversion are calculated through the bed based
C      on flux equations. For HCl, the concentration at the outlet of
C      the reactor is modified with the gas cell correction.
C
C      SUBROUTINE BED(LOAD,PPMH,PPMS,SA,PRESS,TEMP,
&      SFLRT,DT,PAR, NOBS,F,START,END,NPAR,COUNTR,
&      NEXP,RXR,AVGCON,AVCONH,AVCONS)
C
C      IMPLICIT DOUBLE PRECISION (A-H, O-Z)
C      DOUBLE PRECISION MOLE, LOAD,HCLIN,SUM
C      INTEGER START,END,COUNTR,FREQM,FREQD
C      DIMENSION PAR(10),F(2000),HCL(10001,201),SO2(10001,201)
C      DIMENSION CONV(10001,201),AVGCON(2000),XSUM(10001)
C      DIMENSION FLUXH(10001,201),FLUXS(10001,201),RXR(2000)
C      DIMENSION CONVS(10001,201),CONVH(10001,201)
C      DIMENSION AVCONH(2000),AVCONS(2000),XSUMH(10001),
C      DIMENSION XSUMS(10001)
C
C      Define the time vector. FREQM is the frequency of time points
C      in a minute that is calculated with the model. FREQD is
C      the number of data points in a minute. NFACT is the factor
C      of model points compared to data points.
C      NTIME is the total number of time points that will be calculated.
C
C      FREQM=12
C      FREQD=4
C      NFACT=FREQM/FREQD
C      NTIME=NOBS*NFACT
C
C      The next few lines convert the experimental conditions into
C      important variables. MOLE is the number of moles in the rxr.
C      AREA is the normalized total surface area of the sorbent
C      (m**2/g), AFLRT is the actual flowrate (m**3/min.) of the gas C
C      through the reactor. HCLIN and SO2IN are the concentrations of the
C      gases (mol/m**3).
C
C      MOLE=LOAD*1D-3/154.08D0
C      AREA=LOAD*1D-3*SA
```

```

AFLRT=SFLRT*1D-3*(TEMP+273.15D0)
/294.25D0*14.696D0/(14.696D0+PRESS)
HCLIN=(14.696D0+PRESS)*6.89476D3*PPMH*1D-6/
& (273.15D0+TEMP)/8.314D0
SO2IN=(14.696D0+PRESS)*6.89476D3*PPMS*1D-6/
& (273.15D0+TEMP)/8.314D0

```

C
C
C
C
C
C
C
C

Begin the DO loops to determine the concentration at the outlet of the bed. N is the number of differential distances in the bed. The outer loop provides the calculations through time. The inner loop calculates calculation of concentration as a function of distance through the bed. The initial value of conversion in the bed is set to 1×10^{-5} . This was not necessary but generally allowed for more rapid convergence to a solution.

```

N=30
DO 987 I=1,NTIME
  HCL(I,1)=HCLIN
  SO2(I,1)=SO2IN
  SUMH=0.0D0
  SUMS=0.0D0
  DO 876 J=1,N
    CONV(I,J)=1D-5
    CONVS(I,J)=0.0D0
    SUMH=SUMH+CONVH(I,J)
    SUMS=SUMS+CONVS(I,J)
    IF (CONV(I,J) .GE. PAR(3)) THEN
      FLUXH(I,J)=0.0D0
    ELSE
      FLUXH(I,J)=HCL(I,J)/(CONV(I,J)/PAR(1)
& +1D0/HCL(I,J)/PAR(2))
& *(PAR(3)-CONV(I,J))
    ENDIF
    IF (FLUXH(I,J) .LT. 0.0D0) FLUXH(I,J)=0.0
    IF (CONV(I,J) .LT. 0.95D0*PAR(3)) THEN
      FLUXS(I,J)=SO2(I,J)/(CONV(I,J)/PAR(4)
& +1D0/HCL(I,J)/PAR(5))*(PAR(3)-CONV(I,J))
    ELSE IF (CONV(I,J) .GE. 0.95D0*PAR(3)
& .AND. CONV(I,J) .LT. PAR(3)) THEN
      FLUXS(I,J)=SO2(I,J)/(CONV(I,J)/PAR(4)
& +1D0/HCL(I,J)/PAR(5))*(PAR(3)-CONV(I,J))
& +PAR(6)/CONV(I,J)
    ELSE
      FLUXS(I,J)=PAR(6)/CONV(I,J)
    ENDIF
    IF (FLUXS(I,J) .LT. 0.0D0) FLUXS(I,J)=0.0D0

```

C

```

C      The next part of the code calculates the mass balances.
C
      HCL(I,J+1)=HCL(I,J)-FLUXH(I,J)*AREA/DBLE(N)/AFLRT
      SO2(I,J+1)=SO2(I,J)-FLUXS(I,J)*AREA/DBLE(N)/AFLRT
      IF (HCL(I,J+1) .LE. 0.0D0) HCL(I,J+1)=0.0D0
      IF (SO2(I,J+1) .LE. 0.0D0) SO2(I,J+1)=0.0D0
      CON VH(I+1,J)=CON VH(I,J)+AFLRT/DBLE(FREQM)/MOLE
&          *DBLE(N)*(HCL(I,J)-HCL(I,J+1))/2.0D0
      CON VS(I+1,J)=CON VS(I,J)+AFLRT/DBLE(FREQM)/MOLE
&          *DBLE(N)*(SO2(I,J)-SO2(I,J+1))
      CONV(I+1,J)=CON VH(I+1,J)+CON VS(I+1,J)
876      CONTINUE
      IF (NFACT .EQ. 1) ITER=0
      ITER=ITER+1
      XSUMH(I)=SUMH/DBLE(N)
      XSUMS(I)=SUMS/DBLE(N)
987      CONTINUE
C
C      The following part of the code calculates the concentration in
C      the gas cell based on the outlet of the reactor. The concentration of
C      HCl from the outlet of the reactor is corrected to account for the gas
C      cell.. SO2 concentration is not corrected. Modeled points are C
C      generated to match the data points taken. The variable ITER tracks C
C      which of the reactor outlet modeled points is used to compare to the
C      experimental points in GREG.
C
      ITER=1
      DO 765 I=1,NTIME
        IF (I .EQ. 1) THEN
          F(START)=1D0
          F(START+NOBS)=1D0
          RXR(START)=HCL(I,N)/HCLIN
          RXR(START+NOBS)=SO2(I,N)/SO2IN
          AVCONH(START)=XSUMH(I)
          AVCONS(START)=XSUMS(I)
          AVGCON(START)=XSUMH(I)+XSUMS(I)
          GOTO 765
        ENDIF
        IF (ITER .EQ. NFACT) THEN
&          F(START+I/NFACT)=HCL(I,N)/HCLIN
&          -PAR(NPAR-NEXP+COUNTR)
&          *(HCL(I,N)/HCLIN-F(START+I/NFACT-1))
          RXR(START+I/NFACT)=HCL(I,N)/HCLIN
          F(START+NOBS+I/NFACT)=SO2(I,N)/SO2IN
          RXR(START+NOBS+I/NFACT)=SO2(I,N)/SO2IN
          AVCONH(START+I/NFACT)=XSUMH(I)

```

```

                                AVCONS(START+I/NFACT)=XSUMS(I)
                                AVGCON(START+I/NFACT)=XSUMH(I)
                                +XSUMS(I)
                                ITER=0
                                ENDIF
                                IF (NFACT .EQ. 1) ITER=0
                                ITER=ITER+1
765      CONTINUE
C
      RETURN
      END

```

E.2.2 HCl-SO₂ Bag Filter Code

```

C      Program written by Paul Chisholm
C      11 November 1998
C
C      The purpose of this program is to take information from
C      sand bed experiments to predict sorbent performance
C      on a bag filter.
C
C      PROGRAM FILTER
C      PARAMETER (M=1801)
C      IMPLICIT DOUBLE PRECISION (A-H, O-Z)
C      DOUBLE PRECISION MOLEQ,PPMH,PPMS
C      DIMENSION PAR(10),HCL(M,M),CONV(M,M),FLUXH(M,M),
C      DIMENSION SO2(M,M),UTIL(M),TOTCON(M),
C      DIMENSION REMH(M),REMS(M),TOTRMH(M),TOTRMS(M)
C      DIMENSION AVERMH(M),AVERMS(M),FLUXS(M,M),
C
C      OPEN(UNIT=12, FILE='filter',STATUS='UNKNOWN')
C
C      Set important filter conditions. HCLIN is the inlet
C      concentration of HCl in ppm. SO2 is the inlet concentration of
C      SO2 in ppm. RATIO is the mole ratio
C      of hydrated lime to HCl+SO2. WEIGHT is the molecular
C      weight of the sorbent. AREA is the normalized surface
C      area of the sorbent.
C
C      PPMH=250D0
C      PPMS=1000D0
C      RATIO=1.5D0
C      WEIGHT=154.08D0
C      AREA=87.5D0

```

```

C
C      NTIME is the number of time steps. DT is the interval
C      between time steps (min.). A few basic calculations are
C      performed. AFLRT is the actual gas flowrate (m**3/min.);
C      HCLQ and SO2Q are the flowrates of HCl and SO2 (mol/m**3);
C      HCLIN and SO2IN are the concentration of HCl and SO2 in the inlet
C      (mol/m**3); SORBENT is the mole rate of sorbent (mol/min.); and
C      AREART is the rate of addition of sorbent area (m**2/min.)
C
      NTIME=1201
      DT=1D0/20D0
      TEMP=120D0
      Q=1.5D0
      AFLRT=Q/1.0D3*(273.15+TEMP)/(273.15+21.1)
      HCLQ=Q/1.0D3*1.013D5*PPMH/1.0D6/(273.15D0+21.1D0)
&      /8.314D0
      SO2Q=Q/1.0D3*1.013D5*PPMS/1.0D6/
&      (273.15D0+21.1D0)/8.314D0
      HCLIN=1.013D5*PPMH/1E6/(273.15D0+TEMP)/8.314D0
      SO2IN=1.013D5*PPMS/1E6/(273.15D0+TEMP)/8.314D0
      SORBENT=(HCLQ*0.5D0+SO2Q)*RATIO
      AREART=AREA*SORBENT*WEIGHT
C
C      Set the flux equation parameters:
C
      PAR(1)=6.38D-5
      PAR(2)=6.62D-5
      PAR(3)=0.943D0
      PAR(4)=2.08D-6
      PAR(5)=2.78D-2
      PAR(6)=3.8D-9
C
C      The calculations are similar to those from the fixed-bed
C      in many ways. There is no gas cell correction. The
C      origin is at the bag filter surface. The outside of
C      the filter cake is a moving boundary with a moving
C      boundary condition. Some parameters are divided by
C      60 to convert minutes to seconds. TOTCON is the
C      total conversion added up through the entire bed.
C
      N=2
      DO 987 I=1,NTIME
        HCL(I,N)=HCLIN
        SO2(I,N)=SO2IN
        TOTCON(I)=0D0
      DO 876 J=N,2,-1
        CONV(I,N)=1D-5

```

```

      IF (CONV(I,J) .GE. PAR(3)) THEN
        FLUXH(I,J)=0.0D0
      ELSE
        FLUXH(I,J)=HCL(I,J)/(CONV(I,J)/PAR(1)/6D1
&          +1D0/PAR(2)/6D1)*(PAR(3)-CONV(I,J))
      ENDIF
      IF (FLUXH(I,J) .LT. 0.0D0) FLUXH(I,J)=0.0
      IF (CONV(I,J) .LT. 0.95D0*PAR(3)) THEN
        FLUXS(I,J)=SO2(I,J)/(CONV(I,J)/PAR(4)/6D1
&          +1D0/HCL(I,J)/PAR(5)/6D1)*(PAR(3)-CONV(I,J))
      ELSE IF (CONV(I,J) .GE. 0.95D0*PAR(3)
&          .AND. CONV(I,J) .LT. PAR(3)) THEN
        FLUXS(I,J)=SO2(I,J)/(CONV(I,J)/PAR(4)/6D1
&          +1D0/HCL(I,J)/PAR(5)/6D1)
&          *(PAR(3)-CONV(I,J))+PAR(6)*6D1/CONV(I,J)
      ELSE
        FLUXS(I,J)=PAR(6)*6D1/CONV(I,J)
      ENDIF
      HCL(I,J-1)=HCL(I,J)-FLUXH(I,J)*AREART*DT/AFLRT
      SO2(I,J-1)=SO2(I,J)-FLUXS(I,J)*AREART*DT/AFLRT
      IF (HCL(I,J-1) .LE. 0.0D0) HCL(I,J-1)=0.0D0
      IF (SO2(I,J-1) .LE. 0.0D0) SO2(I,J-1)=0.0D0
      CONV(I+1,J)=CONV(I,J)+AFLRT/SORBENT*
&          ((HCL(I,J)-HCL(I,J-1))/2.0D0)+(SO2(I,J)-SO2(I,J-1)))
      TOTCON(I)=TOTCON(I)+CONV(I+1,J)
876 CONTINUE
      REMH(I)=(HCLIN-HCL(I,1))/HCLIN
      REMS(I)=(SO2IN-SO2(I,1))/SO2IN
      IF (I.EQ. 1) THEN
        TOTRMH(I)=REMH(I)
        TOTRMS(I)=REMS(I)
        GOTO 987
      ENDIF
C
C
C
C
      TOTREM is the removal through a single bag. AVEREM
      is the average removal over an entire baghouse.
      UTIL is the sorbent utilization.
      TOTRMH(I)=TOTRMH(I-1)+REMH(I)
      TOTRMS(I)=TOTRMS(I-1)+REMS(I)
      AVERMH(I)=TOTRMH(I)/DBLE(N)
      AVERMS(I)=TOTRMS(I)/DBLE(N)
      UTIL(I)=TOTCON(I)/DBLE(N)
      WRITE(12,1)DBLE(I)*DT,AVERMH(I),1D0-AVERMH(I),
&          AVERMS(I),1D0-AVERMS(I),UTIL(I)
C
C
      This calculation increases the bed thickness.

```

```
C      N=N+1
987  CONTINUE
C      CLOSE(12)
1      FORMAT (E15.6,E15.6,E15.6,E15.6,E15.6,E15.6)
      RETURN
      END
```


Appendix F. Data Archive

This appendix archives experimental data from Experiment Nos. CS18 and CS25. These two experiments were chosen because they were used to draw comparison between municipal waste combustors and coal-fired boilers. A more extensive archive for all of the 64 experiments, 30 for hydrated lime and 34 for calcium silicate, is located with Dr. Gary Rochelle at the Department of Chemical Engineering at the University of Texas at Austin. The data format is the same as shown below for Experiment Nos. CS18 and CS25. All 62 experiments were not included in this dissertation because the tables take up over 100 pages.

Table F.1 Experimental Data (in ppm) for Exp. Nos. CS18 and CS25.

Time (min.)	CS18			CS25			Time (min.)
	HCl	SO ₂	NO ₂	HCl	SO ₂	NO ₂	
0	221	993	47	982	255	51	0
0.25	207	823	33	800	165	38	0.25
0.5	138	223	-1	388	25	21	0.5
0.75	110	248	0	255	2	29	0.75
1	98	426	7	193	3	34	1
1.25	74	548	20	145	18	35	1.25
1.5	65	634	20	121	36	34	1.5
1.75	73	705	23	112	56	31	1.75
2	63	752	24	108	88	38	2
2.25	59	778	27	112	103	33	2.25
2.5	52	809	27	114	118	36	2.5
2.75	49	829	31	116	133	39	2.75
3	43	831	31	146	141	40	3
3.25	43	850	28	206	154	40	3.25
3.5	56	868	31	289	167	42	3.5
3.75	40	874	34	361	180	43	3.75
4	33	885	38	397	191	46	4
4.25	55	803	22	450	196	44	4.25
4.5	66	873	18	497	201	44	4.5
4.75	70	904	19	551	208	37	4.75

Time (min.)	CS18			CS25			Time (min.)
	HCl	SO ₂	NO ₂	HCl	SO ₂	NO ₂	
5	64	901	20	606	216	43	5
5.25	57	899	22	636	220	45	5.25
5.5	28	898	22	680	223	44	5.5
5.75	54	899	28	706	230	39	5.75
6	34	886	26	724	231	49	6
6.25	48	896	25	769	234	46	6.25
6.5	52	880	22	795	236	47	6.5
6.75	36	898	23	819	240	44	6.75
7	37	911	25	829	243	43	7
7.25	38	900	24	850	245	47	7.25
7.5	42	904	25	856	247	54	7.5
7.75	46	914	24	874	244	48	7.75
8	41	910	24	880	247	48	8
8.25	59	919	21	884	247	48	8.25
8.5	50	934	24	889	246	49	8.5
8.75	68	940	27	906	249	46	8.75
9	81	946	28	904	249	48	9
9.25	92	942	27	944	252	49	9.25
9.5	102	944	28	912	251	48	9.5
9.75	127	966	33	941	255	50	9.75
10	120	962	32	924	246	45	10
10.25	128	962	30	952	252	49	10.25
10.5	136	963	29	940	254	50	10.5
10.75	132	963	31	949	253	53	10.75
11	160	957	31	936	254	48	11
11.25	163	981	35	952	254	49	11.25
11.5	171	960	34	960	251	52	11.5
11.75	178	961	30	957	254	48	11.75
12	186	974	33	964	252	45	12
12.25	184	972	36	969	257	52	12.25
12.5	184	965	35	966	256	51	12.5
12.75	174	971	33	960	255	48	12.75
13	194	970	34	973	253	52	13
13.25	202	956	33	981	255	51	13.25
13.5	199	985	35	973	255	53	13.5
13.75	193	967	34	978	254	53	13.75
14	202	992	39	984	253	54	14
14.25	192	955	35	963	255	51	14.25

Time (min.)	CS18			CS25			Time (min.)
	HCl	SO ₂	NO ₂	HCl	SO ₂	NO ₂	
14.5	193	984	36	993	253	51	14.5
14.75	201	966	37	976	250	47	14.75
15	204	968	34	1010	255	48	15
15.25	216	990	36	985	255	51	15.25
15.5	207	982	36	981	256	51	15.5
15.75	198	973	37	982	253	52	15.75
16	209	980	37	1006	253	45	16
16.25	198	965	34	988	255	52	16.25
16.5	197	966	37	991	252	49	16.5
16.75	218	974	34	976	251	48	16.75
17	202	971	34	983	256	52	17
17.25	216	975	35	988	259	52	17.25
17.5	221	993	36	992	254	52	17.5
17.75	216	983	38	1005	253	48	17.75
18	219	963	35	988	252	51	18
18.25	220	984	36	1002	254	48	18.25
18.5	218	972	35	989	254	51	18.5
18.75	214	981	37	980	255	51	18.75
19	217	987	39	989	252	51	19
19.25	230	984	38	995	254	51	19.25
19.5	221	971	38	1001	257	51	19.5
19.75	204	978	36	984	253	51	19.75
20	215	979	39	994	254	49	20
20.25	219	978	38	987	252	49	20.25
20.5	213	973	36	984	253	49	20.5
20.75	207	968	35	999	255	50	20.75
21	222	986	39	991	255	49	21
21.25	225	983	37	989	256	50	21.25
21.5	218	978	35	974	251	49	21.5
21.75	234	976	36	1002	253	48	21.75
22	228	986	38	984	254	53	22
22.25	231	986	36	992	254	50	22.25
22.5	237	984	38	974	253	49	22.5
22.75	222	978	39	985	251	48	22.75
23	230	987	35	990	252	48	23
23.25	230	972	37	999	252	48	23.25
23.5	228	994	37	988	252	48	23.5
23.75	235	975	34	993	254	52	23.75

Time (min.)	CS18			CS25			Time (min.)
	HCl	SO ₂	NO ₂	HCl	SO ₂	NO ₂	
24	239	987	37	976	255	51	24
24.25	227	982	39	978	255	49	24.25
24.5	239	984	37	981	248	49	24.5
24.75	218	984	40	1002	252	46	24.75
25	232	973	35	996	251	49	25
25.25	239	987	38	988	251	51	25.25
25.5	240	992	36	990	253	52	25.5
25.75	237	992	39	991	253	50	25.75
26	234	992	42	981	255	47	26
26.25	233	982	38	996	249	47	26.25
26.5	228	986	38	980	250	46	26.5
26.75	236	984	37	995	247	46	26.75
27	235	974	37	1001	251	46	27
27.25	245	991	36	999	257	51	27.25
27.5	230	981	38	960	249	49	27.5
27.75	236	1000	39	992	250	48	27.75
28	234	982	41	1003	248	46	28
28.25	235	974	37	1003	252	47	28.25
28.5	241	984	38	1002	249	47	28.5
28.75	241	987	39	983	252	47	28.75
29	244	984	39	989	248	48	29
29.25	242	984	39	989	259	50	29.25
29.5	242	982	39	997	248	48	29.5
29.75	239	986	36	993	248	45	29.75
30	234	986	39	995	247	45	30
30.25	230	987	42	1026	250	43	30.25
30.5	235	990	41	980	253	47	30.5
30.75	237	991	40	981	251	46	30.75
31	234	988	39	982	249	44	31
31.25	231	985	39	992	247	44	31.25
31.5	246	975	38	1009	248	46	31.5
31.75	235	983	39	1002	250	45	31.75
32	248	984	40	988	249	48	32
32.25	237	987	39	999	252	42	32.25
32.5	239	989	39	988	248	47	32.5
32.75	242	997	43	1006	246	46	32.75
33	253	975	39	1003	253	44	33
33.25	245	984	40	1010	263	55	33.25

Time (min.)	CS18			CS25			Time (min.)
	HCl	SO ₂	NO ₂	HCl	SO ₂	NO ₂	
33.5	235	980	36	931	225	42	33.5
33.75	228	992	39	1044	234	32	33.75
34	224	995	44	1042	242	35	34
34.25	233	979	41	1014	241	34	34.25
34.5	241	981	40	1003	244	44	34.5
34.75	243	985	37	996	244	43	34.75
35	246	1001	41	978	245	43	35
35.25	234	985	41	988	247	45	35.25
35.5	250	1002	43	1000	251	46	35.5
35.75	227	989	42	984	247	43	35.75
36	230	992	42	992	244	42	36
36.25	234	994	41	1005	245	39	36.25
36.5	248	987	40	1017	245	36	36.5
36.75	241	975	38	1004	247	43	36.75
37	254	993	41	1003	250	47	37
37.25	239	991	40	983	247	40	37.25
37.5	238	987	43	995	248	44	37.5
37.75	231	980	38	991	251	48	37.75
38	238	996	41	1002	246	44	38
38.25	250	980	40	1013	247	45	38.25
38.5	246	991	41	1013	248	43	38.5
38.75	240	987	38	1010	247	47	38.75
39	251	990	43	1020	246	43	39
39.25	234	991	43	999	247	48	39.25
39.5	239	989	42	1002	246	40	39.5
39.75	234	981	37	1000	244	40	39.75
40	245	988	41	1012	246	44	40
40.25	234	1001	43	1010	249	44	40.25
40.5	231	991	44	1001	249	47	40.5
40.75	244	995	44	995	243	44	40.75
41	241	986	41	985	247	41	41
41.25	235	985	41	1002	244	42	41.25
41.5	230	984	42	999	244	41	41.5
41.75	240	986	38	1003	250	45	41.75
42	244	997	36	991	251	46	42
42.25	240	989	43	977	251	46	42.25
42.5	239	985	40	998	248	45	42.5
42.75	239	998	43	991	248	47	42.75

Time (min.)	CS18			CS25			Time (min.)
	HCl	SO ₂	NO ₂	HCl	SO ₂	NO ₂	
43	243	988	41	1015	242	42	43
43.25	248	987	45	1007	246	45	43.25
43.5	243	999	41	999	246	43	43.5
43.75	244	977	41	1013	249	43	43.75
44	260	994	42	1009	247	45	44
44.25	259	983	41	994	246	47	44.25
44.5	244	992	41	995	247	44	44.5
44.75	256	986	41	993	249	45	44.75
45	244	997	41	1019	241	46	45
45.25	237	990	43	1009	247	45	45.25
45.5	239	984	39	976	250	45	45.5
45.75	237	977	39	1006	245	44	45.75
46	241	988	39	983	246	43	46
46.25	266	989	39	1000	246	47	46.25
46.5	258	989	39	1005	245	49	46.5
46.75	250	989	39	1015	247	41	46.75
47	259	1004	44	994	249	43	47
47.25	232	987	43	1007	247	47	47.25
47.5	236	988	43	1002	246	47	47.5
47.75	256	979	39	997	245	47	47.75
48	263	991	41	1015	247	44	48
48.25	244	992	40	1001	245	45	48.25
48.5	239	990	42	1008	247	39	48.5
48.75	244	981	41	1010	245	47	48.75
49	255	990	41	1000	244	45	49
49.25	254	986	40	1016	247	45	49.25
49.5	241	990	41	1001	243	42	49.5
49.75	247	982	40	1022	248	43	49.75
50	250	997	43	991	247	47	50
50.25	236	994	41	1005	250	49	50.25
50.5	242	1017	48	999	245	45	50.5
50.75	236	953	45	1004	247	44	50.75
51	258	956	31	1019	248	47	51
51.25	287	988	33	1017	249	44	51.25
51.5	270	993	36	1004	243	46	51.5
51.75	270	995	36	1028	247	41	51.75
52	270	997	37	1012	248	46	52
52.25	255	987	41	978	248	48	52.25

Time (min.)	HCl	CS18 SO ₂	NO ₂	HCl	CS25 SO ₂	NO ₂	Time (min.)
52.5	254	990	39	998	247	46	52.5
52.75	251	987	43	1001	244	47	52.75
53	253	988	41	993	246	45	53
53.25	251	986	40	998	244	42	53.25
53.5	249	979	39	1003	242	40	53.5
53.75	244	994	40	1019	250	48	53.75
54	248	987	43	1006	249	47	54
54.25	243	983	43	1002	247	44	54.25
54.5	253	988	42	1005	246	44	54.5
54.75	259	985	42	994	246	43	54.75
55	249	985	41	1014	245	43	55
55.25	242	998	40	1018	250	46	55.25
55.5	252	991	41	1000	247	48	55.5
55.75	240	995	44	999	245	44	55.75
56	241	979	41	995	248	49	56
56.25	248	991	42	992	251	52	56.25
56.5	262	992	39	994	244	45	56.5
56.75	256	992	40	1007	249	48	56.75
57	250	989	41	983	249	49	57
57.25	244	986	41	998	246	48	57.25
57.5	250	998	42	1027	245	47	57.5
57.75	258	977	39	1020	244	45	57.75
58	270	987	40	1002	248	47	58
58.25	250	999	39	1005	248	46	58.25
58.5	260	1000	44	985	249	50	58.5
58.75	250	989	41	994	249	49	58.75
59	245	1000	40	1003	249	48	59
59.25	245	975	45	987	246	46	59.25
59.5	266	991	41	1015	246	44	59.5
59.75	261	991	41	1006	247	46	59.75
60	248	997	44	999	246	43	60
60.25	254	998	45	1016	250	48	60.25
60.5	246	984	46	996	249	46	60.5
60.75	250	986	44	1006	248	49	60.75
61	250	985	44	977	243	43	61
61.25	248	990	39	1016	251	45	61.25
61.5	253	991	41	985	246	52	61.5
61.75	250	1001	43	995	250	51	61.75

Time (min.)	CS18 HCl	SO ₂	NO ₂	CS25 HCl	SO ₂	NO ₂	Time (min.)
62	238	987	42	999	246	45	62
62.25	236	987	41	1002	248	51	62.25
62.5	234	987	41	1020	250	48	62.5
62.75	242	989	41	989	244	45	62.75
63	253	997	41	1008	248	44	63
63.25	258	984	39	1024	247	48	63.25
63.5	266	991	40	1003	251	51	63.5
63.75	261	994	41	984	246	49	63.75
64	248	989	42	1011	250	50	64
64.25	256	993	39	1001	250	44	64.25
64.5	247	1002	42	996	249	45	64.5
64.75	243	989	40	990	247	45	64.75
65	246	995	43	1009	246	44	65
65.25	241	998	44	1009	246	48	65.25
65.5	241	984	40	1017	249	48	65.5
65.75	251	989	41	1013	245	46	65.75
66	244	999	42	995	248	47	66
66.25	262	985	41	999	251	53	66.25
66.5	247	991	40	987	247	48	66.5
66.75	242	1006	43	1001	247	50	66.75
67	241	996	44	987	247	46	67
67.25	229	980	42	1000	250	48	67.25
67.5	243	982	42	984	246	47	67.5
67.75	256	984	41	1001	248	48	67.75
68	254	983	41	998	252	49	68
68.25	256	1006	42	993	248	50	68.25
68.5	262	991	44	993	249	51	68.5
68.75	236	988	42	996	251	48	68.75
69	260	984	41	1013	249	47	69
69.25	256	999	43	1012	249	49	69.25
69.5	252	986	40	999	248	48	69.5
69.75	257	998	44	999	247	46	69.75
70	241	995	45	995	248	48	70
70.25	239	996	44	991	249	49	70.25
70.5	234	995	43	1003	250	54	70.5
70.75	254	1003	43	1000	247	48	70.75
71	257	978	42	1006	249	45	71
71.25	250	983	40	1010	251	47	71.25

Time (min.)	CS18			CS25			Time (min.)
	HCl	SO ₂	NO ₂	HCl	SO ₂	NO ₂	
71.5	253	988	42	998	255	54	71.5
71.75	248	1006	44	984	246	50	71.75
72	242	984	45	1013	254	53	72
72.25	258	991	44	1006	250	53	72.25
72.5	253	990	41	1000	253	51	72.5
72.75	257	992	41	1012	250	47	72.75
73	260	995	41	1005	248	54	73
73.25	247	1005	44	1015	250	50	73.25
73.5	254	996	45	1005	253	50	73.5
73.75	241	995	49	994	249	50	73.75
74	244	986	42	1003	243	49	74
74.25	243	992	42	1008	252	47	74.25
74.5	248	993	41	998	249	49	74.5
74.75	255	987	41	995	249	45	74.75
75	251	998	44	992	254	51	75
75.25	257	1005	46				75.25
75.5	245	996	46				75.5
75.75	248	984	43				75.75
76	239	984	44				76
76.25	267	992	42				76.25
76.5	255	998	42				76.5
76.75	243	1014	46				76.75
77	252	975	43				77
77.25	259	988	44				77.25
77.5	253	990	42				77.5
77.75	246	988	41				77.75
78	250	991	41				78
78.25	254	994	41				78.25
78.5	253	999	44				78.5
78.75	243	999	48				78.75
79	240	993	45				79
79.25	264	984	43				79.25
79.5	266	998	43				79.5
79.75	266	991	40				79.75
80	249	999	42				80
80.25	255	996	44				80.25
80.5	258	988	42				80.5
80.75	255	1004	48				80.75

Time (min.)	CS18			CS25			Time (min.)
	HCl	SO ₂	NO ₂	HCl	SO ₂	NO ₂	
81	248	991	43				81
81.25	258	993	45				81.25
81.5	255	1006	45				81.5
81.75	257	986	45				81.75
82	251	991	42				82
82.25	251	1008	48				82.25
82.5	245	975	42				82.5
82.75	264	997	43				82.75
83	253	1001	43				83
83.25	246	1001	45				83.25
83.5	239	1001	48				83.5
83.75	242	992	46				83.75
84	254	993	44				84
84.25	253	995	43				84.25
84.5	270	987	42				84.5
84.75	248	998	42				84.75
85	261	1002	44				85
85.25	244	991	43				85.25
85.5	246	999	45				85.5
85.75	257	989	42				85.75
86	250	997	46				86
86.25	257	1001	44				86.25
86.5	241	1001	45				86.5
86.75	251	991	46				86.75
87	251	1008	47				87
87.25	252	1004	49				87.25
87.5	242	1004	50				87.5
87.75	233	1004	49				87.75
88	246	993	49				88
88.25	242	998	48				88.25
88.5	248	999	48				88.5
88.75	253	1000	48				88.75
89	230	990	50				89
89.25	253	991	47				89.25
89.5	245	1004	46				89.5
89.75	253	990	46				89.75
90	261	997	44				90

Appendix G. Speculation of Absorption Mechanism

As it was mentioned in Section 8.3, the role of relative humidity in the absorption of acid gases is not well understood. In this study, a semi-empirical approach was used to describe the data. A theory explaining the absorption of acid gases was developed but not applied due to its complexity. The purpose of this appendix is to qualitatively describe this theory.

To simplify this discussion, the reactive sorbent is assumed to consist of one planar layer. HCl will be used as the example acid gas, although SO₂ and NO₂ should behave similarly. The theory is comprised of three regimes. During the first regime, HCl is exposed to the sorbent which is covered with a surface layer of water. The thickness of the water layer is in accordance with the water vapor isotherm. Because this layer of water is in contact with alkaline sorbent, its pH is moderately high. HCl is absorbed into the water layer and reacts. The rate of reaction is limited either by the gas film resistance or reaction kinetics.

As the concentration of chloride increases in the water layer, the driving force for nucleation of calcium chloride increases. When the driving force becomes large enough, calcium chloride instantaneously forms a nucleus. Nucleation is the second regime.

After nucleation of a calcium chloride crystal, other calcium and chloride ions diffuse to it and crystallize. As the crystal becomes larger, it spreads across the surface of the fresh sorbent. A schematic of the crystallization process is shown in Figure G.1.1. Crystallization is the third regime. The rate of HCl absorption, then, is the rate at which calcium chloride diffuses to a nucleus to crystallize. As chloride precipitates, it allows another chloride ion to dissolve into the surface water.

The strength of this theory is that it describes the role of relative humidity. With greater humidity, the water layer is thicker. Therefore, calcium and chloride ions diffuse more quickly to a nucleation site. More importantly, further nucleation is prevented because of the ease with which ions can diffuse. Without many nucleation sites, the layer of sorbent is not covered by a layer of

crystallizing reaction product. When the relative humidity is low, ions can not diffuse as quickly and are forced to nucleate throughout the surface of the sorbent. While the resulting crystals may be thinner on the surface of the sorbent, the layer covers more surface area. Therefore, the absorption rate drops to zero because the pH of the solution is too low to allow for HCl sorption.

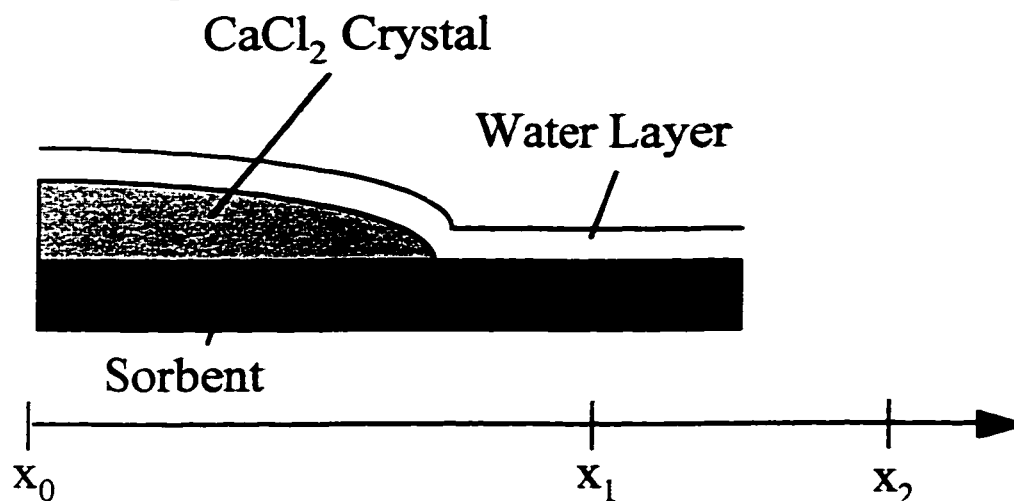


Figure G.1.1 Schematic of crystallization.

Appendix H. Experimental Reproducibility

At the end of Chapter 3, Figure 3.6.1 compared three fixed-bed experiments performed at the same conditions. The data from the three experiments showed that there were some reproducibility limitations with the experimental apparatus. To determine how the uncertainty in a fixed-bed experiment may impact the modeling results, all three experiments shown in Figure 3.6.1 were modeled. The data set for each experiment were regressed both individually and simultaneously with each of the other two data sets.

The parameters estimated and the model fits are shown in Table H.1.1 and Figures H.1.1-3. The parameter estimation shows that D_{eff} and k_s did not vary significantly from one experiment to the next, taking into account the confidence intervals. Regressed values of x_T had the greatest deviation between experiments. The differences between values of x_T are a reflection of the fact that, according to the gas phase mass balance, slightly different final HCl loading values were

Table H.1.1 Comparison of Parameters for Three Experiments at the Conditions of CS9

CS Exp. No.	HCl Conc. (ppm)	Sorb. Load. (mg)	$D_{eff} \times 10^5$ (m/s)	$k_s \times 10^4$ (m/s)	x_T	c (s)	Mean Model Error (%) †	Simult. Mean Model Error (%) †
Simult. Model			1.43	9.82	0.604	-	-	3.27
2 σ :			0.22	14.3	0.015	-		
9(1)	2000	36	1.93	12.7	0.641	9.02	3.46	4.10
2 σ :			0.48	10.7	0.024	0.48		
9(2)	2000	36	1.44	2.68	0.613	7.44	2.33	2.46
2 σ :			0.29	2.58	0.018	0.46		
9(3)	2000	36	1.36	6.48	0.539	6.26	2.42	3.03
2 σ :			0.26	9.47	0.018	0.53		

† The error reported is the square root of the average model error squared multiplied by 100.

calculated. These experiments were all performed at a relatively high concentration, 2000 ppm. Therefore, small relative uncertainties or signal drift would have affected x_T much more an experiment at, for example, 250 ppm.

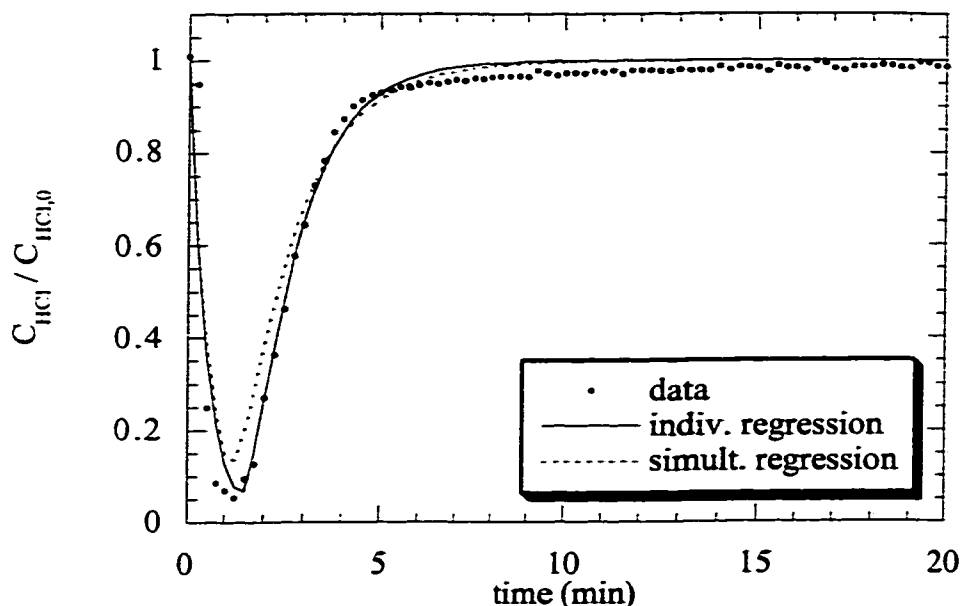


Figure H.1.1 Comparison of data from CS9(1) to a individually regressed model and to the model with all CS9 experiments regressed simultaneously.

The experiments were performed at 3.5% RH, 120 °C, and 1.5 SLPM with 2000 ppm HCl, 36 mg calcium silicate. Regressed parameters documented in Table H.1

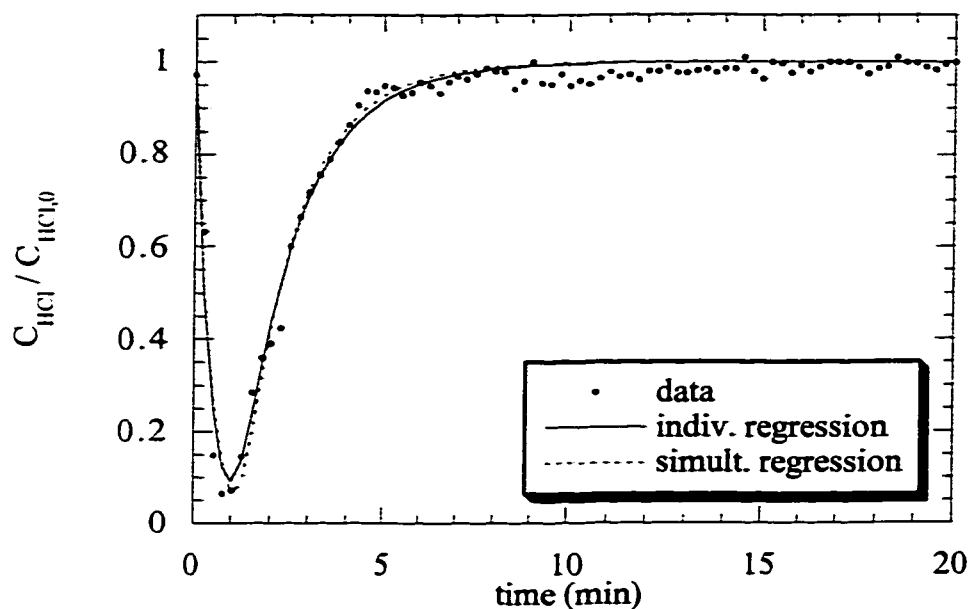


Figure H.1.2 Comparison of data from CS9(2) to a individually regressed model and to the model with all CS9 experiments regressed simultaneously.

The experiments were performed at 3.5% RH, 120 °C, and 1.5 SLPM with 2000 ppm HCl, 36 mg calcium silicate. Regressed parameters documented in Table H.1

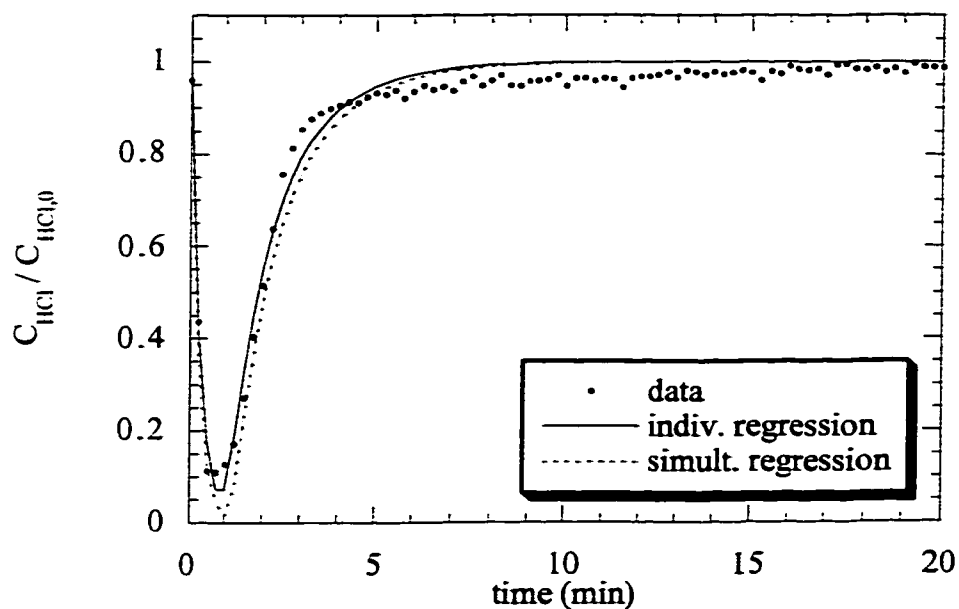


Figure H.1.3 Comparison of data from CS9(3) to a individually regressed model and to the model with all CS9 experiments regressed simultaneously.

The experiments were performed at 3.5% RH, 120 °C, and 1.5 SLPM with 2000 ppm HCl, 36 mg calcium silicate. Regressed parameters documented in Table H.1

References

- Arthur, L. F., "Silicate Sorbents for Flue Gas Cleaning," Ph.D. Dissertation, The University of Texas at Austin, 1998.
- Bhatia, J. K., D. D. Perlmutter, "The Effect of Pore Structure on Fluid-Solid Reactions: Application to the SO_2 -Lime Reaction," *AIChE Journal*, **27**(2), 226, 1981.
- Borgwardt, R. H., K.R. Bruce, J. Blake, "An Investigation of Product-Layer Diffusivity for CaO Sulfation," *Industrial Engineering and Chemistry Research*, **26**, 1993, 1987.
- Cain, P. M., "Removal of Hydrogen Chloride from Flue Gas by Dry Sorbents Prepared from the Hydrothermal Reaction of Silica and Calcium Hydroxide," Ph.D. Dissertation, The University of Tennessee, 1993.
- Caracotsios, M., "Model Parametric Sensitivity Analysis and Nonlinear Parameter Estimation. Theory and Applications," Ph.D. Dissertation, The University of Wisconsin-Madison, 1986.
- Chang, J. C. S., T. G. Brna, and C. B. Sedman, "Pilot Evaluation of Sorbents for Simultaneous Removal of HCl and SO_2 from MSW Incinerator Flue Gas by Dry Injection Process," presented at the International Conference on Municipal Waste Combustion, Hollywood, Florida, 1989.
- Chu, P., G. T. Rochelle, "Removal of SO_2 and NO_x from Stack Gas by Reaction with Calcium Hydroxide Solids," *JAPCA*, **39**(2), 175, 1989.
- Dam-Johansen, K., P. F. B. Hansen, K. Østergaard, "High-Temperature Reaction Between Sulfur Dioxide and Limestone--III. A Grain-Micrograin Model and Its Verification," *Chemical Engineering Science*, **46**(3), 847, 1991.
- Daoudi, M., J. K. Walters, "A Thermogravimetric Study of the Reaction of Hydrogen Chloride Gas with Calcined Limestone: Determination of Kinetic Parameters," *The Chemical Engineering Journal*, **47**, 1, 1991.
- Donnelly J. R., "Overview of Air Pollution Controls for Municipal Waste Combustors," presented at the Second International Conference on Municipal Waste Combustion, Tampa, Florida, 1991.
- Duo, W., N. F. Kirby, J. P. K. Seville, R. Clift, "Alteration with Reaction Progress of the Rate Limiting Step for Solid-Gas Reactions of Ca-Compounds with HCl," *Chemical Engineering Science*, **50**(13), 2017, 1995.

- Duo, W., J. P. K. Seville, N. F. Kirby, R. Clift, "Formation of Product Layers in Solid-Gas Reactions for Removal of Acid Gases," *Chemical Engineering Science*, **49**(24A), 4429, 1994.
- Dutchuk, M., "NO₂ Absorption in Aqueous Dithionite," M. S. Thesis, The University of Texas at Austin, 1999.
- Fernández, J., J. Renedo, A. Garea, J. Viguri, J. A. Iribien, "Preparation and Characterization of Fly Ash/Hydrated Lime Sorbents for SO₂ Removal," *Powder Technology*, **94**, 133, 1997.
- Fonseca, A. M., J. J. Órfão, R. L. Salcedo, "Kinetic Modeling of the Reaction of HCl and Solid Lime at Low Temperatures," *Industrial Engineering and Chemistry Research*, **37**, 4570, 1998.
- Garea, A., J. R. Viguri, A. Iribien, "Kinetics of Flue Gas Desulphurization at Low Temperatures: Fly Ash/Calcium (3/1) Sorbent Behaviour," *Chemical Engineering Science*, **52**(5), 715, 1997.
- Garvin D., V.B. Parker, and H.J. White, Jr., CODTA Thermodynamic Tables, Hemisphere Publishing Corporation, New York, 1987.
- Gullett, B. K., W. Jozewicz, L. A. Stefanski, "Reaction Kinetics of Ca-Based Sorbents with HCl," *Industrial Engineering and Chemistry Research*, **31**, 2437, 1992.
- Hanawalt, J., H. Rinn, L. Frevel, "Chemical Analysis by X-ray Diffraction. Classification and Use of X-Ray Diffraction Patterns," *Analytical Chemistry*, **10**, 457, 1938.
- Hanst, P. L., S. T. Hanst, "Volume 1: Gas Measurements in the Fundamental Infrared Region," Promotional Document, Infrared Analysis, Inc., Anaheim, California, 1995.
- Holzman, M. and R. S. Atkins, "Retrofitting Acid Gas Controls: A Comparison of Technologies," *Solid Waste & Power*, **2**(5), 1988.
- Hsia, C., G. R. St. Pierre, K. Raghunathan, L.-S. Fan, "Diffusion Through CaSO₄ Formed During the Reaction of CaO with SO₂ and O₂," *AIChE Journal*, **39**(4), 1993.
- Iribien, A., F. Cortabitarte, J. I. Ortiz, "Kinetics of Flue gas Desulfurization at Low Temperatures: Nonideal Surface Adsorption Model," *Chemical Engineering Science*, **47**(7), 1533, 1992.
- Jarvis, J. B., P. A. Nassos, D. A. Stewart, "A Study of Sulfur-Nitrogen Compounds in Wet Lime/Limestone FGD Systems," presented at the 1985

EPA/EPRI Symposium on Flue Gas Desulfurization, Cincinnati, Ohio, EPA-600/9-85-033A, Volume 1, 261, 1985.

Jorgensen, C., J. C. S. Chang, T. G. Brna, "Evaluation of Sorbents and Additives for Dry SO₂ Removal," presented at the Spring National AIChE Meeting, New Orleans, LA, 1986.

Jones B. F., P.S. Lowell, F.B. Meserole, "Experimental and Theoretical Studies of Solid Solution Formation in Lime and Limestone SO₂ Scrubbers," EPA-600/2-76-273a, 1976.

Jozewicz, W., J. C. S. Chang, C. B. Sedman, "Bench-Scale Evaluation of Calcium Sorbents for Acid Gas Emission Control," *Environmental Progress*, 9(3), 137, 1990.

Jozewicz, W., B. K. Gullett, S. C. Tseng, "A Novel Calcium-Based Sorbent for the Removal of Flue Gas by Dry Injection," presented at the Second International Conference on Municipal Waste Combustion, Tampa, Florida, 1991.

Jozewicz, W., C. Jorgensen, J. C. S. Chang, C. B. Sedman, T. G. Brna, "Development and Pilot Plant Evaluation of Silica-Enhanced Lime Sorbents for Dry Flue Gas Desulfurization," *JAPCA*, 38, 796, 1988.

Jozewicz, W., G. T. Rochelle, "Fly Ash Recycle in Dry Scrubbing," *Environmental Progress*, 5(4), 219, 1986.

Kind, K. K., P. D. Wasserman, G. T. Rochelle, "Effects of Salts on Preparation and Use of Calcium Silicates for Flue Gas Desulfurization," *Environmental Science and Technology*, 28(2), 277, 1994.

Klingspor, J., A. Stromberg, H. T. Karlsson, I. Bjerle, "Similarities Between Lime and Limestone in Wet-Dry Scrubbing," *Chemical and Engineering Processing*, 18(5), 239, 1984

Levenspiel, O., Chemical Reaction Engineering, John Wiley and Sons, New York, 1972.

Littlejohn, D., Y. Wang, S. Chang, "Oxidation of Aqueous Sulfite Ion by Nitrogen Dioxide," *Environmental Science and Technology*, 27(10), 2162, 1993.

Lyon, R. K., J. A. Cole, J. C. Kramlich, S. L. Chen, "The Selective Reduction of SO₃ to SO₂, and the Oxidation of NO to NO₂ by Methanol," *Combustion and Flame*, 81, 30, 1990.

- Matsukata, M., K. Takeda, T. Miyatani, K. Ueyama, "Simultaneous Chlorination and Sulphation of Calcined Limestone," *Chemical Engineering Science*, **51**(11), 2529, 1996.
- Nelli, C. H., "Nitrogen Dioxide Removal by Calcium Silicate Solids," Ph.D. Dissertation, The University of Texas at Austin, 1997.
- Nelli, C. H., G. T. Rochelle, "Nitrogen Dioxide Reaction with Alkaline Solids," *Industrial Engineering and Chemistry Research*, **35**, 999, 1996.
- Oblath, S. B., S. S. Markowitz, T. Novakov, and S. G. Chang, "Kinetics of the Formation of Hydroxylamine Disulfonate by Reaction with Nitrite with Sulfites," *Journal of Physical Chemistry*, **85**, 1017, 1981.
- Oblath, S. B., S. S. Markowitz, T. Novakov, and S. G. Chang, "Kinetics of the Initial Reaction of Nitrite Ion in Bisulfite Solutions," *Journal of Physical Chemistry*, **86**, 4853, 1982.
- Pakrasi, A., "Kinetic Studies on the Removal of Hydrogen Chloride from Flue Gas by Hydrated Lime Powders in a Bench Scale Fixed Bed Reactor," Ph.D. Dissertation, The University of Tennessee, Knoxville, 1992.
- Perkin-Elmer, "Spectrum 2000 User's Reference," Perkin-Elmer Ltd., Beaconsfield, Buckinghamshire, United Kingdom, 1995.
- Perkin-Elmer, "TR-IR User's Manual," Perkin-Elmer Ltd., Beaconsfield, Buckinghamshire, United Kingdom, 1992.
- Perkin-Elmer, "Spectrum for Windows™ User's Reference," Perkin-Elmer Ltd., Beaconsfield, Buckinghamshire, United Kingdom, 1995b.
- Perry, R. H., D. W. Green, and J. O. Maloney, Perry's Chemical Engineers' Handbook, Sixth Edition, McGraw-Hill Book Company, New York, 1984.
- Ruiz-Alsop, R. N., G. T. Rochelle, "Effect of Deliquescent Salt Additives on the Reaction of SO_2 with $\text{Ca}(\text{OH})_2$," presented at the 189th Meeting of the American Chemical Society, Miami, FL, 1985.
- Simons, G. A., "Parameters Limiting Sulfation by CaO ," *AIChE Journal*, **34**(1), 167, 1988.
- Simons, G. A., A. R. Garman, "Small Pore Closure and the Deactivation of the Limestone Sulfation Reaction," *AIChE Journal*, **32**(9), 1491, 1986.
- Sinke, G. C., E. H. Mossner, J. L. Curnutt, "Enthalpies of Solution and Solubilities of Calcium Chloride and Its Lower Hydrates," *Journal of Chemical Thermodynamics*, **17**, 893, 1985.

- Szekely, J., J. W. Evans, H. Y. Sohn, Gas-Solid Reactions, Academic Press, New York, 1976.
- Stewart, W. E., M. Caracotsios, J. P. Sørensen, "Parameter Estimation from Multiresponse Data," *AIChE Journal*, **38**(5), 1992.
- USEPA, "Standards of Performance for New Stationary Sources and Emission Guidelines for Existing Sources: Hospital/Medical/Infectious Waste Incinerators," 40 CFR 48348, September 15, 1997.
- USEPA, "Standards of Performance for New Stationary Sources and Emission Guidelines for Existing Sources: Municipal Waste Combustors" 40 CFR 65387, December 19, 1995.
- von Rosenberg, D. U., R. P. Chambers, and G. A. Swan, "Numerical Solution of Surface Controlled Fixed-Bed Adsorption," *Industrial Engineering and Chemistry Research Fundamentals*, **16**(1), 154, 1977.
- Wang, W., Z. Ye, I. Bjerle, "The Kinetics of the Reaction of Hydrogen Chloride with Fresh and Spent Ca-Based Desulfurization Sorbents," *Fuel*, **75**(2), 207, 1996.
- Weinell, C. E., P. I. Jensen, K. Dam-Johansen, H. Livbjerg, "Hydrogen Chloride Reaction with Lime and Limestone: Kinetics and Sorption Capacity," *Industrial Engineering and Chemistry Research*, **31**, 164, 1992.
- White, D. M., M. A. Vancil, "Review of Dry Injection Technology for Reducing Emissions from Municipal Waste Combustors," presented at the International Conference on Municipal Waste Combustion, Hollywood, Florida, 1989.
- Yuan, C.-S., Z.-T. Fong, "Experimental Study on Simultaneous SO₂, HCl, and NO Removal via Spray Drying Technology," presented at the 85th Annual Meeting & Exhibition, Kansas City, Missouri, 1992.

Vita

Paul Norman Chisholm was born in Malden, Massachusetts, on 29 March, 1971. With brothers Don and Ted, he is the third son of Edward F. and M. Norma Chisholm. Paul graduated from Reading Memorial High School in Reading, Massachusetts, in 1989. Later that year, he entered the University of Notre Dame in Notre Dame, Indiana, with a scholarship from the U.S. Army. Upon graduation in 1993 with a Bachelor of Science in Chemical Engineering, Paul was commissioned into the U.S. Army Reserves as a Second Lieutenant. While awaiting required military schooling, he worked as a Research Assistant for Dr. Arvind Varma at Notre Dame. After completion of the Officer Basic Course at Aberdeen Proving Ground in Aberdeen, Maryland, in 1994, Paul entered the graduate program at the University of Texas at Austin under the supervision of Dr. Gary Rochelle. During the spring semester of 1998, Paul worked as a Graduate Cooperative Student at Huntsman Corporation's Austin Research Laboratory. He continues to participate in the Texas Army National Guard. Upon completion of graduation from the University of Texas, Paul will be working for Exxon Chemical's Basic and Intermediates Chemical Technology group in Baytown, Texas.

Permanent address: 3 Beech Street, Reading, MA 01867-2731

This dissertation was typed by the author.